SUMMARY AND CRITIQUE OF THE THERMODYNAMIC PROPERTIES OF ROCK-FORMING MINERALS

HAROLD C. HELGESON, JOAN M. DELANY*,
H. WAYNE NESBITT**, and DENNIS K. BIRD***

Department of Geology and Geophysics,
University of California,
Berkeley, California 94720

* Present address: Department of Earth and Space Sciences, University of California, Los Angeles, California 90024

** Present address: Department of Geology, La Trobe University, Bundoora, Victoria, Australia 3083

*** Present address: Department of Geosciences, University of Arizona, Tucson, Arizona 85721

Vol. 278-A 1978

American Journal of Science

Established in 1818 by Benjamin Silliman

KLINE GEOLOGY LABORATORY
YALE UNIVERSITY
NEW HAVEN, CONNECTICUT

The research reported in the following pages was carried out in recognition of the need for a well documented, comprehensive, and critical compilation of thermodynamic data for minerals which can be used with confidence to characterize chemical equilibrium in geologic systems. The credibility of such a compilation is largely a function of the extent to which the authors demonstrate that the thermodynamic data adopted for a given mineral are consistent with those derived from experimental data for all other minerals, and that none contravenes reliable geologic observations. We make no pretense at having achieved these goals with the present contribution, which represents little more than a beginning step in this direction. Nevertheless, we consider it an important step and hope that it will serve as a comprehensive foundation for future refinement of the values adopted for the thermodynamic properties of minerals. At the same time we trust that the near-coincident appearance of the present communication and the revision of U.S. Geological Survey Bulletin 1259 (Robie and Waldbaum, 1968) by Robie, Hemingway, and Fisher (1978), which is based almost entirely on calorimetric data, will in no way polarize the geologic community. The two publications serve different needs and both should enhance the geologist's ability to understand and meet the many challenges inherent in applying thermodynamic analysis to the interpretation of phase relations in natural systems.

Most compilations of thermodynamic data contain few if any illustrations to facilitate assessment of the reliability of the values given for the thermodynamic properties of the species considered. Furthermore, as a rule they contain little or no comparative discussion or documentation of the basis for choosing the values adopted and the extent to which they agree or disagree with other values reported in the literature. Perhaps more importantly, attention is rarely devoted in such compilations to the chemical or geologic consequences of choosing one value over another. We consider these serious shortcomings which we have endeavored to overcome in the present communication.

The calculations summarized below were carried out with the firm conviction that there are no "correct" thermodynamic properties of minerals, just as there are no "correct" physical, compositional, and crystallochemical states of minerals. That this is indeed true can be easily verified by little more than a cursory appraisal of the spectrum of calorimetric enthalpies of formation that have been reported in recent years for different natural and synthetic samples of the same mineral.

The discussion in the following pages combines many elements of a textbook with advanced concepts and numerical results of recent research. We make no apology for this but instead submit that the present state of understanding in the application of thermodynamics to the interpretation of geologic systems requires careful documentation of the equations used in the calculations and continued reappraisal of the factors contributing to the thermodynamic behavior of minerals.

H. C. Helgeson
Berkeley, California
January 15, 1978

American Journal of Science

V. 278-A

1978

CONTENTS

SUMMARY AND CRITIQUE OF THE THERMODYNAMIC PROPERTIES OF ROCK-FORMING MINERALS

ABSTRACT. Critical analysis of experimental high-pressure/temperature solubility data and univariant/divariant phase relations reported in the literature with equations representing the thermodynamic properties of ionic aqueous species, $SiO_{2(aq)}$, H_2O, CO_2, O_2, and the temperature dependence of the standard molal heat capacities of minerals affords an internally consistent set of thermodynamic data for the bulk of the abundant rock-forming silicates, carbonates, and oxides in the crust and upper mantle. Standard molal Gibbs free energies and enthalpies of formation were obtained in this manner for $\sim$ 70 minerals in the system Na_2O–K_2O–CaO–MgO–FeO–Fe_2O_3–Al_2O_3–SiO_2–CO_2–H_2O. The calculations were carried out using standard molal entropies, heat capacities, and volumes derived from calorimetric, crystallographic, and density data or estimated from correlation algorithms and Clapeyron slope constraints. Where necessary and appropriate, provision was included for configurational entropy contributions and enthalpy changes arising from the temperature dependence of substitutional and displacive order/disorder in minerals. In most cases, simultaneous consideration of multiple equilibria reduced relative uncertainties in the standard molal enthalpies and Gibbs free energies of formation generated from the high pressure/temperature data by more than an order of magnitude from those inherent in corresponding values derived from calorimetric measurements. Apparent inconsistencies among experimental data and phase relations in nature were resolved by taking account of geologic observations, the thermodynamic consequences of metastable equilibria, and compositional variation in minerals at both high and low temperatures and pressures. Experimental solution compositions and/or reversal temperatures for more than 130 reactions at various pressures are depicted in phase diagrams, where they can be compared with calculated equilibrium constants and univariant/divariant curves generated from the thermodynamic data summarized in the tables and discussed in the text. These data, together with the equations of state employed in the calculations, permit comprehensive prediction of the thermodynamic consequences of equilibrium and mass transfer among minerals and aqueous solutions in geochemical processes at high pressures and temperatures.

CONVENTIONS AND NOTATION

The standard state for minerals and liquids adopted in the present study is one of unit activity of the pure solid or liquid at any pressure and temperature, but that for gases calls for unit fugacity of the hypothetical gas at 1 bar and any temperature. It follows that the activities of components corresponding to stoichiometric minerals and pure liquids are unity, and the fugacities of gases are equal to their activities at all pressures and temperatures. The standard state for aqueous species corresponds to unit activity of the species in a hypothetical one molal solution referenced to infinite dilution at any pressure and temperature. The activity coefficients of aqueous species thus approach one as the activity of the solvent (relative to the liquid standard state) approaches unity. In contrast, the fugacity coefficients of the components of gas mixtures approach the fugacity coefficients of the pure gases (which are not necessarily unity) as the mole fractions of the gases approach one at any pressure and temperature.

Standard molal Gibbs free energies and enthalpies are reported below in thermochemical calories (cal) or kilocalories (kcal) mole^{-1}, which can be converted to joules (j) or kilojoules (kj) mole^{-1} by multiplying by 4.184 j cal^{-1} or kj kcal^{-1}. Standard molal entropies and heat capacities are given in cal mole^{-1} (°K)$^{-1}$ and standard molal volumes in cm^3 mole^{-1}. The latter values can be converted to cal mole^{-1} bar^{-1} by multiplying by 0.0239 cal cm^{-3} bar^{-1}. These various units were adopted in preference to SI units to facilitate calculation of equilibrium constants using the thermodynamic properties of minerals given below and those for gases, liquids, and aqueous species reported in other publications. The thermodynamic properties reported in many of these are also expressed in cal or kcal mole^{-1}.

The terms K-feldspar, albite, dolomite, and epidote are used in the following pages to refer to $KAlSi_3O_8$, $NaAlSi_3O_8$, $CaMg(CO_3)_2$, and $Ca_2FeAl_2Si_3O_{12}(OH)$ in their stable states of order/disorder at any pressure and temperature. Similarly, except when cited in conjunction with their monoclinic analogs, enstatite and ferrosilite refer to the stable polymorphs of $MgSiO_3$ and $FeSiO_3$ at any pressure and temperature. In contrast, zoisite is used to denote only the orthorhombic form of $Ca_2Al_3Si_3O_{12}(OH)$.

Glossary of Symbols

A_r	— Pre-exponential factor for the rth reaction (eq 102).
A	— Designation of the A lattice site in dolomite.
$\mathbf{A}_r$	— Chemical affinity of the rth reaction.
a, a_i	— Standard molal heat capacity coefficient for the Maier-Kelley power function or (in the case of a_i) the activity of the ith species.
a_α	— Constant defined by eq (112).

a_d — Activity of $CaMg(SiO_3)_2$.

a_i, a_j, a_l — Activity of the subscripted species or (in the case of a_i) the first coefficient in the Maier-Kelley power function for the standard molal heat capacity of the ith mineral.

an — Subscript designating $KFe^{++}{}_3(AlSi_3O_{10})(OH)_2$.

(aq) — Subscript designating the aqueous state.

b, b_i — Standard molal heat capacity coefficient in the Maier-Kelley power function or (in the case of b) the b cell parameter.

b_α — Constant defined by eq (113).

β, Γ, λ — Matrix and column vector notation in eq (33).

(c) — Subscript designating the crystalline state.

$c = 1, 2, \ldots \hat{c}$ — Index designating different structural classes of minerals.

c, c_i — Standard molal heat capacity coefficient in the Maier-Kelley power function or (in the case of c) the c cell parameter.

c_α — Designation of $(\partial V^\circ{}_\alpha/\partial T)_P$.

$C^\circ{}_P$ — Standard molal heat capacity at constant pressure.

$C^\circ{}_{P_r}$ — Standard molal heat capacity at 1 bar.

$\Delta C^\circ{}_P$, $\Delta C^\circ{}_{P,r}$ — Standard molal heat capacity of reaction.

$\Delta C^\circ{}_{P,ds}$ — Standard molal heat capacity of substitutional disorder.

$\Delta C^\circ{}_{P,dt}$ — Standard molal heat capacity of displacive disorder.

$\Delta C^\circ{}_{P,t}$ — Standard molal heat capacity of transition or total standard molal heat capacity of substitutional and displacive disorder.

$\tilde{\gamma}_l$ — Activity coefficient of the lth aqueous species.

δ — Finite difference derivative.

$đQ_{irrev,r}$ — Inexact differential of the heat associated with the rth irreversible reaction.

$\Delta E^*{}_r$ — Activation energy for the rth reaction.

f_l — Fugacity of the lth species.

$\hat{f}_v$ — Fraction of lattice sites corresponding to point defects in a crystal.

G — Gibbs free energy.

G° — Standard molal Gibbs free energy.

$G - G^\circ$ — Ideal molal Gibbs free energy of mixing.

ΔG° — Apparent standard molal Gibbs free energy of formation from the elements defined by eq (14).

ΔG°_f — Standard molal Gibbs free energy of formation from the elements at 298.15°K and 1 bar.

$\Delta G^\bullet_f$ — Intracrystalline standard molal Gibbs free energy of formation from the elements at 298.15°K and 1 bar.

ΔG°_r — Standard molal Gibbs free energy of reaction.

ΔG°_d, ΔG°_{ds} — Standard molal Gibbs free energy of substitutional disorder.

ΔG°_{dt} — Standard molal Gibbs free energy of displacive disorder.

ΔG°_v — Standard Gibbs free energy of formation of a single vacancy in a crystal.

H° — Standard molal enthalpy.

ΔH° — Apparent standard molal enthalpy of formation from the elements defined by eq (15).

ΔH°_d, ΔH°_{ds} — Standard molal enthalpy of substitutional disorder.

ΔH°_{dt} — Standard molal enthalpy of displacive disorder.

ΔH°_f — Standard molal enthalpy of formation from the elements at 298.15°K and 1 bar.

$\Delta H^\bullet_f$ — Intracrystalline standard molal enthalpy of formation from the elements at 298.15°K and 1 bar.

ΔH°_r — Standard molal enthalpy of reaction.

ΔH°_t — Standard molal enthalpy of transition or total standard molal enthalpy of substitutional and displacive disorder.

ΔH^*_r — Enthalpy of activation for the rth reaction.

$H_2O_{(s)}$ — Designation of "structural" H_2O in minerals.

$H_2O_{(z)}$ — Designation of "zeolitic" H_2O in minerals.

$\bar{I}$ — "True" ionic strength of an aqueous electrolyte solution.

i — Index designating minerals, species or thermodynamic components of solid solutions.

j — Index designating minerals or the atoms on the lattice sites of solid solutions.

K — Equilibrium constant.

k — Boltzmann's constant (3.2995×10^{-24} cal $(°K)^{-1}$).

k — Designation of the Clapeyron slope of a univariant curve.

$\hat{k}$ — Proportionality constant in eqs (55) and (73).

k_i — Standard state proportionality constant in eqs (46) and (48).

k_r — Rate constant for the rth reaction.

l — Index designating species in a reaction or the thermodynamic components of a solid solution.

(l), $(liquid)$ — Subscripts designating the liquid state.

λ_a — Activity coefficient of $NaAlSi_2O_6 \cdot H_2O$.

λ_{ab} — Activity coefficient of $NaAlSi_3O_8$.

λ_d — Activity coefficient of $NaAlSi_2O_6$.

λ_l — Activity coefficient of the lth thermodynamic component of a solid solution.

λ_n — Activity coefficient of $NaAlSiO_4$.

M, M(1), M(2), M(3), M(4) — Octahedral site designations for minerals.

M_a, M_c, M_d, M_m, M_s — Molecular weight of Al_2O_3, CaO, $CaMg(SiO_3)_2$, MgO, and SiO_2, respectively.

m_l — Molality of the lth aqueous species.

μ_i — Chemical potential of the ith component or species.

$\mu^\bullet{}_i$ — Standard molal intracrystalline chemical potential of the ith species.

n — Number of moles of the spinel component of an aluminous diopside solid solution (gram formula wt)$^{-1}$ for a unit framework of 6 oxygen atoms.

$\hat{n}_{l,r}$ — Reaction coefficient for the lth species in the rth reaction, which is negative for reactants and positive for products.

$n_{j,s}$ — Number of moles of the jth species on the sth energetically equivalent sites in a mineral.

$n_{s,i}$ — Stoichiometric number of energetically equivalent sth sites in one mole of the ith component of a solid solution.

$\nu_{Al,t}$, $\nu_{Si,t}$ — Number of moles of tetrahedral Al and Si atoms (gram formula unit)$^{-1}$ of a mineral.

$\nu_{i,\psi}$ — Number of moles of the ith oxide or hydroxide formula unit (gram formula unit)$^{-1}$ of the ψth mineral.

$\nu_{j,i}$ — Number of moles of the jth oxide or hydroxide formula unit (gram formula unit)$^{-1}$ of the ith mineral.

ν_O — Number of moles of oxygen other than in OH^- (gram formula unit)$^{-1}$ of a mineral.

$\nu_{s,j,i}$ — Stoichiometric number of sth energetically equivalent sites occupied by the jth species in one mole of the ith component of a solid solution.

ξ_r — Progress variable for the rth reaction.

P — Pressure in bars or kilobars.

P* — Variable pressure integration limit corresponding to P_t for $T > T_{t,P_r}$ and P_r for $T \leqslant T_{t,P_r}$.

p_l — Partial pressure of the lth species.

P_r — Reference pressure (1 bar).

P_t — Transition pressure.

pd — Subscript designating $KFe^{+++}{}_3(AlSi_3O_{10})O_2H_{-1}$.

Q_r — Reaction quotient defined by eq (100).

R — Gas constant (1.9872 cal $mole^{-1}$ $(°K)^{-1}$).

r — Index designating reactions.

$\hat{r}_r$ — Rate of the rth reaction.

S° — Standard molal entropy.

s — Substitutional ordering parameter defined by eq (127), or index designating energetically distinct lattice sites in minerals.

$\hat{s}$ — Designation of the number of aqueous species appearing in a reaction.

σ — Ordering parameter defined by eq (212E).

$\sigma^\circ{}_r$ — Designation of the Gibbs free energy function defined by eq (31).

$S - S^\circ$ — Ideal molal entropy of mixing.

$S^\circ{}_{s,i}$ — Standard molal entropy parameter for the ith species in eqs (62) and (75).

$S^\circ{}_{\Sigma,i}$ — Sum of the standard molal entropies of the oxides in one mole (gram formula unit) of the ith mineral.

ΔS°, $\Delta S^\circ{}_r$ — Standard molal entropy of reaction.

$\Delta S^\circ{}_d$, $\Delta S^\circ{}_{ds}$ — Standard molal entropy of substitutional disorder.

$\Delta S^\circ{}_f$ — Standard molal entropy of formation from the elements at 298.15°K and 1 bar.

$\Delta S^*{}_r$ — Entropy of activation for the rth reaction.

$\Delta S^\circ{}_t$ — Standard molal entropy of transition.

T — Temperature in °C or °K, or in the case of eqs (203) and (204), a subscript designating tetrahedral sites.

t — Time.

t — Subscript designating transition, total, or (in the case of eqs 220 and 221) tetrahedral.

T_1, T_2, T_{1o}, T_{1m}, T_{2o}, T_{2m} — Tetrahedral site designations.

T_c — Temperature at which a phase becomes completely disordered.

T_{ds} — Temperature above which no substitutional order is apparent.

$T_{m/a}$ — Temperature above which albite exhibits only monoclinic symmetry.

T_r — Reference temperature (298.15°K).

T_t — Transition temperature.

v — Subscript designating vacant sites in a crystal.

$V°_{\alpha}$ — Standard molal volume of α-quartz.

$\Delta V°$, $\Delta V°_r$ — Standard molal volume of reaction.

$V°_{\beta}$ — Standard molal volume of β-quartz.

$V°_{s,i}$ — Standard molal volume parameter for the ith mineral in eqs (62) and (75).

$V°_{\Sigma,i}$ — Sum of the standard molal volumes of the oxides in one mole (gram formula unit) of the ith mineral.

$\Delta V°_t$ — Standard molal volume of transition.

w — Weight percent Al_2O_3 in aluminous diopside.

x — Number of moles of Fe^{+++} on the M(1) sites in one gram formula unit of stoichiometric epidote.

X — Mole fraction.

X_a — Mole fraction of $NaAlSi_2O_6 \cdot H_2O$.

X_{ab} — Mole fraction of $NaAlSi_3O_8$.

X_h — Mole fraction of $Mg_2Al_3(AlSi_5O_{18}) \cdot H_2O$.

X_l — Mole fraction of the lth component or species.

$X_{Mg,M(1)}$ — Mole fraction of magnesium on the M(1) sites in a mineral.

X_n — Mole fraction of $NaAlSiO_4$.

$X_{Si,T}$ — Mole fraction of silicon on the tetrahedral sites of a mineral.

χ_l — Fugacity coefficient of the lth species.

Y — Substitutional ordering parameter defined by eq (149).

ψ, Ψ — Mineral designations.

$\Psi \cdot \hat{n}_{H_2O_{(z)}} H_2O_{(z)}$ — General representation of a zeolitic mineral containing $\hat{n}_{H_2O_{(z)}}$ moles of "zeolitic" H_2O.

Z — Substitutional ordering parameter defined by eq (148) for albite and eq (159) for K-feldspar.

Summary of Mineral Names and Formulas

To facilitate cross referencing among the text, figures, and tables presented in the pages that follow, an index number has been assigned to each of the minerals considered in the present communication. These numbers coincide with those in the data file of the computer program discussed under CONCLUDING REMARKS.

Index Number	Name	Formula
1501	Acanthite	Ag_2S
1548	Aegerine	$NaFe(SiO_3)_2$
1044	Akermanite	$Ca_2MgSi_2O_7$
1092	Alabandite	MnS
1531	Albite	$NaAlSi_3O_8$
1560	Albite, High	$NaAlSi_3O_8$
1025	Albite, Low	$NaAlSi_3O_8$
1527	Almandine	$Fe_3Al_2Si_3O_{12}$
1083	Alunite	$KAl_3(OH)_6(SO_4)_2$
1017	Amesite, 7A	$Mg_2Al(AlSiO_5)(OH)_4$
1511	Amesite, 14A	$Mg_4Al_2(Al_2Si_2O_{10})(OH)_8$
1125	Amorphous Silica	$SiO_2 \cdot nH_2O$
1022	Analcime	$NaAlSi_2O_6 \cdot H_2O$
1021	Analcime, Dehydrated	$NaAlSi_2O_6$
1001	Andalusite	Al_2SiO_5
1530	Andradite	$Ca_3Fe_2Si_3O_{12}$
1081	Anglesite	$PbSO_4$
1078	Anhydrite	$CaSO_4$
1015	Annite	$KFe_3(AlSi_3O_{10})(OH)_2$
1030	Anorthite	$CaAl_2Si_2O_8$
1518	Anthophyllite	$Mg_7Si_8O_{22}(OH)_2$
1542	Antigorite	$Mg_{48}Si_{34}O_{85}(OH)_{62}$
1072	Aragonite	$CaCO_3$
1053	Artinite	$Mg_2(OH)_2CO_3 \cdot 3H_2O$
1060	Azurite	$Cu_3(OH)_2(CO_3)_2$
1080	Barite	$BaSO_4$
1116	Boehmite	$AlO(OH)$
1503	Bornite	Cu_5FeS_4
1117	Brucite	$Mg(OH)_2$
1554	Bunsenite	NiO
1040	Ca–Al Pyroxene	$CaAl(AlSiO_6)$
1073	Calcite	$CaCO_3$
1009	Celadonite	$KMgAlSi_4O_{10}(OH)_2$
1082	Celestite	$SrSO_4$
1068	Cerussite	$PbCO_3$
1133	Chabazite	$Ca(Al_2Si_4O_{12}) \cdot 6H_2O$
1128	Chalcedony	SiO_2

Index Number	Name	Formula
1504	Chalcocite	Cu_2S
1502	Chalcopyrite	$CuFeS_2$
1018	Chamosite, 7A	$Fe_2Al(AlSiO_5)(OH)_4$
1058	Chloritoid	$FeAl_2SiO_5(OH)_2$
1007	Chrysotile	$Mg_3Si_2O_5(OH)_4$
1091	Cinnabar	HgS
1512	Clinochlore, 7A	$Mg_5Al(AlSi_3O_{10})(OH)_8$
1513	Clinochlore, 14A	$Mg_5Al(AlSi_3O_{10})(OH)_8$
1515	Clinozoisite	$Ca_2Al_3Si_3O_{12}(OH)$
1557	Coesite	SiO_2
1102	Copper, Native	Cu
1065	Cordierite	$Mg_2Al_3(AlSi_5O_{18})$
1066	Cordierite, Hydrous	$Mg_2Al_3(AlSi_5O_{18}) \cdot H_2O$
1108	Corundum	α–Al_2O_3
1086	Covellite	CuS
1556	Cristobalite	SiO_2
1126	Cristobalite, Alpha	SiO_2
1127	Cristobalite, Beta	SiO_2
1550	Cronstedtite, 7A	$Fe_2Fe(FeSiO_5)(OH)_4$
1043	Cummingtonite	$Mg_7Si_8O_{22}(OH)_2$
1112	Cuprite	Cu_2O
1514	Daphnite, 7A	$Fe_5Al(AlSi_3O_{10})(OH)_8$
1016	Daphnite, 14A	$Fe_5Al(AlSi_3O_{10})(OH)_8$
1115	Diaspore	AlO(OH)
1006	Dickite	$Al_2Si_2O_5(OH)_4$
1039	Diopside	$CaMg(SiO_3)_2$
1075	Dolomite	$CaMg(CO_3)_2$
1070	Dolomite, Disordered	$CaMg(CO_3)_2$
1071	Dolomite, Ordered	$CaMg(CO_3)_2$
1520	Edenite	$NaCa_2Mg_5(AlSi_7O_{22})(OH)_2$
1537	Enstatite	$MgSiO_3$
1545	Epidote, Ordered	$Ca_2FeAl_2Si_3O_{12}(OH)$
1559	Epidote	$Ca_2FeAl_2Si_3O_{12}(OH)$
1536	Epistilbite	$Ca(Al_2Si_6O_{16}) \cdot 5H_2O$
1049	Fayalite	Fe_2SiO_4
1521	Ferroedenite	$NaCa_2Fe_5(AlSi_7O_{22})(OH)_2$
1549	Ferrogedrite	$Fe_5Al_2(Al_2Si_6O_{22})(OH)_2$
1055	Ferropargasite	$NaCa_2Fe_4Al(Al_2Si_6O_{22})(OH)_2$
1508	Ferrosilite	$FeSiO_3$
1041	Ferrotremolite	$Ca_2Fe_5Si_8O_{22}(OH)_2$
1113	Ferrous Oxide	FeO
1522	Fluoredenite	$NaCa_2Mg_5(AlSi_7O_{22})F_2$
1079	Fluorite	CaF_2
1042	Fluortremolite	$Ca_2Mg_5Si_8O_{22}F_2$

Index Number	Name	Formula
1061	Fluorphlogopite	$KMg_3(AlSi_3O_{10})F_2$
1048	Forsterite	Mg_2SiO_4
1087	Galena	PbS
1047	Gehlenite	$Ca_2Al_2SiO_7$
1114	Gibbsite	$Al(OH)_3$
1063	Glaucophane	$Na_2Mg_3Al_2Si_8O_{22}(OH)_2$
1100	Gold, Native	Au
1103	Graphite	C
1010	Greenalite	$Fe_3Si_2O_5(OH)_4$
1529	Grossular	$Ca_3Al_2Si_3O_{12}$
1019	Grunerite	$Fe_7Si_8O_{22}(OH)_2$
1106	Halite	NaCl
1005	Halloysite	$Al_2Si_2O_5(OH)_4$
1523	Hastingsite	$NaCa_2Fe_4Fe(Al_2Si_6O_{22})(OH)_2$
1054	Hedenbergite	$CaFe(SiO_3)_2$
1544	Hematite	Fe_2O_3
1535	Heulandite	$Ca(Al_2Si_7O_{18}) \cdot 6H_2O$
1050	Huntite	$CaMg_3(CO_3)_4$
1062	Hydromagnesite	$Mg_5(OH)_2(CO_3)_4 \cdot 4H_2O$
1067	Jadeite	$NaAl(SiO_3)_2$
1507	Kalsilite	$KAlSiO_4$
1004	Kaolinite	$Al_2Si_2O_5(OH)_4$
1028	K-feldspar	$KAlSi_3O_8$
1002	Kyanite	Al_2SiO_5
1546	Larnite	β–Ca_2SiO_4
1132	Laumontite	$Ca(Al_2Si_4O_{12}) \cdot 4H_2O$
1516	Lawsonite	$CaAl_2Si_2O_7(OH)_2 \cdot H_2O$
1024	Leonhardite	$Ca_2(Al_4Si_8O_{24}) \cdot 7H_2O$
1110	Lime	CaO
1524	Magnesiohastingsite	$NaCa_2Mg_4Fe(Al_2Si_6O_{22})(OH)_2$
1547	Magnesioriebeckite	$Na_2Mg_3Fe_2Si_8O_{22}(OH)_2$
1074	Magnesite	$MgCO_3$
1506	Magnetite	Fe_3O_4
1059	Malachite	$Cu_2(OH)_2CO_3$
1119	Manganosite	MnO
1551	Margarite	$CaAl_2(Al_2Si_2O_{10})(OH)_2$
1045	Merwinite	$Ca_3Mg(SiO_4)_2$
1090	Metacinnabar	HgS
1027	Microcline, Maximum	$KAlSi_3O_8$
1011	Minnesotaite	$Fe_3Si_4O_{10}(OH)_2$
1046	Monticellite	$CaMgSiO_4$
1012	Muscovite	$KAl_2(AlSi_3O_{10})(OH)_2$
1533	Natrolite	$Na_2(Al_2Si_3O_{10}) \cdot 2H_2O$
1031	Nepheline	$NaAlSiO_4$

Index Number	Name	Formula
1558	Nesquehonite	$MgCO_3 \cdot 3H_2O$
1553	Nickel	Ni
1013	Paragonite	$NaAl_2(AlSi_3O_{10})(OH)_2$
1538	Pargasite	$NaCa_2Mg_4Al(Al_2Si_6O_{22})(OH)_2$
1543	PD-oxyannite	$KFe_3(AlSi_3O_{12})H_{-1}$
1109	Periclase	MgO
1541	Phillipsite, Calcium	$Ca(Al_2Si_5O_{14}) \cdot 5H_2O$
1540	Phillipsite, Potassium	$K_2(Al_2Si_5O_{14}) \cdot 5H_2O$
1539	Phillipsite, Sodium	$Na_2(Al_2Si_5O_{14}) \cdot 5H_2O$
1014	Phlogopite	$KMg_3(AlSi_3O_{10})(OH)_2$
1123	Potassium Oxide	K_2O
1532	Prehnite	$Ca_2Al(AlSi_3O_{10})(OH)_2$
1093	Pyrite	FeS_2
1509	Pyrophyllite	$Al_2Si_4O_{10}(OH)_2$
1555	Pyrrhotite	FeS
1505	Quartz	SiO_2
1552	Quicksilver	Hg
1056	Richterite	$Na_2CaMg_5Si_8O_{22}(OH)_2$
1525	Riebeckite	$Na_2Fe_3Fe_2Si_8O_{22}(OH)_2$
1085	Rhodochrosite	$MnCO_3$
1029	Sanidine, High	$KAlSi_3O_8$
1023	Sepiolite	$Mg_4Si_6O_{15}(OH)_2(OH_2)_2 \cdot (OH_2)_4$
1076	Siderite	$FeCO_3$
1003	Sillimanite	Al_2SiO_5
1101	Silver, Native	Ag
1064	Smithsonite	$ZnCO_3$
1124	Sodium Oxide	Na_2O
1528	Spessartine	$Mn_3Al_2Si_3O_{12}$
1088	Sphalerite	ZnS
1120	Spinel	$MgAl_2O_4$
1057	Staurolite	$Fe_2Al_9Si_4O_{23}(OH)$
1534	Stilbite	$NaCa_2(Al_5Si_{13}O_{36}) \cdot 14H_2O$
1069	Strontianite	$SrCO_3$
1107	Sylvite	KCl
1510	Talc	$Mg_3Si_4O_{10}(OH)_2$
1111	Tenorite	CuO
1517	Tremolite	$Ca_2Mg_5Si_8O_{22}(OH)_2$
1130	Wairakite	$Ca(Al_2Si_4O_{12}) \cdot 2H_2O$
1084	Witherite	$BaCO_3$
1035	Wollastonite	$CaSiO_3$
1089	Wurtzite	ZnS
1519	Zoisite	$Ca_2Al_3Si_3O_{12}(OH)$

INTRODUCTION

In the years following the appearance of Robie and Waldbaum's (1968) and Naumov, Ryzenko, and Khodakovskii's (1971) compilations of thermodynamic data for minerals, numerous attempts have been made to resolve inconsistencies among reported values of the standard molal enthalpies and Gibbs free energies of formation of various oxides and silicates (for example, Helgeson, 1969; Anderson, 1970; Zen, 1969a and b, 1971, 1972, 1973, 1977; Fisher and Zen, 1971; Zen and Chernosky, 1976; Parks, 1972; Thompson, 1973a and b, 1974a and b; Bird and Anderson, 1973; Ulbrich and Merino, 1974; Chatterjee, 1977; Chatterjee and Johannes, 1974; Haas and Fisher, 1976; Hemingway and Robie, 1977; Robie, Hemingway, and Fisher, 1978). Unfortunately, most of these are restricted to one or another mineral or system, some are based on invalid assumptions, others fail to take adequate account of thermodynamic constraints on phase relations, and none is compatible with both geologic observations and recent experimental data. These deficiencies can be avoided by simultaneous consideration of multiple reactions in experimental as well as natural systems with equations incorporating rigorous and explicit provision for the thermodynamic behavior of minerals and aqueous species. The object of the present communication is to derive with the aid of such equations a comprehensive and reliable set of internally consistent thermodynamic data for all the abundant minerals in the Earth's crust which will, (1) reproduce accurately geologic phase relations and the many experimental observations of high pressure/temperature phase equilibria that have accumulated over the past twenty years, and (2) afford realistic prediction of the chemical consequences of reversible reactions among minerals and aqueous solutions in multicomponent systems at both high and low temperatures and pressures.

Although many calorimetric investigations of minerals have been carried out over the past several decades (for example, Kracek, Neuvonen, and Burley, 1951; Neuvonen, 1952; Kelley and others, 1953; Kelley, 1960, 1962; Barany and Kelley, 1961; Barany, 1962, 1963, 1964; King and Weller, 1961a and b; Pankratz, 1964a and b; Hlabse and Kleppa, 1968; Holm and Kleppa, 1966, 1968; Navrotsky, 1971; Waldbaum, ms; Waldbaum and Robie, 1971; Robie and Hemingway, 1973; Shearer, ms; Charlu, Newton, and Kleppa, 1975; Newton, Charlu, and Kleppa, 1977; Hemingway and Robie, 1977a), few have resulted in sufficiently accurate standard molal enthalpies of formation to afford reliable prediction of equilibrium constants at high pressures and temperatures. Uncertainties in enthalpies of formation at 25°C and 1 bar derived from high temperature molten salt calorimetry are of the order of 500 cal $mole^{-1}$, and those resulting from measurements of low-temperature heats of solution in hydrofluoric acid solutions commonly exceed a kcal $mole^{-1}$. Uncertainties of this order of magnitude may lead to errors of more than 100°C in computed equilibrium temperatures. In contrast, *relative* uncertainties in standard molal enthalpies and Gibbs free energies of formation

of minerals derived from compositional data and experimental observations of equilibrium temperatures and pressures for a series of independent equilibria involving minerals and a fluid phase are commonly of the order of 50 cal $mole^{-1}$ or less, which permits close approximation of the thermodynamics of reactions among minerals and aqueous solutions at high pressures and temperatures.

Many outstanding studies of reversible reactions among minerals, Na^+, K^+, $SiO_{2(aq)}$, O_2, CO_2, and/or H_2O have been reported in the literature (for example, Hemley, 1959; Hemley, Meyer, and Richter, 1961; Hemley and others, 1971, 1977a and b; Greenwood, 1962, 1967a; Orville, 1963, 1972; Eugster and Skippen, 1967; Skippen, 1971, 1974; Chatterjee and Johannes, 1974) which are now sufficient in number and cover a wide enough spectrum of equilibrium states to permit reliable calculation of the standard molal enthalpies and Gibbs free energies of formation of the bulk of the rock-forming minerals in the crust and upper mantle. Calculations of this kind were carried out by combining data reported in these and similar studies with equations of state for aqueous species (Helgeson and Kirkham, 1974a, 1976, and in press; Walther and Helgeson, 1977; Delany and Helgeson, 1978) and fugacity coefficients for gases (Holloway and Reese, 1974; Holloway, 1977) to evaluate simultaneously equilibrium constants for sets of independent reversible reactions. Calculation of the standard molal Gibbs free energies of the reactions at 25°C and 1 bar were carried out using independently derived volumes and calorimetric and/or estimated entropies and heat capacities of the minerals. The standard molal Gibbs free energies of formation of the minerals were then computed from the standard molal Gibbs free energies of the reactions at 25°C and 1 bar by simultaneous solution of the set of equations. Experimental uncertainties were optimized by carrying out comparative calculations and taking account of Clapeyron slope constraints, which were used to determine the extent to which third law entropies should be adjusted to take account of configurational contributions.

The reliability of standard molal Gibbs free energies of formation of minerals computed from high pressure/temperature phase equilibrium data can be assessed by comparing the results of the calculations with geologic observations and/or calorimetric measurements, which often afford corroboration in spite of (but more commonly because of) the relatively large uncertainties inherent in these data. Contradictions in values of the thermodynamic properties of a given mineral generated from different experimental data may be resolved by comparing the geologic consequences of the discrepancies with phase relations in natural systems. Such comparisons are particularly instructive if the pressure, temperature, and the system considered differ from those in the experimental studies from which the data were obtained. Activity diagrams facilitate correlation of predicted and observed equilibrium states with the compositions of fluid inclusions and interstitial waters in geologic

systems. Correlations of this kind commonly reveal inconsistencies arising from metastability and differences in crystallinity and order/disorder in minerals formed under different conditions in different geologic environments. Because the latter factors affect considerably the extent to which thermodynamic calculations represent geologic reality, the effects of various physical and crystallochemical properties of minerals on their thermodynamic behavior in geologic systems are reviewed briefly below.

THERMODYNAMIC CONSEQUENCES OF THE PHYSICAL AND CRYSTALLOCHEMICAL PROPERTIES OF MINERALS

The crystallochemical properties of anisotropic minerals are vector quantities which may differentially affect the extent to which the minerals react in geochemical processes.[1] Furthermore, a mineral with a given name and composition occurring under the same pressure/temperature conditions in one or another laboratory experiment or different parts of the Earth may have significantly different thermodynamic properties (see below). These differences are manifested in part by differences in the thermodynamic behavior of natural minerals and their synthetic analogs.

In addition to their dependence on pressure, temperature, and composition, the thermodynamic properties of a mineral are sensitive to perturbations in energetic, configurational, and crystallochemical contributions to its stability arising from the cooling rate and strain history of the mineral in different environments. Perturbations of this kind are responsible for differences in crystallinity, substitutional and displacive order/disorder, and the number and kinds of defects and dislocations in the mineral, all of which contribute to metastable equilibrium states both in nature and in laboratory experiments. Metastable states also occur as a consequence of incomplete reaction resulting from kinetic constraints. It thus follows that experimental observations of the behavior of minerals cannot be related precisely to the behavior of minerals in geochemical processes without correlating the measurements with the physical and crystallochemical properties of the minerals. Unfortunately, few experimental investigations reported in the literature are comprehensive enough to permit such correlation. Until recently, the thermodynamic consequences of order/disorder in minerals received little attention in experimental investigations of phase equilibria, and the crystallographic properties of the minerals used in calorimetric studies were rarely determined. Even compositional data reported in many early investigations are inadequate to permit unambiguous interpretation of the experimental results.

Despite the fact that thermodynamic calculations of mineral stabilities using data derived from experimental studies afford little more than

[1] In this respect, the thermodynamic properties of anisotropic crystals are somewhat analogous to the electrostatic properties of polar molecules. Although in both cases overall electrical neutrality and conservation of mass are maintained, the magnitudes of the properties are directional.

approximations of geologic reality, comparison of predicted and observed compatibilities and compositions indicates that many of these are close approximations. Furthermore, experimental results obtained using a variety of starting materials, equipment, and techniques in different laboratory studies of a given equilibrium mineral assemblage are commonly compatible with one another. It thus seems reasonable to conclude that in many reactions, physical and crystallochemical factors have a secondary effect on the thermodynamic behavior of minerals. In others, such as solid/solid phase transitions, they are clearly of primary importance.

Solid state phase transitions.—Phase transitions in minerals range from those manifested by abrupt and obvious changes in morphology (such as clinoenstatite/enstatite) to those caused by gradual and nearly imperceptible changes in bond angles or substitutional order/disorder among atoms on energetically distinct lattice sites. Although chemical equilibrium at constant pressure and temperature requires the Gibbs free energy of transformation to be zero for all phase transitions, the partial derivatives of the Gibbs free energies of minerals may exhibit either abrupt or gradual changes with increasing pressure and/or temperature, depending on the nature of the transition taking place.

Despite a multitude of experimental studies, the nature of many phase transitions exhibited by oxides and silicates remains ambiguous. Some of these are thought to be first-order transitions, which are characterized by discontinuities in the temperature dependence of the entropy, enthalpy, volume, heat capacity, expansibility, and compressibility of the compound. Others are almost certainly lambda transitions[2] with no discontinuity in the temperature dependence of these properties. A lambda transition can be thought of as a continuum of infinitesimal changes in the internal structure and/or distribution of atoms in a mineral in response to changes in pressure and/or temperature. The heat capacity, expansibility, and compressibility of a mineral undergoing a lambda transition change dramatically and (in contrast to their first-order counterparts) their dependence on temperature before and after the transition is strikingly different. Typical perturbations of the heat capacities of minerals by structural changes accompanying first-order and lambda transitions are depicted schematically in figure 1. The heat capacity curve in figure 1B is similar to that of β-brass, which exhibits a lambda transition caused by increasing long-range disorder with increasing temperature.

The nature of a phase transition cannot always be deduced unambiguously from the behavior of the heat capacity of a mineral with increasing temperature. In some cases measurements of the heat capacities of minerals as a function of temperature must be carried out in conjunction with annealing experiments to detect lambda transitions.

[2] All transitions other than first-order are referred to as lambda transitions to avoid theoretical implications inherent in the designations, second-order, third-order, et cetera (Denbigh, 1971).

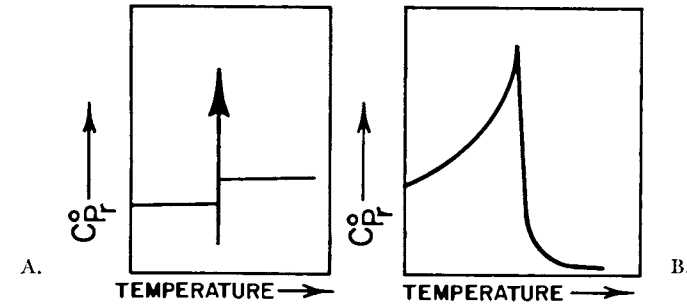

Fig. 1. Schematic illustration of the isobaric temperature dependence of the standard molal heat capacities of minerals undergoing first-order (diagram A) and lambda (diagram B) transitions at 1 bar.

For example, this is almost certainly true of displacive disorder in albite (see below). In other instances, changes in the partial derivatives of the enthalpies and Gibbs free energies of minerals undergoing lambda transitions may occur rapidly over a short temperature range, which also makes them difficult to document experimentally. Some minerals (such as chalcopyrite) apparently undergo both kinds of transitions superimposed on one another. Discontinuities in such cases are nearly impossible to detect without a differential scanning calorimeter or a continuous X-ray read-out as a function of temperature.

In general, first-order transitions in silicates at 1 bar are characterized by enthalpies, entropies, heat capacities, and volumes of transition of the order of 500 cal $mole^{-1}$, 0.5 cal $mole^{-1}$ $(°K)^{-1}$, 0.5 cal $mole^{-1}$ $(°K)^{-1}$, and 0.5 cm^3 $mole^{-1}$, respectively, or less. Comparable or even larger changes may occur in lambda transitions, but over a range of temperature which may be as small as a few degrees, or (as in the case of the alkali feldspars) extend over a thousand degrees. In the latter cases the term transition temperature is a misnomer designating the lambda point, which refers to the temperature at which the heat capacity curve reaches its peak (fig. 1B).

An example of a lambda transition exhibited by a mineral is shown in figure 2, where the standard molal heat capacity of nesquehonite is plotted as a function of temperature at 1 bar. It can be seen that the curve representing the heat capacity of nesquehonite exhibits a classic lambda configuration which has been documented by careful heat capacity measurements at closely spaced temperature intervals. Despite widespread application of the differential scanning calorimeter in recent years, changes in the heat capacities of most other minerals have not been investigated as thoroughly. In fact, even in the case of a mineral as common as quartz, ambiguities remain.

The thermodynamic properties of α and β-quartz are plotted in figure 3, where it is apparent that the data points corresponding to the open and solid circles are spaced too far apart to be definitive with respect to the nature of the entire transition. However, the large differ-

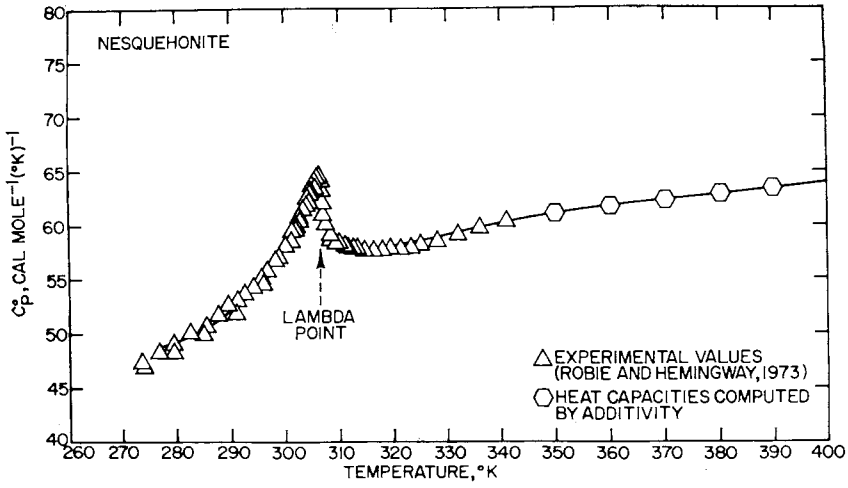

Fig. 2. Standard molal heat capacity of nesquehonite as a function of temperature at 1 bar. The curve was generated from eq (19) and the heat capacity coefficients for nesquehonite given in table 9.

ence in the slope of the heat capacity curve below 700° and that above 900°K, together with the heat capacity measurements obtained with a differential scanning calorimeter by O'Neill and Fyans (ms) strongly suggest that α-quartz goes through a lambda transition between ~700° and ~848°K. However, the possibility still exists (which has been debated extensively) that the lambda transition in this temperature interval is superimposed on a first order transition in the vicinity of 848°K. Although the curve representing the standard molal volume of quartz as a function of temperature in figure 3 suggests the presence of a discontinuity of ~848°K, the corresponding enthalpy and entropy curves are ambiguous in this regard.

In general, calculation of the Clapeyron slopes of univariant curves representing first-order solid/solid transitions requires highly accurate heat capacity and density data for the two polymorphs. Because the Clapeyron slopes of most such curves are essentially independent of pressure and temperature at pressures below ~10 kb, if we let $\mathbf{k} \equiv dP/dT$ for a given first-order transition of this kind and write the Clapeyron equation as

$$\mathbf{k} \equiv \left.\frac{dP}{dT}\right|_{\Delta G^\circ = 0} = \frac{\Delta S^\circ}{\Delta V^\circ} \tag{1}$$

it follows that

$$d(\Delta S^\circ) = \mathbf{k}\, d(\Delta V^\circ) \tag{2}$$

where $\mathbf{k}$ stands for the Clapeyron slope constant and ΔS°, ΔV°, and ΔG° refer to the standard molal entropy, volume, and Gibbs free energy of transition. Combining eq (2) with

$$d(\Delta S^\circ) = \left(\frac{\partial(\Delta S^\circ)}{\partial T}\right)_P dT + \left(\frac{\partial(\Delta S^\circ)}{\partial P}\right)_T dP \quad (3)$$

and

$$d(\Delta V^\circ) = \left(\frac{\partial(\Delta V^\circ)}{\partial T}\right)_P dT + \left(\frac{\partial(\Delta V^\circ)}{\partial P}\right)_T dP \quad (4)$$

together with

$$\left(\frac{\partial(\Delta S^\circ)}{\partial P}\right)_T = -\left(\frac{\partial(\Delta V^\circ)}{\partial T}\right)_P \quad (5)$$

and

$$\Delta C^\circ_P = T\left(\frac{\partial(\Delta S^\circ)}{\partial T}\right)_P \quad (6)$$

leads to

$$\Delta C^\circ_P = 2kT\left(\frac{\partial(\Delta V^\circ)}{\partial T}\right)_P + k^2T\left(\frac{\partial(\Delta V^\circ)}{\partial P}\right)_T \quad (7)$$

which describes the interdependence of the standard molal heat capacity, expansibility, and compressibility of transition if k is essentially independent of pressure and temperature. Note that eq (7) can be rearranged and (after completing the square) expressed as

$$k = \pm\left(\frac{\Delta C^\circ_P\left(\frac{\partial(\Delta V^\circ)}{\partial P}\right)_T + T\left(\frac{\partial(\Delta V^\circ)}{\partial T}\right)^2_P}{T\left(\frac{\partial(\Delta V^\circ)}{\partial P}\right)^2_T}\right)^{1/2} - \frac{\left(\frac{\partial(\Delta V^\circ)}{\partial T}\right)_P}{\left(\frac{\partial(\Delta V^\circ)}{\partial P}\right)_T} \quad (8)$$

Consideration of high-pressure/temperature phase equilibrium data indicates that the kyanite/andalusite transition temperature at 1 bar is ~ 466°K, and that the corresponding temperature for the andalusite/sillimanite transition is ~ 1043°K (see below). Evaluation of eq (1) for these two transitions with the aid of entropy, heat capacity, volume, and expansibility data taken from Stull and Prophet (1971), Robie and Waldbaum (1968), and Skinner (1966) yields $k = 12.8$ and $k = -5.1$ bar $(°K)^{-1}$, respectively. In the case of the kyanite/andalusite transition, the calculations yield a relatively large standard molal entropy and volume of transition at 466°K and 1 bar (2.28 cal mole^{-1} °K^{-1} and 7.47 cm^3 mole^{-1}, respectively) so the calculated value of k is relatively insensitive to small errors in the heat capacities and expansibilities used in the calculations. However, the opposite is true in the case of the andalusite/sillimanite transition, for which the calculated standard molal entropy and volume of transition are 0.28 cal mole^{-1} $(°K)^{-1}$ and −2.28 cm^3 mole^{-1}, respectively, at 1043°K and 1 bar. In the latter case the standard molal entropy of transition is smaller than the aggregate uncertainty in the entropy and heat capacity data used in the calculations. Accordingly, the calculated value of k for the andalusite/sillimanite transition is far less reliable that that computed for the kyanite/anda-

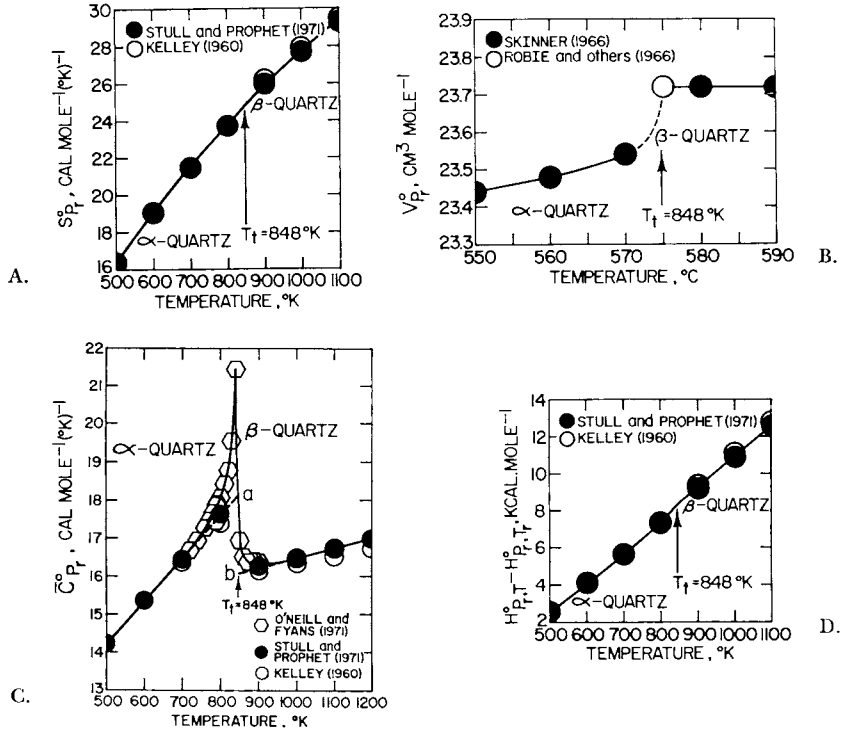

Fig. 3. Standard molal entropy, volume, heat capacity, and relative standard molal enthalpy of α and β-quartz as a function of temperature at 1 bar. Interval ab in diagram C corresponds to the apparent standard molal heat capacity of transition (see text).

lusite transition. In fact, the value of k and the standard molal entropy and volume of transitions computed above for the kyanite/andalusite transition are almost identical to those generated from high pressure/temperature phase equilibrium data assuming constant volumes of the polymorphs, but those for the andalusite/sillimanite transition are not (see below). The discrepancies in the latter case arise primarily from an error of only $\sim$ 0.2 cal mole^{-1} (°K)$^{-1}$ in the value of ΔS° computed above for the andalusite/sillimanite transition at 1043°K and 1 bar.

Because the standard molal entropies of most first-order solid/solid phase transitions are small, the angle at which the standard molal Gibbs free energy curves for the polymorphs intersect at the transition temperature is small. Consequently, large errors may result in calculated transition temperatures if highly accurate entropy and volume data are not available for the two polymorphs. In certain cases, such as the andalusite/sillimanite transition, the heat capacities of the two polymorphs must be known as a function of temperature to at least five significant figures to preclude unacceptable errors in calculated transition temperatures. Otherwise, the calculated temperatures may differ from the actual

temperatures of transition by more than several hundred degrees, *and the computed entropy and enthalpy of transition may have the wrong sign.*

In general, heat capacity, compressibility, and expansibility data for minerals are not sufficiently comprehensive, accurate, or precise to permit reliable calculation of k from eqs (1) or (8). The standard molal entropies and volumes of most first order transitions are not only small, but they may be sensitive functions of temperature and pressure. Nevertheless, experimentally determined univariant curves representing first-order transitions or isopleths of order/disorder for lambda transitions can be reproduced by assuming ΔS° and ΔV° to be constant at all pressures and temperatures corresponding to those along the univariant curves. Density data can then be used to calculate standard molal entropies of transition from the experimental values of k. Alternately, if calorimetric data are available at one bar, standard molal volumes of transition can be computed from experimental Clapeyron slopes. Note that the assumption of constant ΔS° along univariant curves requires the standard molal enthalpy of transition at a given pressure and temperature ($\Delta H^\circ_{P,T}$) to be proportional to the transition temperature (T_t) at all pressures, which can be expressed as

$$\Delta H^\circ_{P,T} = \Delta S^\circ_{P_r,T_t} T_{t,P} \tag{9}$$

where $\Delta S^\circ_{P_r,T_r}$ stands for the standard molal entropy of transition at the reference pressure of 1 bar (P_r). Although eq (9) is almost certainly not strictly true for solid/solid phase transitions, errors in $\Delta H^\circ_{P,T}$ arising from the assumption that the univariant transition curve is both isentropic and isochoric are probably negligible compared to other uncertainties involved in thermodynamic calculations of phase equilibria at high pressures and temperatures. Nevertheless, even if ΔS° and ΔV° of transition were actually independent of pressure and temperature, it does not follow that this assumption necessarily permits accurate values of k to be computed directly from volumetric and calorimetric data. If ΔS° and ΔV° of transition are constant, it follows from eqs (1) and (3) through (6) that

$$\Delta C^\circ_P = kT \left(\frac{\partial(\Delta V^\circ)}{\partial T}\right)_P = -k^2 T \left(\frac{\partial(\Delta V^\circ)}{\partial P}\right)_T , \tag{10}$$

$$\left(\frac{\partial(\Delta V^\circ)}{\partial P}\right)_T = -\frac{1}{k}\left(\frac{\partial(\Delta V^\circ)}{\partial T}\right)_P , \tag{11}$$

and

$$k = \frac{\Delta C^\circ_P}{T\left(\frac{\partial(\Delta V^\circ)}{\partial T}\right)_P} = -\frac{\left(\frac{\partial(\Delta V^\circ)}{\partial T}\right)_P}{\left(\frac{\partial(\Delta V^\circ)}{\partial P}\right)_T} . \tag{12}$$

The extent to which either eqs (8) or (12) represents a close approximation of reality is difficult to assess because the standard molal heat

capacities of first-order transitions are small and of the same order of magnitude as the uncertainties in the calorimetric data from which they are derived. For example, interpolation of heat capacity and expansibility data taken from Stull and Prophet (1971) and Skinner (1966) suggests $\Delta C^\circ_P = 0.09$ cal mole^{-1} (°K)$^{-1}$ and $(\partial(\Delta V^\circ)/\partial T)_P = 4.2 \times 10^{-4}$ cm^3 mole^{-1} (°K)$^{-1}$ for the kyanite/andalusite transition at 1 bar. These values lead to $\mathbf{k} = 19.2$ bar (°K)$^{-1}$ from eq (12). This Clapeyron slope is too large to satisfy high-pressure/temperature data, which require $\mathbf{k} \approx 12.6$ bar (°K)$^{-1}$ (see below). However, the calorimetric ΔC°_P of transition is subject to large enough uncertainties that it may well be in error by the small amount required to make the computed value of $\mathbf{k}$ consistent with the high-pressure/temperature data.

In general, power function coefficients taken from the literature for equations describing the heat capacity of a given polymorph as a function of temperature at 1 bar cannot be used with confidence for temperatures outside the range of the calorimetric measurements. Reliable extrapolations to higher temperatures can be made with such coefficients only if the calorimetric measurements from which they were derived extend well above the "knee" in the curve representing the heat capacity of the mineral as a function of temperature (see below). It should also be emphasized that few of these coefficients are valid for temperatures in the range where a lambda transition takes place. Nevertheless, regardless of whether a given phase undergoes a first-order or lambda transition, if the standard molal enthalpy relative to that at 298.15°K is known as a function of temperature both above and below the temperature (or temperatures) of transition, accurate values of the standard molal entropies and heat capacities of the polymorphs can be computed at higher and lower temperatures. For example, in the case of the superimposed lambda and first order transition represented schematically in figure 4, the standard molal heat capacity at point *b* can be computed from the value at point *a* by taking account of the *apparent* standard molal heat capacity of transition. The apparent standard molal heat capacity of transition corresponds to the difference in the heat capacities obtained by extrapolation of the heat capacity curves for the high and low-temperature polymorphs to the transition temperature or lambda point. Apparent standard molal enthalpies, entropies, and volumes of transition are defined similarly. By taking account of these apparent changes, values of the thermodynamic properties of high-temperature polymorphs can be computed for temperatures above that corresponding to point *b* in figure 4 if the standard molal thermodynamic properties of the low-temperature phase at 25°C and 1 bar are known and heat capacity power function coefficients for the two polymorphs are available for temperatures above and below the interval represented by *ab* in figure 4. For temperatures in the interval *ab*, the calculations generate errors in the standard molal enthalpy of the phase equal to the area between the dashed and solid curves, which is relatively slight for lambda

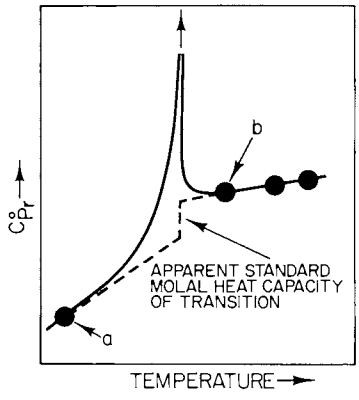

Fig. 4. Schematic illustration of the apparent standard molal heat capacity of transition for a hypothetical superimposed lambda and first-order transition at 1 bar (see text).

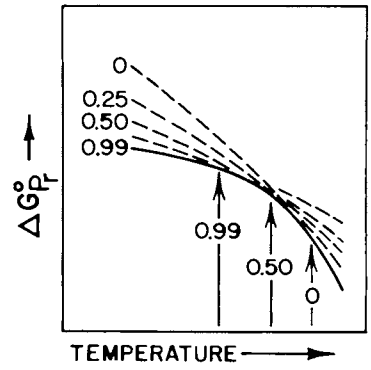

Fig. 5. Schematic illustration of the temperature dependence of the apparent standard molal Gibbs free energy of formation of a phase undergoing a "smeared" lambda transition at 1 bar (see text). The solid curve corresponds to the stable phase and the dashed curves to metastable states of constant order designated by values shown for the ordering parameter, which varies from 1 (complete order) to zero (complete disorder) with increasing temperature.

transitions only if the mineral disorders over a narrow temperature range. In the case of first-order transitions, the apparent and actual properties of transition are coincident, and the error reduces to zero.

Lambda phase transitions which are "smeared out" over a wide temperature interval pose a more difficult problem in thermodynamic calculations than those that occur over a narrow temperature range. Smeared transitions are exhibited by dolomite, albite, epidote, monoclinic potassium feldspar, and other abundant minerals in the Earth's crust (see below). Accurate calculation of the thermodynamic properties of these minerals requires explicit provision for changes in the thermodynamic consequences of substitutional order/disorder with increasing temperature. In contrast to the structural disorder contributing to the thermodynamic behavior of α-quartz between ~700° and 848°K, lambda transitions in many complex silicates are caused by changes in site occupancy with increasing temperature. Although continuous, these changes in substitutional order/disorder are nonlinear functions of temperature which have not been characterized adequately for most minerals.

Substitutional order/disorder.—Although differential site occupancy in minerals is a function of temperature, pressure, and composition, the effect of intracrystalline exchange on the thermodynamic behavior of minerals depends on the extent to which order/disorder is coupled to changes in composition. If more than one kind of atom occurs in either tetrahedral or octahedral coordination in a silicate, substitutional disorder may occur on one or both types of sites, and it may or may not

involve the same atoms responsible for compositional variation in the mineral. For example, as a consequence of the comparable temperature dependence of the Z ordering parameters for albite and K-feldspar (see below), compositional variation resulting from exchange of Na^+ and K^+ among alkali feldspars may occur with little or no accompanying changes in order among Al and Si on the T_1 and T_2 tetrahedral sites. In contrast, substitution of Na for Ca in the plagioclase lattice is coupled through aluminum avoidance and charge balance requirements to disordered substitution of Si for Al on the tetrahedral sites. Changes in order/disorder thus invariably accompany compositional variation in plagioclase solid solutions but not in alkali feldspars. In other cases, such as the orthopyroxenes, substitutional order/disorder affects the thermodynamic behavior of minerals only as a consequence of compositional variation.

The distribution of atoms among energetically nonequivalent sites in minerals is thermodynamically analogous to the association of species to form complexes in an aqueous electrolyte solution. Equilibrium among complexes and dissociated species in an aqueous solution can be described in terms of dissociation constants, which vary with temperature and pressure. The dissociation constants determine (together with activity coefficients) the extent to which various complexes form in a solution of a given composition. Of all the possible configurations that could be taken by the ions in an aqueous electrolyte solution, the distribution of species actually present is the one that contributes to the lowest Gibbs free energy of the system at a given temperature and pressure. Similarly, the distribution of atoms among energetically nonequivalent sites in a stable mineral corresponds to the configuration contributing to the lowest Gibbs free energy of the mineral. However, in contrast to their aqueous counterparts, complexes in crystals are subject to site constraints. Nevertheless, the equilibrium distribution of atoms among different sites in a crystal can be described in terms of distribution constants, which are analogous to dissociation constants for aqueous species. Site occupancy determines the magnitude of long-range ordering parameters, which are related to distribution constants by the law of mass action for intracrystalline exchange reactions.

The thermodynamic consequences of substitutional order/disorder in a mineral of a given composition depend on the complexity and geometry of its crystal structure, the bond angles and energies of attraction among the atoms on the lattice sites, and other crystallochemical and configurational constraints contributing to energetic differences in otherwise comparable lattice positions. Many investigations of interchange energies and changes in the thermodynamic properties of minerals caused by substitutional order/disorder have been carried out in recent years (for example, Mueller, 1962; Matsui and Banno, 1965; Thompson, J. B., 1967, 1969, 1970; Grover and Orville, 1969; Blander, 1970, 1972; Chelischev and Borutskaya, 1972; Saxena, 1969, 1973; Saxena

and Ghose, 1971; Wood and Banno, 1973; Thompson, Waldbaum, and Hovis, 1974; Hovis, 1974; Kerrick and Darken, 1975; Powell, 1977), but most of these are not definitive with respect to the temperature dependence of the thermodynamic properties of minerals that exhibit substitutional order/disorder. Hovis' (1974) and Thompson, Waldbaum, and Hovis' (1974) recent studies are outstanding exceptions. For example, Hovis' calorimetric measurements of the heats of solution of eleven monoclinic K-feldspars of different order (determined from their unit cell dimensions) in 20.1 percent hydrofluoric acid at 49.7°C indicate a difference in the standard molal enthalpy of formation of perfectly ordered and completely disordered K-feldspars of 2650 cal $mole^{-1}$. The standard molal volumes of the feldspars exhibited a corresponding difference of 0.268 cm^3 $mole^{-1}$, and Hovis estimated the difference in the standard molal third law entropy of completely ordered and disordered feldspar to be 3.7 ± 0.3 cal $mole^{-1}$ $(°K)^{-1}$. Variation of the long-range ordering parameter in monoclinic potassium feldspar with temperature and pressure may thus account for more than 2 kcal $mole^{-1}$ in the standard molal Gibbs free energy of the mineral. Although the standard molal enthalpies of both sodium and potassium feldspar apparently exhibit a linear dependence on the long-range ordering parameter (see below), the ordering parameter itself is a nonlinear function of temperature. In contrast, the Bragg-Williams theory of order/disorder (Bragg and Williams, 1934, 1935) requires a nonlinear relation between the standard molal enthalpy of disorder and the ordering parameter. Nevertheless, both functions lead to a dependence of Gibbs free energy on temperature similar to that depicted schematically in figure 5. The solid curve in figure 5 represents the stable ordering state, and the numbers indicate the degree of order.

Vacancy defects.—Few minerals occur in nature without crystallochemical imperfections and inhomogeneities such as Schottky and Frenkel defects, edge and screw dislocations, stacking faults, twin boundaries, domain structures, and sector zoning. All these contribute to the thermodynamic behavior of minerals, both in the laboratory and in geochemical processes. Imperfections in crystal structure occur on all scales from electronic lattice defects caused by local excesses and deficiencies of electrons to macroimperfections in stacking order.

Because the atoms on the lattice sites of a crystal are not stationary but vibrate about an equilibrium position, thermal perturbations in their vibration frequencies cause certain of the atoms to escape from their lattice sites, either to vacant neighboring lattice sites or interstitial space. If this phenomenon occurs on the surface of the crystal, the atom may escape and contribute to the vapor pressure of the mineral. Once atoms escape from the surface of a crystal, point defects are formed that migrate through the crystal as other atoms "jump" into vacant neighboring sites. In a first approximation, the fraction of lattice sites corresponding to

point defects ($\hat{f}_v$) formed by thermal diffusion in a simple crystal can be expressed as

$$\ln \hat{f}_v = \frac{-\Delta G^\circ_v}{kT} \tag{13}$$

where ΔG°_v refers to the standard Gibbs free energy of formation of a single vacancy and k stands for Boltzmann's constant. Eq (13) is an expression of the law of mass action for reversible formation of an ideal defect. As expected, the higher the temperature, the more defects form in a crystal (and the higher the vapor pressure of the mineral).

The energy requirements for point defect formation in simple compounds can be computed from lattice models and elastic constants. Such calculations by Holder and Granato (1969) indicate values of ΔG°_v of the order of an electron volt, or approx 3.8×10^{-20} calories, which is in general agreement with calculations of the energy required to form Schottky defects in simple ionic crystals reported by Rittner, Hutner, and du Pré (1949a and b). Substituting this figure for ΔG°_v in eq (13) along with $k = 3.2995 \times 10^{-24}$ cal $(°K)^{-1}$ yields $\hat{f}_v = 1.0 \times 10^{-5}$ for 1000°K and $\hat{f}_v = 3.2 \times 10^{-3}$ for 2000°K. The higher temperature value compares favorably with experimental density measurements for metals, which commonly exhibit defect concentrations of the order of 0.02 volume percent.

Although vacancy defect concentrations and the Gibbs free energies of point defect formation in simple compounds are hardly representative of minerals in general, we can make a conservative estimate of the order of magnitude of the contribution of vacancy defect formation to the Gibbs free energies of formation of silicates by assuming a minimum defect concentration of 0.02 volume percent, a representative molal volume of 100 cm^3 $mole^{-1}$, and a value of ΔG°_v approximately equal to that in metals (that is, 3.8×10^{-20} calories $defect^{-1}$). These figures indicate that a kcal $(mole\ of\ mineral)^{-1}$ is required to form 0.02 volume percent of 1-angstrom vacancies. Although this calculation is highly approximate, it does reveal that point defects arising from thermal diffusion in crystals may contribute significantly to the thermodynamic properties of silicates.

Vacancy defects are also functions of chemical potential gradients in crystals, which may be controlled by chemical reactions of minerals with their environment. In a geologic context, the thermodynamic consequences of point defect formation in response to chemical potential gradients may be greater than those computed above for vacancy defects caused by thermal diffusion. Experimental studies of diffusion rates of Na^+, K^+, and Rb^+ in single crystals of alkali feldspar by Petrovic (1974) and Foland (1974) indicate diffusion coefficients of the order of 10^{-10} to 10^{-13} cm^2 sec^{-1} at 800°C with activation energies ranging from 53 to 72 kcal $(g\ atom)^{-1}$. The experimental data also suggest that alkali cation diffusion in feldspars may be anisotropic and involve Frenkel defects.

In general, solid state diffusion is too slow (even in the context of geologic time) to permit significant intracrystalline mass transfer and vacancy migration much below 500°C. At higher temperatures, the experimental data indicate that defect formation in response to thermal diffusion, chemical potential gradients, and/or nonhydrostatic stress may contribute significantly to the thermodynamic properties of minerals in geologic systems.

Dislocations.—As might be expected, the energy per unit atomic length required to form a dislocation in a crystal is larger than, but comparable to the energy of formation of point defects. For example, Holder and Granato (1969) report energies of formation for screw and edge dislocations in metals and simple compounds of the order of 1 to 22 electron volts (unit atomic length)$^{-1}$. Their calculations, which are based on elastic theory, compare favorably with experimental measurements on highly deformed materials. Dislocation densities in crystals range from 10^4 dislocations cm^{-2} in near-perfect crystals to 10^{12} dislocations cm^{-2} in crystals that have undergone intense plastic deformation. If we assume Holder and Granato's (1969) value for the energy required to form an edge dislocation in MgO (18.3 electron volts or 6.95×10^{-19} cal (unit atomic length)$^{-1}$) and a dislocation density of 10^{12} dislocations cm^{-2}, it follows that formation of edge dislocations in a one cubic millimeter crystal of plastically deformed periclase may increase its Gibbs free energy of formation by as much as ten calories, *which is equivalent to 11.2 kcal (mole MgO)$^{-1}$*. This calculation leaves little doubt that dislocation energies may affect substantially the stabilities of minerals in geologic processes, especially those involving deformation, radiation, and/or rapid cooling. All these processes favor the persistence of metastable phases in deformed rocks and oppose the effects of annealing, which reduces dislocation densities and promotes achievement of stable equilibrium.

It seems highly probable that differences in the thermodynamic properties of synthetic and natural minerals having the same composition and crystallinity arise primarily from differences in the dislocation densities of the samples. Both calorimetric and phase equilibrium studies indicate that the standard molal Gibbs free energies of formation of synthetic minerals produced over short time periods in laboratory experiments may be several kcal mole^{-1} less negative than those of their natural counterparts. For example, equilibrium temperatures for the reaction shown in figure 41 may vary by as much as 120°C, depending on the sample of stoichiometric synthetic or natural tremolite used in the experiments (G. B. Skippen, 1978, personal commun.). Because the standard molal entropy of the reaction represented by the curve in figure 41 is $\sim$ 18 cal mole^{-1} (°K)$^{-1}$ at high temperatures and pressures, this variation corresponds to a difference of $\sim$ 2.2 kcal mole^{-1} in the standard molal Gibbs free energies of formation of stoichiometric synthetic and natural tremolite.

Crystallinity and particle size.—Because the surface area (and therefore the total surface energy) of the grains in a mole of a cryptocrystal-

line mineral is greater than that of its coarsely crystalline counterpart, fine-grained aggregates of minerals constitute metastable phases. A grain boundary can be thought of as a continuum of dislocations with a Gibbs free energy of formation comparable to that of multiple edge dislocations. Experimental solubility measurements suggest that differences in both particle size and the crystallinities of various specimens of a mineral formed in different environments under identical pressure/temperature conditions may be accompanied by differences of as much as several kilocalories mole^{-1} in their Gibbs free energies of formation (Frink and Peech, 1962; Kittrick, 1966a and b, 1970). Large variations in crystallinity and Gibbs free energy commonly occur in clay minerals such as gibbsite, kaolinite, montmorillonite, et cetera.

Cryptocrystalline minerals, like highly disordered phases, commonly form metastably under conditions of rapid precipitation. In extreme cases, the precipitated phase is amorphous. Upon "aging" or annealing, metastable cryptocrystalline or amorphous minerals recrystallize to their more stable configurations. Although decreasing crystallinity should be accompanied by increasing solubility relative to the more crystalline form of a mineral, this is not always observed. For example, fine grained "massive" NaCl–KCl–$CaCl_2$ salt precipitated from a supersaturated solution and allowed to "age" is slow to dissolve upon subsequent exposure to pure H_2O. Owing to tight packing of the grains and the small exposed surface area, the rate of dissolution is so slight that the salt appears insoluble. However, fine-grinding the massive cryptocrystalline salt restores its ability to reach equilibrium with its environment in a matter of hours. *This observation underscores the importance of recognizing the distinction between crystallinity and particle size in experimental studies of the thermodynamic behavior of minerals.*

Particle size (or more precisely, surface area) has been demonstrated to have a substantial effect (up to 5 kcal mole^{-1}) on the heats of solution of 2α-FeOOH and α-Fe_2O_3 (Ferrier, 1966; Langmuir, 1971a) and (to a much lesser extent) on that of α-quartz (Hemingway and Robie, 1977a). However, to our knowledge comparable studies of the effect of different crystallinities on the heats of solution of samples of the same particle size have not been carried out. Nevertheless, it appears that the contribution of the interfacial energy of the grains in a cryptocrystalline mineral to its thermodynamic behavior is comparable to that of the surface energy of fine particles of the mineral.

As the effects of the crystallochemical and physical properties of minerals on their thermodynamic behavior become better quantified, it will no doubt become advantageous to include explicit physical specifications (such as perfect, completely ordered, single crystals with a given morphology and surface area) in the definition of the standard state, rather than relying on the simple but ambiguous stipulation that the mineral be "in its stable form." Thermodynamic changes caused by crystallochemical departures from the standard state could then be described quantitatively in terms of variables analogous to activity co-

efficients. Although sufficient data are not yet available to permit general application of such an approach, a step in this direction has been made by Mueller (1962), Thompson (1969), and others who describe the thermodynamic consequences of differential site occupancy in feldspars in terms of long-range ordering parameters.

SUMMARY OF THERMODYNAMIC RELATIONS

As indicated above, the standard state for minerals adopted in the present study is one in which the activities of the components of pure (stoichiometric) minerals are unity at any pressure and temperature.[3] Because this standard state is unrestricted with respect to pressure and temperature, the *apparent* standard molal Gibbs free energy and enthalpy of formation of a mineral from its elements at a given pressure and temperature ($\Delta G^\circ_{P,T}$ and $\Delta H^\circ_{P,T}$, respectively) can be expressed as[4]

$$\Delta G^\circ_{P,T} \equiv \Delta G^\circ_f + (G^\circ_{P,T} - G^\circ_{P_r,T_r}) \tag{14}$$

and

$$\Delta H^\circ_{P,T} \equiv \Delta H^\circ_f + (H^\circ_{P,T} - H^\circ_{P_r,T_r}) \tag{15}$$

where

$$G^\circ_{P,T} - G^\circ_{P_r,T_r} = -S^\circ_{P_r,T_r}(T - T_r) + \int_{T_r}^{T} C^\circ_{P_r} dT - T\int_{T_r}^{T} C^\circ_{P_r} d\ln T + \int_{P_r}^{P} V^\circ_T dP \tag{16}$$

and

$$H^\circ_{P,T} - H^\circ_{P_r,T_r} = \int_{T_r}^{T} C^\circ_{P_r} dT + \int_{P_r}^{P}\left(V^\circ - T\left(\frac{\partial V^\circ}{\partial T}\right)_P\right)_T dP \tag{17}$$

where T refers to temperature in °K and P to pressure in bars, ΔG°_f and ΔH°_f designate the standard molal Gibbs free energy and enthalpy of formation of the mineral from its elements in their stable form

[3] The term component is used in this communication in its strict thermodynamic sense. A thermodynamic component of a mineral corresponds to a chemical formula unit representing one of the minimum number of independent variables required to describe the composition of the mineral. All stoichiometric minerals are thus composed of a single component corresponding to the formula of the mineral. However, because the term component has no physical connotation, the minerals themselves are *not* components.

[4] Use of the word apparent in referring to $\Delta G^\circ_{P,T}$ (and its enthalpy analog, $\Delta H^\circ_{P,T}$) was suggested by Benson (1968) to preclude confusion with corresponding standard molal properties of formation from the elements at high pressures and temperatures, such as those tabulated by Robie and Waldbaum (1968). The latter properties include provision for changes in the standard molal Gibbs free energies and enthalpies of the elements with increasing pressure and temperature, which cancel in computing the thermodynamic properties of chemical reactions.

at 298.15°K (T_r) and 1 bar (P_r), and $G°_{P,T}$, $G°_{P_r,T_r}$, $H°_{P,T}$, $H°_{P_r,T_r}$, $S°_{P_r,T_r}$, $C°_{P_r}$, and $V°_T$ represent the standard molal Gibbs free energy, enthalpy, entropy, heat capacity, and volume of the mineral at the subscripted pressures and temperatures. The corresponding expression for the standard molal entropy of a mineral at a given pressure and temperature ($S°_{P,T}$) is given by

$$S°_{P,T} - S°_{P_r,T_r} = \int_{T_r}^{T} C°_{P_r} d\ ln\ T - T \int_{P_r}^{P} \left(\left(\frac{\partial V°}{\partial T} \right)_P \right)_T dP \tag{18}$$

Standard molal heat capacities of minerals at 1 bar.—Experimental standard molal heat capacities of minerals at 1 bar and temperatures $\geqslant$ 298.15°K can be represented closely by the Maier-Kelley (1932) power function, which can be written as

$$C°_{P_r} = a + b\ T - c\ T^{-2} \tag{19}$$

and integrated to give

$$\int_{T_r}^{T} C°_{P_r} dT = a\ (T - T_r) + \frac{b\ (T^2 - T_r^2)}{2} + c \left(\frac{1}{T} - \frac{1}{T_r} \right) \tag{20}$$

and

$$\int_{T_r}^{T} C°_{P_r} d\ ln\ T = a\ ln\ (T/T_r) + b\ (T - T_r) + \frac{c}{2} \left(\frac{1}{T^2} - \frac{1}{T_r^2} \right) \tag{21}$$

where a, b, and c stand for temperature-independent coefficients characteristic of the mineral. Except for minerals with high Debye temperatures, eq (19) yields fits of experimental heat capacities at temperatures $>$ 298.15°K to within ~0.1 cal mole^{-1} (°K)$^{-1}$ or less. The maximum fit residuals occur in the vicinity of the "knee" in the heat capacity curve, which is more pronounced and occurs at higher temperatures for minerals with high Debye temperatures. For example, it can be seen in figure 6 that the curvature of the heat capacity curve for periclase is considerably greater than that for α-quartz.

Although errors resulting from fits of eq (19) to experimental high-temperature heat capacities of minerals with high Debye temperatures may exceed 0.1 or even 1 cal mole^{-1} (°K)$^{-1}$, such large discrepancies are rare. As emphasized by Kelley (1960), a single algebraic function capable of fitting the heat capacities of all minerals equally well would contain a large number of terms, many of which would be redundant for many substances. Nevertheless, it is highly desirable from a computational point of view to have such a function. Eq (19) represents a compromise in this respect. It sacrifices a small degree of accuracy in the case of

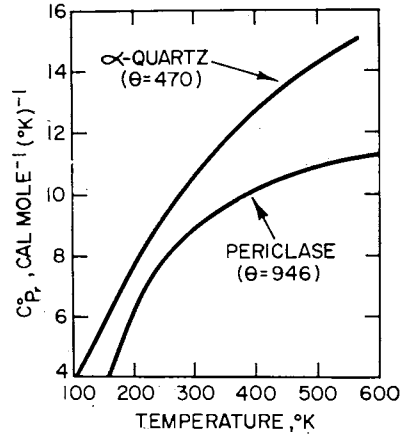

Fig. 6. Standard molal heat capacity of α-quartz and periclase as a function of temperature at 1 bar (Kelley, 1960). The symbol θ designates the Debye temperatures of the minerals.

compounds with relatively high Debye temperatures for simplicity and generality but still affords close approximation of the heat capacities of most minerals. As a rule, the inconvenience of using diverse and more complicated power functions such as those employed by Haas and Fisher (1976), Krupka, Kerrick, and Robie (1977), and others is not warranted by the corresponding improvement in accuracy.

In most cases, errors introduced by representing the standard molal heat capacities of minerals with eq (19) tend to cancel in calculating the thermodynamic properties of reactions. Even in cases where estimated coefficients are used (see below), eq (19) usually leads to significantly more accurate standard molal entropies of reaction at high temperatures than assuming the difference in the sums of the standard molal heat capacities of formation from the elements of the product and reactant minerals (multiplied by their absolute reaction coefficients) to be zero, which (if calorimetric heat capacities are not available) is the approach advocated by Fisher and Zen (1971), Zen and Chernosky (1976), and others.

Standard molal volumes of minerals.—In general, $(\partial V^\circ/\partial P)_T$ and $(\partial V^\circ/\partial T)_P$ for minerals can be regarded as zero without introducing undue uncertainty in thermodynamic calculations of mineral stabilities at pressures and temperatures corresponding to those in the crust of the Earth. It can be seen in figures 7 and 8 that (with the exception of quartz) thermal expansion and compression of minerals cause opposing changes in V° of the order of 3 percent or less at temperatures $< 800°$ to 1200°C at 1 bar and pressures $<$ 20 to 40 kb at 25°C. In contrast, the standard molal volume of α-quartz increases by more than 3 percent as temperature increases to 575°C at 1 bar and decreases by $\sim$ 3 percent as pressure increases to $\sim$ 12 kb. With a few exceptions such as α-quartz,

the compressibilities of silicates at 25°C are of the order of 1 percent or less at pressures < 10 kb.

Few compressibility data are available for minerals at high temperatures, but those reported by Spetzler (1970) and Spetzler, Sammis, and O'Connell (1972) for MgO and NaCl, together with lattice model calculations for NaCl reported by Demarest (1972) suggest that the isothermal bulk modulus of simple compounds may decrease by as much as an order of magnitude as temperature increases to ~1000°C. Although NaCl is hardly representative of minerals in general, it seems reasonable to conclude from these observations that the effects of thermal expansion on the standard molal volumes of minerals are essentially offset by the effects of compressibility at pressures and temperatures in the vicinity of 5 to 10 kb and 500° to 1000°C. For this reason, and because compressibilities decrease with increasing pressure, calculation of the thermodynamic properties of reactions involving a gas or fluid phase at high pressures and temperatures assuming $V°_{P,T}$ to be equal to $V°_{1\ bar,\ 298.15°K}$ for the minerals in the reaction probably leads to negligible errors, even in many cases for pressures as high as 50 to 100 kb (Delany and Helgeson, 1978). In contrast, because $\Delta S°_r$ and $\Delta V°_r$ are commonly small for reactions involving only solids, the compressibilities and expansibilities of minerals may have a dominant effect on the thermodynamic properties of solid/solid reactions at high pressures and temperatures.

If we assume an average thermal expansion of 3×10^{-3} cm^3 (°K)$^{-1}$ at 1 bar on the basis of the curves shown in figure 7 and take the average high-temperature compressibility to be 5×10^{-4} cm^3 bar^{-1} (which seems reasonable in the light of available experimental data), compensation of the effects of compressibility and thermal expansion would cause the standard molal volume of a mineral at 2 kb and ~ 300°C, 4 kb and 600°C, and 6 kb and 900°C to be the same as its value at 25°C and 1 bar. The assumption of constant volume equal to $V°_{P_r,T_r}$ would thus

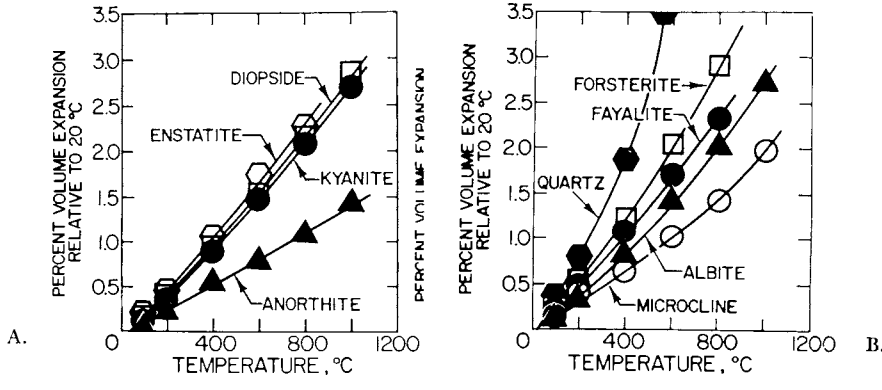

Fig. 7. Expansibility of minerals as a function of temperature at 1 bar. The symbols represent experimental data reported by Skinner (1966).

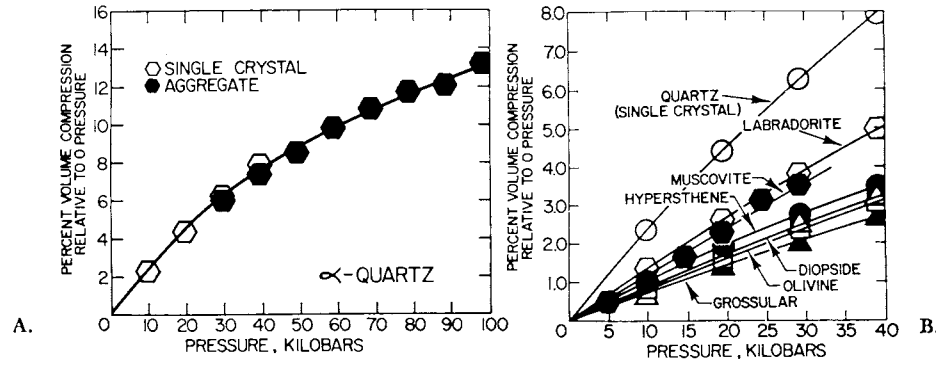

Fig. 8. Compressibility of minerals as a function of pressure at 25°C. The symbols represent experimental data reported by Bridgman (1948a and b, 1949).

introduce only slight errors in calculated values of $\Delta G^\circ_{P,T}$ at these temperatures and pressures (~ 25, 50, and 75 cal mole^{-1}, respectively). For the representative thermal expansion and compressibility adopted above, these are the largest absolute errors that result from constant volume calculations for minerals at pressures < 6 kb at 300°C, 12 kb at 600°C, and 16 kb at 900°C. Because thermal expansion decreases dramatically with increasing pressure (Skinner, 1966), the maximum error in $S^\circ_{P,T}$ caused by the constant volume assumption is < 0.24 cal mole^{-1} (°K)$^{-1}$ at pressures < 10 kb. Owing to the opposing effect of ΔV° and $(\partial(\Delta V^\circ)/\partial T)_P$ on the standard molal enthalpies of minerals as a function of pressure, errors in $\Delta H^\circ_{P,T}$ caused by the constant volume assumption should be smaller than coresponding errors in $\Delta G^\circ_{P,T}$ at pressures $\lesssim$ 10 kb.

Although uncertainties in $\Delta H^\circ_{P,T}$ and $\Delta G^\circ_{P,T}$ of the order of 75 cal mole^{-1} and errors in $S^\circ_{P,T}$ of ~ 0.25 cal mole^{-1} (°K)$^{-1}$ may affect significantly calculated equilibrium temperatures for solid/solid phase transitions (see above), for most dehydration/decarbonation equilibria, the assumption of constant mineral volumes has a negligible effect on calculated equilibrium temperatures. The standard molal entropies of such reactions are of the order of 20 cal mole^{-1} (°K)$^{-1}$ or more, which means that a relative uncertainty of 75 cal mole^{-1} in $\Delta H^\circ_{P,T}$ for a given mineral introduces only 5°C or less uncertainty in calculated equilibrium temperatures (see below). This calculation takes no account of the fact that errors introduced by the assumption of constant volume for minerals tend to cancel in calculation of the thermodynamic properties of reactions, which reduces considerably relative uncertainties in values of the standard molal Gibbs free energies of formation of minerals computed from high pressure/temperature data.

Near-cancellation of $(\partial(\Delta V^\circ)/\partial P)_T$ and $(\partial(\Delta V^\circ)/\partial T)_P$, respectively, for the reactant and product minerals in a given reaction would be expected on theoretical grounds but can be demonstrated only for re-

actions involving minerals for which highly accurate elastic constant data are available. Cancellation of the effects of these variables on the thermodynamic properties of reactions may occur even in the case of dehydration/decarbonation equilibria. For example, expansibility and volume data taken from Cameron and others (1973), Sueno and others (1973), Skinner (1966), and Robie and Waldbaum (1968) for the minerals in the reaction,

$$\text{tremolite} \rightleftharpoons 2 \text{ diopside} + 3 \text{ enstatite} + \text{quartz} + H_2O \qquad (22)$$

indicate that the sum of $(\partial(\Delta V^\circ)/\partial T)_P$ for 2 diopside + 3 enstatite + α-quartz is approximately equal to $(\partial(V^\circ)/\partial T)_P$ of tremolite (9.6×10^{-3} cm^3 mole^{-1} (°K)$^{-1}$) at $\sim$ 550°C and 1 bar. At other pressures and temperatures the difference is finite but certainly negligible compared to $(\partial(V^\circ)/\partial T)_P$ of H_2O.

Retrieval equations.—Assuming the standard molal volumes of minerals to be independent of pressure and temperature leads to

$$\int_{P_r}^{P} V^\circ_T \, dP = V^\circ_{P_r,T_r} (P - P_r) \qquad (23)$$

which can be combined with eqs (16), (17), (18), (20), (21), and the approximation

$$\left(\frac{\partial V^\circ}{\partial T}\right)_P = 0 \qquad (24)$$

for minerals to give

$$G^\circ_{P,T} - G^\circ_{P_r,T_r} = -S^\circ_{P_r,T_r}(T - T_r) + a(T - T_r - T \ln (T/T_r)) + \frac{(c - bTT_r^2)(T - T_r)^2}{2TT_r^2} + V^\circ_{P_r,T_r}(P - P_r) \qquad (25)$$

$$H^\circ_{P,T} - H^\circ_{P_r,T_r} = a(T - T_r) + \frac{b}{2}(T^2 - T_r^2) + c\left(\frac{1}{T} - \frac{1}{T_r}\right) + V^\circ_{P_r,T_r}(P - P_r), \qquad (26)$$

and

$$S^\circ_{P,T} - S^\circ_{P_r,T_r} = a \ln (T/T_r) + b(T - T_r) + \frac{c}{2}\left(\frac{1}{T^2} - \frac{1}{T_r^2}\right) \qquad (27)$$

Eqs (14) and (25) permit calculation of ΔG°_f for minerals from values of $V^\circ_{P_r,T_r}$, $S^\circ_{P_r,T_r}$ and heat capacity power function coefficients using equations of state and thermodynamic data for aqueous and gaseous

species to evaluate experimental standard molal Gibbs free energies of reaction (ΔG°_r) at high pressures and temperatures. However, the approach used to calculate the requisite values of ΔG°_r from high pressure/temperature experimental data depends on the type of reaction being considered.

Taking account of eq (14), the standard molal Gibbs free energy of a reaction at a given pressure and temperature ($\Delta G^\circ_{r,P,T}$) can be expressed as

$$\Delta G^\circ_{r,P,T} = \sum_l \hat{n}_l \, \Delta G^\circ_{l,P,T} = \sum_l \hat{n}_l \, (\Delta G^\circ_{f,l} + (G^\circ_{l,P,T} - G^\circ_{l,P_r,T_r})) = -RT \, ln \, K_{P,T} \tag{28}$$

where $\hat{n}_l$ stands for the stoichiometric coefficient of the lth species ($l = 1, 2, \ldots \hat{l}$) in the reaction (which is positive for products and negative for reactants), and $K_{P,T}$ refers to the equilibrium constant for the reaction at the subscripted pressure and temperature. The equilibrium constant is related to composition by

$$\prod_l a_l^{\hat{n}_l} = K_{P,T} \tag{29}$$

where $a_{l,P,T}$ denotes the activity of the lth species at the pressure and temperature of interest.

For $\hat{r}$ independent reactions involving $\hat{\imath}$ species for which values of $\Delta G^\circ_{f,i}$ are unknown ($i = 1, 2, \ldots \hat{\imath}$) and $\hat{\jmath}$ species for which values of $\Delta G^\circ_{f,j}$ are known ($j = 1, 2, \ldots \hat{\jmath}$), it follows from eq (28) for $\hat{l} = \hat{\imath} + \hat{\jmath}$ that we can write

$$\sum_r^{\hat{r}} \sum_i^{\hat{\imath}} \hat{n}_{i,r} \, \Delta G^\circ_{f,i} = \sum_r^{\hat{r}} \sigma^\circ_{r,P,T} \tag{30}$$

where

$$\sigma^\circ_{r,P,T} \equiv \Delta G^\circ_{r,P,T} - \sum_j^{\hat{\jmath}} \hat{n}_{j,r} \, \Delta G^\circ_{j,P,T} - \sum_i^{\hat{\imath}} \hat{n}_i \, (G^\circ_{i,P,T} - G^\circ_{i,P_r,T_r}) \tag{31}$$

where $\Delta G^\circ_{j,P,T}$ refers to the apparent standard molal Gibbs free energy of formation of the jth species (eq 14) and $\Delta G^\circ_{r,P,T}$ to the standard molal Gibbs free energy of the rth reaction at the subscripted pressure and

temperature. Eq (30) can be expressed as a linear matrix equation of the form

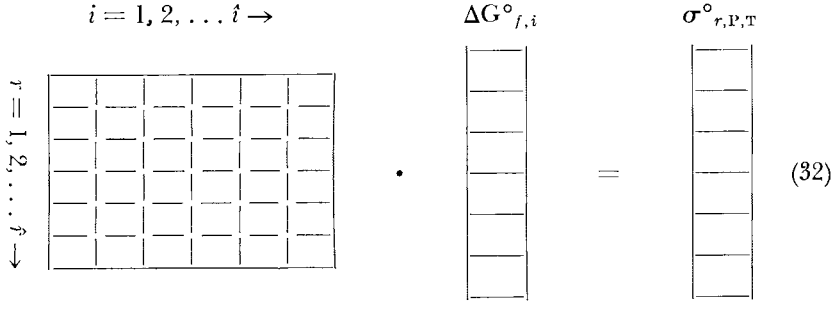

(32)

which can be represented by

$$\beta = \Gamma^{-1} \lambda \tag{33}$$

where β refers to the column vector of unknown values of $\Delta G^\circ_{f,i,r}$, Γ denotes the matrix of stoichiometric reaction coefficients ($\hat{n}_{i,r}$), and λ stands for the $\sigma^\circ_{r,P,T}$ column vector. If $\hat{r} = \hat{\imath}$ and $\hat{r}$ values of $\sigma^\circ_{r,P,T}$ are known, the matrix is nonsingular and the equation can be solved using any one of several standard algorithms to yield $\hat{\imath}$ values of $\Delta G^\circ_{f,i}$. Provided $\hat{r}$ experimental values of $\Delta G^\circ_{r,P,T}$ are known experimentally and values of S°_{i,P_r,T_r}, S°_{j,P_r,T_r}, V°_{i,P_r,T_r}, V°_{j,P_r,T_r}, and heat capacity power function coefficients for eq (19) are available for all the minerals, the requisite values of $\sigma^\circ_{r,P,T}$ can be computed from eqs (14), (25), and (31) with the aid of thermodynamic data and equations for the gases and aqueous species appearing in the reactions. Values of $\Delta G^\circ_{f,i}$ generated by the calculations permit calculation of corresponding values of $\Delta H^\circ_{f,i}$ from

$$\Delta H^\circ_{f,i} = \Delta G^\circ_{f,i} + T_r \Delta S^\circ_{f,i} \tag{34}$$

where $\Delta S^\circ_{f,i}$ stands for the standard molal entropy of formation of the ith species from its elements in their stable form at 298.15°K and 1 bar.

Eq (33) ensures internal consistency among values of $\Delta G^\circ_{f,i}$ computed from a given set of high pressure-temperature phase equilibrium data. However, if matrix equations for more than one set of reactions are evaluated, the values of $\Delta G^\circ_{f,i}$ computed from any one of the matrix equations will be consistent with those derived from another only if the one or more values of the index j in each of the equations refers to a mineral indexed by j or i in at least one of the elements in each of the other matrix equations. *Failure to incorporate this constraint may lead to contradictions in the thermodynamic properties of minerals computed from different sets of experimental data, which is the cause of many such discrepancies reported in the literature.*

Equilibrium constants and Gibbs free energies of reaction.—Adopting alternate standard states for H_2O facilitates calculation of $\sigma^\circ_{r,P,T}$

for different kinds of reactions. For example, if the reactions involve only minerals and aqueous solutions, it is convenient to employ standard states that are independent of pressure and temperature for all species. Hence, if we specify a liquid standard state for H_2O together with that adopted above for minerals, the activity of pure H_2O as well as the activities of all thermodynamic components of stoichiometric minerals are unity at any pressure and temperature. The most convenient standard state for aqueous species other than H_2O is one of unit activity in a hypothetical one molal solution referenced to infinite dilution at any pressure and temperature. The standard molal thermodynamic properties of aqueous solute species can then be calculated for pressures and temperatures to 5 kb and 600°C from equations given by Helgeson and Kirkham (1976 and in press) and Walther and Helgeson (1977). Similarly, values of $\Delta G^\circ_{H_2O,P,T}$ and the other thermodynamic properties of H_2O consistent with the liquid standard state can be computed for pressures and temperatures to $\sim$ 100 kb and $<$ 1000°C from equations summarized by Helgeson and Kirkham (1974a) and Delany and Helgeson (1978). As an example, let us consider a reversible reaction involving only minerals, H_2O, and $SiO_{2(aq)}$ and let $\hat{l}$ and $\hat{l}$–1 in eqs (28) and (29) refer to the latter two species, respectively. We can then write

$$a_{H_2O}^{\hat{n}_{H_2O}}\ a_{SiO_{2(aq)}}^{\hat{n}_{SiO_{2(aq)}}}\ \prod_{l}^{\hat{l}-2} a_l^{\hat{n}_l} =$$

$$a_{H_2O}^{\hat{n}_{H_2O}}\ m_{SiO_{2(aq)}}^{\hat{n}_{SiO_{2(aq)}}}\ \bar{\gamma}_{SiO_{2(aq)}}^{\hat{n}_{SiO_{2(aq)}}}\ \prod_{l}^{\hat{l}-2} X_l^{\hat{n}_l}\ \lambda_l^{\hat{n}_l} = K_{P,T} \tag{34}$$

where $m_{SiO_{2(aq)}}$ and $\bar{\gamma}_{SiO_{2(aq)}}$ stand for the molality and activity coefficient of $SiO_{2(aq)}$, and X_l and λ_l refer to the mole fraction and activity coefficient of the lth component of the minerals involved in the reaction. The activity coefficients are related to composition by

$$\bar{\gamma}_{SiO_{2(aq)}} = \frac{a_{SiO_{2(aq)}}}{m_{SiO_{2(aq)}}} \tag{35}$$

and

$$\lambda_l = \frac{a_l}{X_l} \tag{36}$$

where X_l stands for the mole fraction of the lth component of a solid solution. Note that regardless of the pressure and temperature, the standard states adopted above require that $\lambda_l \rightarrow 1$ as $X_l \rightarrow 1$, but $\bar{\gamma}_{SiO_2} \rightarrow 1$ as $a_{H_2O} \rightarrow 1$.

Because departures from unit activity of H_2O caused by dissolution of slightly soluble minerals in aqueous solutions are negligible, the

standard state for H_2O described above is closely approximated by experimental conditions in many phase equilibrium studies. Solubility data (for example, Morey, 1957) indicate that in the absence of CO_2, CH_4, and other gases, the fluid phase involved in most experimental studies is > 98 wt percent H_2O, which corresponds to ~ 99.8 mole percent. Under these conditions the activity of H_2O can be regarded as unity. The activity coefficient of $SiO_{2(aq)}$ in such solutions can also be taken as unity without introducing significant error in thermodynamic calculations (Walther and Helgeson, 1977). Consequently, if the reactions involve only minerals that exhibit little or no solid solution so that $\lambda_l \approx X_l \approx 1$, eq (34) reduces to

$$m_{SiO_{2(aq)}} = K_{P,T} \tag{37}$$

For reversible reactions among stoichiometric minerals, H_2O, and $SiO_{2(aq)}$, analyses of silica in the aqueous phase thus yield values of log $K_{P,T}$ which can be used together with eq (28) to compute values of $\Delta G^\circ_{r,P,T}$ for eq (31). If the reactions involve only stoichiometric minerals and H_2O, eq (37) reduces to

$$\log K_{P,T} = 0 \tag{38}$$

and $\Delta G^\circ_{r,P,T} = 0$ at the equilibrium pressures and temperatures determined in the experimental study.

Values of $\Delta G^\circ_{r,P,T}$ can be computed for reactions involving aqueous species other than H_2O and $SiO_{2(aq)}$ in a manner analogous to that for dehydration/desilication reactions. If we let $\hat{l}$ designate H_2O and $\hat{l}$–1, $\hat{l}$–2, . . . $\hat{l}$–$\hat{s}$ refer to the aqueous solute species, a general statement of eq (29) can be written for a reaction involving $\hat{s}$ such species as

$$a_{H_2O}^{\hat{n}_{H_2O}} \prod_{\hat{l}}^{\hat{l}-(\hat{s}+1)} X_l^{\hat{n}_l} \lambda_l^{\hat{n}_l} \prod_{\hat{l}-\hat{s}}^{\hat{l}-1} m_l^{\hat{n}_l} \bar{\gamma}_l^{\hat{n}_l} = K_{P,T} \tag{39}$$

Where $\bar{\gamma}_l$ is defined by a general statement of eq (35). In most instances $\bar{\gamma}_l$ for nonpolar neutral species at high pressures and temperatures can be regarded as unity without introducing significant error in the calculations. However, for ionic species, $\bar{\gamma}_l$ may be much smaller or greater than 1, depending on the "true" ionic strength ($\bar{I}$) of the aqueous phase. The ionic strength in turn depends on the degree of ion association in solution, which is a function of pressure and temperature. Values of $\bar{I}$, a_{H_2O}, and $\bar{\gamma}_l$ for ionic species in chloride-rich solutions at high pressures and temperatures can be computed with the aid of equations and data summarized by Helgeson (1969) and Helgeson and Kirkham (1974b and in press). Such calculations indicate that the ratios of $\bar{\gamma}_l$ for similar ionic species (such as Na^+ and K^+) are close to one in solutions of relatively low ionic strength at high pressures and temperatures. Under these conditions, the electrostatic properties of the solvent favor ion association and the formation of neutral complexes, which lowers the "true" ionic

strength of electrolyte solutions. In general, the activity of H_2O in electrolyte solutions at temperatures $\lesssim$ 200°C can also be regarded as unity without introducing unacceptable uncertainty in values of $K_{P,T}$ computed from eq (39), even in concentrated solutions. At higher temperatures, the osmotic coefficients of electrolyte solutions reported by Liu and Lindsay (1972), Lietzke and Stoughton (1974), and Silvester and Pitzer (1977) indicate that a_{H_2O} may be as low as $\sim$ 0.6.

As a rule, it is convenient to regard CO_2 as an aqueous species at temperatures and pressures corresponding to those in the two-phase region of the phase diagram for the system CO_2–H_2O in figure 9. The standard state for $CO_{2(aq)}$ is then taken to be the same as that adopted above for other aqueous species. In contrast, at higher temperatures where H_2O and CO_2 are completely miscible, it is advantageous to adopt a gas standard state for CO_2. The gas standard state is one of unit fugacity of the hypothetical ideal gas at 1 bar and any temperature. The standard molal Gibbs free energy of the gas is then independent of pressure. Despite the fact that the activity of H_2O may be $<<$ 1 in fluids coexisting with both carbonates and silicates at high temperatures, it is convenient in certain instances to compute values of $\Delta G°_{r,P,T}$ for dehydration/decarbonation reactions by employing the gas standard state for CO_2 in conjunction with the liquid standard state for H_2O. In contrast to the standard molal Gibbs free energy of CO_2, the standard molal Gibbs free energy of H_2O is then a function of pressure. If ideal mixing occurs in a fluid phase composed of CO_2 and H_2O, the activity of H_2O relative to the liquid standard state is equal to its mole fraction. However, the activity of CO_2 consistent with the gas standard state is equal to its fugacity, which is related to the mole fraction of CO_2 in the fluid by Dalton's law; that is, for fluid pressure (P_f) equal to total pressure (P),

$$f_{CO_2} = p_{CO_2}\,\chi_{CO_2} = X_{CO_2}\,\chi_{CO_2}\,P \tag{40}$$

where f_{CO_2}, p_{CO_2}, X_{CO_2}, and χ_{CO_2} stand for the fugacity, partial pressure, mole fraction, and fugacity coefficient of CO_2. The law of mass action

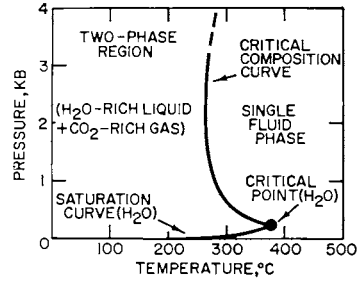

Fig. 9. Phase relations in the system CO_2–H_2O at high pressures and temperatures (Tödheide and Franck, 1963).

for a dehydration/decarbonation reaction consistent with ideal mixing of CO_2 and H_2O can be written for these standard states as

$$a_{H_2O}^{\hat{n}_{H_2O}} \; f_{CO_2}^{\hat{n}_{CO_2}} \prod_{l}^{\hat{l}-2} a_l^{\hat{n}_l} =$$

$$X_{H_2O}^{\hat{n}_{H_2O}} \; X_{CO_2}^{\hat{n}_{CO_2}} \; \chi_{CO_2}^{\hat{n}_{CO_2}} \; P^{\hat{n}_{CO_2}} \prod_{l}^{\hat{l}-2} X_l^{\hat{n}_l} \; \lambda_l^{\hat{n}_l} = K_{P,T} \qquad (41)$$

which corresponds to a statement of eq (29) with $\hat{l}$ and $\hat{l}$–1 designating H_2O and CO_2, respectively. If all minerals involved in the reaction are stoichiometric, so that $\lambda_l = 1$ in eq (36) for $l = 1, 2, \ldots (\hat{l}-2)$ at all pressures and temperatures, eq (41) reduces to

$$X_{H_2O}^{\hat{n}_{H_2O}} \; X_{CO_2}^{\hat{n}_{CO_2}} \; \chi_{CO_2}^{\hat{n}_{CO_2}} \; P^{\hat{n}_{CO_2}} = K_{P,T} \qquad (42)$$

which permits calculation of $\Delta G^\circ_{r,P,T}$ for eq (31) from eq (28) and experimentally determined fluid compositions.

If the gas standard state is adopted for both CO_2 and H_2O in calculating the thermodynamic properties of decarbonation/dehydration reactions, an equation for H_2O analogous to eq (40) can be written, and eqs (41) and (42 become (for $P_f = P$)

$$f_{H_2O}^{\hat{n}_{H_2O}} \; f_{CO_2}^{\hat{n}_{CO_2}} \prod_{l}^{\hat{l}-2} a_l^{\hat{n}_l} = \left(X_{H_2O}^{\hat{n}_{H_2O}} \; X_{CO_2}^{\hat{n}_{CO_2}} \; \chi_{H_2O}^{\hat{n}_{H_2O}} \; \chi_{CO_2}^{\hat{n}_{CO_2}} \right)$$

$$P^{(\hat{n}_{H_2O} + \hat{n}_{CO_2})} \prod_{l}^{\hat{l}-2} X_l^{\hat{n}_l} \; \lambda_l^{\hat{n}_l} = K_{P,T} \qquad (43)$$

and

$$X_{H_2O}^{\hat{n}_{H_2O}} \; X_{CO_2}^{\hat{n}_{CO_2}} \; \chi_{H_2O}^{\hat{n}_{H_2O}} \; \chi_{CO_2}^{\hat{n}_{CO_2}} \; P^{(\hat{n}_{H_2O} + \hat{n}_{CO_2})} = K_{P,T} \qquad (44)$$

where χ_{H_2O} refers to the fugacity coefficient of H_2O.

Pressure–volume–temperature data for the system CO_2–H_2O indicate that under certain restricted pressure/temperature conditions the mixing properties of these components are essentially ideal (Greenwood, 1973; Holloway, 1977), which means that for reactions at these pressures and temperatures the fugacity coefficients of pure CO_2 and H_2O at the temperature and total pressure of interest can be used for χ_{CO_2} and χ_{H_2O} in eqs (43) and (44). For ideal mixing of CO_2 and H_2O, values of χ_{CO_2} and χ_{H_2O} at high pressures and temperatures can be calculated from equations summarized by Holloway and Reese (1974), Holloway (1977), and Helgeson and Kirkham (1974a). If provision for nonideal mixing is incorporated in the calculations, fugacity coefficients for both CO_2 and H_2O as a function of X_{CO_2} can be computed from the modified Redlich-Kwong algorithm

given by Holloway (1977). Note that if H_2O is not involved in the reaction, $\hat{n}_{H_2O} = 0$ and ${X_{H_2O}}^{\hat{n}_{H_2O}} = {\chi_{H_2O}}^{\hat{n}_{H_2O}} = 1$ in both eqs (42) and (44). However, if CO_2 is absent, eq (42) reduces to zero, and eq (44) becomes (for $P_f = P$)

$${\chi_{H_2O}}^{\hat{n}_{H_2O}}\ P^{\hat{n}_{H_2O}} = {f_{H_2O}}^{\hat{n}_{H_2O}} = K_{P,T} \tag{45}$$

The equilibrium constants in eqs (41) and (43) require $G°_{P,T} - G°_{P_r,T_r}$ in a statement of eq (14) for CO_2 to be equal to $G°_{P_r,T} - G°_{P_r,T_r}$, which is true for H_2O only if eqs (43) and (44) or (45) are used to describe the equilibrium states. Values of $G°_{P_r,T} - G°_{P_r,T_r}$, $H°_{P_r,T} - H°_{P_r,T_r}$, $S°_{P_r,T} - S°_{P_r,T_r}$, and $C°_{P_r,T}$ for gases can be computed from eqs (19) and (25) through (27) using heat capacity coefficients given by Kelley (1960), which permits calculation of $\Delta G°_{P_r,T}$ and $\Delta H°_{P_r,T}$ with the aid of eqs (14) and (15) and the values of $\Delta G°_f$ and $\Delta H°_f$ for gases reported by Wagman and others (1968). The thermodynamic properties at 25°C and 1 bar of a number of gases of geologic interest are summarized in table 9.

Solid solutions.—Calculation of $\Delta G°_{r,P,T}$ from experimental data for reactions involving solid solutions requires provision for mixing of atoms among energetically equivalent sites in the mineral, as well as exchange of atoms between energetically distinct sites. The thermodynamic consequence of mixing and exchange of atoms among energetically equivalent and distinct sites in solid solutions has received considerable attention in recent years (Mueller, 1962; Matsui and Banno, 1965; Thompson, 1967, 1969; Blander, 1970, 1972; Saxena and Ghose, 1971; Saxena, 1969, 1973; Grover and Orville, 1969; Wood and Banno, 1973; Kerrick and Darken, 1975; Powell, 1977; Aagaard, Helgeson, and Benson, 1979). Because silicate solid solutions commonly exhibit compositional variation on more than one kind of site, the activities of the thermodynamic components of the solutions rarely equal the mole fractions of the components. However, if no exchange of atoms between energetically distinct sites accompanies compositional variation, the activities of the thermodynamic components of the mineral can be approximated by assuming random mixing and equal interaction of atoms on energetically equivalent sites. A general equation relating site occupancy in such solutions to the activity of the ith thermodynamic component (a_i) can be written as[5]

$$a_i = k_i \prod_s \prod_j {X_{j,s}}^{\nu_{s,j,i}} \tag{46}$$

where k_i denotes a proportionality constant determined by temperature, pressure, and the stoichiometry of the ith component (see below), $\nu_{s,j,i}$

[5] It should perhaps be emphasized that no assumptions other than those stated above are necessary to derive eqs (46) through (52) from first principles of either classical or statistical thermodynamics (for example, see Kerrick and Darken, 1975; and Aagaard, Helgeson, and Benson, 1979).

stands for the stoichiometric number of sth energetically equivalent sites occupied by the jth species in one mole (gram formula unit) of the ith component, and $X_{j,s}$ represents the mole fraction of the jth species on the sth sites in the solid solution, which is given by

$$X_{j,s} = \frac{n_{j,s}}{\sum_{j} n_{j,s}} \tag{47}$$

where $n_{j,s}$ stands for the number of moles of the jth species on the sth sites. The proportionality constant k_i in eq (46) can be expressed as

$$k_i = \prod_{s} \prod_{j} \left(\frac{\nu_{s,j,i}}{\nu_{s,i}} \right)^{-\nu_{s,j,i}} \tag{48}$$

so that at all pressures and temperatures,

$$\lim_{X_i \to 1} a_i = 1 \tag{49}$$

where X_i stands for the mole fraction of the ith thermodynamic component of the solid solution, and $\nu_{s,i}$ designates the stoichiometric number of energetically equivalent sth sites in one mole of the ith component. Note that $\nu_{s,i} = \nu_{s,j,i}$ only if one kind of atom occupies the sth sites. Otherwise,

$$\nu_{s,i} = \sum_{j} \nu_{s,j,i} \tag{50}$$

Similarly, $k_i = 1$ only if one kind of atom occupies each kind of energetically equivalent sites in the mineral

Although eq (46) is strictly valid only for solid solutions of thermodynamic components with equal standard molal volumes, it can be used to obtain close approximations of a_i if the standard molal volumes of the components are within ~5 (or even in some cases ~10) percent of each other. Eq (46) is consistent with

$$G - G^\circ = RT \sum_{i} X_i \left(\ln k_i + \sum_{s} \sum_{j} \nu_{s,j,i} \ln X_{j,s} \right) \tag{51}$$

where $G - G^\circ$ stands for the molal Gibbs free energy of mixing. Differentiating eq (51) leads to

$$\begin{aligned} S - S^\circ = &- R \sum_{i} X_i \left(\ln k_i + \sum_{s} \sum_{j} \nu_{s,j,i} \ln X_{j,s} \right) \\ &- RT \sum_{i} X_i \left(\left(\frac{\partial \ln k_i}{\partial T} \right)_P + \sum_{s} \sum_{j} \ln X_{j,s} \left(\frac{\partial \nu_{s,j,i}}{\partial T} \right)_P \right. \\ &\left. + \nu_{s,j,i} \left(\frac{\partial \ln X_{j,s}}{\partial T} \right)_{P,X_i} \right) \end{aligned} \tag{52}$$

where $S - S^\circ$ corresponds to the molal entropy of mixing for a random distribution of atoms on all energetically distinct sites and the subscript X_i stands for constant X_i for all values of i. Note that $(\partial \nu_{s,j,i}/\partial T)_P$, $(\partial \ ln \ k_i/\partial T)_P$, and $(\partial \ ln \ X_{j,s}/\partial T)_{P,x_i}$ are finite only for components that exhibit disorder as a function of temperature. In these cases, $\nu_{s,j,i}$, k_i, $(\partial \ ln \ k_i/\partial T)_P$ $(\partial ln \ \nu_{s,j,i}/\partial T)_P$, and $(\partial \ ln \ X_{j,s}/\partial T)_{P,x_i}$ can be computed from long-range ordering parameters, equilibrium constants, and standard molal enthalpies of reaction for exchange of atoms among energetically distinct sites.

Provision for exchange of atoms between energetically distinct sites can be made in thermodynamic calculations by taking account of constraints imposed by homogeneous equilibrium among the various species on the sites. The law of mass action for an interchange reaction involving atoms designated by $j = 1$ and $j = 2$ on energetically distinct sites represented by $s = 1$ and $s = 2$ can be written as

$$\prod_{s=1}^{2} \prod_{j=1}^{2} a_{j,s}^{\hat{n}_{j,s}} = \prod_{s=1}^{2} \prod_{j=1}^{2} X_{j,s}^{\hat{n}_{j,s}} \lambda_{j,s}^{\hat{n}_{j,s}} = K \tag{53}$$

where $a_{j,s}$ and $\lambda_{j,s}$ refer to the activity and activity coefficient of the jth atom on the sth sites, $\hat{n}_{j,s}$ stands for the reaction coefficient of the subscripted atom on the sth sites (which is negative for reactants and positive for products), and K denotes the equilibrium (distribution) constant for the reaction. Because K is independent of composition, if $\lambda_{j,s} = 1$ for all values of j and s so that all atoms on each kind of energetically equivalent sites mix randomly with equal interaction, eq (53) reduces to

$$\prod_{s=1}^{2} \prod_{j=1}^{2} X_{j,s}^{\hat{n}_{j,s}} = K \tag{54}$$

which can be used together with X-ray, neutron diffraction, or Mössbauer spectral data and eqs (46) and (52) to calculate the activities of the thermodynamic components of solid solutions and the entropies of mixing from compositional data.

In contrast to the mixing equation derived by Kerrick and Darken (1975), eqs (46), (51), (52), and (54) apply to mixing of ordered, disordered, and partially ordered components, but only if substitutional order/disorder is not coupled to compositional variation in the mineral. In the latter case (which includes orthopyroxene and plagioclase solid solutions), intrasite mixing is accompanied by intersite exchange, and $\lambda_{j,s}$ is a function of composition. Either $\lambda_{j,s}$ or λ_i must then be described with the aid of regular solution theory or higher order Margules expansions, such as those summarized by Thompson (1967), Saxena (1973), and others.

ESTIMATION OF ENTROPIES, VOLUMES, AND HEAT CAPACITIES OF MINERALS

The equations summarized above permit calculation of the standard molal Gibbs free energies of formation of minerals at P_r and T_r from experimental observations of phase equilibria at high pressures and temperatures. However, the calculations require values of $S°_{P_r,T_r}$, $V°_{P_r,T_r}$, and heat capacity coefficients for all the minerals involved in the reactions. These data are available for most of the minerals considered below, but in certain cases it was necessary to use estimated entropies, volumes, and heat capacities to compute $G°_{P,T} - G°_{P_r,T_r}$, $H°_{P,T} - H°_{P_r,T_r}$, and $S°_{P,T} - S°_{P_r,T_r}$ for minerals at high pressures and temperatures. Configurational contributions were included in the estimates only in cases where the magnitude of the contributions could be established unambiguously. This procedure seems preferable to that advocated by Waldbaum (1973), Ulbrich and Waldbaum (1976), Zen (1977), and others, who argue in favor of adding ideal configurational entropy contributions to the calorimetric third law entropies of minerals that exhibit order/disorder. Consideration of substitutional order/disorder in alkali feldspars, Ca–Al pyroxene, and other minerals (see below) suggests that actual configurational contributions to the entropies of minerals may be substantially less than ideal.

Although calorimetric third law entropies and heat capacities of minerals are uncertain to the extent of a few tenths of a cal $mole^{-1}$ $(°K)^{-1}$, the uncertainties generally fail to justify unweighted optimization of standard molal entropies of reaction by linear programming, as suggested by Gordon (1973), who treats both entropies and Gibbs free energies of reactions equally as adjustable parameters.[6] Accordingly, most of the calculations reported below were carried out using entropies and heat capacities of minerals derived from calorimetic data or estimation algorithms, rather than generating them from high pressure/temperature phase equilibrium data. Adjustments were made only in those cases where the thermodynamic consequences of order/disorder have been documented or the predicted Clapeyron slopes of univariant curves failed to satisfy experimental observations at high pressures and temperatures. This procedure ensured compatibility of the calculations with low-temperature heat capacity data and precluded erroneous assignment of uncertainties in reversal temperatures to the standard molal entropies of minerals. It also minimized errors caused by assuming unwarranted configurational contributions to the entropy, which tend to cancel in reactions among disordered minerals.

In general, the standard molal volumes, entropies, and heat capacities of minerals at 25°C and 1 bar can be estimated to within a few percent of their experimental values. In most (but not all) cases (see above), discrepancies of this order of magnitude have a negligible effect

[6] Although weighting factors can be incorporated in linear programming routines for thermodynamic analysis of high pressure/temperature phase equilibrium data, comprehensive calculations of this kind have yet to be carried out.

on calculated standard molal enthalpies and Gibbs free energies of reactions at high pressures and temperatures.

Entropy and volume.—Various empirical algorithms have been used to estimate the standard molal entropies of minerals (Latimer, 1952; Pitzer and Brewer, 1961; Kelley, private commun. cited by Stull, 1965; Fyfe, Turner, and Verhoogen, 1958; Helgeson, 1969; Saxena, 1976; Cantor, 1977). All these yield close approximations for certain classes of compounds, but none is valid for all minerals. Most such algorithms are based on corresponding states relations and/or models in which simple additivity rules or the entropies of structural analogs are modified to take explicit account of atomic mass, ionic size and charge, and/or the standard molal volumes of minerals. For example, Fyfe, Turner, and Verhoogen (1958) employed the relation,

$$S^\circ_{i,P_r,T_r} = S^\circ_{\Sigma,i,P_r,T_r} + \hat{k}(V^\circ_{i,P_r,T_r} - V^\circ_{\Sigma,i,P_r,T_r}) \tag{55}$$

where the subscript i denotes the mineral for which the standard molal entropy at 25°C and 1 bar is to be estimated, $\hat{k}$ denotes a constant, and

$$S^\circ_{\Sigma,i,P_r,T_r} \equiv \sum_j \nu_{j,i} S^\circ_{j,P_r,T_r} \tag{56}$$

and

$$V^\circ_{\Sigma,i,P_r,T_r} \equiv \sum_j \nu_{j,i} V^\circ_{j,P_r,T_r} \tag{57}$$

where $\nu_{j,i}$ stands for the number of moles of the jth oxide formula unit ($j = 1, 2, \ldots \hat{j}$) in one mole of the ith mineral, and S°_{j,P_r,T_r} and V°_{j,P_r,T_r} represent the standard molal entropy and volume of the pure oxide at 25°C and 1 bar. A value of 0.6 appears to be the "best" value of $\hat{k}$ for most silicates (Fyfe, Turner, and Verhoogen, 1958; Beane, ms), but comparative calculations indicate that $\hat{k}$ may vary significantly for minerals in different structural classes.

In most cases eq (55) affords estimates of the standard molal entropies of minerals within a few percent of those obtained experimentally. Although this equation is clearly more accurate than assuming the standard molal entropy of formation of a mineral from it oxides to be zero (see below), which leads to

$$S^\circ_{i,P_r,T_r} = S^\circ_{\Sigma,i,P_r,T_r}, \tag{58}$$

closer approximations can usually be obtained by first writing a reversible reaction between the mineral for which the standard molal entropy at 25°C and 1 bar is to be estimated and another mineral (or minerals) in the same or a similar structural class using oxide formula units to balance the reaction. For example, the standard molal entropy of akermanite at 25°C and 1 bar can be estimated from the calorimetric entropy of gehlenite by taking account of

$$\underset{\text{(akermanite)}}{Ca_2MgSi_2O_7} + \underset{\text{(corundum)}}{\alpha\text{-}Al_2O_3} \rightleftharpoons \underset{\text{(gehlenite)}}{Ca_2Al_2SiO_7} + \underset{\text{(periclase)}}{MgO} + \underset{\text{(}\alpha\text{-quartz)}}{SiO_2} \tag{59}$$

for which

$$S^\circ_{akermanite} + \Delta S^\circ_r = S^\circ_{gehlenite} + S^\circ_{periclase} + S^\circ_{\alpha\text{-}quartz} - S^\circ_{corundum} \tag{60}$$

and

$$V^\circ_{akermanite} + \Delta V^\circ_r = V^\circ_{gehlenite} + V^\circ_{periclase} + V^\circ_{\alpha\text{-}quartz} - V^\circ_{corundum} \tag{61}$$

If we now write general expressions of the form of eqs (60) and (61) and designate the left sides of these expressions as S°_s and V°_s, respectively, close estimates of the standard molal entropies of *nonferrous* minerals (see below) at 25°C and 1 bar can be computed from

$$S^\circ_{i,P_r,T_r} = \frac{S^\circ_{s,i,P_r,T_r}\,(V^\circ_{s,i,P_r,T_r} + V^\circ_{i,P_r,T_r})}{2V^\circ_{s,i,P_r,T_r}} \tag{62}$$

by first calculating S°_{s,i,P_r,T_r} and V°_{s,i,P_r,T_r} from expressions such as eqs (60) and (61). For example, in the case of akermanite, substituting experimental standard molal entropies and volumes of gehlenite, periclase, α-quartz, and corundum, together with the standard molal volume of akermanite in eqs (60) through (62) yields an estimate of 50.0 cal mole^{-1} (°K)$^{-1}$ for S°_{i,P_r,T_r}, which is equal to the calorimetric value reported by Robie and Waldbaum (1968). In contrast, eq (55) results in an estimate of 46.8 cal mole^{-1} (°K)$^{-1}$, and simple addition of the standard molal entropies of the oxide formula units in akermanite (eq 58) yields 45.2 cal mole^{-1} (°K)$^{-1}$.

Alternate entropy estimates computed from eqs (55), (58), and (62) for various nonferrous silicates are shown in table 1 and plotted in figure 10, where they can be compared with their experimental counterparts. The standard molal entropy and volume of H_2O used to calculate the estimates for tremolite and kaolinite correspond to those for "structural" H_2O in table 2 (see below). It can be seen in table 1 and figure 10 that both eqs (55) and (62) yield reasonably close approximations of experimental entropies that are significantly better than those obtained from eq (58), but the estimates computed from eq (62) are more consistently reliable and generally closer to their exprimental counterparts than those obtained from eq (55). Note that in certain cases (for example, clinoenstatite, diopside, and merwinite), relatively large errors result from eq (55) but not from eq (62). The latter equation also affords close estimates of the standard molal entropies of nonferrous carbonates, chlorides, sulfates, and multiple oxides, which is not true of eq (55). However, none of the algorithms yields accurate estimates of the standard molal entropies of sulfides, which can be approximated more closely by using Latimer's (1952) or Kelley's (private commun., cited by Stull, 1965) approach.

Differences between the standard molal entropies estimated from eq (58) and the calorimetric values shown in table 1 range from 0.1 to

TABLE 1

Comparative summary of experimental and estimated standard molal entropies of minerals at 298.15°K and 1 bar

Mineral	Formula	$V^\circ_{P_r,T_r}$ [a,d]	Experimental $S^\circ_{P_r,T_r}$ [c,d]	Estimated $S^\circ_{P_r,T_r}$ [c,e]		
				(eq 58)	(eq 55)	(eq 62)
Clinoenstatite	$MgSiO_3$	31.276	16.2	16.3	14.7	16.2
Wollastonite	$CaSiO_3$	39.93	19.6	19.4	19.7	20.0
Diopside	$CaMg(SiO_3)_2$	66.09	34.2	35.7	31.3	34.4
Jadeite	$NaAl(SiO_3)_2$	60.40	31.9	34.8	28.7	32.5
Tephroite	Mn_2SiO_4	48.61[b]	39.0[b]	38.4	38.1	38.8
Calcium-olivine	γ-Ca_2SiO_4	59.11[b]	28.8[b]	28.9	30.6	28.9
Phenacite	Be_2SiO_4	37.19[b]	15.4[b]	16.6	15.4	16.5
Willemite	Zn_2SiO_4	52.42[b]	31.4[b]	30.7	31.4	31.5
Akermanite	$Ca_2MgSi_2O_7$	92.81	50.0	45.2	46.8	50.0
Merwinite	$Ca_3Mg(SiO_4)_2$	104.4	60.5	54.7	54.3	59.9
Low Albite	$NaAlSi_3O_8$	100.07	49.5	44.7	48.7	48.6
Nepheline	$NaAlSiO_4$	54.16	29.7	24.9	28.7	30.1
Tremolite	$Ca_2Mg_5Si_8O_{22}(OH)_2$	272.92	131.2	139.8	132.6	131.8
Kaolinite	$Al_2Si_2O_5(OH)_4$	99.52	48.5	51.1	51.8	48.2

Mineral	Reference reactions for the estimates shown in column 7 above
Clinoenstatite	$MgSiO_3 + MnO \rightleftharpoons MnSiO_3 + MgO$
Wollastonite	$CaSiO_3 + MnO \rightleftharpoons MnSiO_3 + CaO$
Diopside	$CaMg(SiO_3)_2 \rightleftharpoons MgSiO_3 + CaO + SiO_2$[h]
Jadeite	$NaAl(SiO_3)_2 + CaO + MgO \rightleftharpoons CaMg(SiO_3)_2 + 0.5Na_2O + 0.5\alpha\text{-}Al_2O_3$
Tephroite	$Mn_2SiO_4 + 2MgO \rightleftharpoons Mg_2SiO_4 + 2MnO$
Calcium-olivine	γ-$Ca_2SiO_4 + 2BeO \rightleftharpoons Be_2SiO_4 + 2CaO$
Phenacite	$Be_2SiO_4 + 2MgO \rightleftharpoons Mg_2SiO_4 + 2BeO$
Willemite	$Zn_2SiO_4 + 2MgO \rightleftharpoons Mg_2SiO_4 + 2ZnO$
Akermanite	$Ca_2MgSi_2O_7 + \alpha\text{-}Al_2O_3 \rightleftharpoons Ca_2Al_2SiO_7$[f] $+ MgO + SiO_2$[h]
Merwinite	$Ca_3Mg(SiO_4)_2 + CaO \rightleftharpoons 2Ca_2SiO_4$[g] $+ MgO$
Low Albite	$NaAlSi_3O_8 + 0.5K_2O \rightleftharpoons KAlSi_3O_8$[g] $+ 0.5Na_2O$
Nepheline	$NaAlSiO_4 + 0.5K_2O \rightleftharpoons KAlSiO_4 + 0.5Na_2O$
Tremolite	$Ca_2Mg_5Si_8O_{22}(OH)_2 \rightleftharpoons Mg_3Si_4O_{10}(OH)_2 + 2CaMg(SiO_3)_2$
Kaolinite	$Al_2Si_2O_5(OH)_4 + 2SiO_2$[h] $\rightleftharpoons Al_2Si_4O_{10}(OH)_2 + H_2O_{(s)}$

[a] $cm^3\ mole^{-1}$. [b] Robie and Waldbaum (1968). [c] $cal\ mole^{-1}(°K)^{-1}$. [d] Except where indicated otherwise, the values of $V^\circ_{P_r,T_r}$ and $S^\circ_{P_r,T_r}$ shown in these columns were taken from table 8. [e] Computed using experimental standard molal entropies and volumes for the minerals shown above and/or those for oxides and minerals in tables 2 and 8 together with the values of $V^\circ_{P_r,T_r}$ and $S^\circ_{P_r,T_r}$ for rhodonite (35.16 $cm^3\ mole^{-1}$ and 24.5 $cal\ mole^{-1}(°K)^{-1}$, respectively) and larnite (51.60 $cm^3\ mole^{-1}$ and 30.50 $cal\ mole^{-1}(°K)^{-1}$, respectively) given by Robie and Waldbaum (1968). [f] Larnite. [g] Microcline. [h] α-quartz.

8.6 cal mole^{-1} (°K)$^{-1}$. Corresponding discrepancies resulting from eq (55) are smaller (from 0 to 6 cal mole^{-1} (°K)$^{-1}$), but many are nevertheless large. In contrast, none of the errors intoduced by the structural algorithm (eq 62) exceeds 1.1 cal mole^{-1} (°K)$^{-1}$, and all but two of the estimates calculated from eq (62) are within 0.6 cal mole^{-1} (°K)$^{-1}$ of the experimental values shown in table 1. These and other comparisons of this kind indicate that eq (62) yields estimates within ~ 1 percent of the calorimetric entropies of most silicates at 25°C and 1 bar. It should perhaps be emphasized in this regard that errors in estimated standard molal entropies of minerals computed from eq (62) which exceed ~ 1 percent of the corresponding calorimetric values can usually be attributed to the use of an inappropriate structural analog in the reference reaction employed in the calculations. In certain cases the estimates may be affected considerably by the extent to which the structural analogs represent adequately the various structural domains in the minerals in question. Where a dearth of data requires use of a quasi-analog, the uncertainty in the estimate may exceed several cal mole^{-1} (°K)$^{-1}$. In these cases, eq (55) may yield a better estimate.

With the exception of solid/solid phase transitions, errors in the standard molal entropies of minerals of the order of ~ 1 percent have a negligible effect on calculated standard molal entropies of reactions at high temperatures, which are commonly of the order of 20 cal mole^{-1} (°K)$^{-1}$ or more. Although uncertainties in $G°_{P,T} - G°_{P_r,T_r}$ caused by

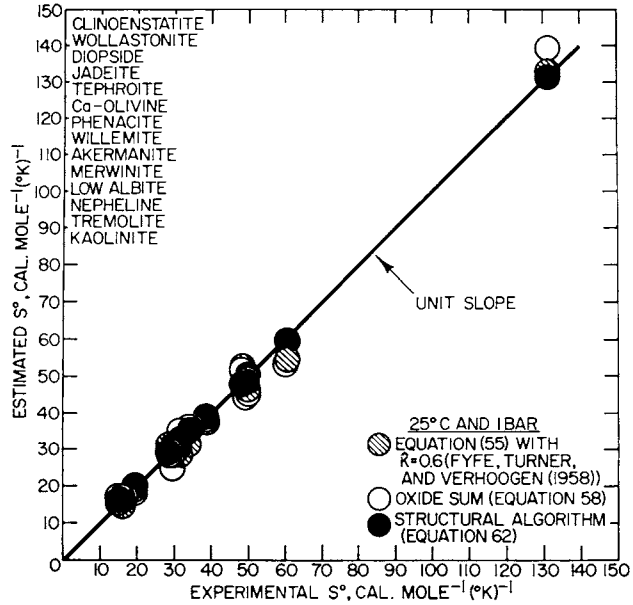

Fig. 10. Correlation of estimated and experimental standard molal entropies of minerals at 25°C and 1 bar.

errors in estimated entropies may exceed several hundred cal^{-1} mole^{-1} at high temperatures, if all estimates are consistent with one another and more than one estimate is involved, errors in $G°_{P,T} - G°_{P_r,T_r}$ caused by the structural algorithm tend to cancel in calculating the standard molal Gibbs free energies of reactions at high temperatures and pressures.

The contribution of structural H_2O to the standard molal entropies of silicates ($S°_{H_2O_{(s)}}$) can be estimated from eq (62) using calorimetric data for hydrous minerals together with the contribution of structural H_2O to their standard molal volumes ($V°_{H_2O_{(s)}}$), which is ~13.7 cm^3 (mole H_2O)$^{-1}$ (Fyfe, Turner, and Verhoogen, 1958). This value of $V°_{H_2O_{(s)}}$ and the standard molal volumes and entropies of α-quartz, kao-

TABLE 2

Summary of experimental standard molal volumes, entropies, and heat capacity power function coefficients for oxides

Mineral	Formula	$V°_{P_r,T_r}$ [a]	$S°_{P_r,T_r}$ [b]	$c°_{P_r,T_r}$ [b,p]	Coefficients for equation (19)			Temperature Range, °K
					a [b]	$b \times 10^3$ [d]	$c \times 10^{-5}$ [e]	
Lime	CaO	16.764[f]	9.50[f,g,x]	10.24	11.67[q]	1.08[q]	1.56[q]	298-2000[q]
Periclase	MgO	11.248[f]	6.44[f,g,g]	9.03	10.18[q]	1.74[q]	1.48[q]	298-2100[q]
Manganosite	MnO	13.221[f]	14.27[f,j]	10.70	11.11[q]	1.94[q]	0.88[q]	298-1800[q]
Ferrous Oxide	FeO	12.00[f]	14.52[f,g,j]	11.89	12.12[r]	2.07[r]	0.75[r]	298-1600[q]
Bromellite	BeO	8.309[f]	3.38[g,g]	6.08	8.45[q]	4.00[q]	3.17[q]	298-1200[q]
Zincite	ZnO	14.338[f]	10.43[f,j]	9.62	11.71[q]	1.22[q]	2.18[q]	298-2000[q]
Potassium Oxide	K_2O	40.38[f]	22.5[f,g]	20.10	18.51[r]	8.65[r]	0.88[r]	298-1100[q]
Sodium Oxide	Na_2O	25[h]	17.935[q]	16.46	18.25[r]	4.89[r]	2.89[r]	298-1000[q]
Corundum	α-Al_2O_3	25.575[f]	12.18[f,j]	18.90	27.49[q]	2.82[q]	8.38[q]	298-1800[q]
Hematite	α-Fe_2O_3	30.274[f]	20.94[u]	25.04	23.49[q]	18.60[q]	3.55[q]	298- 950[q,w]
	β-Fe_2O_3				36.00[q]	0.00[q]	0.00[q]	950-1050[q,w]
	γ-Fe_2O_3				31.71[q]	1.76[q]	0.00[q]	1050-1800[q]
α-quartz	SiO_2	22.688[f]	9.88[f]	10.63	11.22[q]	8.20[q]	2.70[q]	298- 848[q,w]
β-quartz	SiO_2	23.72[k]		14.99	14.41[q]	1.94[q]	0.00[q]	848-2000[q]
"Structural" H_2O	$H_2O_{(s)}$	13.7[m]	9.6[n]	9.57	7.11[s]	8.24[s]	0.00[s]	298-1000[s]
"Zeolitic" H_2O	$H_2O_{(z)}$	8[c]	14.1[t]	11.4	11.4[v]	0.0[v]	0.0[v]	

[a] cm^3 mole^{-1}. [b] cal mole^{-1} (°K)$^{-1}$. [c] Estimated from standard molal volumes of zeolites (see text). [d] cal mole^{-1}(°K)$^{-2}$. [e] cal (°K) mole^{-1}. [f] Robie and Waldbaum (1968). [g] Stull and Prophet (1971). [h] Estimated from equation (62) using standard molal entropies and volumes of sodium aluminum silicates given in table 8 (see text). [j] Wagman and others (1968). [k] Standard molal volume at 575°C given by Robie and others (1966). [g] Parker, Wagman, and Evans (1971). [m] Fyfe, Turner, and Verhoogen (1958). [n] Estimated from equation (62) and the standard molal volumes and entropies of α-quartz, pyrophyllite, chrysotile, kaolinite, and talc shown in table 8 (see text). [p] Computed from equation (19) using the heat capacity coefficients given above. [q] Kelley (1960). [r] Generated by regression of heat capacity data reported by Stull and Prophet (1971) with equation (19). [s] Pankratz (1964b). [t] Estimated from the standard molal entropies of analcime and dehydrated analcime given in table 8 (see text). [u] Haas and Robie (1973). [v] Estimated from equations (86) through (88) and calorimetric data reported by King (1955) and King and Weller (1961b) - see text. [w] Equation (19) fails to represent adequately changes in the standard molal heat capacities of α, β, and γ polymorphs in the vicinity of α/β and β/γ transition temperatures (see text). [x] This value was adopted in preference to that computed by Chase and others (1975) because it appears to be more consistent with the standard molal entropies of other calcium compounds at 25°C and 1 bar.

linite, chrysotile, pyrophyllite, and talc permit calculation of $S°_{H_2O_{(s)}}$ at 25°C and 1 bar from alternate statements of eq (62) for

$$\text{kaolinite} + 2\ \alpha\text{-quartz} \rightleftharpoons \text{pyrophyllite} + H_2O_{(s)} \tag{63}$$

and

$$\text{chrysotile} + 2\ \alpha\text{-quartz} \rightleftharpoons \text{talc} + H_2O_{(s)} \tag{64}$$

which yields 9.9 and 9.3 cal mole^{-1} (°K)$^{-1}$, respectively. The mean of these (9.6 cal mole^{-1} (°K)$^{-1}$) is close to the value of $S°_{H_2O_{(s)}}$ computed from eq (55) using $V°_{H_2O_{(s)}} = 13.7$ cm^3 mole^{-1} and the standard molal entropies and volumes of K_2O, corundum, α-quartz, and muscovite (9.4 cal mole^{-1} (°K)$^{-1}$). The latter value corresponds to that suggested by Latimer (1952) for estimating the entropies of nonsilicates containing loosely bound H_2O, but it is 1.3 cal mole^{-1} (°K)$^{-1}$ lower than the standard molal entropy of metastable ice at 25°C and 1 bar (10.7 cal mole^{-1} (°K)$^{-1}$). It appears from these and similar calculations and comparisons that a value of 9.6 cal mole^{-1} (°K)$^{-1}$ for $S°_{H_2O_{(s)}}$ yields closer estimates of $S°_{P_r,T_r}$ for hydrous silicates from eq (62) than those generated from eqs (55) or (58) using 9.4, 9.6, or 10.7 cal mole^{-1} (°K)$^{-1}$ for $S°_{H_2O_{(s)}}$ at 25°C and 1 bar. Accordingly, 9.6 cal mole^{-1} (°K)$^{-1}$ was adopted for $S°_{H_2O_{(s)},P_r,T_r}$ in the present study (table 2).

It can be deduced from table 1 that eq (62) yields estimates for tremolite and kaolinite that are within 0.6 percent of the calorimetric values, which is also true for chrysotile. With the exception of muscovite, larger discrepancies result if eq (55) is used with $S°_{H_2O_{(s)}} = 9.6$ cal mole^{-1} (°K)$^{-1}$. The latter discrepancies range from $\sim$ 2 to 5 cal mole^{-1} (°K)$^{-1}$ for kaolinite, pyrophyllite, chrysotile, and tremolite.

The contribution of loosely held H_2O molecules ($S°_{H_2O_{(z)}}$) in the structural channels of zeolites and related minerals to their standard molal entropies can be estimated by assuming $\Delta S°_{r,P_r,T_r} = 0$ for a hypothetical reaction of the form

$$\psi + \hat{n}_{H_2O_{(z)}} H_2O_{(z)} \rightleftharpoons \psi \cdot \hat{n}_{H_2O_{(z)}} H_2O_{(z)} \tag{65}$$

where ψ represents a dehydrated zeolitic mineral, $\hat{n}_{H_2O}$ stands for the reaction coefficient for H_2O, and $\psi \cdot \hat{n}_{H_2O}\ H_2O$ designates a hydrated equivalent of ψ in which the H_2O molecules are loosely bound. Assuming $\Delta S°_{r,P_r,T_r} = 0$ for reaction (65) is equivalent to regarding $S°_{H_2O_{(z)}}$ as an additive contribution to the standard molal entropies of zeolitic minerals. This assumption seems reasonable in view of the relatively weak hydrogen bonds responsible for holding $H_2O_{(z)}$ in the channels of zeolites.

If $\Delta S°_{r,P_r,T_r}$ is taken to be zero for a statement of reaction (65) for analcime and dehydrated analcime, calorimetric data reported by King (1955) and King and Weller (1961b) indicate a value of 14.1 cal mole^{-1} (°K)$^{-1}$ for $S°_{H_2O_{(z)}}$. As expected, this value lies between $S°_{H_2O_{(s)}}$ (9.6 cal mole^{-1} (°K)$^{-1}$) and S° for liquid H_2O at 25°C and 1 bar (16.7 cal

mole^{-1} (°K)$^{-1}$). The observation that the entropy contribution of $H_2O_{(z)}$ is 4.5 cal mole^{-1} (°K)$^{-1}$ larger than that of "tightly" bound structural H_2O but only 2.6 cal mole^{-1} (°K)$^{-1}$ smaller than $S°_{P_r,T_r}$ for liquid H_2O is consistent with the relative magnitude of the translational, vibrational, and rotational degrees of freedom that one would postulate for the three types of H_2O.

In contrast to the observation that $S°_{H_2O_{(s)}} < S°_{H_2O_{(z)}} < S°_{H_2O_{(liquid)}}$, structurally bound H_2O would be expected to contribute to a greater extent to the volume of a mineral such as muscovite than the corresponding contribution of loosely bound "nonessential" H_2O to the volumes of zeolites. The channels in zeolites are relatively large, and, unlike clay minerals, their structure retains much of its integrity during dehydration. Hence, $H_2O_{(z)}$ should not contribute substantially to the volume of a zeolite. This reasoning is supported by estimates of $V°_{H_2O_{(z)}}$, which can be made by adopting an approach analogous to that employed above to estimate $S°_{H_2O_{(z)}}$; that is, by assuming $\Delta V°_{r,P_r,T_r} = 0$ for hypothetical reactions among zeolites or "zeolitic" minerals and $H_2O_{(z)}$. For example, data given in table 2 and the assumption that the standard molal volumes of reaction are zero for

$$\text{laumontite} \rightleftharpoons \text{wairakite} + 2\ H_2O_{(z)}, \tag{66}$$

$$2\ \text{laumontite} \rightleftharpoons \text{leonhardite} + H_2O_{(z)}, \tag{67}$$

and

$$\text{leonhardite} \rightleftharpoons 2\ \text{wairakite} + 3\ H_2O_{(z)} \tag{68}$$

leads, respectively, to estimates of 8.2, 7.1, and 8.5 cm^3 mole^{-1} for $V°_{H_2O_{(z)}}$. Despite the large uncertainty in $V°_{P_r,T_r}$ for Na_2O (see below), these values compare favorably with that (10.7 cm^3 mole^{-1}) computed from eq (55) using $S°_{H_2O_{(z)}} = 14.1$ cal mole^{-1} (°K)$^{-1}$ and the standard molal volumes and entropies of analcime, α-quartz, corundum, and Na_2O. All these estimates, which are $\sim$ 3 to 6 cm^3 mole^{-1} less than the value of $V°_{H_2O_{(s)}}$ in table 2, are consistent with the observations summarized above. Although they are not necessarily representative of natural zeolites, which exhibit considerable variation in their cell parameters, a value of $V°_{H_2O_{(z)}} = 8$ should afford reasonably close estimates of the standard molal entropies of most zeolitic minerals. Accordingly, this value was used in the present study together with eqs (55) and (62) to estimate the standard molal entropies of minerals containing loosely bound H_2O molecules.

Eq (62) was also used to estimate the standard molal volume of Na_2O (table 2) using the following reference reactions:

$$Na_2O + 2\ \text{microcline} \rightleftharpoons 2\ \text{low albite} + K_2O \tag{69}$$

and

$$Na_2O + 2\ \text{kalsilite} \rightleftharpoons 2\ \text{nepheline} + K_2O \tag{70}$$

The calculations resulted in 19.9 and 28.0 cm^3 mole^{-1} for $V°_{P_r,T_r}$ of

Na_2O. Corresponding estimates of 21.4 and 22.4 cm^3 $mole^{-1}$ were obtained from eq (55) using experimental data for low albite and nepheline, respectively. Because uncertainties in the data used to calculate these estimates are magnified in the calculations, and because larger discrepancies result from similar calculations using data for other minerals, the mean of these values is not necessarily the best estimate. After exploring various alternatives, it was decided to adopt 25 ± 5 cm^3 $mole^{-1}$ for $V^\circ_{P_r,T_r}$ of Na_2O.

None of the algorithms discussed above is suitable for estimating the standard molal entropies of minerals containing ferrous iron. For example, experimental data shown in tables 2 and 8 together with statements of eq (62) for the reactions

$$\text{fayalite} + 2\ \text{periclase} \rightleftharpoons \text{forsterite} + 2\ \text{ferrous oxide} \tag{71}$$

and

$$\text{fayalite} + 2\ \text{manganosite} \rightleftharpoons \text{tephroite} + 2\ \text{ferrous oxide} \tag{72}$$

yield an estimate of $S^\circ_{P_r,T_r}$ for fayalite of 39.4 and 39.6 cal $mole^{-1}$ $(°K)^{-1}$. Eqs (55) and (58) lead to corresponding estimates of 38.7 and 38.9 cal $mole^{-1}$ $(°K)^{-1}$, respectively. In contrast, the calorimetric entropy reported by Kelley and King (1961) is 34.7 ± 0.4 cal $mole^{-1}$ $(°K)^{-1}$, and Robie and Waldbaum (1968) give 35.4 cal $mole^{-1}$ $(°K)^{-1}$, which differ from all four estimates by ~ 4 cal $mole^{-1}$ $(°K)^{-1}$. The disparity is probably a consequence of a large difference in the electronic configuration and crystal field stabilization energy of Fe^{++} (Burns and Fyfe, 1967; Burns, 1970) in FeO and Fe_2SiO_4. Assuming this to be the general case, estimates of the standard molal entropies of ferrous silicates can be calculated by subtracting 2 cal $mole^{-1}$ $(°K)^{-1}$ (mole FeO)$^{-1}$ from the right sides of eqs (55), (58), and (62), which leads to the following general algorithms

$$S^\circ_{i,P_r,T_r} = S^\circ_{\Sigma,i,P_r,T_r} + \hat{k}(V^\circ_{i,P_r,T_r} - V^\circ_{\Sigma,i,P_r,T_r}) - 2\nu_{Fe,i} \tag{73}$$

$$S^\circ_{i,P_r,T_r} = S^\circ_{\Sigma,i,P_r,T_r} - 2\nu_{Fe,i} \tag{74}$$

and

$$S^\circ_{i,P_r,T_r} = \frac{S^\circ_{s,i,P_r,T_r}\ (V^\circ_{s,i,P_r,T_r} + V^\circ_{i,P_r,T_r})}{2\ V^\circ_{s,i,P_r,T_r}} - 2\nu_{Fe,i} \tag{75}$$

where $\nu_{Fe,i}$ stands for the number of moles of ferrous iron in one mole of the ith mineral.

The value of -2 cal $mole^{-1}$ $(°K)^{-1}$ assigned to the electronic configuration and crystal field stabilization contribution to S°_{i,P_r,T_r} arising from the presence of ferrous iron in silicates is obviously a first approximation which takes no account of the dependence of this contribution on structural factors, such as those considered by Wood and Strens (1971, 1972). Nevertheless, in the absence of more definitive and comprehensive calorimetric data, it seems to afford reasonable estimates of the standard molal entropies of ferrous silicates.

Estimates of $S^\circ_{P_r,T_r}$ are given in table 3 for a large number of silicates for which calorimetric data are either not available or suspect. The latter cases are discussed below. Most of the estimates shown in the table were calculated from eq (75). Wherever possible, structural analogs were used in the reference reactions, but in some cases a dearth of experimental data made it necessary to use structurally similar compounds or composites of structural elements in the mineral in lieu of structural analogs. If a paucity of experimental data precluded this approach, eq (73) was used as an alternative to eq (75). In a few cases, additivity algorithms analogous to eq (74) were employed. For example, the standard molal entropies and volumes of PD-oxyannite and hydrous cordierite at 25°C and 1 bar were estimated by assuming $\Delta S^\circ_{r,P_r,T_r} = \Delta V^\circ_{r,P_r,T_r} = 0$ for

$$KFe_3AlSi_3O_{12}(H_{-1}) + 3\ FeO + 3/2\ H_2O_{(s)} \rightleftharpoons KFe_3AlSi_3O_{10}(OH)_2 + 3/2\ \alpha\text{-}Fe_2O_3 \quad (76)$$

and

$$\text{hydrous cordierite} \rightleftharpoons \text{cordierite} + H_2O_{(z)} \quad (77)$$

Taking the standard molal entropy and volume change for reaction (77) as zero is consistent with the assumption made (above) in calculating $S^\circ_{H_2O_{(z)}}$ from the standard molal entropies of analcime and dehydrated analcime.

Heat capacity.—Close estimates of the standard molal heat capacities of minerals at 25°C and 1 bar can be obtained by summing in appropriate proportions the calorimetric standard molal heat capacities of their constituent oxide formula groups according to

$$C^\circ_{P_r,T_r,i} = \sum_j \nu_{j,i} C^\circ_{P_r,T_r,j} \quad (78)$$

where $\nu_{j,i}$ again refers to the number of moles of the jth oxide formula unit in one mole of the ith mineral. However, better estimates can generally be obtained by assuming the standard molal heat capacities of reactions among oxides and silicates of the same or a similar structural class to be zero at 25°C and 1 bar. Estimates based on this assumption provide at least in part for the temperature dependence of bond energies within the structural components of minerals. The order of magnitude of this contribution can be assessed by comparing alternate estimates of the standard molal heat capacities of minerals with highly accurate calorimetric data. For example, substitution of data taken from table 2 in eq (78) yields an estimate of 79.9 cal mole^{-1} (°K)$^{-1}$ for the standard molal heat capacity of muscovite at 25°C and 1 bar.[7] In contrast, assuming $\Delta C^\circ_{P_r,r} = 0$ at 25°C for the reaction

$$\text{muscovite} + \alpha\text{-quartz} \rightleftharpoons \text{pyrophyllite} + 1/2\ \text{corundum} + 1/2\ K_2O \quad (79)$$

[7] The heat capacity contribution of structural H_2O used to estimate the standard molal heat capacity of muscovite is discussed below.

TABLE 3

Summary of estimated standard molal entropies of minerals at 298.15°K and 1 bar

Mineral Class	Name	Formula	$\bar{V}^\circ_{P_r,T_r}$ [a]	$\bar{S}^\circ_{P_r,T_r}$ [b]	Reference reactions for the estimates shown in column 5
Ortho and Ring Silicates	Monticellite	$CaMgSiO_4$	51.47[d]	26.4[m]	$CaMgSiO_4 + MgO \rightleftharpoons Mg_2SiO_4 + CaO$
	Hydrous Cordierite	$Mg_2Al_3(AlSi_5O_{18}) \cdot H_2O$	241.22[f]	111.43[f]	$Mg_2Al_3(AlSi_5O_{18}) \cdot H_2O \rightleftharpoons Mg_2Al_3(AlSi_5O_{18}) + H_2O_{(z)}$
	Almandine	$Fe_3Al_2Si_3O_{12}$	115.28[c]	75.6[m,q]	$Fe_3Al_2Si_3O_{12} + 3CaO \rightleftharpoons Ca_3Al_2Si_3O_{12} + 3FeO$
	Andradite	$Ca_3Fe_2Si_3O_{12}$	131.85[d]	70.13[m]	$Ca_3Fe_2Si_3O_{12} + \alpha\text{-}Al_2O_3 \rightleftharpoons Ca_3Al_2Si_3O_{12} + \alpha\text{-}Fe_2O_3$
	Spessartine	$Mn_3Al_2Si_3O_{12}$	117.90[d]	74.5[m]	$Mn_3Al_2Si_3O_{12} + 3CaO \rightleftharpoons Ca_3Al_2Si_3O_{12} + 3MnO$
	Clinozoisite	$Ca_2Al_3Si_3O_{12}(OH)$	136.2[c]	70.64[ww]	$Ca_2Al_3Si_3O_{12}(OH)$[x] $\rightleftharpoons Ca_2Al_3Si_3O_{12}(OH)$[pp]
	Epidote[v]	$Ca_2FeAl_2Si_3O_{12}(OH)$[v]	139.2[xx]	75.2[m]	$Ca_2FeAl_2Si_3O_{12}(OH)$[v] $+ 0.5\alpha\text{-}Al_2O_3 \rightleftharpoons Ca_2Al_3Si_3O_{12}(OH)$[x] $+ 0.5\alpha\text{-}Fe_2O_3$
	Chloritoid	$FeAl_2SiO_5(OH)_2$	69.8[d]	42.1[m,q]	$FeAl_2SiO_5(OH)_2 \rightleftharpoons Al_2SiO_5$[jj] $+ FeO + H_2O_{(s)}$
	Staurolite	$Fe_2Al_9Si_4O_{23}(OH)$	224.4[d]	117.1[m,q]	$Fe_2Al_9Si_4O_{23}(OH) \rightleftharpoons 4Al_2SiO_5$[jj] $+ 2FeO + 0.5\alpha\text{-}Al_2O_3 + 0.5H_2O_{(s)}$
Chain and Band Silicates	Ca-Al Pyroxene[u]	$CaAl(AlSiO_6)$[u]	63.5[h]	35.0[w]	$CaAl_2SiO_6$[v] $MgSiO_3 \rightleftharpoons \alpha\text{-}Al_2O_3 + CaMg(SiO_3)_2$
	Clinoferrosilite	$FeSiO_3$	32.952[cc]	22.6[m,q]	$FeSiO_3 + MgO \rightleftharpoons MgSiO_3$[ll] $+ FeO$
	Hedenbergite	$CaFe(SiO_3)_2$	68.27[d]	40.7[m,q]	$CaFe(SiO_3)_2 + MgO \rightleftharpoons CaMg(SiO_3)_2 + FeO$
	Aegerine	$NaFe(SiO_3)_2$	64.37[e]	36.7[m]	$NaFe(SiO_3)_2 + 0.5\alpha\text{-}Al_2O_3 \rightleftharpoons NaAl(SiO_3)_2$[hh] $+ 0.5\alpha\text{-}Fe_2O_3$
	Anthophyllite	$Mg_7[Si_8O_{22}](OH)_2$	264.43[d]	128.6[m]	$Mg_7Si_8O_{22}(OH)_2 \rightleftharpoons Mg_3Si_4O_{10}(OH)_2 + 4MgSiO_3$[y]
	Ferrogedrite	$Fe_5Al_2(Al_2Si_6O_{22})(OH)_2$	265.9[p]	153.5[m,q]	$Fe_5Al_2(Al_2Si_6O_{22})(OH)_2 + 2MgSiO_3$[y] $+ 5MgO \rightleftharpoons Mg_7Si_8O_{22}(OH)_2$[ss] $+ 5FeO + 2\alpha\text{-}Al_2O_3$

continued →

TABLE 3 (continued)

Mineral Class	Name	Formula	$\bar{V}^{\circ}_{P_r,T_r}$ [a]	$\bar{S}^{\circ}_{P_r,T_r}$ [b]	Reference reaction for the estimates shown in column 5
Chain and Band Silicates	Ferrotremolite	$Ca_2Fe_5Si_8O_{22}(OH)_2$	282.8 [ee]	163.5 [m,q]	$Ca_2Fe_5Si_8O_{22}(OH)_2 + 5MgO \rightleftharpoons Ca_2Mg_5Si_8O_{22}(OH)_2 + 5FeO$
	Fluortremolite	$Ca_2Mg_5Si_8O_{22}F_2$	270.45 [c]	129.4 [m]	$Ca_2Mg_5Si_8O_{22}(F_2) + H_2O_{(s)} + CaO \rightleftharpoons Ca_2Mg_5Si_8O_{22}(OH)_2 + CaF_2$ [gg]
	Cummingtonite	$Mg_7Si_8O_{22}(OH)_2$	271.9 [e]	127.5 [m]	$Mg_7Si_8O_{22}(OH)_2 + 2CaO \rightleftharpoons Ca_2Mg_5Si_8O_{22}(OH)_2 + 2MgO$
	Grunerite	$Fe_7Si_8O_{22}(OH)_2$	256.67 [d]	163.3 [m,q]	$Fe_7Si_8O_{22}(OH)_2 + 7MgO \rightleftharpoons Mg_7Si_8O_{22}(OH)_2$ [dd] $+ 7FeO$
	Edenite	$NaCa_2Mg_5(AlSi_7O_{22})(OH)_2$	271.0 [ee]	161.0 [m]	$NaCa_2Mg_5(AlSi_7O_{22})(OH)_2 + \alpha\text{-}Al_2O_3 \rightleftharpoons NaCa_2Mg_4Al(Al_2Si_6O_{22})(OH)_2 + SiO_2$ [s] $+ MgO$
	Ferroedenite	$NaCa_2Fe_5(AlSi_7O_{22})(OH)_2$	280.9 [ee]	193.7 [m,q]	$NaCa_2Fe_5(AlSi_7O_{22})(OH)_2 + 5MgO \rightleftharpoons NaCa_2Mg_5(AlSi_7O_{22})(OH)_2 + 5FeO$
	Fluoredenite	$NaCa_2Mg_5(AlSi_7O_{22})F_2$	272.5 [ee]	146.7 [m]	$NaCa_2Mg_5(AlSi_7O_{22})F_2 + CaO + H_2O_{(s)} \rightleftharpoons NaCa_2Mg_5(AlSi_7O_{22})(OH)_2 + CaF_2$ [gg]
	Pargasite	$NaCa_2Mg_4Al(Al_2Si_6O_{22})(OH)_2$	273.5 [j]	160.0 [w]	$NaCa_2Mg_4Al(Al_2Si_6O_{22})(OH)_2 + 0.5K_2O + \alpha\text{-}Al_2O_3 \rightleftharpoons KMg_3(AlSi_3O_{10})(OH)_2 + 2CaAl_2SiO_6 + MgSiO_3$ [ll] $+ 0.5Na_2O$
	Ferropargasite	$NaCa_2Fe_4Al(Al_2Si_6O_{22})(OH)_2$	279.89 [d]	185.5 [m,q]	$NaCa_2Fe_4Al(Al_2Si_6O_{22})(OH)_2 + 4MgO \rightleftharpoons NaCa_2Mg_4Al(Al_2Si_6O_{22})(OH)_2 + 4FeO$
	Magnesiohastingsite	$NaCa_2Mg_4Fe(Al_2Si_6O_{22})(OH)_2$	273.8 [ee]	163.8 [m]	$NaCa_2Mg_4Fe(Al_2Si_6O_{22})(OH)_2 + 0.5\alpha\text{-}Al_2O_3 \rightleftharpoons NaCa_2Mg_4Al(Al_2Si_6O_{22})(OH)_2 + 0.5\alpha\text{-}Fe_2O_3$
	Hastingsite	$NaCa_2Fe_4Fe(Al_2Si_6O_{22})(OH)_2$	280.3 [ee]	189.2 [m]	$NaCa_2Fe_4Fe(Al_2Si_6O_{22})(OH)_2 + 0.5\alpha\text{-}Al_2O_3 \rightleftharpoons NaCa_2Fe_4Al(Al_2Si_6O_{22})(OH)_2 + 0.5\alpha\text{-}Fe_2O_3$
	Glaucophane	$Na_2Mg_3Al_2Si_8O_{22}(OH)_2$	269.7 [c]	130.0 [m]	$Na_2Mg_3Al_2Si_8O_{22}(OH)_2 + 2MgO + 2CaO \rightleftharpoons Ca_2Mg_5Si_8O_{22}(OH)_2 + \alpha\text{-}Al_2O_3 + Na_2O$
	Magnesioriebeckite	$Na_2Mg_3Fe_2Si_8O_{22}(OH)_2$	271.3 [ee]	138.0 [m]	$Na_2Mg_3Fe_2Si_8O_{22}(OH)_2 + \alpha\text{-}Al_2O_3 \rightleftharpoons Na_2Mg_3Al_2Si_8O_{22}(OH)_2 + \alpha\text{-}Fe_2O_3$
	Riebeckite	$Na_2Fe_3Fe_2Si_8O_{22}(OH)_2$	274.9 [ee]	156.6 [m,q]	$Na_2Fe_3Fe_2Si_8O_{22}(OH)_2 + 3MgO \rightleftharpoons Na_2Mg_3Fe_2Si_8O_{22}(OH)_2 + 3FeO$
	Richterite	$Na_2CaMg_5Si_8O_{22}(OH)_2$	272.8 [ee]	137.6 [m]	$Na_2CaMg_5Si_8O_{22}(OH)_2 + CaO \rightleftharpoons Ca_2Mg_5Si_8O_{22}(OH)_2 + Na_2O$
Framework Silicates	Wairakite	$Ca(Al_2Si_4O_{12}) \cdot 2H_2O$	191.17 [d]	105.1 [m]	$Ca(Al_2Si_4O_{12}) \cdot 2H_2O + Na_2O \rightleftharpoons 2NaAlSi_2O_6 \cdot H_2O + CaO$
	Laumontite	$Ca(Al_2Si_4O_{12}) \cdot 4H_2O$	207.55 [d]	117.1 [m]	$Ca(Al_2Si_4O_{12}) \cdot 4H_2O \rightleftharpoons 0.5Ca_2(Al_4Si_8O_{24}) \cdot 7H_2O$ [ii] $+ 0.5H_2O_{(z)}$

Mineral Class	Name	Formula	$\bar{V}^\circ_{P_r,T_r}$ [a]	$\bar{S}^\circ_{P_r,T_r}$ [b]	Reference reaction for the estimates shown in column 5
Framework Silicates	Chabazite	$Ca(Al_2Si_4O_{12}) \cdot 6H_2O$	247.76[d]	152.9[m]	$Ca(Al_2Si_4O_{12}) \cdot 6H_2O + 2SiO_2$[s] $\rightleftharpoons Ca(Al_2Si_6O_{16}) \cdot 5H_2O + H_2O_{(z)}$
	Epistilbite	$Ca(Al_2Si_6O_{16}) \cdot 5H_2O$	267.56[d]	152.9[m]	$Ca(Al_2Si_6O_{16}) \cdot 5H_2O \rightleftharpoons 0.5Ca_2(Al_4Si_8O_{24}) \cdot 7H_2O$[ii] $+ 2SiO_2$[s] $+ 1.5H_2O_{(z)}$
	Heulandite	$Ca(Al_2Si_7O_{18}) \cdot 6H_2O$	316.37[d]	182.4[m]	$Ca(Al_2Si_7O_{18}) \cdot 6H_2O \rightleftharpoons Ca(Al_2Si_6O_{16}) \cdot 5H_2O + SiO_2$[s] $+ H_2O_{(z)}$
	Stilbite	$NaCa_2(Al_5Si_{13}O_{36}) \cdot 14H_2O$	649.91[d]	399.3[m]	$Ca_2Na(Al_5Si_{13}O_{36}) \cdot 4H_2O + 0.5SiO_2$[s] $\rightleftharpoons 2Ca(Al_2Si_6O_{16}) \cdot 5H_2O + 0.5Na_2(Al_2Si_3O_{10}) \cdot 2H_2O + 3H_2O_{(z)}$
	Natrolite	$Na_2(Al_2Si_3O_{10}) \cdot 2H_2O$	169.72[d]	101.6[m]	$Na_2(Al_2Si_3O_{10}) \cdot 2H_2O + SiO_2$[s] $\rightleftharpoons 2NaAlSi_2O_6 \cdot H_2O$
	Na-Phillipsite	$Na_2(Al_2Si_5O_{14}) \cdot 5H_2O$[nn]	265[mm]	172.4[m,rr]	$Na_2(Al_2Si_5O_{14}) \cdot 5H_2O \rightleftharpoons 2NaAlSi_2O_6 \cdot H_2O + SiO_2$[s] $+ 3H_2O_{(z)}$
	K-Phillipsite	$K_2(Al_2Si_5O_{14}) \cdot 5H_2O$[nn]	265[mm]	172.1[m,rr]	$K_2(Al_2Si_5O_{14}) \cdot 5H_2O + Na_2O \rightleftharpoons Na_2(Al_2Si_5O_{14}) \cdot 5H_2O + K_2O$
	Ca-Phillipsite	$Ca(Al_2Si_5O_{14}) \cdot 5H_2O$[nn]	265[mm]	166.6[m,rr]	$Ca(Al_2Si_5O_{14}) \cdot 5H_2O + Na_2O \rightleftharpoons Na_2(Al_2Si_5O_{14}) \cdot 5H_2O + CaO$
Sheet Silicates	Greenalite	$Fe_3Si_2O_5(OH)_4$	115.0[j]	72.6[m,q]	$Fe_3Si_2O_5(OH)_4 + 3MgO \rightleftharpoons Mg_3Si_2O_5(OH)_4 + 3FeO$
	Minnesotaite	$Fe_3Si_4O_{10}(OH)_2$	147.86[j]	83.5[m,q]	$Fe_3Si_4O_{10}(OH)_2 + 3MgO \rightleftharpoons Mg_3Si_4O_{10}(OH)_2 + 3FeO$
	Celadonite	$KMgAlSi_4O_{10}(OH)_2$	157.1[d]	74.9[m]	$KMgAlSi_4O_{10}(OH)_2 + \alpha\text{-}Al_2O_3 \rightleftharpoons KAl(Al_2Si_3O_{10})(OH)_2 + MgO + SiO_2$[s]
	Margarite	$CaAl_2(Al_2Si_2O_{10})(OH)_2$	129.4[d]	63.8[m]	$CaAl_2(Al_2Si_2O_{16})(OH)_2 + SiO_2$[s] $+ 0.5K_2O \rightleftharpoons KAl_2(AlSi_3O_{10})(OH)_2 + 0.5\alpha\text{-}Al_2O_3 + CaO$
	Paragonite	$NaAl_2(AlSi_3O_{10})(OH)_2$	132.53[r]	66.4[m]	$NaAl_2(AlSi_3O_{10})(OH)_2 + 0.5K_2O \rightleftharpoons KAl_2(AlSi_3O_{10})(OH)_2 + 0.5Na_2O$
	Phlogopite	$KMg_3(AlSi_3O_{10})(OH)_2$	149.66[c]	76.1[m]	$KMg_3(AlSi_3O_{10})(OH)_2 + \alpha\text{-}Al_2O_3 \rightleftharpoons KAl_2(AlSi_3O_{10})(OH)_2 + 3MgO$
	Annite	$KFe_3(AlSi_3O_{10})(OH)_2$	154.32[c]	95.2[m,q]	$KFe_3(AlSi_3O_{10})(OH)_2 + \alpha\text{-}Al_2O_3 \rightleftharpoons KAl_2(AlSi_3O_{10})(OH)_2 + 3FeO$
	PD-Oxyannite	$KFe_3(AlSi_3O_{12}\square(H_{-1})$	143.2[k]	68.5[n]	
	7A-Clinochlore	$Mg_5Al(AlSi_3O_{10})(OH)_8$	211.5[q]	106.5[m]	$Mg_5Al(AlSi_3O_{10})(OH)_8 \rightleftharpoons Mg_3Si_2O_5(OH)_4 + 2Mg(OH)_2 + \alpha\text{-}Al_2O_3 + SiO_2$[s]
	7A-Daphnite	$Fe_5Al(AlSi_3O_{10})(OH)_8$	221.2[ℓ]	138.9[m,q]	$Fe_5Al(AlSi_3O_{10})(OH)_8 + 5MgO \rightleftharpoons Mg_5Al(AlSi_3O_{10})(OH)_8$[z] $+ 5FeO$
	7A-Amesite	$Mg_2Al(AlSiO_5)(OH)_4$	103.00[d]	52.0[m]	$Mg_2Al(AlSiO_5)(OH)_4 \rightleftharpoons 0.5Mg_3Si_2O_5(OH)_4 + 0.5Mg(OH)_2 + \alpha\text{-}Al_2O_3 + 0.5H_2O_{(s)}$

continued →

TABLE 3 (continued)

Mineral Class	Name	Formula	$\bar{V}^\circ_{P_r,T_r}$ [a]	$\bar{S}^\circ_{P_r,T_r}$ [b]	Reference reaction for the estimates shown in column 5
Sheet Silicates	Antigorite	$Mg_{48}Si_{34}O_{85}(OH)_{62}$	1749.13[vv]	861.36[t]	
	7A-Chamosite	$Fe_2Al(AlSiO_5)(OH)_4$	106.2[d]	64.7[m,q]	$Fe_2Al(AlSiO_5)(OH)_4 + 2MgO \rightleftharpoons MgAl(AlSiO_5)(OH)_4$[bb] $- 2FeO$
	7A-Cronstedtite	$Fe_2Fe(FeSiO_5)(OH)_4$	110.9[d]	73.5[m]	$Fe_2Fe(FeSiO_5)(OH)_4 + \alpha\text{-}Al_2O_3 \rightleftharpoons Fe_2Al(AlSiO_5)(OH)_4$[kk] $+ \alpha\text{-}Fe_2O_3$
	14A-Clinochlore	$Mg_5Al(AlSi_3O_{10})(OH)_8$	207.11[e]	111.2[m]	$Mg_5Al(AlSi_3O_{10})(OH)_8 + 0.5K_2O \rightleftharpoons KMg_3(AlSi_3O_{10})(OH)_2 + 2Mg(OH)_2 + 0.5\alpha\text{-}Al_2O_3 + H_2O_{(s)}$
	14A Daphnite	$Fe_5Al(AlSi_3O_{10})(OH)_8$	213.42[e]	142.5[m,q]	$Fe_5Al(AlSi_3O_{10})(OH)_8 + 5MgO \rightleftharpoons Mg_5Al(AlSi_3O_{10})(OH)_8$[aa] $+ 5FeO$
	14-A Amesite	$Mg_4Al_2(Al_2Si_2O_{10})(OH)_8$	205.4[qq]	108.9[m]	$Mg_4Al_2(Al_2Si_2O_{10})(OH)_8 + MgO + SiO_2$[s] $\rightleftharpoons Mg_5Al(AlSi_3O_{10})(OH)_8$[aa] $+ \alpha\text{-}Al_2O_3$
	Sepiolite	$Mg_4Si_6O_{15}(OH)_2(OH_2)_2 \cdot (OH_2)_4$[ww]	285.6[ff]	146.6[m,tt]	$Mg_4Si_6O_{15}(OH)_2(OH_2)_2 \cdot (OH_2)_4 + 0.5Mg(OH)_2 \rightleftharpoons 1.5Mg_3Si_4O_{10}(OH)_2 + 6H_2O_{(s)}$

[a] $cm^3\ mole^{-1}$. [b] $cal\ mole^{-1}\ (°K)^{-1}$. [c] Robie and others (1966). [d] Computed from cell parameters reported by Donnay and Ondik (1973). [e] Calculated from cell parameters reported by Deer, Howie, and Zussman (1962). [f] Computed by adding the values of $V^\circ_{P_r,T_r}$ and $S^\circ_{P_r,T_r}$ for anhydrous cordierite in table 8 to the volume and entropy contributions of "zeolitic" H_2O (table 2) -- see text. [g] Mean of the value of $V^\circ_{P_r,T_r}$ for chrysotile given by Robie and Waldbaum (1968) and that for amesite computed from cell parameters reported by Donnay and Ondik (1973). [h] Robie and Waldbaum (1968). [i] Computed from cell parameters reported by Berry (1974). [k] Estimated from the sum of the values of $V^\circ_{P_r,T_r}$ for annite and 3/2 $\alpha\text{-}Fe_2O_3$ by subtracting $V^\circ_{P_r,T_r}$ for 3FeO and 3/2 $H_2O_{(s)}$. [l] Mean of the values of $V^\circ_{P_r,T_r}$ for chamosite and greenalite calculated from cell parameters reported by Donnay and Ondik (1973) and Berry (1974). [m] Computed from equation (75) for the reference reactions shown in column 5 using values of $V^\circ_{P_r,T_r}$ and $S^\circ_{P_r,T_r}$ given in columns 4 and 5 above and those for minerals and/or oxides in tables 2 and 8. [n] Estimated from the sum of $S^\circ_{P_r,T_r}$ for annite and 3/2 $\alpha\text{-}Fe_2O_3$ minus 3FeO and 3/2 $H_2O_{(s)}$.

[p] Computed from equation (73) using values of $V^\circ_{P_r,T_r}$ for minerals given above and those for the appropriate oxides in table 3. [q] The entropy estimates shown for these minerals include a correction of -2.0 cal (mole FeO)$^{-1}$ (°K)$^{-1}$ to provide for the electronic configuration of Fe^{++} in the silicate lattice (see text). [r] Chatterjee (1970). [s] α-quartz. [t] Estimated by recalculating the entropy reported by King and others (1967) for antigorite with a stoichiometry of $Mg_3Si_2O_3(OH)_4$ to $Mg_{48}Si_{34}O_{85}(OH)_{62}$ using values of $S^\circ_{P_r,T_r}$ for α-quartz and $H_2O_{(s)}$ taken from table 3. [u] Disordered. [v] Ordered. [w] Estimated using data taken from tables 2 and 8 to evaluate equation (62) for the reaction shown above with provision for disorder based on observations of high pressure/temperature phase equilibria (see text). [x] Clinozoisite. [y] The values of $S^\circ_{P_r,T_r}$ and $V^\circ_{P_r,T_r}$ for enstatite used in the calculations correspond to $S^\circ_{P_r,T_r,\text{clinoenstatite}} + \Delta S^\circ_{t,1\text{ bar, clinoenstatite/enstatite}}$ and $V^\circ_{P_r,T_r,\text{clinoenstatite}} + \Delta V^\circ_{t,1\text{ bar,clinoenstatite/enstatite}}$ (table 8). [z] 7A-clinochlore. [aa] 14A-clinchlore. [bb] 7A-amesite. [cc] Computed from cell parameters reported by Burnham (1965). [dd] Cummingtonite. [ee] Ernst (1968). [ff] Computed by Stoessell (ms). from cell parameters reported by Preisinger (1959). [gg] The values of $V^\circ_{P_r,T_r}$ and $S^\circ_{P_r,T_r}$ for CaF_2 used in the calculations (24.542 cm^3 mole^{-1}) and (16.46 cal mole^{-1} (°K)$^{-1}$), respectively, are those reported by Robie and Waldbaum (1968). [hh] Jadeite. [ii] The value of $V^\circ_{P_r,T_r}$ for leonhardite used in the calculations (407.86 cm^3 mole^{-1}) was computed from cell parameters reported by Donnay and Ondik (1973). The corresponding value of $S^\circ_{P_r,T_r}$ (220.4 cal mole^{-1} (°K)$^{-1}$) is that reported by King and Weller (1961b). [jj] Kyanite. [kk] 7A-chamosite. [ll] Clinoenstatite. [mm] Estimated from data reported by Sheppard and Gude (1970). [nn] Idealized formulas consistent with data reported by Sheppard and Gude (1970). [pp] Zoisite. [qq] Estimated from a and β lattice constants reported by Steinfink (1958) and values of the b and cell parameters computed from algorithms given by Bailey (1972). [rr] Highly uncertain estimates owing to ambiguities in the compositional dependence of the molal volume of phillipsite. [ss] Anthophyllite. [tt] Estimated by Stoessell (ms). [uu] The formula for sepiolite is that adopted by Stoessell (ms) to differentiate among different types of structural H_2O in the mineral. [vv] Kunze (1961). [ww] Estimated by assuming ΔS°_t for the clinozoisite/zoisite transition to be 0.1 cal mole^{-1} (°K)$^{-1}$ (see text). [xx] Bird (ms) and Bird and Helgeson (1977) -- see text.

TABLE 4

Comparative summary of experimental and estimated standard molal heat capacities of minerals at 298.15°K and 1 bar

Mineral	Formula	Experimental $C^\circ_{P_r,T_r}$ [a,b]	Estimated $C^\circ_{P_r,T_r}$ [a]	
			Equation (78) [c]	Calculated (eq 80) assuming $\Delta C^\circ_{P_r,T_r} = 0$ for the reactions shown below [d]
Wollastonite	$CaSiO_3$	20.4	20.9	20.1
Clinoenstatite	$MgSiO_3$	18.9	19.7	19.2
Forsterite	Mg_2SiO_4	28.2	28.7	27.9
Fayalite	Fe_2SiO_4	31.8	34.4	33.9
Diopside	$CaMg(SiO_3)_2$	37.5	40.5	39.3
Akermanite	$Ca_2MgSi_2O_7$	50.7	50.8	49.9
Merwinite	$Ca_3Mg(SiO_4)_2$	60.3	61.0	60.6
Low Albite	$NaAlSi_3O_8$	49.0	49.6	48.7
Microcline	$KAlSi_3O_8$	48.5	51.4	50.8

Mineral	Reference reactions for the estimates shown in column 5 above
Wollastonite	$CaSiO_3 + MgO \rightleftharpoons MgSiO_3 + CaO$
Clinoenstatite	$MgSiO_3 + CaO \rightleftharpoons CaSiO_3 + MgO$
Forsterite	$Mg_2SiO_4 + 2CaO \rightleftharpoons \gamma\text{-}Ca_2SiO_4 + 2MgO$
Fayalite	$Fe_2SiO_4 + 2MgO \rightleftharpoons Mg_2SiO_4 + 2FeO$
Diopside	$CaMg(SiO_3)_2 \rightleftharpoons MgSiO_3 + CaSiO_3$
Akermanite	$Ca_2MgSi_2O_7 + \alpha\text{-}Al_2O_3 \rightleftharpoons Ca_2Al_2SiO_7 + MgO + SiO_2$ [e]
Merwinite	$Ca_3Mg(SiO_4)_2 \rightleftharpoons Ca_2MgSi_2O_7 + CaO$
Low Albite	$NaAlSi_3O_8 + CaO + 0.5\alpha\text{-}Al_2O_3 \rightleftharpoons CaAl_2Si_2O_8 + SiO_2$ [e] $+ 0.5Na_2O$
Microcline	$KAlSi_3O_8 + 0.5Na_2O \rightleftharpoons NaAlSi_3O_8 + 0.5K_2O$

[a] cal $mole^{-1}(°K)^{-1}$. [b] Calculated from equation (19) using experimental coefficients given in tables 2 and 8. [c] Computed using values of $C^\circ_{P_r,T_r}$ for oxides given in table 2. [d] Calculated using values of $C^\circ_{P_r,T_r}$ generated from equation (19) and experimental heat capacity power function coefficients for $\gamma\text{-}Ca_2SiO_4$ reported by Kelley (1960), together with corresponding values for oxides and other minerals given in tables 2 and 8. [e] α-quartz.

using experimental heat capacities shown in table 2 and that for pyrophyllite reported by Robie, Hemingway, and Wilson (1976) leads to an estimate of the standard molal heat capacity of muscovite at 25°C and 1 bar of 79.1 cal mole^{-1} (°K)$^{-1}$. The corresponding calorimetric value given by Robie, Hemingway, and Wilson is 77.9 cal mole^{-1} (°K)$^{-1}$, which differs from the latter estimate by 1.5 percent or 1.2 cal mole^{-1} (°K)$^{-1}$. In contrast, the estimate computed from eq (78) differs from the calorimetric value by 2.6 percent.

If we let $\hat{\imath}$ designate a mineral for which the standard molal heat capacity at 25°C and 1 bar is to be estimated, the structural algorithm discussed above can be expressed as

$$C^\circ_{P_r,T_r,\hat{\imath}} = \sum_{i}^{i-1} \hat{n}_{i,r} C^\circ_{P_r,T_r,i} / \hat{n}_{\hat{\imath},r} \tag{80}$$

where $\hat{n}_{i,r}$ and $\hat{n}_{\hat{\imath},r}$ refer to the stoichiometric coefficients of the ith and $\hat{\imath}$th species in the rth reference reaction, which are positive for products and negative for reactants. Standard molal heat capacities of various minerals at 25°C and 1 bar are shown in table 4, where estimates generated assuming $\Delta C^\circ_{P_r,r} = 0$ for reactions among minerals in the same or a similar structural class (eq 80) can be compared with their experimental counterparts and those estimated from eq (78). It can be seen in table 4 that the estimates computed from eq (80) are generally closer to the calorimetric values than those derived from eq (78). The discrepancies in the latter case are within 0.1 to 3.0 cal mole^{-1} (°K)$^{-1}$ of the experimental values, with a mean discrepancy of 1.2 cal mole^{-1} (°K)$^{-1}$. Corresponding differences for the values estimated from eq (80) range from 0.3 to 2.3 cal mole^{-1} (°K)$^{-1}$, with a mean of 0.9 cal mole^{-1} (°K)$^{-1}$. In most cases errors generated by eq (80) are of the order of 2 percent or less.

The calculations summarized in table 4 leave little doubt that additivity algorithms afford close approximation of the standard molal heat capacities of minerals at 25°C and 1 bar. In many cases, correspondingly close estimates of $C^\circ_{P_r}$ as a function of temperature can be calculated by combining eq (78) for the ith mineral with eq (19) for its oxide formula units (designated by the index j) to give

$$C^\circ_{P_r,i} = \sum_j \nu_{j,i}\, a_j + \nu_{j,i}\, b_j T - \nu_{j,i}\, c_j T^{-2} \tag{81}$$

which is equivalent to assuming

$$a_i = \sum_j \nu_{j,i}\, a_j \tag{82}$$

$$b_i = \sum_j \nu_{j,i}\, b_j \tag{83}$$

and

$$c_i = \sum_j \nu_{j,i}\, c_j \tag{84}$$

However, even better estimates of a_i, b_i, and c_i can be obtained by assuming $\Delta C^\circ_{P_r,r} = 0$ at all temperatures for reactions among structurally related minerals, which lead to

$$C^\circ_{P_r,\hat{i}} = \sum_i^{\hat{i}-1} \hat{n}_{i,r}\,(a_i + b_i T - c_i T^{-2})/\hat{n}_{\hat{i},r} \tag{85}$$

Eq (85) is analogous to eq (80) and consistent with

$$a_{\hat{i}} = \sum_i^{\hat{i}-1} \hat{n}_{i,r}\, a_i/\hat{n}_{\hat{i},r} \tag{86}$$

$$b_{\hat{i}} = \sum_i^{\hat{i}-1} \hat{n}_{i,r}\, b_i/\hat{n}_{\hat{i},r} \tag{87}$$

and

$$c_{\hat{i}} = \sum_i^{\hat{i}-1} \hat{n}_{i,r}\, c_i/\hat{n}_{\hat{i},r} \tag{88}$$

A number of examples of estimated coefficients are shown in table 5, where those generated from eqs (86) through (88) for the minerals listed in table 4 can be compared with corresponding estimates from eqs (82) through (84) and the coefficients obtained directly by regression of calorimetric data.

To preclude unwarranted uncertainty, all estimates of heat capacity power function coefficients must take into account temperature limitations on the validity of the regression coefficients used in the estimates. Because the heat capacity coefficients given by Kelley (1960) for α-quartz are not valid for temperatures above the α/β transition temperature (848°K), two sets of coefficients are given in table 5 for minerals with estimates that include heat capacity coefficients for quartz. The first set incorporates coefficients for α-quartz, which are replaced in the second by those for β-quartz.

It can be seen in table 5 that many of the estimated coefficients differ considerably from their experimental counterparts. Nevertheless, owing to compensation among the terms of the Maier-Kelley regression equation (eq 19), the estimated coefficients afford close approximation of experimental heat capacities at both low and high temperatures. For example, it can be deduced from table 6 and figure 11 that the estimated coefficients given in table 5 yield values of $C^\circ_{P_r,T}$ calculated from eq (81)

TABLE 5

Comparative summary of experimental and estimated standard molal heat capacity power function coefficients for minerals

Mineral[a]	Experimental[e,j]				Estimated from equation (81)[i]				Estimated from equation (85) assuming $\Delta C^\circ_{P_r,T}=0$ for the reactions shown in table 4[i]			
	a[b]	b[c] x 10^3	c[d] x 10^{-5}	Temperature Range, °K	a[b,f]	b[c,f] x 10^3	c[d,f] x 10^{-5}	Temperature Range, °K[g]	a[b,h]	b[c,h] x 10^3	c[d,h] x 10^{-5}	Temperature Range, °K[g]
Wollastonite	26.64	3.6	6.52	298 - 1400	22.89 26.08	9.28 3.02	4.26 1.56	298 - 848 848 - 2000	26.04	4.08	6.36	298 - 1800
Clinoenstatite	24.55	4.74	6.28	298 - 1800	21.40 24.59	9.94 3.68	4.18 1.48	298 - 848 848 - 2000	25.15	4.26	6.44	298 - 1400
Forsterite	35.81	6.54	8.52	298 - 1800	31.58 34.77	11.68 5.42	5.66 2.96	298 - 848 848 - 2000	28.88	13.64	4.48	298 - 1120
Fayalite	36.51	9.36	6.70	298 - 1490	35.46 38.65	12.34 6.08	4.20 1.50	298 - 848 848 - 1600	39.69	7.20	7.06	298 - 1600
Diopside	52.87	7.84	15.74	298 - 1600	44.29 50.67	19.22 6.70	8.44 3.04	298 - 848 848 - 2000	51.19	8.34	12.80	298 - 1400
Akermanite	60.09	11.40	11.40	298 - 1700	55.96 62.34	20.30 7.78	10.00 4.60	298 - 848 848 - 2000	57.65 60.84	15.12 8.86	10.92 8.72	298 - 848 848 - 1600
Merwinite	72.97	11.96	14.44	298 - 1700	67.63 74.01	21.38 10.04	11.56 6.16	298 - 848 848 - 2000	71.76	12.48	12.96	298 - 1600
Low Albite	61.70	13.9	15.01	298 - 1400	56.53 66.10	28.46 9.67	13.74 5.64	298 - 848 848 - 1000	59.35 62.54	21.86 15.60	15.29 12.59	298 - 848 848 - 1000
Microcline	63.83	12.9	17.05	298 - 1400	56.66 66.23	30.34 11.56	12.73 4.63	298 - 848 848 - 1100	61.83	15.78	14.00	298 - 1100

[a]Formulas for the minerals are given in table 4. [b]cal $mole^{-1}(°K)^{-1}$. [c]cal $mole^{-1}(°K)^{-2}$. [d]cal (°K) $mole^{-1}$. [e]Kelley (1960). [f]Computed using experimental coefficients for oxides taken from table 2. [g]Minimum experimental temperature range for the minerals and/or oxides used in the calculations (see tables 2 and 8). [h]Computed using experimental coefficients for γ-Ca_2SiO_4 reported by Kelley (1960) and those for oxides and other minerals given in tables 2 and 8. [i]Where appropriate, two sets of estimated coefficients are shown for different temperature ranges corresponding to those for which the heat capacity power function coefficients for α and β-quartz are applicable. These coefficients should not be used for temperatures in the vicinity of the α/β-quartz transition where equation (19) fails to represent adequately the heat capacity of quartz (see text). [j]Pankratz and Kelley (1964).

that differ from their experimental counterparts by 0 to 3.0 cal mole^{-1} (°K)$^{-1}$ at 200°C, 0.3 to 7.0 cal mole^{-1} (°K)$^{-1}$ at 500°C, and 0.7 to 3.0 cal mole^{-1} (°K)$^{-1}$ at 800°C. In contrast, those computed from the structural algorithm (eq 85) for the reference reactions in table 4 differ by 0.2 to 1.9 cal mole^{-1} (°K)$^{-1}$ at 200°, and 0.2 to 3.8 cal mole^{-1} (°K)$^{-1}$ at 500°, and 0.0 to 2.9 cal mole^{-1} (°K)$^{-1}$ at 800°C. The discrepancies are not systematic functions of temperature, but they are related indirectly to the Debye temperatures of the minerals and the extent to which eqs (81) and (85) represent accurately the calorimetric heat capacity data for the compounds in the temperature range of the "knee" in the heat capacity curves (fig. 6).

In most cases, the structural algorithm affords estimates of $C°_{P_r}$ at high temperatures that are within ~ 2 percent of the calorimetric values. Where the discrepancies are larger, even greater differences result from eq (81), which generally affords estimates within ~ 5 percent of the calorimetric values. Although the structural algorithm is thus more consistently reliable, either method of estimation may introduce as much

TABLE 6

Comparative summary of experimental and estimated standard molal heat capacities of minerals at high temperatures and 1 bar[a]

Mineral[b]	Computed (eq 19) from the experimental coefficients in columns 2 through 4 of table 5			Computed (eq 19) from the estimated coefficients in columns 6 through 8 of table 5			Computed (eq 19) from the estimated coefficients in columns 10 through 12 of table 5		
	200°C	500°C	800°C	200°C	500°C	800°C	200°C	500°C	800°C
Wollastonite	25.4	28.3	29.9	25.4	29.4	32.48 29.2	25.1	28.1	29.9
Clinoenstatite	24.0	27.2	29.1	24.2	28.4	31.70 28.4	24.3	27.4	29.2
Forsterite	35.1	39.4	42.1	34.6	39.7	43.62 40.3	33.3	38.7	43.1
Fayalite	38.0	41.4	46.0	39.4	44.3	48.3 45.0	39.9	44.1	46.8
Diopside	49.6	56.3	59.9	49.6	57.7	64.18 57.6	49.4	55.5	59.0
Akermanite	60.4	67.0	71.3	61.1	70.0	76.88 70.3	59.9	67.5	72.93 69.6
Merwinite	72.2	79.8	84.6	72.6	82.2	89.57 81.6	71.9	79.2	84.0
Low Albite	61.6	69.9	75.3	63.9	76.2	85.88 76.0	62.9	73.7	81.48 78.2
Microcline	62.3	71.0	76.2	65.3	78.0	88.11 78.2	63.0	71.7	77.6

[a] cal mole^{-1} (°K)$^{-1}$. [b] Formulas for the minerals are given in table 5.

as a cal mole^{-1} (°K)$^{-1}$ and a kcal mole^{-1} of error in calculated values of $S°_{P_r,T} - S°_{P_r,T_r}$ and $H°_{P_r,T} - H°_{P_r,T_r}$, respectively, at high temperatures. However, the errors in $S°_{P_r,T} - S°_{P_r,T_r}$ and $H°_{P_r,T} - H°_{P_r,T_r}$ tend to cancel in calculating $G°_{P_r,T} - G°_{P_r,T_r}$, which as a result is subject to less uncertainty than $H°_{P_r,T} - H°_{P_r,T_r}$. For example, it can be seen in figure 12 that a constant error of 1 cal mole^{-1} (°K)$^{-1}$ in $C°_{P_r,T}$ results in an error of ~ 360 cal mole^{-1} in $\Delta G°_{P_r,T}$ at 600°C, but the corresponding error in $\Delta H°_{P_r,T}$ is 575 cal mole^{-1}. It should also be noted that if estimated heat capacity coefficients are used for both product and reactant minerals in a given reaction, and if all of the estimates are consistent with one another, errors introduced by the estimates in the high-temperature thermodynamic properties of the minerals tend to cancel in calculating the standard molal entropies, enthalpies, and Gibbs free energies of reaction.

The importance of restricting regression coefficients used in estimation algorithms to the temperature ranges of their validity can also be assessed in table 6 and figure 11. Where two estimates are given for 800°C in table 6, the first corresponds to an extrapolated heat capacity generated from the set of estimated coefficients in table 5 for temperatures < 848°K. The second corresponds to an estimate based in part on the heat capacity coefficients for β-quartz, which is the stable polymorph

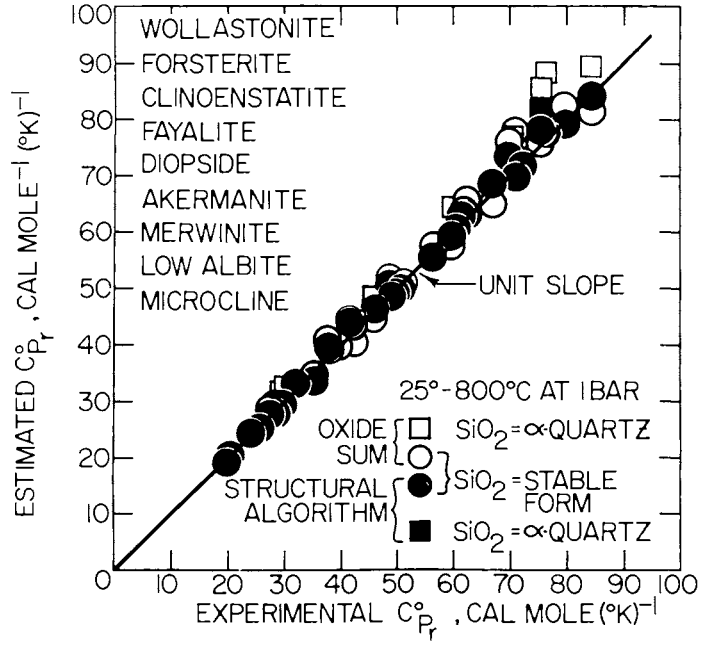

Fig. 11. Correlation of estimated and experimental standard molal heat capacities of minerals at 25°, 200°, 500°, and 800°C at 1 bar.

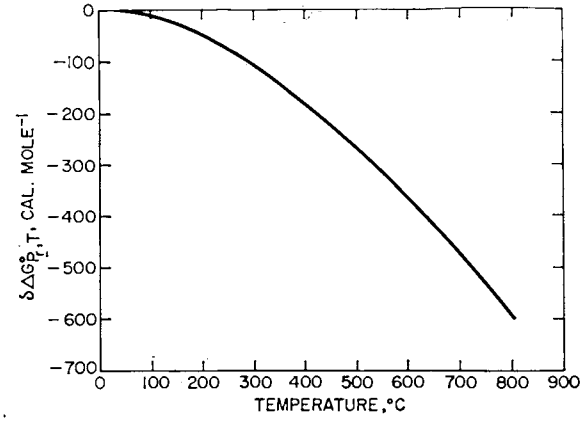

Fig. 12. Temperature dependence of the error in the apparent standard molal Gibbs free energy of formation of a mineral at 1 bar ($\delta\Delta G^{\circ}_{P_r,T}$) caused by a constant error of 1 cal mole^{-1} (°K)$^{-1}$ in $C^{\circ}_{P_r,T}$.

at 800°C and 1 bar. It can be seen that the differences between the latter values and the corresponding estimates generated in part from the coefficients for α-quartz are of the order of $\sim$ 3 cal mole^{-1} (°K)$^{-1}$ (mole SiO_2)$^{-1}$.

Despite the fact that replacing the coefficients for α-quartz with those for β-quartz for temperatures > 848°K introduces a discontinuity in estimates of $C^{\circ}_{P_r}$ for minerals as a function of temperature (fig. 13), it can be deduced from figures 11 and 13 that this procedure affords closer approximation of reality than using the coefficients for α-quartz to compute high-temperature estimates or replacing only the b and c coefficients of α-quartz with those for β-quartz, which requires estimates of $C^{\circ}_{P_r}$ to be continuous functions of temperature. Consideration of figure 117 indicates that this observation is also true for α, β, and γ-Fe_2O_3. It should perhaps be emphasized in this regard that the discontinuities in the estimated heat capacities of minerals as a function of temperature must be taken into account explicitly in calculating standard molal entropies and apparent standard molal enthalpies and Gibbs free energies of minerals from the integrals of eq (19).

The contribution of structural and zeolitic H_2O to the standard molal heat capacities of minerals can be estimated by assuming $\Delta C^{\circ}_{P_r,T} = 0$ for

$$\text{muscovite} \rightleftharpoons \text{dehydrated muscovite} + H_2O_{(s)} \tag{89}$$

and

$$\text{analcime} \rightleftharpoons \text{dehydrated analcime} + H_2O_{(z)}. \tag{90}$$

High-temperature calorimetric data reported by Pankratz (1964b) for muscovite and dehydrated muscovite led to the values of a, b, and c shown in table 2 for $H_2O_{(s)}$. Although comparable data are available for dehydrated analcime (Pankratz, 1968b), the heat capacity of analcime

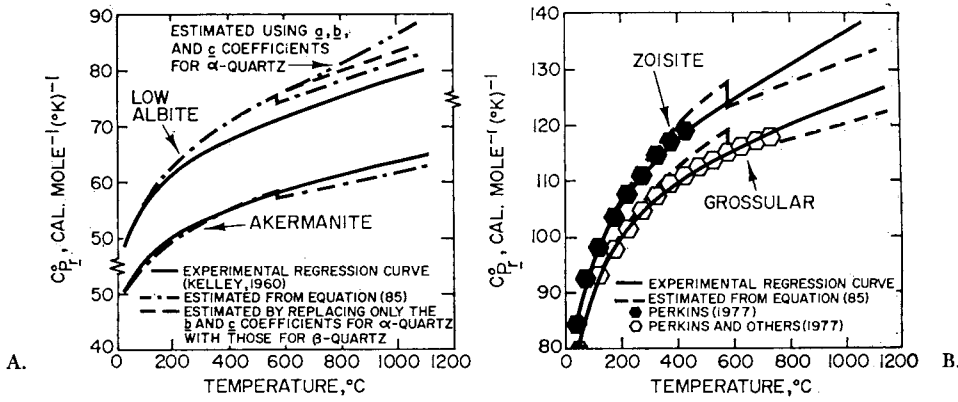

Fig. 13. Calculated, estimated, and experimental standard molal heat capacities of low albite, akermanite, zoisite, and grossular as a function of temperature at 1 bar (see text). Perkins (1977) refers to Dexter Perkins III (1977, written commun.).

has been measured only at temperatures $\leqslant$ 298.15°K. These data, together with corresponding heat capacities of dehydrated analcime, are plotted in figure 14. Although King (1955) took the dashed curve shown in figure 14A to be the best representation of his data above 280°K, it appears from the temperature dependence of the difference in the standard molal heat capacities of analcime and dehydrated analcime (fig. 15) that the solid curve in figure 14A is probably a better representation of his data. The three solid curves in figures 14 and 15, which are consistent with one another, suggest that $C^\circ_{P_r,H_2O_{(z)}}$ is essentially constant above 25°C. Accordingly, the *b* and *c* power function coefficients for $H_2O_{(z)}$ are shown as zero in table 2. As expected, $C^\circ_{P_r,T_r}$ for $H_2O_{(z)}$ is larger than that for $H_2O_{(s)}$. The latter value is nearly equal to the standard molal heat capacity of metastable ice at 25°C and 1 bar.

Estimated coefficients for eq (19) are given in table 7 for a large number of minerals for which high-temperature heat capacity data are not available. Most of the estimates were calculated from the structural algorithm, but in certain instances lack of pertinent calorimetric data

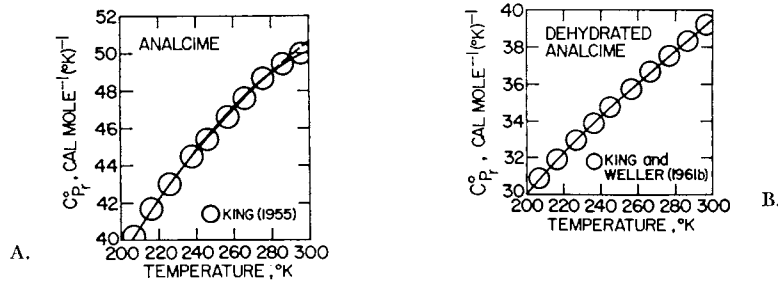

Fig. 14. Standard molal heat capacities of analcime and dehydrated analcime as a function of temperature at 1 bar.

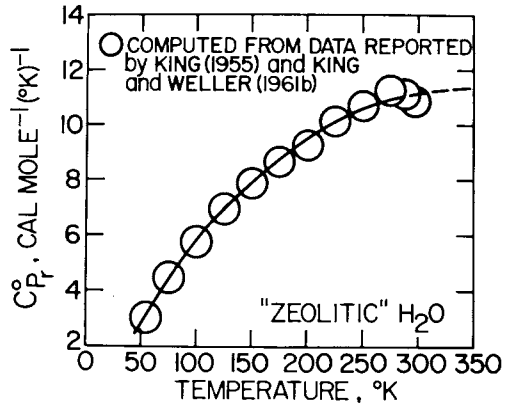

Fig. 15. Standard molal heat capacity of "zeolitic" H_2O as a function of temperature at 1 bar (see text).

made it necessary to use eqs (82) through (84). Up to four sets of coefficients are shown in table 7 for each mineral, together with the temperature ranges for which they are valid. It should be emphasized that none of the coefficients should be used for temperatures in the vicinity of the intermediate temperature limits shown in the table, which correspond to transition temperatures for minerals such as quartz or hematite (see above).

RETRIEVAL CALCULATIONS

Eqs (14), (27), and (30) through (32) together with standard molal entropies, volumes, and heat capacity power function coefficients given in tables 2, 3, 7, and 8 permit calculation of ΔG°_f from high pressure/temperature experimental data reported in the literature. The results of calculations of this kind for a large number of rock-forming minerals are summarized in table 8. The requisite values of $\Delta G^\circ_{r,P,T}$ were computed using experimentally determined equilibrium temperatures, mineral and fluid compositions, and (where necessary) a few selected calorimetric values of ΔH°_f.[8] The thermodynamic properties of H_2O, $SiO_{2(aq)}$, K^+, and Na^+ were calculated with the aid of equations and data summarized by Helgeson and Kirkham (1974a, 1976, and in press), Walther and Helgeson (1977), and Delany and Helgeson (1978).[9] Calculations for dehydration/decarbonation reactions were carried out assuming, alter-

[8] Calorimetric values of ΔH°_f were used only for α-quartz, periclase, magnetite, gibbsite, and monticellite (see below).

[9] In view of the recent paper by Hemingway and Robie (1977b) on the thermodynamic properties of the aluminum ion, it should be emphasized that the validity of none of the calculations reported in the present communication depends on the thermodynamic properties of Al^{+++}. It should also be noted that all the retrieval calculations discussed below that involved H_2O, Na^+, and/or K^+ took account of typographical errors in a number of the equations given by Helgeson and Kirkham (1974a and b, 1976), which are corrected in footnote 1 of Helgeson and Kirkham (1976), footnotes 1 and 2 of Walther and Helgeson (1977), and footnote 1 of Delany and Helgeson (1978).

nately, ideal and nonideal mixing of CO_2 and H_2O. Fugacity coefficients of CO_2 for the ideal case were computed from the Redlich-Kwong algorithm generated by Holloway and Reese (1974), which yields values of χ_{CO_2} in close agreement with the calculated values reported by Ryzhenko and Volkov (1971) at pressures below ~ 5 kb as well as with the corresponding states relations summarized by Breedveld and Prausnitz (1973). However, discrepancies among fugacity coefficients generated from different algorithms, regression equations, and/or extrapolation techniques used to represent various arrays of experimental data increase dramatically at high pressures, where relatively large differences are apparent in the values of χ_{CO_2} calculated by Mel'nik (1972), C. W. Burnham and V. J. Wall (1974, written commun.), Greenwood (1969, 1973), Holloway and Reese (1974), Holloway (1977), Ryzhenko and Malinin (1971), and Ryzhenko and Volkov (1971).

Comparative calculations of equilibrium temperatures for dehydration/decarbonation reactions were carried out with the aid of equations summarized by Holloway (1977) representing nonideal mixing of CO_2 and H_2O. The results of these calculations were compared with those based on the assumption of ideal mixing to assess quantitatively the reliability of Holloway's equations and the effects of nonideal mixing on equilibrium temperatures and fluid compositions. Although in some instances these effects appear to be large (see below), the modified Redlich-Kwong equation of state for gas mixtures employed by Holloway failed to afford consistent improvement in the agreement of calculated and experimental fluid compositions and equilibrium temperatures, which precluded general application of the equation in the retrieval calculations.

Because CO_2 exhibits large positive deviations from ideality at high pressures, considerable uncertainty attends retrieval of standard molal Gibbs free energies of formation at 25°C and 1 bar from high-pressure experimental data for decarbonation equilibria that involve more than 1 or 2 moles of CO_2. Fortunately, most of the experimental data reported in the literature for such equilibria pertain to 1 or 2 kb, where uncertainties introduced by calculated fugacity coefficients for CO_2 are not as great. Nevertheless, even under these conditions certain dehydration/decarbonation reactions are not suitable for retrieval of reliable standard molal Gibbs free energies of formation of minerals. These are reactions for which $\Delta H°_r$ is relatively small, which causes calculated equilibrium temperatures for a given composition to be highly sensitive to small errors in fugacity coefficients. For this reason, and because relatively large uncertainties attend calculation of the fugacity coefficients of CO_2 and H_2O in mixtures of these components (see above), experimental data for decarbonation equilibria were used in the retrieval calculations only in those (few) cases where data for dehydration reactions were not available.

Before carrying out retrieval calculations using experimental data for dehydration reactions, reversal temperature "brackets" reported in

TABLE 7

Summary of estimated standard molal heat capacity power function coefficients for minerals

Mineral Class	Name	Formula	$C^\circ_{P_r,T_r}$ [a,e]	[a,f,i]	[b,f,i] $\times 10^3$	[c,f,i] $\times 10^{-5}$	Temperature Range, °K [d]
Ortho and Ring Silicates	Monticellite	$CaMgSiO_4$	29.4	36.82 [t]	5.34 [t]	8.0 [t]	298-1400
	Hydrous Cordierite	$Mg_2Al_3(AlSi_5O_{18}) \cdot H_2O$	119.5	155.23	25.80	38.60	298-1700
	Lawsonite	$Ca_2Al_2Si_2O_7(OH)_2 \cdot H_2O$	70.5	81.80 [r]	23.36 [r]	16.26 [r]	298-848
				84.99 [r]	17.10 [r]	13.56 [r]	848-1000
	Almandine	$Fe_3Al_2Si_3O_{12}$	86.5	97.55 [j]	33.64 [j]	18.73 [j]	298-848
				107.09 [j]	14.86 [j]	10.63 [j]	848-1600
	Spessartine	$Mn_3Al_2Si_3O_{12}$	82.9	94.48 [j]	33.24 [j]	19.12 [j]	298-848
				104.05 [j]	14.46 [j]	11.02 [j]	848-1800
	Chloritoid	$FeAl_2SiO_5(OH)_2$	50.4	60.63	17.13	13.63	298-1000
	Staurolite	$Fe_2Al_9Si_4O_{23}(OH)_2$	153.8	207.12	36.94	57.22	298-1000
Chain and Band Silicates	Ca-Al Pyroxene	$CaAl_2SiO_6$	39.3	54.13	6.42	14.9	298-1400
	Clinoferrosilite	$FeSiO_3$	21.8	26.49	5.07	5.55	298-1600
	Hedenbergite	$CaFe(SiO_3)_2$	40.4	54.81	8.17	15.01	298-1600
	Aegerine	$NaFe(SiO_3)_2$	41.3	46.16	19.31	9.46	298-950
				52.42	10.01	7.68	950-1050
				50.27	10.89	7.68	1050-1400
	Anthophyllite	$Mg_7[Si_8O_{22}](OH)_2$	75.5	180.68	60.57	38.46	298-903
				197.54	41.61	13.34	903-1250
				199.52	41.61	13.34	1258-1500 [g]
	Ferrogedrite	$Fe_5Al_2(Al_2Si_6O_{22})(OH_2)$	169.8	196.27	58.39	39.01	298-903
				204.70	48.91	26.45	903-1258
				205.69	48.91	26.45	1258-1500 [g]

Mineral Class	Name	Formula	$C^*_{P_r,T_r}$ [a,e]	a [a,f,i]	b [b,f,i] × 10^3	c [c,f,i] × 10^{-5}	Temperature Range, °K [d]
Chain and Band Silicates	Tremolite	$Ca_2Mg_5[Si_8O_{22}](OH)_2$	154.9	188.22 [s]	57.29 [s]	44.82 [s]	298-800
	Ferrotremolite	$Ca_2Fe_5Si_8O_{22}(OH)_2$	169.2	197.93	58.95	41.17	298-800
	Fluortremolite	$Ca_2Mg_5Si_8O_{22}F_2$	151.0	183.74 [u]	55.25 [u]	43.73 [u]	298-800
	Cummingtonite	$Mg_7Si_8O_{22}(OH)_2$	152.5	185.24	58.61	41.66	298-800
	Grunerite	$Fe_7Si_8O_{22}(OH)_2$	172.5	198.83	60.93	39.55	298-800
	Edenite	$NaCa_2Mg_5(AlSi_7O_{22})(OH)_2$	162.5	199.71	48.78	46.01	298-848
				202.90	42.52	43.31	848-1000
	Ferroedenite	$NaCa_2Fe_5(AlSi_7O_{22})(OH)_2$	176.8	209.42	50.44	42.36	298-848
				212.61	44.18	39.66	848-1000
	Fluoredenite	$NaCa_2Mg_5(AlSi_7O_{22})F_2$	158.6	195.23	46.74	44.92	298-848
				198.42	40.48	42.22	848-1000
	Pargasite	$NaCa_2Mg_4Al(Al_2Si_6O_{22})(OH)_2$	161.7	205.80	41.66	50.21	298-1000
	Ferropargasite	$NaCa_2Fe_4Al(Al_2Si_6O_{22})(OH)_2$	173.2	213.57	42.99	47.29	298-1000
	Magnesiohastingsite	$NaCa_2Mg_4Fe(Al_2Si_6O_{22})(OH)_2$	164.8	203.80	49.55	47.80	298-950
				203.80	49.55	47.80	298-950
				210.06	40.25	46.02	950-1050
	Hastingsite	$NaCa_2Fe_4Fe(Al_2Si_6O_{22})(OH)_2$	176.3	211.57	50.88	44.88	298-950
				217.82	41.58	43.10	950-1050
				215.68	42.46	43.10	1050-1500 [g]

continued →

TABLE 7 (continued)

Mineral Class	Name	Formula	$C^{\circ}_{P_r,T_r}$ [a,e]	a [a,f,i]	b [b,f,i] × 10^3	c [c,f,i] × 10^{-5}	Temperature Range, °K [d]
Chain and Band Silicates	Glaucophane	$Na_2Mg_3Al_2Si_8O_{22}(OH)_2$	151.7	190.26	59.36	50.01	298-800
	Magnesioriebeckite	$Na_2Mg_3Fe_2Si_8O_{22}(OH)_2$	157.8	186.26	75.14	45.18	298-950
				198.77	56.54	41.63	950-1050
				194.48	58.30	41.63	1050-1500 [g]
	Riebeckite	$Na_2Fe_3Fe_2Si_8O_{22}(OH)_2$	166.4	192.09	76.14	42.99	298-950
				204.60	57.54	39.44	950-1050
				200.31	59.30	39.44	1050-1500 [g]
	Richterite	$Na_2CaMg_5Si_8O_{22}(OH)_2$	161.1	194.80	61.10	46.15	298-800
Framework Silicates	Analcime	$NaAlSi_2O_6 \cdot H_2O$	50.7	53.49 [h]	24.14 [h]	8.88 [h]	298-1000
	Leonhardite	$Ca_2(Al_4Si_8O_{24}) \cdot 7H_2O$	224.6	235.00 [g]	88.94 [g]	32.86 [g]	298-1000
	Wairakite	$Ca(Al_2Si_4O_4O_{12}) \cdot 2H_2O$	95.2	100.40	44.47	16.43	298-1000
	Laumontite	$Ca(Al_2Si_4O_{12}) \cdot 4H_2O$	118.0	123.20	44.47	16.43	298-1000
	Chabazite	$Ca(Al_2Si_4O_{12}) \cdot 6H_2O$	140.8	146.00	44.47	16.43	298-1000
	Epistilbite	$Ca(Al_2Si_6O_{16}) \cdot 5H_2O$	150.6	157.04	60.87	21.83	298-848
				163.42	48.35	16.43	848-1000
	Heulandite	$Ca(Al_2Si_7O_{18}) \cdot 6H_2O$	172.7	179.66	69.07	24.53	298-848
				189.23	50.29	16.43	848-1000
	Stilbite	$NaCa_2(Al_5Si_{13}O_{36}) \cdot 14H_2O$	375.5	390.55	137.68	49.84	298-848
				400.12	118.90	41.74	848-1000

Mineral Class	Name	Formula	$C°_{P_r,T_r}$ [a,e]	a [a,f,i]	b [b,f,i] × 10^3	c [c,f,i] × 10^{-5}	Temperature Range, °K [d]
Framework Silicates	Natrolite	$Na_2(Al_2Si_3O_{10}) \cdot 2H_2O$	90.8	95.76	40.08	15.06	298-848
				92.57	46.34	17.76	848-1000
	Na-Phillipsite	$Na_2(Al_2Si_5O_{14}) \cdot 5H_2O$	146.2	152.40	56.48	20.46	298-848
				155.59	50.22	17.76	848-1000
	K-Phillipsite	$K_2(Al_2Si_5O_{14}) \cdot 5H_2O$	149.9	152.66	60.24	18.45	298-848
				155.85	53.98	15.75	848-1000
	Ca-Phillipsite	$Ca(Al_2Si_5O_{14}) \cdot 5H_2O$	140.0	145.82	52.67	19.13	298-848
				149.01	46.41	16.43	848-1000
Sheet Silicates	Kaolinite	$Al_2Si_2O_5(OH)_4$	57.3	72.77[k]	29.20[k]	21.52[k]	298-1000
	Halloysite	$Al_2Si_2O_5(OH)_4$	57.3	72.77[ℓ]	29.20[ℓ]	21.52[ℓ]	298-1000
	Dickite	$Al_2Si_2O_5(OH)_4$	57.3	72.77[m]	29.20[m]	21.52[m]	298-1000
	Talc	$Mg_3Si_4O_{10}(OH)_2$	79.9	82.48[n]	41.61[n]	13.34[n]	298-800
	Antigorite	$Mg_{48}Si_{34}O_{85}(OH)_{62}$	1059.1	1,228.45[x]	513.76[x]	286.68[x]	298-848
				1,234.83[x]	501.24[x]	281.28[x]	298-1000
	Greenalite	$Fe_3Si_2O_5(OH)_4$	74.1	81.65	32.60	15.39	298-1000
	Minnesotaite	$Fe_3Si_4O_{10}(OH)_2$	88.5	88.31	42.61	11.15	298-800
	Celadonite	$KMgAlSi_4O_{10}(OH)_2$	66.9	80.25	25.30	18.54	298-1000
	Margarite	$CaAl(Al_2Si_2O_{10})(OH)_2$	75.8	102.50	16.35	28.05	298-848
				99.31	22.61	30.75	848-1000

continued →

TABLE 7 (continued)

Mineral Class	Name	Formula	$C^{\circ}_{P_r,T_r}$ [a,e]	a [a,f,i]	b [b,f,i] × 10^3	c [c,f,i] × 10^{-5}	Temperature Range, °K [d]
Sheet Silicates	Paragonite	$NaAl_2(AlSi_3O_{10})(OH)_2$	75.0	97.43	24.50	26.44	298-1000
	Phlogopite	$KMg_3(AlSi_3O_{10})(OH)_2$	85.0	100.61	28.78	21.50	298-1000
	Fluorphlogopite	$KMg_3(AlSi_3O_{10})F_2$		96.13	26.74	20.41	298-1000
	Annite	$KFe_3(AlSi_3O_{10})(OH)_2$	93.6	106.43	29.77	19.31	298-1000
	PD-oxyannite	$KFe_3AlSi_3O_{12}(H_{-1})$	84.2	88.34[j]	54.12[j]	18.06[j]	298-848
				97.91[j]	35.34[j]	9.96[j]	848-950
				116.68[j]	7.44[j]	4.63[j]	950-1050
				110.24[j]	10.08[j]	4.63[j]	1050-1100
	7A-Clinochlore	$Mg_5Al(AlSi_3O_{10})(OH)_8$	131.9	162.82	50.62	40.88	298-848
				166.01	44.36	38.18	848-1000[g]
	7A-Daphnite	$Fe_5Al(AlSi_3O_{10})(OH)_8$	146.2	172.53	52.28	37.23	298-848
				175.72	46.02	34.63	848-1000[g]
	7A-Amesite	$Mg_2Al(AlSiO_5)(OH)_4$	65.6	81.03	24.74	20.23	298-1000[g]
	7A-Chamosite	$Fe_2Al(AlSiO_5)(OH)_4$	71.4	84.91	25.40	18.77	298-1000[g]
	7A-Cronstedtite	$Fe_2Fe(FeSiO_5)(OH)_4$	77.5	84.79	41.84	12.48	298-950
				97.30	23.24	8.93	950-1050[g]
				93.01	25.00	8.93	1050-1500[g]
	14A-Clinochlore	$Mg_5Al(AlSi_3O_{10})(OH)_8$	136.8	166.50	42.10	37.47	298-1000[g]

Mineral Class	Name	Formula	$C^\circ_{P_r,T_r}$ [a,e]	a [a,f,i]	b [b,f,i] $\times 10^3$	c [c,f,i] $\times 10^{-5}$	Temperature Range, °K [d]
Sheet Silicates	14A-Daphnite	$Fe_5Al(AlSi_3O_{10})(OH)_8$	151.1	176.21	43.76	33.82	298-1000 [g]
	14A-Amesite	$Mg_4Al_2(Al_2Si_2O_{10})(OH)_8$	136.1	172.59	34.98	41.67	298-848 [g]
				169.40	41.24	44.37	848-1000 [g]
	Prehnite	$Ca_2Al(AlSi_3O_{10})(OH)_2$	80.8	91.60 [j]	37.82 [j]	19.60 [j]	298-848
				101.17 [j]	19.04 [j]	11.50 [j]	848-1800
	Sepiolite	$Mg_4Si_6O_{15}(OH)_2(OH_2)_2 \cdot (OH_2)_4$ [w]	168.0	157.92 [v]	104.30 [v]	18.68 [v]	298-800 [v]
Carbonates	Dolomite	$CaMg(CO_3)_2$	37.7	44.71 [h]	17.78 [h]	10.95 [h]	298-1000

[a] cal mole^{-1}(°K)$^{-1}$. [b] cal mole^{-1}(°K)$^{-2}$. [c] cal (°K) mole^{-1}. [d] Except where indicated otherwise, the numbers shown in this column designate the minimum experimental temperature range for the minerals and/or oxides used in the calculations (see tables 2, 5, and 8). [e] Computed from equation (19) and the coefficients shown above. [f] Calculated using estimates of a, b, and c shown above and/or experimental coefficients for minerals and/or oxides taken from tables 2, 5 and 8. Multiple sets of coefficients and temperature ranges are given where appropriate to avoid uncertainties inherent in using heat capacity coefficients for oxides and minerals outside of their temperature range of applicability (see text). The estimated coefficients should not be used for temperatures in the vicinity of phase transitions where equations (19) fails to represent adequately the heat capacities of polymorphs. [g] Extrapolated. [h] Computed assuming $\Delta C^\circ_{P_r,T} = 0$ for dolomite $\rightleftharpoons$ calcite + magnesite. The estimated coefficients apply to ordered dolomite. [i] Except where indicated otherwise, the values shown for a, b, and c were estimated from equations (86) through (88) assuming $\Delta C^\circ_{P_r,T} = 0$ for the reference reactions shown in table 3. [j] Computed from equations (82) through (84). [k] Computed assuming $\Delta C^\circ_{P_r,T} = 0$ for kaolinite + 3 periclase $\rightleftharpoons$ corundum + chrysotile. [l] Computed assuming $\Delta C^\circ_{P_r,T} = 0$ for halloysite $\rightleftharpoons$ kaolinite. [m] Calculated assuming $\Delta C^\circ_{P_r,T} = 0$ for dickite $\rightleftharpoons$ kaolinite. [n] Computed assuming $\Delta C^\circ_{P_r,T} = 0$ for talc + corundum pyrophyllite + 3 periclase. [p] Computed assuming $\Delta C^\circ_{P_r,T} = 0$ for analcime $\rightleftharpoons$ dehydrated analcime + $H_2O_{(z)}$. [q] Computed assuming $\Delta C^\circ_{P_r,T} = 0$ for leonhardite $\rightleftharpoons$ 2 wairakite + $3H_2O_{(z)}$ [r] Computed assuming $\Delta C^\circ_{P_r,T} = 0$ for lawsonite $\rightleftharpoons$ gehlenite + quartz + $H_2O_{(s)}$ + $H_2O_{(z)}$. [s] Computed assuming $\Delta C^\circ_{P_r,T} = 0$ for tremolite $\rightleftharpoons$ talc + 2 diopside. [t] Computed assuming $\Delta C^\circ_{P_r,T} = 0$ for monticellite $\rightleftharpoons$ wollastonite + periclase. [u] Computed using experimental Maier-Kelley heat capacity coefficients for α-CaF_2 (a = 14.30, b = 7.28×10^{-3}, and c = 0.47×10^5) reported by Kelley (1960). [v] Estimated by Stoessell (ms) assuming $\Delta C^\circ_{P_r} = 0$ for the reference reaction shown in table 3. [w] See footnote uu in Table 3. [x] Recalculated from the heat capacity coefficients reported by King and others (1967) for antigorite with the stoichiometry $Mg_3Si_2O_5(OH)_4$ to $Mg_{48}Si_{34}O_{85}(OH)_{62}$ using data given in table 2 (see text).

the literature were tested for internal consistency by comparing the pressure distribution of the brackets with Clapeyron slopes calculated independently from eqs (1), (27), and the approximation for solid phases represented by

$$V^\circ_{P,T} = V^\circ_{P_r,T_r} \tag{91}$$

using standard molal entropies, volumes, and heat capacity power function coefficients given in tables 2, 3, 7, and 8 for the minerals involved in the reaction. This procedure was also used to assess the relative reliability of data reported for various pressures by different investigators and to determine the extent to which the data warranted modification of standard molal third law entropies to take account of configurational contributions. Wherever possible, solubility measurements were correlated with independent observations of equilibrium pressures and temperatures. In certain instances it was necessary to invoke subjective judgement in choosing among conflicting sets of experimental data, but in most cases contradictions could be resolved by comparing the results of alternate calculations with experimental solubilities, calorimetric data, and/or geologic observations. In this way, optimum values of $\sigma^\circ_{r,P,T}$ were selected to satisfy available data. In all cases, at least one value of j in eq (31) in each matrix equation (eq 32) referred to a mineral indexed as j or i in the other matrix equations, which insured internal consistency in the computed values of ΔG°_f for all the minerals. Provision was included in the calculations for phase transitions, and wherever possible, experimental Clapeyron slopes were adopted for these equilibria. Values of ΔH°_f were calculated from the standard molal Gibbs free energies of formation retrieved from the high pressure/temperature data by evaluating

$$\Delta H^\circ_f = \Delta G^\circ_f + T\Delta S^\circ_f \tag{92}$$

where ΔS°_f stands for the standard molal entropy of formation from the elements in their stable form at 298.15°K and 1 bar. Relative uncertainties in the calculated values of ΔG°_f and ΔH°_f were assessed with the aid of equations summarized below.

Uncertainties and ambiguities.—Uncertainties and ambiguities inherent in calculating standard molal enthalpies and Gibbs free energies of formation of minerals from calorimetric data, solubility measurements, and experimental observations of phase equilibria have received considerable attention in recent years (Fyfe, Turner, and Verhoogen, 1958; Greenwood, 1971; Zen, 1971, 1972, 1973, 1977; Parks, 1972; Thompson, 1974a; Ulbrich and Merino, 1974; Anderson, 1976, 1977; Chatterjee, 1977). Nevertheless, the relative extent to which various experimental and interpretative factors contribute to these uncertainties is still a subject of conjecture and debate. Ambiguities and uncertainties commonly stem from inadequate compositional analyses of starting materials and reaction products, internal inconsistencies, inaccurate data reduction, erroneous assumptions, or failure to demonstrate reproducible reversibility. Other

uncertainties result from short-term experimental runs, failure to vary the proportions of reactants and products to promote achievement of stable equilibrium, unreliable experimental techniques, inaccurate cell parameters, lack of information concerning the ordering state of the reactants and products, changes induced by quenching, reliance on X-ray evidence for reaction progress, insufficient annealing, failure to optimize fluid to mineral ratios, sluggish reaction kinetics and metastability, undetected reaction products, indiscriminate use of both natural and synthetic materials, lack of compositional data for the fluid phase, and omission of numerical data from published reports of investigation. *Calculated uncertainties in standard molal Gibbs free energies of formation derived from such data are thus themselves highly uncertain.*

Experimental uncertainties in the standard molal third law entropies of most minerals at 25°C and 1 bar are of the order of a few tenths of a cal mole^{-1} (°K)$^{-1}$ or less, but in some instances entropy errors may exceed a cal mole^{-1} (°K)$^{-1}$. Corresponding uncertainties in calorimetric standard molal enthalpies of formation from the elements at 25°C and 1 bar range from $\sim$ 500 to $>$ 2000 cal mole^{-1}. As emphasized above, uncertainties of this order of magnitude in ΔH°_f are far too large to permit accurate calculation of equilibrium temperatures for high pressure/temperature univariant equilibria. This can be demonstrated by evaluating the finite difference derivative of

$$T = \frac{\Delta H^\circ_{r,P,T}}{\Delta S^\circ_{r,P,T}} \tag{93}$$

where $\Delta H^\circ_{r,P,T}$ and $\Delta S^\circ_{r,P,T}$ refer to the standard molal enthalpy and entropy of reaction for an unrestricted standard state with respect to pressure and temperature. The finite difference derivative (δ) of eq (93) can be written as

$$\delta T = \frac{\delta(\Delta H^\circ_{r,P,T}) - T\delta(\Delta S^\circ_{r,P,T})}{\Delta S^\circ_{r,P,T}} \tag{94}$$

Standard molal entropy changes accompanying dehydration reactions are commonly of the order of 20 cal mole^{-1} (°K)$^{-1}$, which means that for a "typical" dehydration temperature of 600°C, $\Delta H^\circ_{r,P,T} \approx 17{,}500$ cal mole^{-1}. It follows from eq (94) and these "representative" values of T, $\Delta S^\circ_{r,P,T}$, and $\Delta H^\circ_{r,P,T}$ that an uncertainty of $\pm$ 0.5 cal mole^{-1} (°K)$^{-1}$ in $\Delta S^\circ_{r,P,T}$ together with an uncertainty of $\pm$ 1 kcal mole^{-1} in $\Delta H^\circ_{r,P,T}$ results in an uncertainty of $\pm$ 72°C in equilibrium temperatures computed from the thermodynamic data. In contrast, if δT is known experimentally to be $\pm$ 10°C and $\Delta S^\circ_{r,P,T} = 20$ cal mole^{-1} (°K)$^{-1}$, it follows from

$$\delta(\Delta G^\circ_{r,P,T}) = -\Delta S^\circ_{r,P,T}\delta T \tag{95}$$

that an uncertainty of $\pm$ 10°C in T introduces an uncertainty of $\pm$ 200 cal mole^{-1} in $\sigma^\circ_{r,P,T}$, which is transmitted to computed values of ΔG°_f and ΔH°_f at 25°C and 1 bar. However, if experimental reversals are

available at more than one pressure, Clapeyron slope constraints may reduce considerably even this relatively small uncertainty. Because the Clapeyron equation requires reversals at all pressures to be consistent with one another, the maximum uncertainty in $\Delta G^\circ_{r,P,T}$ represented by δT at any one pressure may be reduced significantly by the distribution of reversal brackets at other pressures. Accordingly, uncertainties in values of ΔG°_f that satisfy more than one reversal may be much smaller than those attending retrieval of ΔG°_f from a single reversal. In addition, simultaneous consideration of more than one reaction at a series of pressures reduces relative uncertainties even further. As a result, the relative uncertainties in many of the calculated values of ΔG°_f discussed below are of the order of tens of calories mole^{-1}. Although the absolute uncertainties in ΔG°_f are certainly much greater, because the set of data given in table 8 is comprehensive, it matters little whether the absolute errors in the values of ΔG°_f are large, as long as the *relative* errors are small. This observation is valid for any internally consistent *set* of thermodynamic data, but its practical significance depends on whether additional data from other sources are required to carry out a given calculation. Despite the fact that relative uncertainties in the standard molal volumes, entropies, and heat capacities of minerals used in retrieval calculations are magnified and transmitted to values of ΔG°_f derived from high pressure/temperature phase equilibrium data, extrapolation errors are minimal if the same values of $V^\circ_{P_r,T_r}$, $S^\circ_{P_r,T_r}$, and a, b, and c in eq (19) are used in all subsequent calculations.

Uncertainties in Clapeyron slopes of univariant curves computed from standard molal volume data using calorimetric and/or estimated values of $S^\circ_{P_r,T_r}$ and standard molal heat capacity coefficients can be assessed by taking the finite difference derivative of

$$\left.\frac{dP}{dT}\right|_{\Delta G^\circ_r = 0} = \frac{\Delta S^\circ_r}{\Delta V^\circ_r} \tag{96}$$

which can be written for $\Delta G^\circ_r = 0$ as

$$\delta(dP/dT) = \frac{\delta(\Delta S^\circ_r)}{\Delta V^\circ_r} - \frac{\Delta S^\circ_r \delta(\Delta V^\circ_r)}{(\Delta V^\circ_r)^2} \tag{97}$$

where ΔG°_r, ΔV°_r, and ΔS°_r again refer to the standard molal Gibbs free energy, volume, and entropy of reaction for an unrestricted standard state with respect to temperature and pressure. If we take 20 cal mole^{-1} (°K)$^{-1}$ and 20 cm^3 mole^{-1} as "typical" values of ΔS°_r and ΔV°_r for dehydration reactions, it follows from eq (97) that uncertainties of $\pm$ 0.5 cal mole^{-1} (°K)$^{-1}$ in ΔS°_r and $\pm$ 0.5 cm^3 mole^{-1} (°K)$^{-1}$ in ΔV°_r (which are probably representative of univariant reactions in general) result in an uncertainty of $\pm$ 2 bars (°K)$^{-1}$ for a Clapeyron slope of 42 bars (°K)$^{-1}$. Uncertainties of this order of magnitude introduce corresponding uncertainties of $\sim \pm$ 1°C kb^{-1} in calculated equilibrium tem-

peratures at higher pressures. In general, uncertainties in Clapeyron slope calculations caused by uncertainties in standard molal entropies, heat capacities, and volumes of minerals have a negligible effect on retrieval calculations if the absolute values of $\Delta V°_r$ and $\Delta S°_r$ are of the order of 10 cm^3 $mole^{-1}$ and 10 cal $mole^{-1}$ $(°K)^{-1}$ or more. However, if $\Delta S°_r$ and $\Delta V°_r$ are small, as they are for solid/solid phase transitions and certain dehydration reactions, calculated values of dP/dT may be affected drastically by small errors in $\Delta S°_r$ and/or $\Delta V°_r$.

As emphasized by Fyfe, Turner, and Verhoogen (1958), uncertainties attending both experimental determination and thermodynamic calculation of equilibrium temperatures are controlled to a large extent by the magnitude of $\Delta S°_r$. For example, it can be deduced from the curves in figure 16 that $\Delta S°_r$ is small for reaction 1 and large for reaction 2. Consequently, the uncertainty bracket represented by *ab* is much greater for reaction 1 than reaction 2. Although these brackets are symmetrical in the case of reactions 1 and 2, it can be seen that the equilibrium temperature for reaction 3 is close to the upper end of the uncertainty interval represented by *ab*. The latter case is typical of dehydration reactions taking place at pressures < 1 kb at temperatures from $\sim$ 300° to 500°C, where the heat capacity of H_2O increases dramatically with increasing temperature.

The energy required to activate the three reactions discussed above is represented in figure 16 by intervals *a* and *b*. If the kinetics of the reactions near equilibrium are controlled primarily by their chemical affinities (which seems likely; see, for example, Prigogine, 1967; Aagaard and Helgeson, 1977; Helgeson, 1978), it follows that the small value of

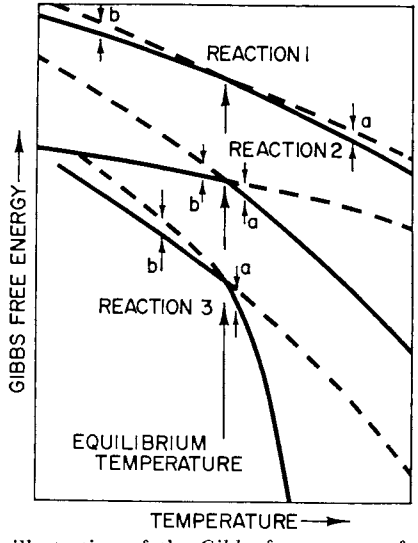

Fig. 16. Schematic illustration of the Gibbs free energy of three hypothetical systems as a function of temperature at constant pressure (see text).

$\Delta S°_r$ for reaction 1 promotes metastability, which is also the case for reaction 3 at low temperatures.

The chemical affinity of the rth reaction ($\mathbf{A}_r$) is defined by

$$\mathbf{A}_r = -\frac{dQ_{irrev,r}}{d\xi_r} \tag{98}$$

where $dQ_{irrev,r}$ stands for the inexact differential of the heat associated with the rth irreversible reaction, and ξ_r represents the progress variable for the process. However, $\mathbf{A}_r$ can also be expressed as

$$\mathbf{A}_r = -\left(\frac{\partial G}{\partial \xi_r}\right)_{P,T} = -\sum_i \mu_i \hat{n}_{i,r} = RT \ln K_r/Q_r \tag{99}$$

where G refers to the Gibbs free energy of the system, $\hat{n}_{i,r}$ represents the stoichiometric coefficient of the ith species involved in the rth reaction ($\hat{n}_{i,r} = dn_i/d\xi_r$, where n_i stands for the number of moles of the ith species in the system), K_r denotes the equilibrium constant for the reaction, and

$$Q_r \equiv \prod_i a_i^{\hat{n}_{i,r}} \tag{100}$$

where a_i stands for the activity of the ith species in the system. At equilibrium, $Q_r = K_r$ and $\mathbf{A}_r = 0$. The rate at which reactions among minerals and aqueous solutions proceed from an activated state toward equilibrium is a function of $\mathbf{A}_r$. If we regard such reactions as sequences of elementary steps in the overall process, near equilibrium the rate of the rth reaction ($\hat{r}_r$) can be expressed as (Prigogine, 1967)

$$\hat{r}_r = \frac{d\xi_r}{dt} = \frac{k_r \mathbf{A}_r}{RT} \tag{101}$$

where k_r is the rate constant given by

$$k_r = A_r e^{-\Delta E^*_r/RT} \tag{102}$$

where A_r designates the pre-exponential factor (which includes the equilibrium concentrations of the species involved in the reaction) and ΔE^*_r stands for the activation energy for the reaction. Because in most cases the volume change associated with the activation process is negligible, and ΔE^*_r is insensitive to changes in pressure and temperature, $\Delta H^*_r \approx \Delta E^*_r$, and both ΔS^*_r and ΔH^*_r can be regarded as constants. Taking account of the fact that ΔE^*_r is positive, it follows from eq (102) that the rates of reactions caused by increasing temperature may be considerably faster than those of reactions caused by decreasing temperature. Because of this, kinetic constraints may result in asymmetric uncertainties in experimentally determined reversal temperatures. These constraints as well as others affecting attainment of equilibrium are discussed in detail by Fyfe, Turner, and Verhoogen (1958).

Many of the observations summarized above concerning the effect of uncertainties in thermodynamic data on calculated equilibrium temperatures for univariant equilibria apply also to multivariant reactions among minerals, gases, and/or aqueous species. However, in the latter cases small calorimetric uncertainties in ΔH°_r and ΔS°_r may be manifested by large errors in computed activities or fugacities instead of equilibrium temperatures. Conversely, small errors in fluid compositions determined experimentally are magnified in corresponding values of $\Delta G^\circ_{r,P,T}$. For example, if accurate values of χ_{CO_2} and χ_{H_2O} are known at a given pressure and temperature, it follows from eqs (28) and (44), together with the constraint

$$X_{CO_2} + X_{H_2O} = 1 \tag{103}$$

that

$$\begin{aligned}\delta(\Delta G^\circ_{r,P,T}) &= -2.303RT\ \delta(\log K_{P,T}) \\ &= -RT\left(\frac{\hat{n}_{CO_2} - X_{CO_2}\ (\hat{n}_{CO_2} + \hat{n}_{H_2O})}{X_{CO_2}\ X_{H_2O}}\right)\delta X_{CO_2}\end{aligned} \tag{104}$$

for reactions involving only CO_2, H_2O, and stoichiometric minerals. Hence if $\hat{n}_{CO_2} = 3$ and $\hat{n}_{H_2O} = -1$ (which is typical), a value of $X_{CO_2} = 0.5$ must be known to $\pm$ 0.01 at 500°C to keep the uncertainty in calculated values of $\Delta G^\circ_{r,P,T}$ within $\sim \pm$ 125 cal mole^{-1}. Note that the uncertainty in $\Delta G^\circ_{r,P,T}$ is magnified considerably for a given δX_{CO_2} as either X_{CO_2} or X_{H_2O} become small. It is also under these conditions that errors stemming from the assumption of ideal mixing of CO_2 and H_2O may have a large effect on calculated equilibrium temperatures, which underscores the inadvisability of retrieving values of ΔG°_f for minerals from temperature-X_{CO_2} data in the dilute regions of concentration without incorporating reliable fugacity coefficients for CO_2 and H_2O in CO_2–H_2O mixtures. In general, calculated equilibrium temperatures and fluid compositions are highly sensitive to χ_{CO_2} in H_2O-rich fluids and χ_{H_2O} in CO_2-rich fluids. As a result, small errors in these fugacity coefficients may result in large errors in σ°_r.

The effect of uncertainties in χ_{H_2O} and χ_{CO_2} on σ°_r for reversible reactions among stoichiometric minerals and a CO_2–H_2O fluid can be assessed from

$$\delta(\Delta G^\circ_{r,P,T}) = -RT(\hat{n}_{CO_2}\ \delta(ln\ \chi_{CO_2}) + \hat{n}_{H_2O}\ \delta(ln\ \chi_{H_2O})) \tag{104A}$$

which can be derived for a given (constant) pressure, temperature, and fluid composition from eqs (28), (44), and (103). If we again let $\hat{n}_{CO_2} = 3$ and $\hat{n}_{H_2O} = -1$, it follows from eq (104A) that errors of $\pm$ 0.1 in the natural logarithms of χ_{CO_2} and χ_{H_2O} may result in a corresponding error of $\sim \pm$ 600 cal mole^{-1} in ΔG°_r, which would be transmitted in retrieval calculations to σ°_r and hence to calculated values of ΔG°_f. Errors in calculated equilibrium temperatures caused by uncertainties in fugacity co-

efficients can be computed for accurately known fluid compositions by evaluating

$$\delta T = \frac{RT^2}{\Delta H^\circ_{r,P,T}} \left(\hat{n}_{CO_2}\, \delta(ln\ \chi_{CO_2}) + \hat{n}_{H_2O}\, \delta(ln\ \chi_{H_2O})\right) \qquad (104B)$$

This relation can be derived by taking account of the van't Hoff equation. Assuming $\Delta H^\circ_{r,P,T} = 35$ kcal mole^{-1} at 500°C for a reaction in which $\hat{n}_{CO_2} = 3$ and $\hat{n}_{H_2O} = -1$ (which is reasonable), evaluation of eq (104B) for uncertainties of $\pm$ 0.1 in $ln\ \chi_{CO_2}$ and $ln\ \chi_{H_2O}$ indicates that errors of the order of $\pm$ 14°C may result in predicted equilibrium temperatures for a given X_{CO_2}.

Under certain circumstances, uncertainties in $ln\ \chi_{CO_2}$ and $ln\ \chi_{H_2O}$ arising from experimental error, equation of state extrapolations, and/or erroneous assumptions regarding ideality or nonideality in CO_2–H_2O mixtures may well exceed $\pm$ 0.1. Because these uncertainties are magnified by RT in eq (104A) and $RT^2/\Delta H^\circ_{r,P,T}$ in eq (104B), considerable care must be exercised in retrieving standard molal Gibbs free energies of formation of minerals from experimental temperature-X_{CO_2} data. The latter observation applies also to retrieval of values of ΔG°_f from solubility measurements. For example, it follows from the first identity in eq (104) that $\hat{n}_{SiO_{2(aq)}} \log a_{SiO_{2(aq)}}$ must be known to $\pm$ 0.03 to preclude errors > 100 cal mole^{-1} in computed values of ΔG°_r for desilication reactions at 500°C.

Relative uncertainties in the values of ΔG°_f and ΔH°_f shown in table 8 are discussed below, but no absolute counterparts are given in the table. Owing to limitations imposed by simultaneous consideration of multiple equilibria and the diverse sources of experimental ambiguities discussed above, attempts to assign with confidence absolute numerical uncertainties to the computed values of ΔG°_f and ΔH°_f were unsuccessful. In fact, these efforts led to the conclusion that (in contrast to arguments advanced by Zen, 1972) weighting vagaries and the nonrandom nature of experimental uncertainties inherent in most high pressure/temperature phase equilibrium data preclude meaningful application of a statistical approach to assigning absolute numerical uncertainties to values of ΔG°_f and ΔH°_f retrieved from such data.[10] This is particularly true of averaging techniques such as the practice of assigning the square root of the sum of the squares of the relative uncertainties for each experimental observation to the thermodynamic properties of minerals retrieved from high pressure/temperature phase equilibrium data. Although estimates of absolute uncertainties could be made with the aid of Monte Carlo calculations (Anderson, 1976), the task would be monumental, and the usefulness of the results would be highly questionable (G. M. Anderson, 1977, written commun.). It thus appears preferable (at least to us) to give no estimates of absolute uncertainties,

[10] It is also for these reasons that satistical regression analysis of experimental reversal temperatures and solubility data commonly leads to unacceptable uncertainties in values of ΔG°_f retrieved from the data.

rather than assigning values that may be both inaccurate and misleading. It should perhaps be emphasized in this regard that differences between the values of $\Delta G°_f$ and $\Delta H°_f$ derived in the present study and those reported elsewhere for the same minerals are not necessarily valid measures of absolute uncertainties. Calculation of uncertainties from comparisons of this kind must take into account all the equilibria employed in the retrieval calculations.

The fact that absolute uncertainties are not given in table 8 affords no justification in itself for questioning the validity of the thermodynamic data shown in the table. To the contrary, because in most cases the *relative* uncertainties in the calculated values of $\Delta G°_f$ and $\Delta H°_f$ are small (of the order of a hundred cal mole^{-1} or less), and because with only a few exceptions (see below), no calorimetric values of $\Delta H°_f$ with aggregate absolute uncertainties > 400 cal mole^{-1} were used in any of the retrieval calculations, it can be argued subjectively that the absolute uncertainties in the values of $\Delta G°_f$ and $\Delta H°_f$ derived in the present study are almost certainly much smaller than those inherent in their calorimetric counterparts. This observation is strongly supported by comparison of equilibrium constants and univariant curves generated from the thermodynamic data in table 8 with the myriad of experimental observations summarized in the following pages.

THE SYSTEM SiO_2

The thermodynamic properties of quartz, coesite, cristobalite, chalcedony, and amorphous silica are shown in table 8. In the case of α-quartz, the value of $\Delta H°_f$ corresponds to that obtained from calorimetric measurements, but the standard molal enthalpies of formation of the other SiO_2 polymorphs were retrieved from high-temperature solubility measurements reported in the literature.

Quartz.—The standard molal volume and calorimetric values of $S°_{P_r,T_r}$ and $\Delta H°_f$ given by Robie and Waldbaum (1968) for α-quartz were adopted in the present study. This value differs by only 12 cal mole^{-1} from that recommended by the CODATA task group in 1975 (CODATA, 1976), which is the value adopted by Hemingway and Robie (1977a). The heat capacity power function coefficients shown in table 8 for α and β-quartz were taken from Kelley (1960), who reports 290 cal mole^{-1} for the apparent standard molal enthalpy of transition ($\Delta H°_t$) at 848°K and 1 bar. This value, which is 116 cal mole^{-1} larger than that reported by Stull and Prophet (1971), was used together with the transition temperature at 1 bar (848°K) and the slope of the curve shown in figure 17 (38.5 bar (°K)$^{-1}$) to calculate the apparent standard molal entropy and volume of transition ($\Delta S°_t$ and $\Delta V°_t$, respectively) given in table 8. Because the standard molal volume of β-quartz was measured at 575°C and 1 bar (table 2), the calculated value of $\Delta V°_t$ (0.372 cm^3 mole^{-1}) requires the standard molal volume of α-quartz to be 23.35 cm^3 mole^{-1} at the transition temperature at 1 bar. However, thermal expansion data (Skinner, 1966) indicate that the standard molal

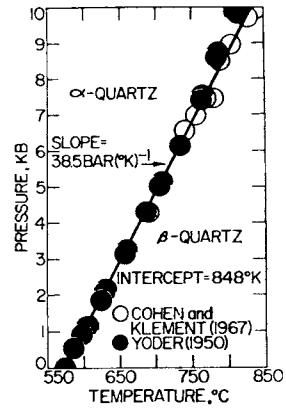

Fig. 17. Calculated equilibrium pressures and temperatures (curve) and experimental data (symbols) documenting the α/β-quartz transition at high pressures and temperatures.

volume of α-quartz reaches 23.35 cm^3 mole^{-1} at $\sim$ 520°C and 1 bar, which is in the vicinity of the lowest temperature at which the standard molal heat capacity of α-quartz exhibits evidence of the occurrence of a lambda transition with increasing temperature (see above). This observation reinforces evidence obtained calorimetrically by O'Neill and Fyans (ms) suggesting that the α/β-quartz transition is a displacive lambda transition, rather than a superimposed lambda/first order transition (fig. 3C). In contrast, if the value of $\Delta H°_t$ reported by Stull and Prophet (174 cal mole^{-1}) is used in the calculation, the computed value of $\Delta V°_t$ (0.223 cm^3 mole^{-1}) requires V° for α-quartz to be 23.50 cm^3 mole^{-1} at the transition temperature. It can be seen in figure 3D that the standard molal volume of α-quartz reaches this value at $\sim$ 565°C, which is well above the temperature at which the lambda transition apparently sets in, but ten degrees below the transition temperature. It should perhaps be emphasized that if an apparent standard molal volume of transition consistent with the curve shown in figure 3D is adopted (0.12 cm^3 mole^{-1}), $\Delta H°_t$ must be 94 cal mole^{-1} to be consistent with the position and slope of the curve in figure 17. Few of the calorimetric data available are consistent with such a small value of $\Delta H°_t$.

Although the curves representing the standard molal volume and heat capacity of α-quartz in figure 3 indicate that the phase begins to disorder as temperature increases above $\sim$ 700°K, the bulk of the shift in the bond angles responsible for the change in symmetry between the two polymorphs takes place within a few degrees of 848°K, where the α/β-quartz transition is rapidly reversible. As a consequence, pressure-temperature isopleths representing displacive disorder manifested by detectable changes in symmetry are telescoped together, resulting in what appears experimentally to be a single univariant curve (fig. 17). The α/β-quartz transition at 848°K can thus be regarded for practical

purposes as a quasi-first-order transition. Because β-quartz is unquenchable, no thermodynamic properties are given for this polymorph in table 8.

The value of $\Delta V°_t$ shown in table 8 is compatible with the standard molal volume of β-quartz at 575°C in table 2, but (as noted in previous discussion) not with the assumption that $V°_{P,T} = V°_{P_r,T_r}$ for α-quartz. This inconsistency (which is the only one of its kind encountered in the present study) can be resolved by incorporating provision for the thermal expansion of α-quartz in thermodynamic calculations. For example, if we designate the temperature and pressure of transition as T_t and P_t, respectively, and assume that the apparent standard molal volume and entropy of transition are independent of pressure and temperature (see above), the thermodynamic consequences of the expansibility and compressibility of α-quartz can be approximated by writing

$$\left(\frac{\partial V°_\alpha}{\partial T}\right)_P = \frac{V°_{\alpha,P_t,T_t} - V°_{\alpha,P_t,T_r}}{T_t - T_r} \tag{105}$$

where $V°_{\alpha,P_t,T_t}$ and $V°_{\alpha,P_t,T_r}$ correspond to the standard molal volume of α-quartz at the subscripted pressures and temperatures. Eq (105) is based on the observation that $(\partial V°/\partial T)_P$ for α-quartz is essentially independent of temperature at 1 bar (fig. 7). It thus follows that we can assume in a first approximation that $(\partial C°_P/\partial P)_T = -T(\partial^2 V°/\partial T^2) \approx 0$.

It can be seen in figure 8 that $(\partial V°/\partial P)_T$ for α-quartz is also essentially constant at 25°C and pressures below ~ 30 kb, which permits us to write

$$V°_{\alpha,P,T_r} = V°_{\alpha,P_r,T_r} + c_\alpha (P - P_r) \tag{106}$$

where c_α stands for $(\partial V°_\alpha/\partial P)_{T_r}$. Combining eqs (105), (106), and

$$V°_{\alpha,P,T} = V°_{\alpha,P,T_r} + \left(\frac{\partial V°_\alpha}{\partial T}\right)_P (T - T_r) \tag{107}$$

with

$$T_{t,P} = T_{t,P_r} + k^{-1} (P - P_r) \tag{108}$$

leads to

$$V°_{\alpha,P,T} = V°_{\alpha,P_r,T_r} + c_\alpha (P - P_r) + \frac{(V°_{\alpha,P_t,T_t} - V°_{\alpha,P_r,T_r} - c_\alpha (P - P_r))(T - T_r)}{T_{t,P_r} + k^{-1} (P - P_r) - T_r} \tag{109}$$

where k refers to the slope of the univariant curve in figure 17. Note that $(\partial V°_\alpha/\partial T)_P$ in eqs (105) and (107) is constrained to be independent of temperature but not of pressure. Conversely, $(\partial V°_\alpha/\partial P)_T$ is taken to be independent of pressure but not of temperature.

If we now combine the integral of eq (109) with

$$\Delta G°_{\beta,P*,T} - \Delta G°_{\beta,P_r,T} = \int_{P_r}^{P*} V°_{\beta,T} dP = V°_{\beta,P_r,T_t} (P* - P_r) \tag{110}$$

we can write for the stable polymorph of quartz at any given pressure and temperature,

$$\Delta G^\circ_{P,T} - \Delta G^\circ_{P_r,T} = V^\circ_{\alpha,P_r,T_r}(P - P^*) + V^\circ_{\beta,P_r,T_t}(P^* - P_r) - \frac{c_\alpha(2P_r(P - P^*) - (P^2 - P^{*2}))}{2} - c_\alpha \mathbf{k}(T - T_r)(P - P^*) + \mathbf{k}(b_\alpha + a_\alpha c_\alpha \mathbf{k})(T - T_r)(\ln(a_\alpha + \mathbf{k}^{-1}P)/(a_\alpha + \mathbf{k}^{-1}P^*)) \quad (111)$$

where P^* stands for P_t if $T > T_{t,P_r}$, but $P^* = P_r$ for $T \leqslant T_{t,P_r}$ and

$$a_\alpha \equiv T_{t,P_r} - \mathbf{k}^{-1}P_r - T_r \quad (112)$$

and

$$b_\alpha \equiv V^\circ_{\alpha,P_t,T_t} - V^\circ_{\alpha,P_r,T_r} + c_\alpha P_r \quad (113)$$

The corresponding expression for the standard molal entropy appears as

$$S^\circ_{P,T} - S^\circ_{P_r,T} = -\mathbf{k}(b_\alpha + a_\alpha c_\alpha \mathbf{k})(\ln(a_\alpha + \mathbf{k}^{-1}P)/(a_\alpha + \mathbf{k}^{-1}P^*)) + c_\alpha \mathbf{k}(P - P^*) \quad (114)$$

which permits calculation of $\Delta H^\circ_{P,T} - \Delta H^\circ_{P_r,T}$ from

$$\Delta H^\circ_{P,T} - \Delta H^\circ_{P_r,T} = \Delta G^\circ_{P,T} - \Delta G^\circ_{P_r,T} + T(S^\circ_{P,T} - S^\circ_{P_r,T}) \quad (115)$$

Values of $\Delta G^\circ_{\alpha,P,T}$ computed from eqs (14) and (111) consistent with $\Delta V^\circ_t = 0.372$ cm^3 mole^{-1}, $V^\circ_{\alpha,P_r,T_r} = 22.688$ cm^3 mole^{-1}, $V^\circ_\beta = 23.72$ cm^3 mole^{-1}, $\mathbf{k} = 38.5$ bar (°K)$^{-1}$, and $c_\alpha = 4.973 \times 10^{-5}$ cm^3 mole^{-1}

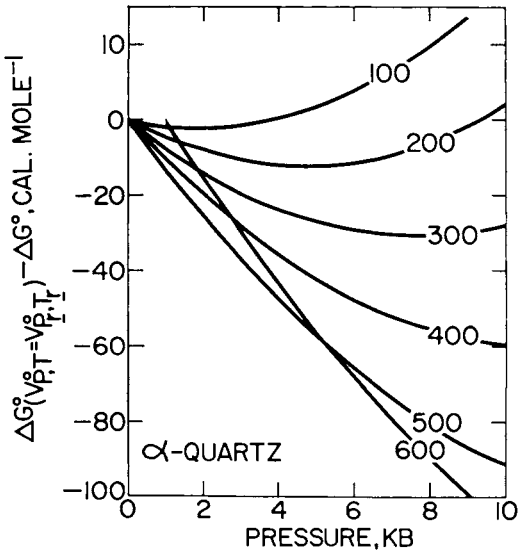

Fig. 18. Difference in the apparent standard molal Gibbs free energy of α-quartz computed assuming $V^\circ_{P,T} = V^\circ_{P_r,T_r}$ and that generated from eq (111) as a function of pressure at constant temperature (labeled in °C).

bar^{-1} differ from corresponding values calculated assuming $V°_{\alpha,P,T} = V°_{\alpha,P_r,T_r}$ by up to $\sim$ 100 cal mole^{-1} at pressures below 10 kb (fig. 18). Although in most cases differences of this order of magnitude have a negligible effect on thermodynamic calculation of mineral stabilities, eq (111) insures compatibility of such calculations with the univariant curve shown in figure 17. For this reason, and because the approach described above affords better approximation of the thermodynamic behavior of α-quartz at high pressures than the assumption that $V°_{\alpha,P,T} = V°_{\alpha,P_r,T_r}$, eqs (111), (114), and (115) were used in the present study to represent the pressure dependence of $\Delta G°_{P,T}$, $S°_{P,T}$, and $\Delta H°_{P,T}$ of quartz.

Coesite.—Experimental observations of the quartz/coesite transition are summarized in figure 19, where it can be seen that the calculated univariant curve for the transition is slightly curved. The Clapeyron slope of the curve is consistent with calorimetric data obtained by Holm, Kleppa, and Westrum (1967), who report $S°_{P_r,T_r} = 9.65$ cal mole^{-1} (°K)$^{-1}$ for coesite. The results of their high-temperature drop calorimetry experiments indicate that the difference in the standard molal heat capacity of coesite and quartz is essentially independent of temperature and equal to 0.22 cal mole^{-1} (°K)$^{-1}$. This value is identical to that at 25°C obtained from low-temperature heat capacity measurements (Holm, Kleppa, and Westrum, 1967). Taking the standard molal volume of coesite to be proportional to that of quartz and adding 0.22 cal mole^{-1} (°K)$^{-1}$ to the a heat capacity coefficients for α and β quartz generated the value of $\Delta G°_f$ for coesite in table 8 from the experimental data shown in figure 19. It can be deduced from the agreement of the curve with

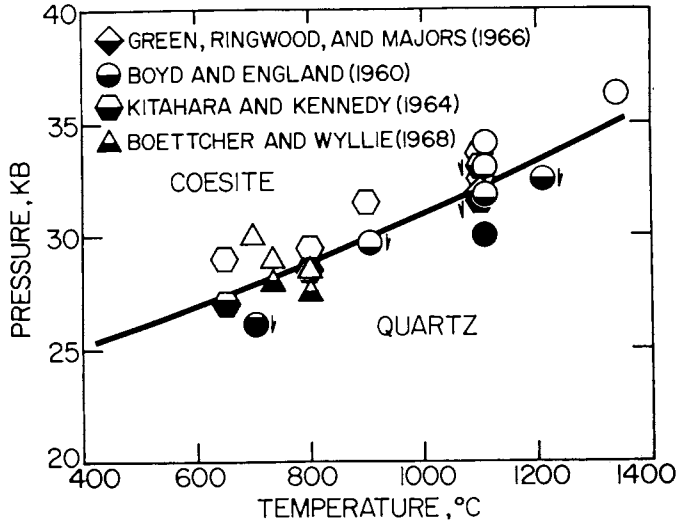

Fig. 19. Calculated equilibrium pressures and temperatures (curve) and experimental data (symbols) documenting the quartz/coesite transition at high pressures and temperatures.

the reversals shown in the figure that the calorimetric heat capacity and entropy data reported by Holm, Kleppa, and Westrum are consistent with the high pressure/temperature phase equilibrium data, as are their relative heat of solution measurements at 970°K and 1 bar. They report 750 ± 150 cal $mole^{-1}$ $(°K)^{-1}$ for the enthalpy change accompanying transformation of quartz to metastable coesite at 970°K and 1 bar, which compares favorably with the corresponding value of 888 cal $mole^{-1}$ calculated from the thermodynamic data for quartz and coesite given in table 8. Nevertheless, because the standard molal entropy of transition is only ~ −0.5 cal $mole^{-1}$ $(°K)^{-1}$ at high pressures and temperatures, the discrepancy of 138 cal $mole^{-1}$, together with the assumptions Holm, Kleppa, and Westrum made concerning the pressure dependence of the standard molal volumes of quartz and coesite introduced isobaric differences of more than 500°C in the univariant curve they predicted compared to that shown in figure 19. Corresponding uncertainties in the calorimetric data reported by Holm, Kleppa, and Westrum (1967) for the coesite/stishovite transition at 1 bar, combined with large uncertainties in the experimental data at higher pressures reported by Sclar and others (1962), Wentorf (1962), Stishov (1963), and others precludes reliable calculation of the thermodynamic properties of stishovite.

Chalcedony, cristobalite, and amorphous silica.—The thermodynamic data given in table 8 for these minerals (which are consistent with those shown for quartz) were adopted by Walther and Helgeson (1977) in their study of the thermodynamic behavior of aqueous silica as a function of pressure and temperature. Differences in crystallinity are apparently responsible for disparities in the thermodynamic properties of chalcedony and α-quartz. In contrast, it appears that differences in the thermodynamic behavior of silica glass and amorphous silica can be attributed (at least in part) to incorporation of interstitial H_2O in the latter phase.

Both α and β cristobalite as well as α-tridymite and its various polymorphs are metastable with respect to quartz at temperatures below 1079° ± 250°K at 1 bar, where β-quartz goes through a sluggish transition to (metastable?) β-cristobalite (Stull and Prophet, 1971). Because metastable cryptocrystalline β-cristobalite commonly occurs in volcanic rocks, the thermodynamic properties of this phase are also shown in table 8. However, corresponding properties of α, β, and γ tridymite are not given. Uncertainties in the experimental data reported for these polymorphs preclude unequivocal designation of the stable polymorphs of SiO_2 at high temperatures and low pressures.

$MgO–CaO–H_2O–CO_2$

Of the minerals in this system, only brucite, magnesite, dolomite, calcite, and aragonite are relatively abundant in the Earth's crust. With the exception of periclase and dolomite (which is considered in later pages) the values of $\Delta G°_f$ and $\Delta H°_f$ given in table 8 for these minerals were derived from the experimental observations of phase equilibria

summarized in figures 20 and 21. The thermodynamic data shown in table 8 for periclase were taken from calorimetric studies.

Periclase, brucite, and magnesite.—The standard molal volume and calorimetric data given in table 8 for periclase were used together with the standard molal volumes, entropies, and heat capacity coefficients for brucite and magnesite to calculate values of $\Delta G°_f$ and $\Delta H°_f$ for the latter two phases from the experimental data plotted in figure 20. The calculated values of $\Delta G°_f$ and $\Delta H°_f$ for brucite (table 8) fall within the uncertainty range of the corresponding values reported by Robie and Waldbaum (1968), but those for magnesite do not. Nevertheless, the value of $\Delta H°_f$ for magnesite in table 8 differs by only 70 cal mole^{-1} from that adopted by Stull and Prophet (1971).

The thermodynamic data given by Robie and Waldbaum (1968) for magnesite require the univariant curve in figure 20B to be > 10° to 20°C higher than that defined by the experimental reversal temperatures. In contrast, it can be seen that the curve generated in the present study is in close agreement with all the experimental data. Except for a single low-pressure reversal for the dehydration of brucite, the same observation holds for the curve in figure 20A. The value of $\Delta H°_f$ for brucite in table 8 is 390 cal mole^{-1} more negative than that given by Stull and Prophet (1971), who report −221,000 ± 500 cal mole^{-1}.

Calcite and aragonite.—To insure agreement with low-temperature experimental data, the standard molal Gibbs free energies of formation of calcite and aragonite in table 8 were calculated from solubilities reported by Christ, Hostetler, and Siebert (1974) using thermodynamic data for Ca^{++} and CO_3^{--} given by Wagman and others (1968). These values were then used together with the standard molal volumes, entropies, and heat capacity coefficients for calcite and aragonite in table 8

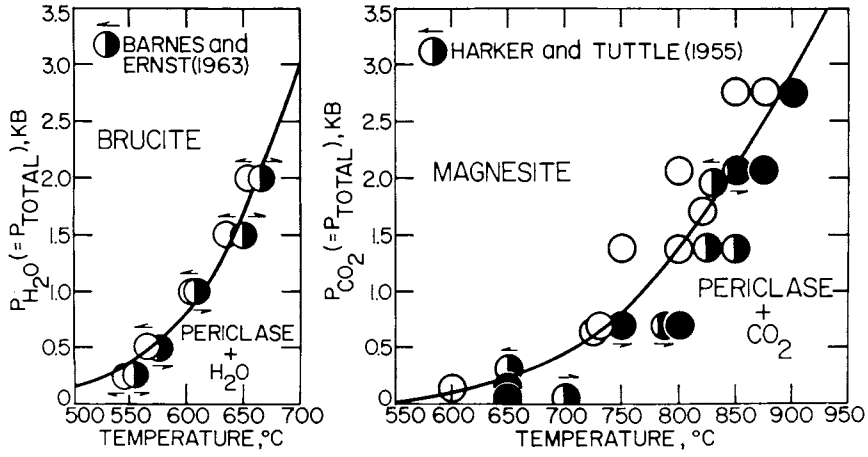

Fig. 20. Univariant equilibrium curves (generated from thermodynamic data given in table 8) and experimental observations of phase relations (symbols) in the system MgO–CO_2–H_2O at high pressures and temperatures.

to calculate equilibrium temperatures and pressures for the calcite/aragonite transition (fig. 21).

The value of $S°_{P_r,T_r}$ for calcite adopted in the present study (22.15 cal mole^{-1} (°K)$^{-1}$, which was taken from Kelley and King, 1961) is 0.23 cal mole^{-1} (°K)$^{-1}$ greater than that given by Staveley and Linford (1969), who also report 21.03 cal mole^{-1} (°K)$^{-1}$ for the standard molal entropy at 25°C and 1 bar of an aragonite sample containing 0.13 mole percent $SrCO_3$. This entropy is 0.15 cal mole^{-1} (°K)$^{-1}$ smaller than the calorimetric value for aragonite given by Kelley and King (1961), who report 21.18 cal mole^{-1} (°K)$^{-1}$. The latter value was adjusted in the present study by 0.38 cal mole^{-1} (°K)$^{-1}$ to bring the calculated Clapeyron slope of the univariant transition curve into close agreement with the distribution of data shown in figure 21. The adjustment of 0.38 cal mole^{-1} (°K)$^{-1}$ is 0.08 cal mole^{-1} (°K)$^{-1}$ greater than the uncertainty in the calorimetric value of $S°_{P_r,T_r}$ for aragonite given by Robie and Waldbaum (1968).

It can be seen in figure 21 that the univariant curve generated from the calculations described above is in close agreement with all the experimental data at high pressures. Owing to ambiguities in the high-pressure transition temperatures for calcite I (which corresponds to calcite) to calcite II, no attempt was made in the present study to retrieve thermodynamic properties for the high pressure/temperature polymorph, calcite

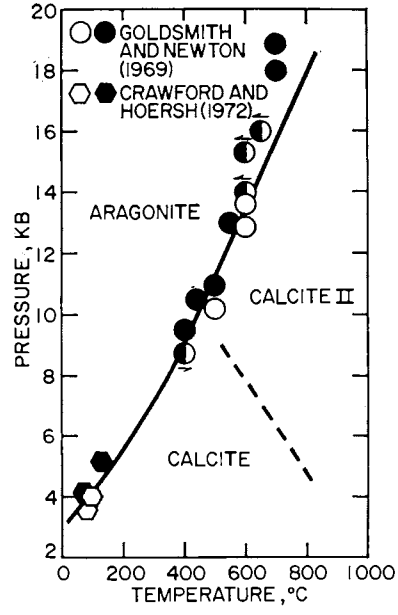

Fig. 21. Calculated equilibrium pressures and temperatures (curve) and experimental data (symbols) documenting the aragonite/calcite transition at high pressures and temperatures.

II. The values of $\Delta G°_f$ and $\Delta H°_f$ given in table 8 for calcite and aragonite fall within the uncertainties in the corresponding values reported by Robie and Waldbaum (1968). The fact that they are consistent with both low-temperature solubility measurements and high pressure/temperature phase equilibrium data reinforce the reliability of the thermodynamic data given in table 8 for aragonite and calcite.

MgO–SiO_2–H_2O

Although equilibrium phase relations in this system have received considerable geologic, experimental, and theoretical attention over the years, many ambiguities and uncertainties in the thermodynamic properties of magnesian silicates have yet to be resolved. Owing to the high sensitivity of calculated equilibrium temperatures and pressures to small errors in the thermodynamic properties of minerals in the system MgO–SiO_2–H_2O, relative uncertainties in the values of $\Delta G°_f$ and $\Delta H°_f$ for these minerals must be of the order of a few tens of cal mole^{-1} or less to reproduce all the various experimental observations. This requirement served as an implicit constraint in the retrieval calculations reported below.

Enstatite, forsterite, talc, anthophyllite, chrysotile, and antigorite.— Simultaneous consideration of high pressure/temperature experimental data shown in figures 24 through 28 for

$$\text{talc} \rightleftharpoons 3 \text{ enstatite} + \text{quartz} + H_2O, \tag{116}$$

$$\text{talc} + \text{forsterite} \rightleftharpoons 5 \text{ enstatite} + H_2O, \tag{117}$$

$$\text{anthophyllite} \rightleftharpoons 7 \text{ enstatite} + \text{quartz} + H_2O, \tag{118}$$

$$2 \text{ talc} \rightleftharpoons 3 \text{ forsterite} + 5\ SiO_{2(aq)} + 2\ H_2O, \tag{119}$$

$$\text{talc} + H_2O \rightleftharpoons \text{chrysotile} + 2\ SiO_{2(aq)}, \tag{120}$$

and

$$16 \text{ talc} + 15\ H_2O \rightleftharpoons \text{antigorite} + 30\ SiO_{2(aq)} \tag{121}$$

generated the values of $\Delta G°_f$ and $\Delta H°_f$ in table 8 for the minerals appearing in these reactions. The calculations were carried out using the standard molal volumes, entropies, and heat capacity coefficients given in the table for the minerals in reactions (116) through (121), together with the thermodynamic data and equations of state for H_2O and $SiO_{2(aq)}$ summarized by Helgeson and Kirkham (1974a) and Walther and Helgeson (1977). Wherever appropriate, provision was incorporated in the calculations for the thermodynamic consequences of the clinoenstatite/enstatite phase transition.

The Clapeyron slope of the univariant curve in figure 22 was used to calculate the standard molal entropy of the clinoenstatite/enstatite transition from density data reported by Stephenson, Sclar, and Smith (1966). Similarly, the value of $\Delta S°_{P_r,T_t}$ given in table 8 for the enstatite/

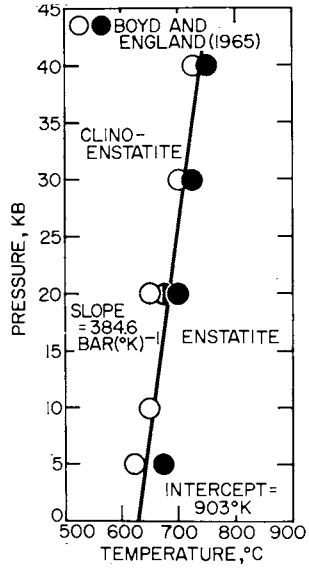

Fig. 22. Calculated equilibrium pressures and temperatures (curve) and experimental data (symbols) documenting the clinoenstatite/enstatite transition at high pressures and temperatures.

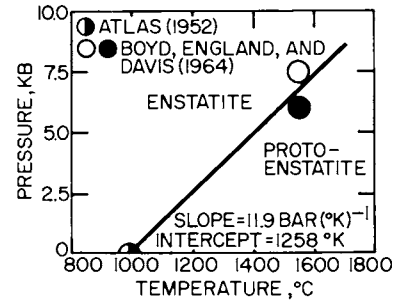

Fig. 23. Calculated equilibrium pressures and temperatures (curve) and experimental data (symbols) documenting the enstatite/protoenstatite transition at high pressures and temperatures.

protoenstatite transition was generated from the Clapeyron slope of the univariant curve in figure 23 using density data given by Smith (1959). The standard molal heat capacity coefficients for enstatite and protoenstatite in table 8 were calculated from calorimetric data tabulated by Stull and Prophet (1971). Note that the term enstatite in table 8 refers to the stable polymorph of $MgSiO_3$ at any temperature.

Univariant curves and equilibrium constants for a large number of reactions among phases in the system MgO–SiO_2–H_2O are shown in figures 24 through 32. The thermodynamic data given in table 8 for talc, enstatite, forsterite, anthophyllite, chrysotile, and antigorite were used to generate the curves in these figures, which (with a few exceptions discussed below) are in remarkably close agreement with the many experimental data represented by the symbols. The agreement is particularly impressive in view of the fact that relatively few laboratory observations were used in the retrieval calculations. Nevertheless, the computed values of $\Delta G°_f$ and $\Delta H°_f$ satisfy a wide range of solubility data and experimental observations of dehydration equilibria. Although the calculations were carried out using estimated heat capacity coefficients for talc (tables 7 and 8), it can be deduced from figure 33 that these estimates afford close approximation of the calorimetric heat capacities of talc reported recently by Krupka, Kerrick, and Robie (1977).

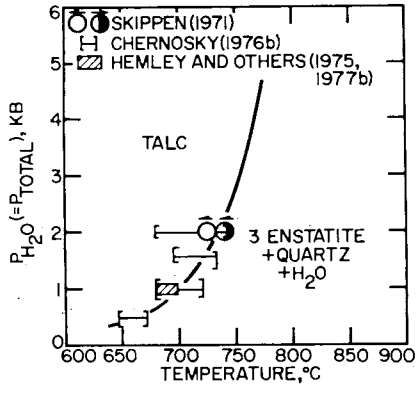

Fig. 24. Univariant equilibrium curve (generated from thermodynamic data given in table 8) and experimental observations of phase relations (symbols) in the system MgO–SiO_2–H_2O at high pressures and temperatures.

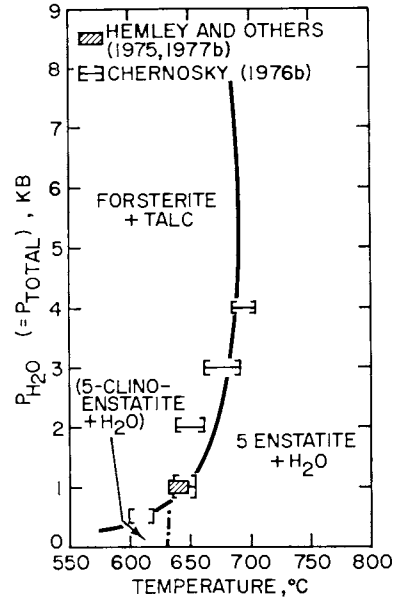

Fig. 25. Univariant equilibrium curve (generated from thermodynamic data given in table 8) and experimental observations of phase relations (symbols) in the system MgO–SiO_2–H_2O at high pressures and temperatures.

It can be seen in figure 26 that the curves generated in the present study are in close agreement with many of the experimental data reported by Greenwood (1963), Hemley and others (1977b), and Chernosky and Knapp (1977), but some discrepancies occur. Nevertheless, on the whole the curves represent the experimental data remarkably well. The discrepancies are almost certainly a consequence of metastability and sluggish reactions rates, which probably account also for thermodynamic inconsistencies in the results of some of the experiments. For example, if a curve were drawn through all the experimental "reversals" in figure 26A, the Clapeyron slope of the curve would require unrealistic values of the standard molal entropies of the reactants and products to satisfy experimental standard molal volume data for the minerals. At 2 kb, the calculated standard molal entropies and volumes of the 4 reactions shown in figure 26 are (in cal $mole^{-1}$ $(°K)^{-1}$ and cm^3 $mole^{-1}$, respectively):

Figure number	$\Delta S°_{P,T}$	$\Delta V°_{P,T}$
26A	76	54
26B	17	9
26C	81	84
26D	19	18

As a consequence, the positions of the curves in figure 26B and D are relatively sensitive to small errors in $\Delta G°_{r,P,T}$ and $\Delta H°_{r,P,T}$, but those in figures 26A and C are not. It was for this reason that experimental data for the reactions shown in figures 26A and C were not used in the retrieval calculations.

Because the Clapeyron slopes of all four curves in figure 26 are large above ~ 2 kb, invariant points limiting the stability of anthophyllite cannot be located with confidence simply by extrapolating the various univariant curves shown in the figure. Calculations of mineral stabilities in the system MgO–SiO_2–H_2O (Delany and Helgeson, 1978) using thermodynamic data taken from table 8 indicate that the equilibria depicted in figures 24 and 25 are metastable below 7.4 and 6.3 kb, respectively, where the univariant curve representing the decomposition of anthophyllite to talc and enstatite intersects the curves shown in figures 24 through 26 at two invariant points.

The observations summarized in the preceding paragraph, as well as the thermodynamic data given in table 8 for anthophyllite, forsterite, enstatite, and talc are not consistent with the phase relations proposed recently by Hemley and others (1977b), who report calculations indicating the existence of two invariant points limiting the stability of anthophyllite at low pressure (~ 200 and ~ 500 bars at ~ 600°C) rather than high. The disparity in the results of the two sets of calculations reported by Delany and Helgeson (1978) and Hemley and others (1977b)

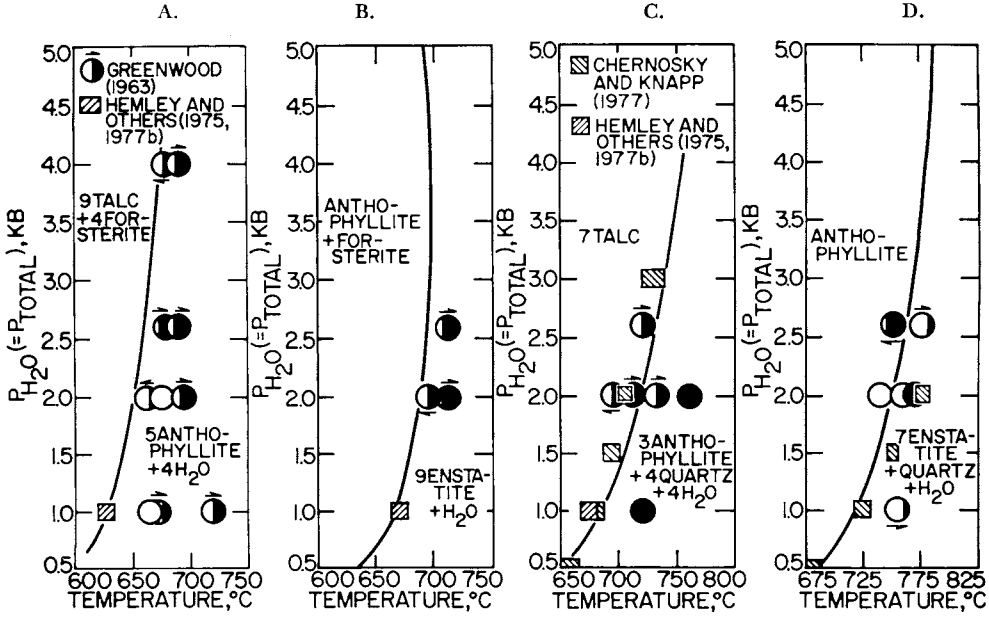

Fig. 26. Univariant equilibrium curves (generated from thermodynamic data given in table 8) and experimental observations of phase relations (symbols) in the system MgO–SiO_2–H_2O at high pressures and temperatures.

arises primarily from differences in the values adopted for $S°_{P_r,T_r}$ and the heat capacity power function coefficients for anthophyllite. The standard molal entropy of anthophyllite at 25°C and 1 bar used by Hemley and his coworkers (133.62 cal mole^{-1} (°K)$^{-1}$ is that computed by Mel'nik and Onopriyenko (1969), which is 5.0 cal mole^{-1} (°K)$^{-1}$ larger than the standard molal entropy estimated in the present study (table 3) using the structural algorithm represented by eq (62) and the values of $S°_{P_r,T_r}$ given in table 8 for talc and enstatite. This estimate differs from the sum of $S°_{P_r,T_r,talc}$ + 4 $S°_{P_r,T_r,clinoenstatite}$ by 1.5 cal mole^{-1} (°K)$^{-1}$, which is consistent with what one would expect from consideration of J. B. Thompson's (1970, 1978) polysomatic model of the amphibole structure. Despite use of the standard molal entropy of clinoenstatite in estimating $S°_{P_r,T_r}$ for anthophyllite, the relevance of the above comparison is underscored by the fact that the calorimetric standard molal entropy of tremolite at 25°C and 1 bar in table 8 differs by only 0.5 cal mole^{-1} (°K)$^{-1}$ from 2 $S°_{P_r,T_r,diopside}$ + $S°_{P_r,T_r,talc}$. Furthermore, again taking account of the structure of anthophyllite, Mel'nik and Onopriyenko's calculations (which at best yield a first approximation based in part on Greenwood's data in fig. 26) generate a value of $S°_{P_r,T_r}$ for anthophyllite that requires (what appears to us to be) an unrealistic

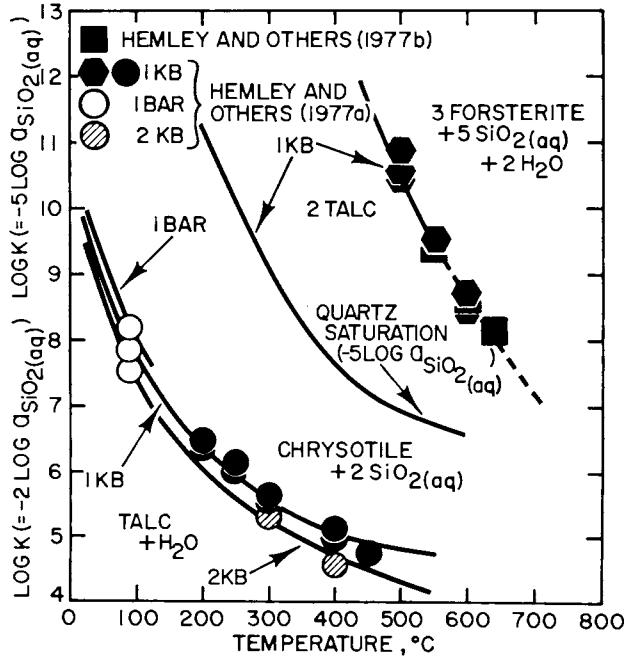

Fig. 27. Calculated (solid curves), extrapolated (dashed curve), and experimental (symbols) equilibrium constants for reactions in the system MgO–SiO_2–H_2O at high pressures and temperatures.

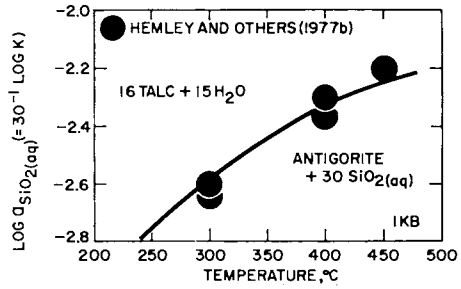

Fig. 28. Calculated (curve) and experimental (symbols) equilibrium constants for reaction (121) as a function of temperature at 1 kb.

Clapeyron slope (see Hemley and others, 1977b) for the high-temperature decomposition of anthophyllite to talc + 4 enstatite.

As indicated above, the validity of the heat capacity power function coefficients for anthophyllite adopted by Hemley and his colleagues is also highly suspect. The coefficients they employed were obtained by multiplying those given by Kelley (1960) for $MgSiO_3$ (amphibole type) by a factor of 8, as an approximate correction for the stoichiometry of anthophyllite. Although both Hemley and his coworkers and Chernosky and Knapp (1977) assert that their experimental data support the calculations reported by Hemley and others (1977b), it can be seen in figure 26 that their data at and below 1 kb are in nearly perfect agreement with the curves generated in the present study, which do not intersect at low pressures.

The value of $\Delta H°_f$ for enstatite in table 8 (which refers to the stable polymorph of $MgSiO_3$ at 298.15°K) is 14 cal $mole^{-1}$ outside the uncertainty range for the calorimetric value given by Robie and Waldbaum (1968), but it falls within that reported by Stull and Prophet (1971) and is consistent with the heat of solution data reported by Shearer (ms) and Charlu, Newton, and Kleppa (1975). The corresponding values of $\Delta H°_f$ in table 8 for forsterite and chrysotile fall well within the uncertainties in their calorimetric values. The standard molal Gibbs free energy of talc given in the table is nearly identical to the values estimated by Bricker, Nesbitt, and Gunter (1973) and computed by Hemley and others (1977a), but the value of $\Delta H°_f$ for talc differs by more than 4 kcal $mole^{-1}$ from the calorimetric enthalpy of formation reported by Barany (1963).

Owing in part to constraints imposed by the relatively large values of many of the coefficients in the reactions depicted in figures 24 through 28, the relative uncertainties in the calculated values of $\Delta G°_f$ and $\Delta H°_f$ in table 8 for the minerals appearing in the reactions are of the order of tens of cal $mole^{-1}$ or less. These small relative uncertainties, together with correspondingly small uncertainties in predictions of the thermodynamic behavior of aqueous silica, are responsible for the remarkably close agreement between the calculated and experimental equilibrium

constants in figures 29 and 30. The dashed curves in figures 27, 29, and 30 represent smooth extrapolations of the solid curves, which correspond to equilibrium constants calculated with the aid of the equation of state for $SiO_{2(aq)}$ given by Walther and Helgeson (1977), which is limited to temperatures $\leqslant 600°C$.

It can be deduced from figure 31A that the calculated equilibrium pressures and temperatures for

$$5 \text{ chrysotile} \rightleftharpoons \text{talc} + 6 \text{ forsterite} + 9\ H_2O \qquad (122)$$

are consistent with both Chernosky's (1973) experimental data for reaction (122) and the solubility measurements reported by Hemley and others (1977a) for chrysotile, talc, and forsterite, which are plotted in figure 27. However, discrepancies are apparent in figure 31B, where the curve generated in the present study for

$$\text{chrysotile} + \text{brucite} \rightleftharpoons 2 \text{ forsterite} + 3\ H_2O \qquad (123)$$

can be compared with Johannes' (1968) experimental observations of equilibrium pressures and temperatures for reaction (123). Correspond-

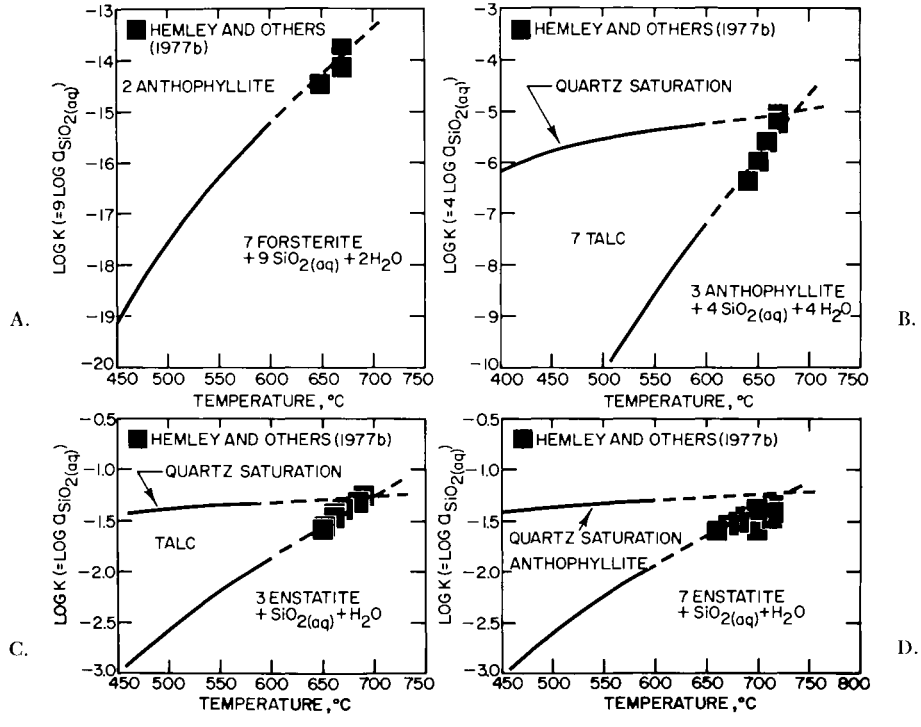

Fig. 29. Calculated (solid curves), extrapolated (dashed curve), and experimental (symbols) equilibrium constants for reactions in the system MgO–SiO_2–H_2O at high pressures and temperatures.

ing curves (generated from thermodynamic data given in table 8) are shown in figure 31 for the antigorite analogs of reactions (122) and (123).

The exact nature of the serpentine used by Johannes is somewhat ambiguous, but the X-ray data he reports suggest that it was chrysotile or a variant thereof. As pointed out by Oterdoom (1977, written commun.) it may well have been orthochrysotile, which was the serpentine used in his earlier studies of the system MgO–SiO_2–H_2O (Johannes, 1967). On the other hand, it can be seen in figure 31B that his experimental data are closely consistent with the curve generated in the present study representing

$$\text{antigorite} + 20\ \text{brucite} \rightleftharpoons 34\ \text{forsterite} + 51\ H_2O \qquad (124)$$

Although the apparent agreement between the curve corresponding to reaction (124) and the experimental data for reaction (123) in figure 31B could be a fortuitous consequence of polytypism and/or compositional variation, it leaves little doubt that Johannes' experimental reactants and products were not comparable to those in Chernosky's experiments. Hemley and others (1977a) attribute the discrepancies in figure 31 to the use of synthetic and natural reactant minerals in the different experimental studies.

Comparison of the curves representing analogous reactions involving chrysotile and antigorite in figure 31, together with comparisons of this kind for other univariant reactions among minerals in the system MgO–SiO_2–H_2O using thermodynamic data taken from table 8, suggests that stoichiometric chrysotile is a metastable phase at all pressures and temperatures (Delany and Helgeson, 1978). This conclusion on the basis of thermodynamic considerations is both supported and contradicted by field observations, which is consistent with the fact that the temperature intervals separating the curves in figures 31A and B would reduce to zero, if $\Delta G°_f$ for chrysotile were $\sim$ 500 cal mole^{-1} more negative. Consequently, chrysotile may be stabilized in nature by slight departures

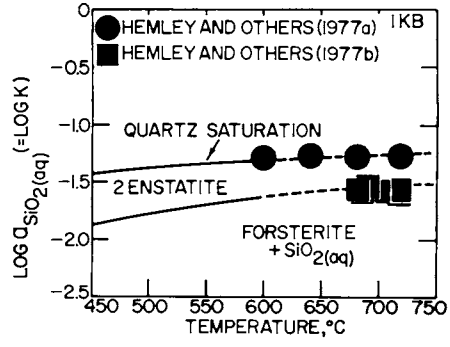

Fig. 30. Calculated (solid curves), extrapolated (dashed curve), and experimental (symbols) equilibrium constants for reactions in the system MgO–SiO_2–H_2O at high pressures and temperatures.

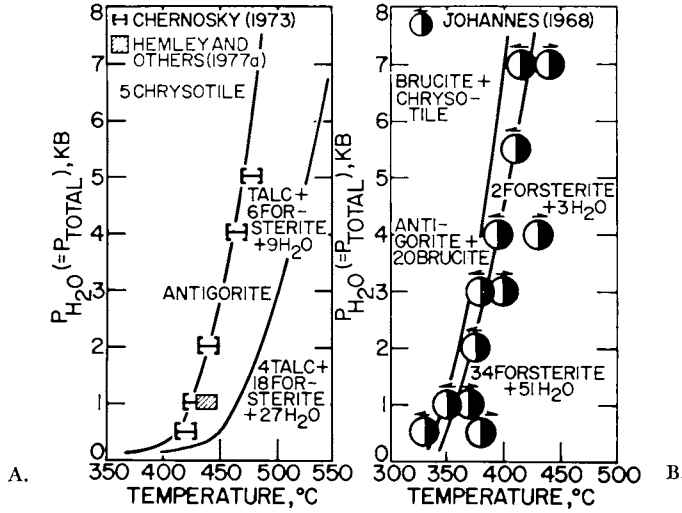

Fig. 31. Univariant equilibrium curves (generated from thermodynamic data given in table 8) and experimental observations of phase relations (symbols) in the system MgO–SiO_2–H_2O at high pressures and temperatures.

from stoichiometric composition (see below) or persist as an early-formed metastable stoichiometric phase if kinetic constraints imposed in geologic systems inhibit its breakdown to antigorite + brucite.

It can be seen in figure 32 that the experimental data reported by Evans and others (1976) for the reaction

$$\text{antigorite} \rightleftharpoons 18 \text{ forsterite} + 4 \text{ talc} + 27 \text{ } H_2O \qquad (125)$$

at 6, 10, and 15 kb are not in agreement with the univariant curve generated from the thermodynamic data in table 8 for antigorite coexisting with forsterite and talc.[11] The discrepancies in figure 32 cannot be resolved by modifying the value of $\Delta G°_f$ adopted for antigorite without contradicting the solubility data shown in figure 28. Similarly, adjusting the estimated value of $S°_{P_r,T_r}$ and/or the standard molal heat capacity power function coefficients of antigorite or talc to bring the curve through the high-pressure reversals contravenes the calorimetric data from which they were derived (table 8) as well as experimental observations of other equilibria involving minerals in the system MgO–SiO_2–H_2O. On the other hand, the discrepancies in figure 32 could be attributed to experimental error if the high-pressure reversals represented by the symbols are inconsistent with those at lower pressures. Such inconsistencies might arise from several factors. The experiments at

[11] The equilibrium temperature bracket reported by Hemley and others (1977b) for reaction (125) is not shown in figure 32. It was based on extrapolation of lower temperature solubility data as a function of T^{-1}. Our extrapolation of the same data (fig. 28) with the equation of state given by Walther and Helgeson (1977) led to the curve shown in figure 32, which is not consistent with that proposed by Hemley and his coworkers.

10 and 15 kb were carried out in a piston-cylinder apparatus, but hydrothermal bombs were used at 2, 4, and 6 kb. Although this observation alone cannot explain the discrepancy at 6 kb, compositional variation may also have affected the experimental results obtained by Evans and others (1976). Evans and his coworkers used vein antigorite in their experiments, which exhibits slight compositional and structural differences from rock-forming antigorite (Oterdoom, 1977, written commun.). The idealized formula of antigorite ($Mg_{48}Si_{34}O_{85}(OH)_{62}$) requires it to be colinear with brucite and chrysotile. Hence, minor variation in the stoichiometry of the phase could affect significantly its thermodynamic behavior under different experimental and natural conditions.

Sepiolite.—The thermodynamic properties of sepiolite in table 8 are those given by Stoessell (ms), which are consistent with the thermodynamic properties given in the table for the other magnesian silicates. It can be seen in figure 34 that calculated equilibrium constants for

$$Mg_4Si_6O_{15}(OH)_2(OH_2)_2 \cdot (OH_2)_4 + 8\ H^+ \rightleftharpoons 4\ Mg^{++} + 6\ SiO_{2(aq)} + 11\ H_2O \qquad (126)$$

using the thermodynamic data for sepiolite in table 8, together with equations and data for Mg^{++}, H^+, and $SiO_{2(aq)}$ given by Helgeson and Kirkham (1976 and in press) and Walther and Helgeson (1977) are consistent with their experimental counterparts at both low and high temperatures. The formula given for sepiolite in reaction (126) is that adopted by Stoessell to distinguish different kinds of H_2O (and OH^- groups) in the crystal lattice.

CaO–MgO–SiO_2–H_2O–CO_2

Of the values of $\Delta G°_f$ and $\Delta H°_f$ shown in table 8 for minerals in this system, only those for quartz, periclase, and monticellite are based on calorimetric measurements. In all other cases, the standard molal Gibbs free energies and enthalpies of formation from the elements at 25°C and 1 bar were retrieved from the high pressure/temperature phase equilibrium data summarized below.

Dolomite, wollastonite, diopside, and tremolite.—The values of $\Delta G°_f$ and $\Delta H°_f$ given in table 8 for these minerals were calculated from the experimental data shown in figures 35 through 37 using the thermodynamic properties of calcite, enstatite, quartz, forsterite, and talc adopted above together with the standard molal volumes, entropies, and heat capacity power function coefficients for dolomite, wollastonite, diopside, and tremolite in table 8. The thermodynamic consequences of order/disorder in dolomite were taken into account in the calculations by adopting the approach taken by Navrotsky and Loucks (1977), who used the Bragg-Williams theory (Bragg and Williams, 1934, 1935; Moelwyn-Hughes, 1961) to calculate the temperature dependence of the ordering parameter (s) for dolomite, which is defined by

$$s \equiv 2X_{Ca,A} - 1 \qquad (127)$$

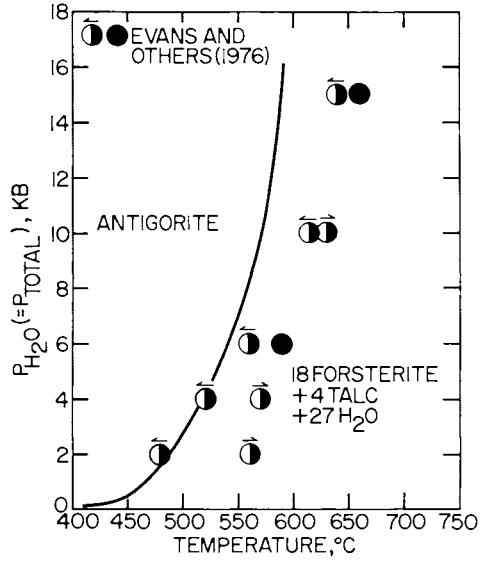

Fig. 32. Univariant equilibrium curve (generated from thermodynamic data given in table 8) and experimental observations of phase relations (symbols) in the system MgO–SiO_2–H_2O at high pressures and temperatures.

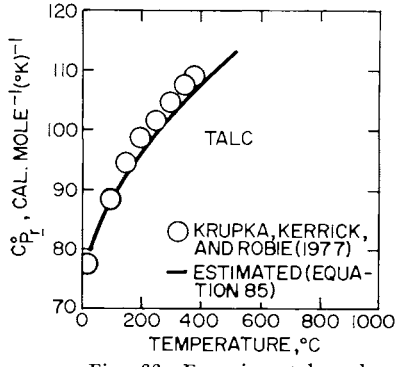

Fig. 33. Experimental and estimated standard molal heat capacities of talc as a function of temperature at 1 bar.

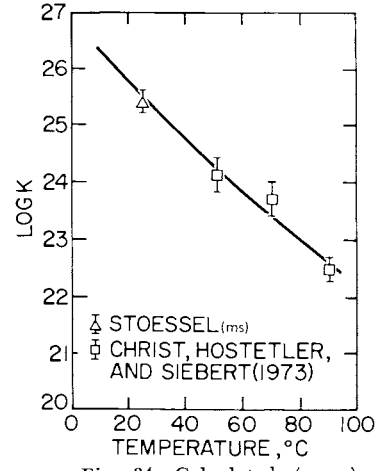

Fig. 34. Calculated (curve) and experimental (symbols) equilibrium constants for reaction (126) as a function of temperature at pressures corresponding to the vapor/liquid equilibrium curve for H_2O.

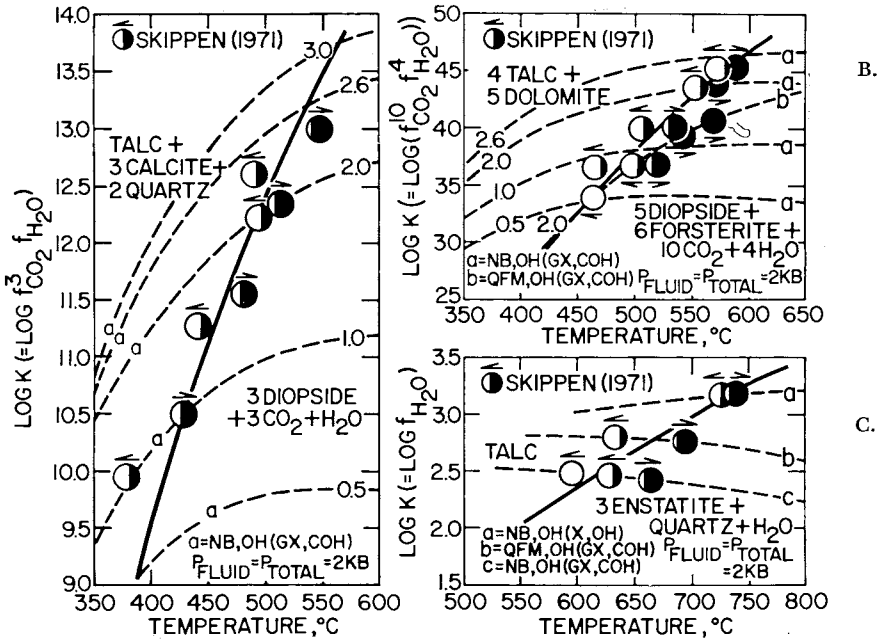

Fig. 35. Calculated (solid curves) and experimental (symbols) equilibrium constants for reactions in the system $CaO–MgO–SiO_2–CO_2–H_2O$ at high temperatures and 2 kb. The dashed curves represent equilibrium constants for various buffers designated by symbols and notation summarized by Eugster and Skippen (1967). In certain cases, the symbols refer to experimental data reported by Skippen (1971) for pressures other than 2 kb, which were used together with standard molal volume data taken from table 8 to calculate corresponding values at 2 kb consistent with the gas standard state for CO_2 and H_2O.

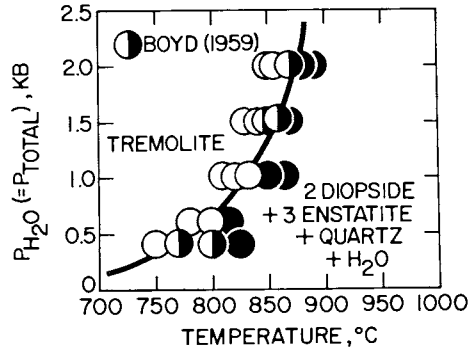

Fig. 36. Univariant equilibrium curve (generated from thermodynamic data given in table 8) and experimental observations of phase relations (symbols) in the system $CaO–MgO–SiO_2–H_2O$ at high pressures and temperatures.

where $X_{Ca,A}$ stands for the mole fraction of calcium atoms on the A sites in dolomite. The s ordering parameter is thus unity if the phase is completely ordered and zero if it is completely disordered. The temperature dependence of the ordering parameter is given by

$$s = \tanh(sT_c/T) \tag{128}$$

where T_c represents the temperature at which the phase becomes completely disordered. Taking this value to be 1200°C (Goldsmith and Heard, 1961) leads to the curve shown in figure 38.

It follows from the Bragg-Williams theory that the standard molal enthalpy of disorder in dolomite ($\Delta H°_d$) can be expressed as

$$\Delta H°_d = RT_c(1 - s^2) \tag{129}$$

Eq (129) was used to calculate $\Delta H°_d$ at a series of temperatures from 25° to 1200°C. Combining the results of these calculations with values of $H°_{P_r,T} - H°_{P_r,T_r}$ computed from eq (26) and the estimated heat capacity coefficients for ordered dolomite (table 7) generated corresponding values of $H°_{P_r,T} - H°_{P_r,T_r}$ for dolomite in its stable ordering state from 25° to 1200°C. Regression of finite difference derivatives of the latter values with eq (19) resulted in the heat capacity coefficients for dolomite given in table 8. Those shown in the table for ordered and disordered dolomite are based on the assumption that $(\partial C°_{P_r}/\partial T)_s$ is independent of s.

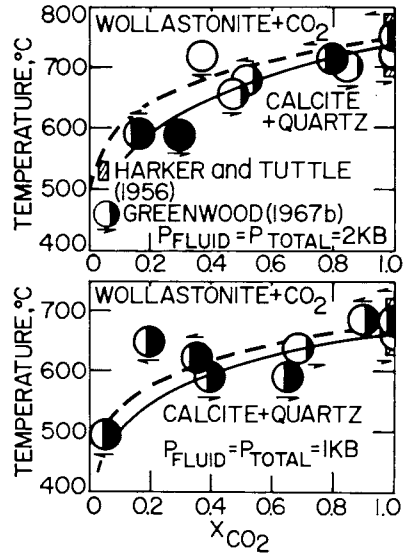

Fig. 37. Calculated (curves) and experimental (symbols) equilibrium temperatures and fluid compositions for coexisting wollastonite, calcite, quartz, and H_2O–CO_2 fluids at high pressures and temperatures. The calculations were carried out assuming, alternately, ideal (solid curves) and nonideal (dashed curves) mixing of CO_2 and H_2O (see text).

It can be seen in figure 39 that the regression equation closely approximates the finite difference standard molal heat capacities of dolomite up to ~ 1350°K. Calculation of the standard molal entropy of disorder at 1 bar for $s = 1$ to $s = 0$ from eq (18) and the heat capacity coefficients in table 8 for dolomite and its completely ordered counterpart yields 2.79 cal mole^{-1} (°K)$^{-1}$, which is only 0.04 cal mole^{-1} (°K)$^{-1}$ greater than that generated by the Bragg-Williams equation for $\Delta S°_d$, which can be written as

$$\Delta S°_d = -2R((1 - s)ln(1 - s) - ln\ 2) \qquad (130)$$

It can be deduced from table 8 that similar calculations lead to $\Delta H°_d = 2927$ and $\Delta G°_d = 2107$ cal mole^{-1} for $s = 1$ to $s = 0$. Consequently, metastable disorder in dolomite may affect significantly its thermodynamic behavior, both in the laboratory and in geochemical processes.

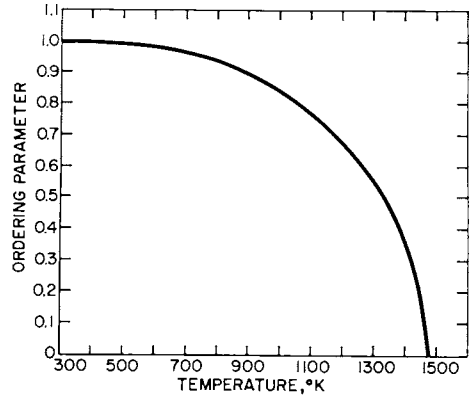

Fig. 38. Bragg-Williams ordering parameter (s) for dolomite as a function of temperature.

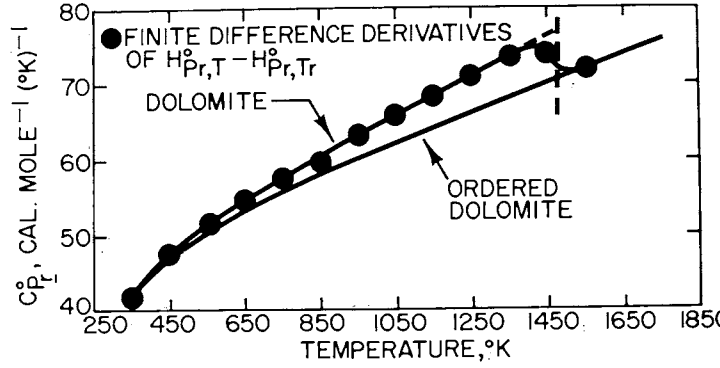

Fig. 39. Standard molal heat capacity of ordered dolomite and dolomite (which refers to $CaMg(CO_3)_2$ in its equilibrium state of order/disorder) as a function of temperature at 1 bar. The curves were generated from eq (19) and heat capacity coefficients given in table 8.

On the other hand, because the s ordering parameter decreases only slightly with increasing temperature below ~ 500°C (fig. 38), the contribution of equilibrium disorder in dolomite to the thermodynamic properties of reactions is substantial only at higher temperatures. The standard molal volume of disorder in dolomite can be calculated from lattice constants reported by Goldsmith, Graf, and Heard (1961). Extrapolation of their data leads to 0.05 cm^3 $mole^{-1}$ for $\Delta V°_d$. The value shown in table 8 for $V°_{P_r,T_r}$ of dolomite corresponds to the mean of the values for the completely ordered and disordered phase.

Although the calculations described above were carried out using estimated heat capacity coefficients for ordered dolomite, disordered dolomite, and tremolite, it can be seen in figure 40 that these estimates afford close approximation of the calorimetric heat capacities of dolomite (in an unreported state of order) and tremolite measured recently by Krupka, Kerrick, and Robie (1977). Owing to partial compensation of the entropy and enthalpy contributions to $\Delta G°_{P,T}$, the differences between the estimated and experimental heat capacities of these minerals have a relatively minor effect on computed values of the apparent standard molal Gibbs free energies of formation of dolomite and tremolite at high pressures and temperatures.

Because energetic distinctions between the M sites in diopside and tremolite apparently become small enough to permit significant disorder in the stoichiometric phases only at high temperatures, no provision was included in the retrieval calculations for disorder in these minerals.

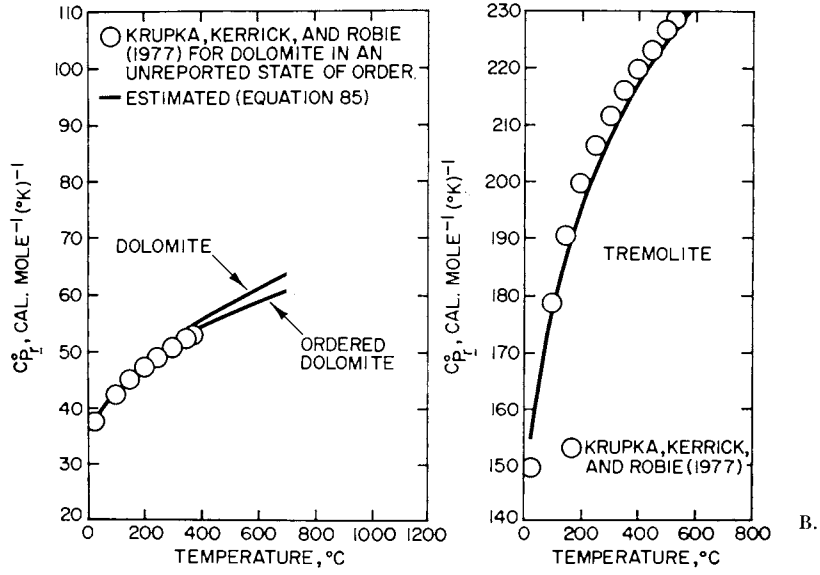

Fig. 40. Experimental and estimated standard molal heat capacities of ordered dolomite, dolomite, and tremolite as a function of temperature at 1 bar.

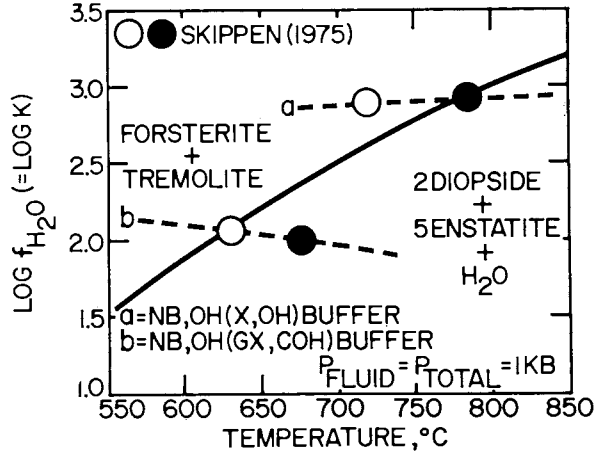

Fig. 41. Calculated (solid curve) and experimental (symbols) equilibrium constants for coexisting forsterite, tremolite, diopside, enstatite, and H_2O at high temperatures and 1 kb. The dashed curves represent equilibrium constants for buffers designated by symbols and notation summarized by Eugster and Skippen (1967). Skippen (1975) refers to G. B. Skippen (1975, written commun.).

However, as in the case of dolomite, calculation of the thermodynamic consequences of compositional variation in diopside and tremolite requires provision for order/disorder such as that suggested by Navrotsky and Loucks (1977).

It can be seen in figures 35 through 37 and 41 through 43 that the curves generated from the thermodynamic data in table 8 are in close agreement with experimental data for a large number of reactions among dolomite, diopside, tremolite, enstatite, talc, calcite, and wollastonite at high pressures and temperatures. It is also evident in figure 35C that the thermodynamic properties of talc and enstatite given in table 8 are consistent with Skippen's (1971) data for reaction (116).

No information is available concerning the ordering state of the dolomite used as a reactant or formed as a product in the experimental studies cited in figures 35, 42, and 43. For this reason, alternate calculations were carried out to determine to what extent order/disorder in dolomite (which is used in the present communication to designate $CaMg(CO_3)_2$ in its stable ordering state at any pressure and temperature) affects equilibrium temperatures and pressures for

$$4 \text{ talc} + 5 \text{ dolomite} \rightleftharpoons 5 \text{ diopside} + 6 \text{ forsterite} + 10\ CO_2 + 4\ H_2O, \quad (131)$$

$$\text{talc} + 3 \text{ calcite} + 3\ CO_2 \rightleftharpoons 3 \text{ dolomite} + 4 \text{ quartz} + H_2O, \quad (132)$$

$$4 \text{ diopside} + \text{dolomite} + CO_2 + H_2O \rightleftharpoons \text{tremolite} + 3 \text{ calcite}, \quad (133)$$

$$\text{diopside} + 2\ CO_2 \rightleftharpoons \text{dolomite} + 2 \text{ quartz}, \quad (134)$$

and

$$\text{tremolite} + 3\ \text{calcite} + 7\ CO_2 \rightleftharpoons 5\ \text{dolomite} + 8\ \text{quartz} + H_2O. \quad (135)$$

With the exception of reaction (133), the calculations indicate that equilibrium disorder in dolomite has a negligible effect on the equilibrium constants of these reactions at the temperatures and pressures for which experimental data are shown in figures 35B, 42, and 43B, D, and E. At these temperatures, the *s* ordering parameter is not much smaller than unity (fig. 38). However, if disordered dolomite were precipitated metastably in the experiments, or samples of dolomite with different states of order were used as reactants, considerable ambiguity could result.

It can be seen in figure 42 that the curve generated for dolomite in its equilibrium state of order from the thermodynamic data in table 8 assuming ideal mixing of CO_2 and H_2O (solid curve) agrees with the reversals reported by Gordon and Greenwood (1970) for $X_{CO_2} > 0.5$ but not for $X_{CO_2} < 0.5$, which cannot be explained by undetected formation of metastable disordered dolomite in the experiments. In contrast, the calculations for dolomite represented by the dashed curve labeled b in figure 42, which were carried out for dolomite in its equilibrium state of order with provision for nonideal mixing of CO_2 and H_2O using Holloway's (1977) equations for χ_{CO_2} and χ_{H_2O} in CO_2–H_2O mixtures, agree with all of Gordon and Greenwood's reversals. On the other

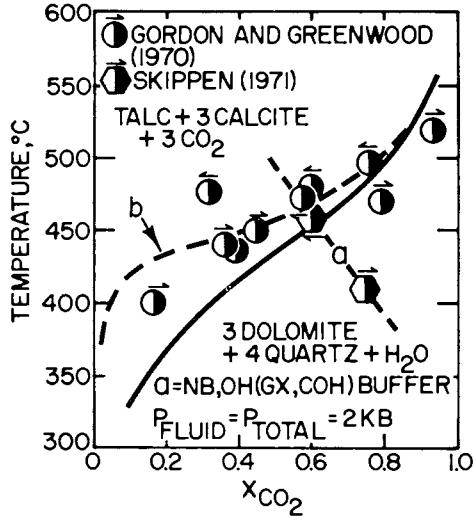

Fig. 42. Calculated (curves) and experimental (symbols) equilibrium temperatures and fluid compositions for coexisting talc, calcite, dolomite, quartz, and H_2O–CO_2 fluids at high pressures and temperatures. The dashed curve labeled *a* represents equilibrium constants for the buffer designated by symbols and notation summarized by Eugster and Skippen (1967), but that labeled *b* corresponds to the nonideal analog of the solid equilibrium curve. The latter curve was generated assuming ideal mixing of CO_2 and H_2O (see text).

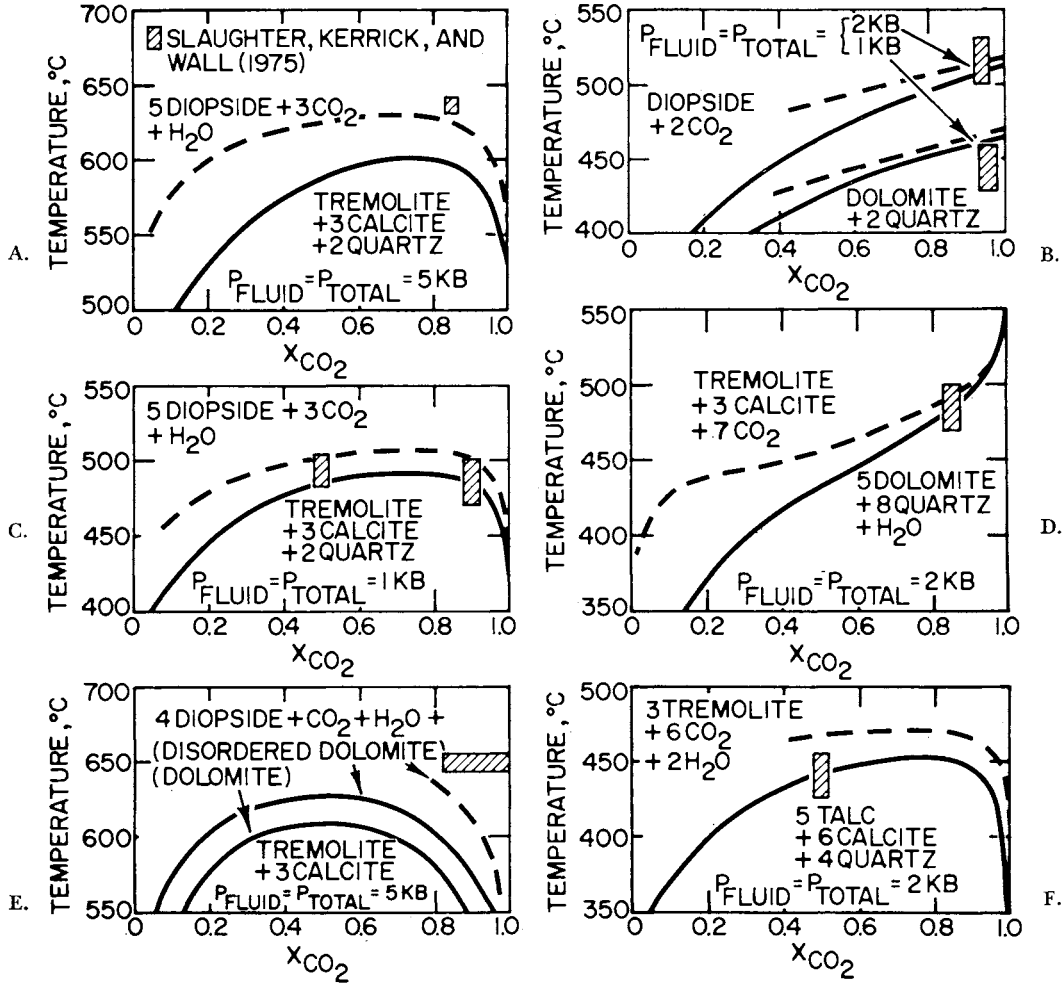

Fig. 43. Calculated (curves) and experimental (symbols) equilibrium temperatures and fluid compositions for reactions among phases in the system CaO–MgO–SiO_2–CO_2–H_2O at high pressures and temperatures. The calculations were carried out assuming, alternately, ideal (solid curves) and nonideal (dashed curves) mixing of CO_2 and H_2O (see text).

hand curve b is slightly inconsistent with the reversal reported by Skippen (1971). Similar comparison of the solid and dashed curves in figure 37 reveals agreement of the calculations for nonideal CO_2–H_2O mixtures in equilibrium with wollastonite, calcite, quartz, and CO_2 at 1 kb, but not at 2 kb. Although it can be argued solely from the distribution of the curves and symbols in figure 37 that the value of $\Delta G°_f$ for wollastonite should be slightly more negative (relative to calcite) than that shown in table 8, other constraints (discussed below) suggest that the value in table 8 is the best "compromise." This conclusion is consistent with reservations expressed above concerning the general applicability and reliability of Holloway's (1977) algorithm for calculating χ_{CO_2} and χ_{H_2O} as a function of X_{CO_2} at all pressures and temperatures.

In contrast to figure 42, the curves in figure 43 suggest that both metastable order/disorder in dolomite and nonideal mixing of CO_2–H_2O may be responsible at least in part for the discrepancies in the calculated and experimental equilibrium temperatures and fluid compositions shown in the figure. However, it can also be deduced from figure 43 that these factors fail to account adequately for all the discrepancies. This observation precluded use in the retrieval calculations of the experimental data shown in figure 43. Note that the curves generated from the thermodynamic calculations differ significantly from the experimental data shown in this figure only at 5 kb, which casts doubt on the reliability of the high-pressure fugacity coefficients of CO_2 used to generate the curves in figures 43A and E. At the very least, the relatively large differences, both in position and configuration of the dashed and solid curves in figure 43 suggest that considerable caution should be exercised in drawing geologic conclusions from temperature-X_{CO_2} diagrams which are based on assumptions concerning the ideality or nonideality of mixing in the system CO_2–H_2O.

Combining the standard molal Gibbs free energies of formation from the elements of ordered and disordered dolomite in table 8 with values of $\Delta G°_f$ for Ca^{++}, Mg^{++}, and CO_3^{--} taken from Wagman and others (1968) and Parker, Wagman, and Evans (1971) leads to $10^{-18.1}$ and $10^{-16.5}$ for the activity product constant of ordered and disordered dolomite, respectively, at 25°C and 1 bar. Corresponding values for dolomite of undetermined order range from $10^{-16.4}$ to $10^{-19.3}$, but most are close to $10^{-17.0}$ (Kramer, 1959; Garrels, Thompson, and Siever, 1960; Van Tassel, 1962; Hsu, 1963; Berner, 1967; Holland and others, 1964; Barnes and Back, 1964; Langmuir, 1964, 1971b). A value of $10^{-17.0}$ corresponds to the solubility product of a metastable partially disordered dolomite with an *s* ordering parameter of 0.7, which is probably typical of modern sedimentary dolomites.

The value of $\Delta H°_f$ shown in table 8 for diopside falls within the uncertainty range for the average of two different calorimetric values (Kracek, 1953; Neuvonen, 1952) cited by Robie and Waldbaum (1968) and is 1.1 kcal $mole^{-1}$ more negative than that reported by Navrotsky

and Coons (1976), who give an uncertainty of ± 700 cal mole^{-1}. However the standard molal enthalpy of formation of diopside from its oxides at 970°K and 1 bar reported recently by Charlu, Newton, and Kleppa (1978) differs from that calculated in the present study by only 550 cal mole^{-1}. In contrast, the standard molal enthalpy of formation of tremolite in table 8 is > 8 kcal mole^{-1} less negative than that obtained calorimetrically by Weeks (1956) and 4 kcal mole^{-1} outside the uncertainty range given for the calorimetric value by Robie and Waldbaum (1968). However, owing to nonstoichiometry and uncertainties regarding the physical state of the tremolite used in Weeks' calorimetric study, it can be argued that the uncertainty in his value is much greater than 4 kcal mole^{-1}. The value of $\Delta H°_f$ for wollastonite in table 8 is within the uncertainty in the calorimetric value given by Robie and Waldbaum (1968), and it differs by 670 cal mole^{-1} from that consistent with Charlu, Newton, and Kleppa's (1978) calorimetric data. The standard molal enthalpy of formation of dolomite given in table 8 is slightly outside the uncertainty range given by Robie and Waldbaum (1968).

Corrections required to account for nonstoichiometry in the samples used in calorimetric studies, as well as experimental vagaries arising from order/disorder, crystallinity, and other factors (such as uncertainties in the computed fugacity coefficients of CO_2 and H_2O in CO_2–H_2O mixtures) all contribute to the various discrepancies discussed in the preceding paragraph. Nevertheless, there can be little doubt from the close correspondence of the curves with the bulk of the experimental data shown in figure 35 through 37 and 41 through 43 that the values of $\Delta H°_f$ given in table 8 for dolomite, wollastonite, tremolite, and diopside are more reliable than those obtained calorimetrically.

Monticellite, merwinite, and akermanite.—Although Walter (1963a and b) and Yoder (1968) report experimental data for more than six reactions involving these minerals, thermodynamic analysis reveals large experimental uncertainties and internal inconsistencies in much of their data. For example, the experimental reversal temperatures reported by Walter for

$$\text{calcite} + \text{forsterite} \rightleftharpoons \text{monticellite} + \text{periclase} + CO_2, \quad (135A)$$

$$\text{forsterite} + \text{diopside} + 2\ \text{calcite} \rightleftharpoons 3\ \text{monticellite} + 2\ CO_2, \quad (135B)$$

and

$$\text{diopside} + \text{calcite} \rightleftharpoons \text{akermanite} + CO_2 \quad (135C)$$

all plot on top of each other, which contravenes the phase rule and leaves little doubt that metastable phases formed in the experiments. Furthermore, neither Walter (1963a and b) nor Yoder (1968) determined the extent of solid solution in merwinite, akermanite, and monticellite, but it nevertheless appears that their results were affected significantly by compositional variation in these minerals.

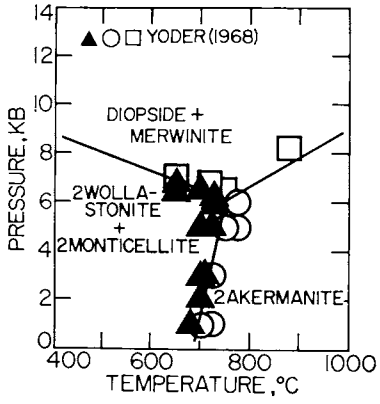

Fig. 44. Univariant equilibrium curves (generated from thermodynamic data given in table 8) and experimental observations of phase relations (symbols) in the system $CaO–MgO–SiO_2$ at high pressures and temperatures.

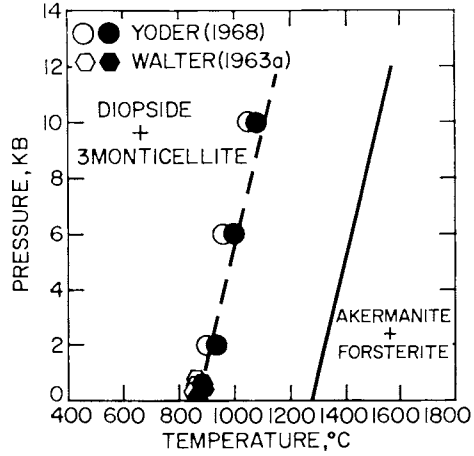

Fig. 45. Univariant equilibrium curve generated from thermodynamic data given in table 8 (solid curve) and experimental observations of phase relations (symbols) in the system $CaO–MgO–SiO_2$ at high pressures and temperatures.

The thermodynamic inconsistencies and ambiguities summarized briefly above led to the decision in the present study to adopt provisionally the calorimetric value of $\Delta H°_f$ for monticellite given by Robie and Waldbaum (1968). This value was then used to retrieve corresponding values for the two melilites from the experimental data shown in figure 44. However, it was necessary to omit provision in the calculations for possible effects of solid solution on the reversal temperatures reported by Yoder, which reduces the values of $\Delta H°_f$ and $\Delta G°_f$ for akermanite, merwinite, and monticellite in table 8 to the status of first approximations. Nevertheless the values of $\Delta H°_f$ shown in the table for merwinite and akermanite both fall well within the reported uncertainty range for the corresponding calorimetric values given by Robie and Waldbaum (1968). It should be noted that the latter observation would no longer be true if the experimental reversals in figures 44 and 45 are valid for stoichiometric akermanite and monticellite. The curves coinciding with the experimental data shown in both these figures, taken together, require $\Delta H°_f$ for akermanite and monticellite to be 3580 cal $mole^{-1}$ and that for merwinite to be 7160 cal $mole^{-1}$ less negative than the corresponding values in table 8. On the other hand, the data in table 8 are consistent with the solid curve in figure 45, which plots at much higher temperatures than those corresponding to the experimental reversals shown in the figure. This inconsistency remains unresolved, but it is of interest to note that the Clapeyron slope of a curve consistent

only with the distribution of Walter's (1963) experimental data at pressures < 1 kb in figure 45 would *not* be compatible with those of the curves in figure 44.

Al_2O_3–SiO_2–H_2O

Considerable controversy has arisen in recent years over the validity and internal consistency of the thermodynamic properties of aluminous minerals reported by different investigators. For example, Zen (1969b, 1972) calculated Gibbs free energies of formation of muscovite from high pressure/temperature phase equilibrium data reported by Velde (1966) and Day (1970) that differ by as much as 10 kcal mole^{-1} from the corrected calorimetric value given by Robie and Waldbaum (1968). Zen (1972), Chatterjee (1972), Ulbrich and Merino (1974), and others attribute this and other similar discrepancies in the thermodynamic properties of aluminosilicates to possible errors in the values of $\Delta H°_f$ for corundum, andalusite, kyanite, and sillimanite reported by Mah (1957), Waldbaum (1965), and Holm and Kleppa (1966), which are internally consistent. In contrast, Thompson (1974a) assumed that such contradictions arise from errors in the standard molal enthalpy of formation from the elements of gibbsite used by Barany (1962, 1963, 1964) to derive standard molal enthalpies of formation from the elements of anorthite, gehlenite, muscovite, and other aluminosilicates from their calorimetric data. This value (−306,380 cal mole^{-1}) was computed by Barany and Kelley (1961) with the aid of Coughlin's (1958) calorimetric enthalpy of reaction for

$$2Al_{(c)} + 6(HCl \cdot 12.73\ H_2O)_{(l)} \rightleftharpoons 2(AlCl_3 \cdot 6H_2O)_{(c)} + 64.386\ H_2O_{(l)} + 3\ H_{2(g)} \qquad (136)$$

where the subscripts (*c*), (*l*), and (*g*) stand for crystalline, liquid, and gas. Coughlin's data for reaction (136) was also used by Barany to calculate values of $\Delta H°_f$ for other aluminosilicates.

In contrast to the calorimetric reaction schemes used by Barany and Kelley (1961), Barany (1962, 1963, 1964), and Barany and Adami (1966) for kaolinite, halloysite, dickite, analcime, dehydrated analcime, and leucite, in which $AlCl_3 \cdot 6\ H_2O$ appears, those for anorthite, gehlenite, muscovite, lawsonite, kalsilite, and other aluminosilicates involve gibbsite. In the case of gibbsite and all the minerals in the first of these groups, heats of solution of 47 to 70 moles of H_2O also appear in the reaction schemes. Both the enthalpy change accompanying reaction (136) and the latter heats of solution have been suggested as possible sources of error in values of $\Delta H°_f$ for gibbsite and aluminosilicates computed by Barany and his coworkers (Thompson, 1974a; Hemingway and Robie, 1977a).

The recent calorimetric value of $\Delta H°_f$ for gibbsite (−309,065 ± 284 cal mole^{-1}) reported by Hemingway and Robie (1977a) is independent of the heat of solution of $AlCl_3 \cdot 6\ H_2O$. The fact that it differs by 2685 cal mole^{-1} from that obtained by Barany and Kelley led Thompson

(1974a) and Chatterjee and Johannes (1974) to suggest that the enthalpy of reaction (136) reported by Coughlin (1958) is in error by an equivalent amount, thereby explaining the discrepancy in the old and new values of $\Delta H°_f$ for gibbsite. However, Coughlin's enthalpy of reaction has since been corroborated by a more recent calorimetric determination (E. G. King, 1975, written commun.). Consequently, the discrepancy cannot be attributed to errors in the heat of solution of $AlCl_3 \cdot 6\ H_2O$.

Hemingway and Robie (1977a) attribute the difference in the old and new values of $\Delta H°_f$ for gibbsite to possible errors in the heats of solution of H_2O measured by Barany and Kelley (1961). However, the error in the measurements required to account for the discrepancy far exceeds the uncertainty reported by Barany and Kelley, who made five separate measurements of the heat of solution of 70.386 moles of H_2O, all of which fall within a range of 360 cal $mole^{-1}$. In the case of kaolinite, five corresponding measurements of the heat of solution of 69.386 moles of H_2O again resulted in values within 360 cal $mole^{-1}$ of each other. The mean of each of these sets of heats of solution measurements $(mole\ H_2O)^{-1}$ is 838 cal $mole^{-1}$. However, later measurements in different solutions (Barany, 1962) yielded 860 and 840 cal $mole^{-1}$, and Hemingway and Robie report 874 cal $mole^{-1}$ for the same reaction with a 20.1 wt percent HF solution. The fact that these heats of solution differ does not appear to us to be in itself a valid basis for concluding that the early measurements are in error. Such differences would be expected for reaction of H_2O with solutions of different composition, which was the case in the calorimetric experiments.

As emphasized above, both calorimetric and solubility data reported by Frink and Peech (1962), Ferrier (1966), Langmuir (1971a), and Kittrick (1966a and b, 1967, 1969, 1970, 1971a, b, c, and d) indicate that the standard molal Gibbs free energies and enthalpies of formation of gibbsite, goethite, ferric oxide, kaolinite, montmorillonite, illite, and (by inference) other clay minerals may vary by as much as several kcal $mole^{-1}$, depending on the crystallinity and particle size of the mineral. It should perhaps be reiterated in this context that particle size and crystallinity are not synonymous terms. Coarse particles may be cryptocrystalline and vice versa, and both crystallinity and particle size may have a significant effect on heats of solution obtained in calorimetric studies.

The recent calorimetric value of $\Delta H°_f$ for gibbsite applies to coarsely crystalline material (R. A. Robie, 1976, personal commun.), and the corresponding value of $\Delta G°_f$ is in excellent agreement with Kittrick's (1966a) solubility data for coarsely crystalline gibbsite. Unfortunately, no information is available concerning the crystallinity of the gibbsite used by Barany and Kelley (1961), because the sample has since been discarded or lost (K. K. Kelley, 1975, personal commun.; E. G. King, 1975, written commun.). However, as emphasized by R. A. Robie (1977, written commun.), the heats of solution of gibbsite measured by Heming-

way and Robie (1977a) at 303.4°, 323°, and 333°K are in excellent agreement with the average of those at 346.85°K reported by Barany and Kelley (1961). On the face of it, this observation would seem to rule out differences in crystallinity as a contributing factor to the discrepancy between the old and new values of $\Delta H°_{f,gibbsite}$. However, even assuming a constant heat capacity of solution (which seems unlikely) the uncertainty ranges represented by the spread of Barany and Kelley's and Hemingway and Robie's data lead to an extrapolation ambiguity in excess of 500 cal mole^{-1} at 346.85°K. If any part of the discrepancy in the values of $\Delta H°_f$ reported by Barany and Kelley (1961) and Hemingway and Robie (1977a) is indeed a result of differences in crystallinity, the "corrections" Thompson (1974a) applied to the calorimetric values of $\Delta H°_f$ reported by the Bureau of Mines for muscovite, anorthite, gehlenite, and other aluminosilicates would themselves be incorrect. In making the corrections he accepted the enthalpy of solution of gibbsite determined by Barany and Kelley (1961) but used the new calorimetric value of $\Delta H°_f$ for gibbsite to calculate standard molal enthalpies of formation from the elements of aluminosilicates from the calorimetric data reported by Barany and his coworkers. However, if the gibbsite used in the calorimetric experiments was cryptocrystalline, this procedure is invalid because it introduces a systematic inconsistency in the recalculated values of $\Delta H°_f$. For this reason, and because the validity of similar corrections applied by Hemingway and Robie on the basis of assumed errors in the heats of solution of H_2O reported by the Bureau of Mines is open to question, none of the "corrected" values of $\Delta H°_f$ for aluminosilicates given by Thompson (1974a) and Hemingway and Robie (1977a) was adopted in the present study. However, the same reservations do not apply to Hemingway and Robie's calorimetric value of $\Delta H°_{f,gibbsite}$ (309,065 cal mole^{-1}), which was used to retrieve corresponding values for aluminosilicates from natural water compositions and the high pressure/temperature phase equilibrium data summarized below.

Gibbsite and kaolinite.—As noted above, the thermodynamic properties of aluminosilicates given in table 8 are compatible with the recent calorimetric value of $\Delta H°_f$ for gibbsite reported by Hemingway and Robie (1977), which is independent of $\Delta H°_{f,corundum}$. However, they are not consistent with the calorimetric data for corundum reported by Holley and Huber (1951) and Mah (1957). To ensure agreement of computed values of $\Delta G°_f$ for aluminosilicates with both experimental and geologic observations of phase equilibria at low as well as high temperatures and pressures, the value of $\Delta G°_f$ for gibbsite computed from the calorimetric value of $\Delta H°_f$ for gibbsite reported by Hemingway and Robie (table 8) was used together with the compositions of mineral assemblages and coexisting interstitial waters in Jamaican bauxite deposits and weathered Hawaiian basalts (Hill and Ellington, 1961; Patterson and Roberson, 1961; Garrels and Mackenzie, 1967; Bricker and

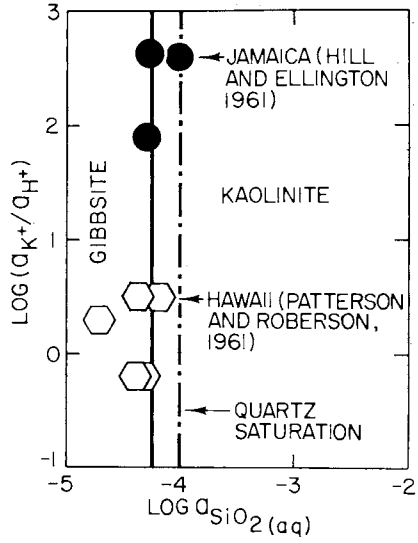

Fig. 46. Logarithmic activity diagram depicting phase relations in a part of the system K_2O–Al_2O_3–SiO_2–H_2O at 25°C, 1 bar, and unit activity of H_2O. The equilibrium constant corresponding to the gibbsite–kaolinite boundary was calculated from thermodynamic data given in table 8. The symbols represent compositions of Jamaican and Hawaiian ground waters, which coexist with kaolinite and/or gibbsite.

Garrels, 1967) to calculate $\Delta G°_f$ for kaolinite. The compositions of these waters (fig. 46) indicate that the equilibrium constant for

$$\text{kaolinite} + H_2O \rightleftharpoons 2\ \text{gibbsite} + 2\ SiO_{2(aq)} \qquad (137)$$

is $\sim 10^{-8.5}$ at 25°C and 1 bar. This figure and the thermodynamic data for aqueous silica given by Walther and Helgeson (1977) lead to a value of $\Delta G°_f$ for kaolinite (table 8) which is in excellent agreement with Kittrick's (1966b, 1970) solubility data for coarsely crystalline kaolinite. In contrast, the value of $\Delta H°_f$ for kaolinite in table 8 is 2356 cal mole^{-1} more negative than that calculated by Robie and Waldbaum (1968) from Barany and Kelley's (1961) data. The latter enthalpy of formation is consistent with Kittrick's solubility data for cryptocrystalline kaolinite, which implies that cryptocrystalline kaolinite was used in Barany and Kelley's calorimetric experiments. The standard molal enthalpy of formation of kaolinite from its elements in table 8 is 2510 cal mole^{-1} less negative than the "corrected" value given by Hemingway and Robie (1977a). The latter value (relative to that for gibbsite) is inconsistent with the water compositions shown in figure 46.

Pyrophyllite, boehmite, diaspore, corundum, andalusite, kyanite, and sillimanite.—Standard molal Gibbs free energies and enthalpies of formation from the elements of these minerals were calculated from high pressure/temperature experimental data for

$$\text{pyrophyllite} + H_2O \rightleftharpoons \text{kaolinite} + 2\ SiO_{2(aq)}, \qquad (138)$$

$$\text{andalusite} \rightleftharpoons \text{corundum} + SiO_{2(aq)}, \quad (139)$$

$$2\ \text{diaspore} \rightleftharpoons \text{corundum} + H_2O, \quad (140)$$

$$\text{andalusite} + H_2O \rightleftharpoons 2\ \text{boehmite} + SiO_{2(aq)}, \quad (141)$$

$$\text{pyrophyllite} \rightleftharpoons \text{andalusite} + 3\ SiO_{2(aq)} + H_2O, \quad (142)$$

$$\text{andalusite} \rightleftharpoons \text{sillimanite}, \quad (143)$$

and

$$\text{andalusite} \rightleftharpoons \text{kyanite}, \quad (144)$$

which ensured compatibility of the results of the calculations with the values of $\Delta G°_f$ and $\Delta H°_f$ for gibbsite and kaolinite adopted above. The values of $S°_{P_r,T_r}$ and the standard molal heat capacity of diaspore employed in the calculations (table 8) correspond to those given by Robie and Waldbaum (1968) and Kelley (1960), which are nearly identical to the more recent values reported by Perkins, Essene, and Westrum (1978). In contrast, the value of $S°_{P_r,T_r}$ given by Kelley and King (1961) and Robie and Waldbaum (1968) for gibbsite (table 8) differs by 0.39 cal $mole^{-1}$ from that adopted by Hemingway and Robie (1977a).

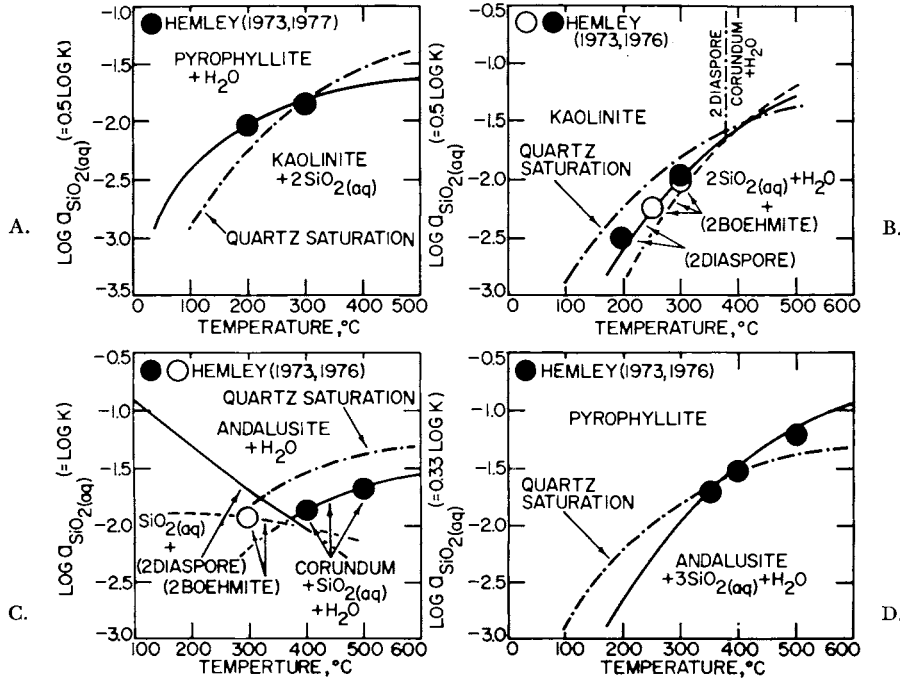

Fig. 47. Calculated (curves) and experimental (symbols) equilibrium constants for reactions among phases in the system Al_2O_3–SiO_2–H_2O as a function of temperature at 1 kb. Hemley (1973, 1976, 1977) refers to J. J. Hemley (1973, 1976, 1977, written and personal commun.).

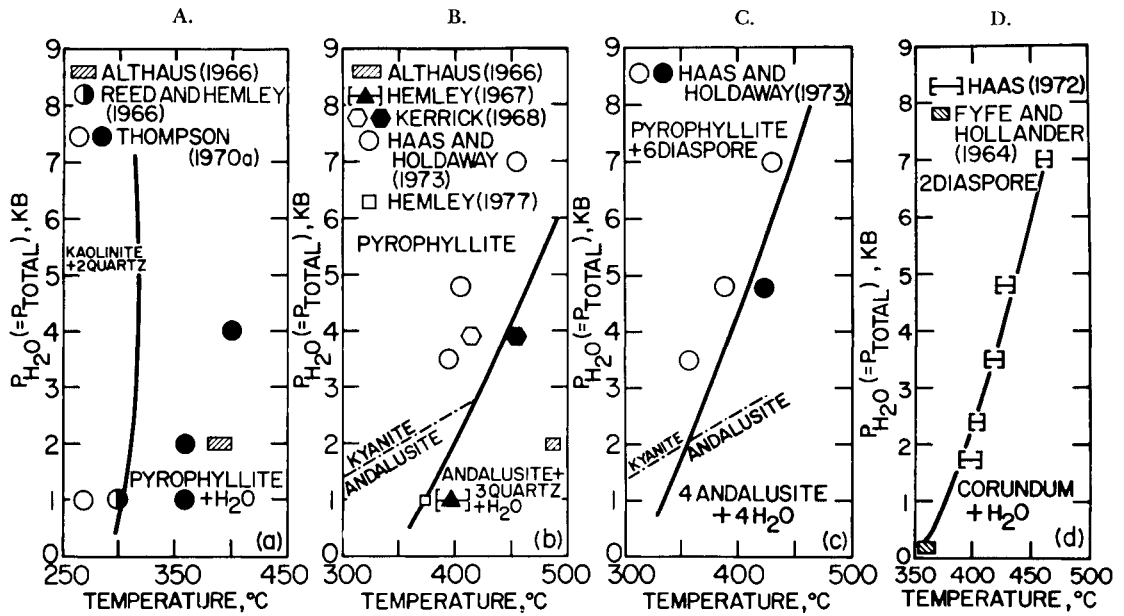

Fig. 48. Univariant equilibrium curves (generated from thermodynamic data given in table 8) and experimental observations of phase relations (symbols) in the system Al_2O_3–SiO_2–H_2O at high pressures and temperatures. Hemley (1977) refers to J. J. Hemley (1977, written commun.).

Equilibrium constants and univariant curves generated from the thermodynamic data in table 8 for the minerals appearing in reactions (138) through (144) can be compared with their experimental counterparts in figures 47 through 49. It can be seen that the curves shown in these figures are in excellent agreement with the experimental data represented by the symbols.

The value of $\Delta H°_f$ for corundum calculated in the present study (table 8) differs significantly from the calorimetric values reported in the literature, which range from −399,040 ± 240 (Snyder and Seltz, 1945) to −402,000 ± 2000 cal mole^{-1} (Schneider and Gattow, 1954). Robie and Waldbaum (1968) and Stull and Prophet (1971) adopted −400,400 ± 300 cal mole^{-1}. This value was obtained calorimetrically by both Holley and Huber (1951) and Mah (1957). The CODATA task group on key values for thermodynamics (CODATA, 1976) recommends −400,500 ± 300 cal mole^{-1}, which is more negative by 3355 cal mole^{-1} than that shown in table 8.

All the calorimetric values of $\Delta H°_f$ for corundum are inconsistent with Haas' (1972) experimental phase equilibrium data in figure 48D, but no evidence is apparent in Haas' paper that throws suspicion on the reliability of his experimental results. In fact, his data are supported by those shown in figure 47C. Because he observed epitaxial overgrowths of diaspore on corundum, Haas (1972) at the very least established minimal temperatures of stability for corundum + H_2O. If values of $\Delta G°_f$ for diaspore, pyrophyllite, kaolinite, andalusite, kyanite, and sillimanite are calculated from the experimental data shown in figures 47 through 49 using the calorimetric data for corundum summarized above, the results are incompatible with the compositions of natural waters and Hemingway and Robie's (1977a) calorimetric data for gibbsite. For example, the calculated equilibrium constant for reaction (137) would be of the order of 10^{-11} at 25°C and 1 bar, which is clearly inconsistent with the water compositions shown in figure 46.

Despite recent arguments to the contrary (Waldbaum, 1971; Thompson, 1974a; Zen, 1977) it appears from the observations summarized above that the source of the contradiction of the calorimetric data for corundum with geologic observations and other experimental data lies in the calorimetric studies. Although it is true that incomplete combustion and (as emphasized by Waldbaum, 1971) formation of a metastable polymorph of Al_2O_3 in the calorimeter would result in a less negative value of $\Delta H°_f$ than that of the stable polymorph, strain energy or interstitial hydrogen in the aluminum samples would have the opposite effect. It seems unlikely, but it is nevertheless possible that the same (or a similar) source of error occurred in all the calorimetric studies of corundum that have been carried out to date (C. E. Holley, Jr., 1977, personal commun.). Despite differences in certain materials used by the various investigators, the procedures, techniques, and experimental equipment were essentially the same.

Recent electrochemical determination of the standard molal Gibbs free energy of formation of corundum (Ghosh, 1976) supports the evidence adduced above suggesting that the calorimetric value of $\Delta H°_f$ for corundum is in error. Third law analysis of emf data from two different high-temperature cells (which yielded results in close agreement with one another) led to an average value of $\Delta H°_f = -392{,}600 \pm 920$ cal mole^{-1}. This value is 7800 cal mole^{-1} *less* negative than the calorimetric value of $\Delta H°_f$ obtained by Holley and Huber (1951) and Mah (1957). However, it is also 4545 cal mole^{-1} less negative than that computed in the present study. Because the results of high-temperature emf studies are subject to relatively large uncertainties, the absolute magnitudes of these differences are not necessarily significant. Nevertheless, the fact that the emf measurements are in serious disagreement with the calorimetric results lends support to the conclusions reached above and underscores the need for renewed calorimetric investigation to resolve the discrepancies.

Although Kerrick (1968), A. B. Thompson (1970a), and Haas and Holdaway (1973) report reversal temperature brackets for

$$\text{kaolinite} + 2\ \text{quartz} \rightleftharpoons \text{pyrophyllite} + H_2O, \tag{145}$$

$$\text{pyrophyllite} \rightleftharpoons \text{andalusite} + 3\ \text{quartz} + H_2O, \tag{146}$$

and

$$\text{pyrophyllite} + 6\ \text{diaspore} \rightleftharpoons 4\ \text{andalusite} + 4\ H_2O, \tag{147}$$

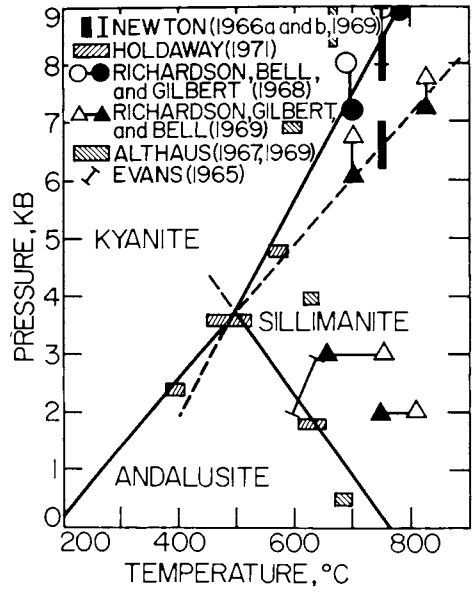

Fig. 49. Univariant equilibrium curves (generated from thermodynamic data given in table 8) and experimental observations of phase relations (symbols) in the system Al_2O_3–SiO_2–H_2O at high pressures and temperatures.

the validity of many of their experimental results is open to serious question. Fine-grained kaolinite and/or pyrophyllite were used as starting materials in all but a few of the experiments, and reversal temperatures were determined by measuring gains or losses in the weight of andalusite and/or quartz crystals. However, in none of the experiments was the proportions of reactants and products varied to promote achievement of stable equilibrium. Because determination of equilibrium temperatures by measuring weight gains and losses is generally unreliable unless the gains and losses are substantial, only those data reported by Kerrick (1968), A. B. Thompson (1970a), and Haas and Holdaway (1973) that are not subject to large uncertainties are shown in figure 48. It is of interest to note in this regard that the equilibrium temperature reported by Reed and Hemley (1966) for reaction (145) at 1 kb (fig. 48A) is "maximal" (J. J. Hemley, 1977, written commun.), and that the Clapeyron slope of the curve in figure 48B is incompatible with the pressure distribution of all the "reversals" reported by Haas and Holdaway (1973).

Owing to the small magnitude of $\Delta S°_{r,P,T}$ and $\Delta V°_{r,P,T}$ for reactions (143) and (144), the Clapeyron slopes of the curves in figure 49 are sensitive to small errors in the standard molal volumes, entropies, and heat capacities of the Al_2SiO_5 polymorphs. Accordingly, the calorimetric standard molal entropies of these phases at 25°C and 1 bar were adjusted slightly in the first or second decimals to optimize agreement of the curves with the experimental data. As indicated above, accurate calculation of the equilibrium pressures and temperatures shown in figure 49 requires 5 significant figures in the heat capacity power function coefficients for the polymorphs. The curves in figure 49 representing the kyanite/andalusite and andalusite/sillimanite transitions intersect 1 bar at 466° and 1043°K, where $\Delta H°_f$ is 1043 and 529 cal $mole^{-1}$, respectively. The Clapeyron slopes of these curves at 1 bar (12.6 and −13.0 bar $(°K)^{-1}$) are in close agreement with those computed recently from hydrothermal and calorimetric data by Anderson, Newton, and Kleppa (1977), and the location of the triple point is nearly identical to that adopted by Holdaway (1971).

After taking account of the difference in the value of $\Delta H°_f$ for corundum reported by Mah (1957) and that derived above from high pressure/temperature data, the calculated values of $\Delta H°_f$ in table 8 for kyanite, andalusite, and sillimanite fall within the uncertainties in the calorimetric values given by Robie and Waldbaum (1968), Stull and Prophet (1971), and Hemingway and Robie (1977a). Equilibrium calculations and the thermodynamic data for the AlO(OH) polymorphs in table 8 indicate that boehmite is metastable with respect to diaspore at all pressures and temperatures, which is consistent with conclusions reached by Apps (ms) and Perkins, Essene, and Westrum (1978) as well as with stability relations observed in nature.

Na_2O–K_2O–Al_2O_3–SiO_2–H_2O

Accurate calculation of the thermodynamic properties of minerals in this system from high pressure/temperature experimental data requires explicit provision for the thermodynamic consequences of both substitutional and displacive order/disorder in the alkali feldspars.

Order/disorder in albite.—The calorimetric values of $\Delta H°_f$ for low albite given by Robie and Waldbaum (1968) and Hemingway and Robie (1977) are based in part on heats of solution of the sample of Amelia albite used by Waldbaum (ms and 1968) and Waldbaum and Robie (1971). Although Waldbaum (1968) concluded that the lattice parameters of the low albite used in his experiments "indicate it to be highly ordered, if not completely ordered," consideration of the relation between the Z ordering parameter and the lattice constants of albite given by Thompson, Waldbaum, and Hovis (1974) suggests that the sample used by Waldbaum may have been somewhat disordered. Holm and Kleppa (1968) reached the same conclusion on the basis of site populations for Amelia albite determined by Ferguson, Ribbe, Traill, and Taylor but reported by Bragg and Claringbull (1965).

The site population reported by Bragg and Claringbull for Amelia albite corresponds to Z = 0.89, which compares favorably with values of Z computed directly from cell constants. According to Thompson, Waldbaum, and Hovis (1974), the Z ordering parameter for pure Na-feldspars can be expressed as[12]

$$\begin{aligned} Z &\equiv (X_{Al,T_{1O}} + X_{Al,T_{1m}}) - (X_{Al,T_{2O}} + X_{Al,T_{2m}}) \\ &= -12.523 - 3.4065b + 7.9454c \end{aligned} \tag{148}$$

where $X_{Al,T_{1O}}$, $X_{Al,T_{2O}}$, $X_{Al,T_{1m}}$, and $X_{Al,T_{2m}}$ stand for the mole fractions of aluminum on the subscripted sites, and b and c refer to the lattice parameters of albite. Eq (148) and the cell constants reported by Waldbaum (1968) yield Z = 0.80 for the Amelia albite used in the calorimetric experiments.

The thermodynamic consequences of substitional order/disorder in albite can be assessed with the aid of the heat of solution data reported by Waldbaum and Robie (1971) and Thompson, Waldbaum, and Hovis (1974). These data are plotted in figure 50, where it can be seen that the data points fall on two parallel linear curves. The separation of the curves ($\sim$ 900 cal mole^{-1}) apparently results from the cooling history of the samples and the displacive transformation from monoclinic to triclinic symmetry at high temperatures (see below). It can be seen in figure 50 that the Y ordering parameter is nonzero in only one of the disordered samples represented by the symbols. Both the Y ordering parameter, which is defined by

$$Y \equiv X_{Al,T_{1O}} - X_{Al,T_{1m}} \tag{149}$$

[12] The coefficient in the last term of eq (148) has been changed to correct a typographical error in the corresponding coefficient given by Thompson, Waldbaum, and Hovis (1974).

TABLE 8

Summary of thermodynamic data for minerals at 298.15°K and 1 bar consistent with experimental solubility data and observations of phase equilibria at high pressures and temperatures

Mineral Class	Name	Index Number[aa]	Formula	Gram Formula Weight[ffff]	ΔG°_f [c,g]	ΔH°_f [c,d]
Oxides	Corundum	1108	α-Al_2O_3	101.961	-374,824	-397,145
	Ferrous Oxide	1113	FeO	71.846	-60,097[ee]	-65,020[g]
	Hematite	1544	Fe_2O_3 (α, β, and γ)	159.692	-178,155[ee]	-197,720[r]
	Magnetite	1506	Fe_3O_4 (α and β)	231.539	-242,574[ee]	-267,250[r]
	Lime	1110	CaO	56.079	-144,366[ee]	-151,790[t]
	Periclase	1109	MgO	40.311	-136,086[ee]	-143,800[g]
	Potassium Oxide	1123	K_2O	94.203	-77,056[ee]	-86,800[g]
	Sodium Oxide	1124	Na_2O	61.979	-89,883[ee]	-99,140[u]
	Quartz (α and β)	1505	SiO_2	60.085	-204,646[bb]	-217,650[bb]
	Cristobalite (α and β)	1556	SiO_2	60.085	-203,895[s]	-216,755
	α-Cristobalite	1126	SiO_2	60.085	-203,895[s]	-216,755
	(β-Cristobalite)[wwww]	1127	SiO_2	60.085	-203,290[s]	-215,675
	Coesite	1557	SiO_2	60.085	-203,541	-216,614
	Chalcedony	1128	SiO_2	60.085	-204,276[s]	-217,282
	Amorphous Silica	1125	$SiO_2 \cdot nH_2O$[z]	60.085	-202,892[s]	-214,568
	Spinel	1120	$MgAl_2O_4$	142.273	-517,006	-546,847
Hydroxides	Boehmite	1116	AlO(OH)	59.988	-217,250	-235,078
	Diaspore	1115	AlO(OH)	59.988	-218,402	-237,170
	Gibbsite	1114	$Al(OH)_3$	78.004	-276,168[ee]	-309,065[w]
	Brucite	1117	$Mg(OH)_2$	58.327	-199,646	-221,390
Carbonates	Calcite	1073	$CaCO_3$	100.089	-270,100[ff]	-288,772
	Aragonite	1072	$CaCO_3$	100.089	-269,875[xxx]	-288,723
	Ordered Dolomite[uuu]	1071	$CaMg(CO_3)_2$	184.411	-517,980[uuu]	-556,851[uuu]
	Disordered Dolomite[uuu]	1070	$CaMg(CO_3)_2$	184.411	-515,873[ee]	-553,924[uuu]
	Dolomite[uuu]	1075	$CaMg(CO_3)_2$	184.411	-517,980	-556,851
	Magnesite	1074	$MgCO_3$	84.321	-245,658	-265,630
Sulfides	Chalcopyrite	1502	$CuFeS_2$	183.515	-44,900[kkkk]	-44,453[kkkk]
	Bornite	1503	Cu_5FeS_4	501.803	-86,704[kkkk]	-79,922[kkkk]
Ortho and Ring Silicates	Kyanite	1002	Al_2SiO_5	162.046	-580,356	-616,897
	Andalusite	1001	Al_2SiO_5	162.046	-580,587	-615,866
	Sillimanite	1003	Al_2SiO_5	162.046	-580,091	-615,099
	Gehlenite	1047	$Ca_2Al_2SiO_7$	274.205	-903,588	-951,665
	Grossular	1529	$Ca_3Al_2Si_3O_{12}$	450.454	-1,496,967	-1,583,397

[a] cal mole^{-1} (°K)$^{-1}$. [b] cm^3 mole^{-1}. [c] cal mole^{-1}. [d] Except where indicated otherwise, the values of ΔH°_f shown in this column were computed from equation (92) and the values of S° and ΔG°_f shown above using 12.24, 6.77, 4.5, 49.003, 31.208, 9.9, 7.81, 15.34, and 1.372 cal mole^{-1} (°K)$^{-1}$ for S° of $Na_{(c)}$, $Al_{(c)}$, $Si_{(c)}$, $O_{2(g)}$, $H_{2(g)}$, $Ca_{(c)}$, $Mg_{(c)}$, $K_{(c)}$, and $C_{(c)}$, respectively, at 298.15°K and 1 bar taken from Wagman and others (1968) and Parker, Wagman, and Evans (1971). The value of S° at 298.15°K and 1 bar for $Fe_{(c)}$ (6.529 cal mole^{-1} (°K)$^{-1}$) used in the calculations is that given by Stull and Prophet (1971). [e] Transition temperature at 1 bar in °K for α/β and β/γ transitions, except where no values of ΔS°_t, ΔH°_t, or ΔV°_t are shown. In the latter cases, T_t designates the upper temperature limit in °K for the heat capacity power function coefficients given for the mineral (see footnote [h]). [f] Computed from equation (9) using the values of T_t and ΔH°_t shown above. [g] Except where

TABLE 8 (continued)

Index Number[aa]	S°[a,i]	V°[b,i]	$C^{\circ}_{P_r}$ Coefficients[h,i] a[a]	$b \times 10^{3}$[j]	$c \times 10^{-5}$[k]	Transition Data (1 bar)[yyyy] T_t[e,l]	ΔS°_t[a]	ΔH°_t[c]	ΔV°_t[b]
1108	12.18	25.575	27.49	2.82	8.38	1800			
1113	14.52	12.00	12.122[m]	2.072[m]	0.750[m]	1600[g]			
1544	20.94	30.274	23.49	18.60	3.55	950[x]	0.168[f]	160[x]	
			36.0	0.00	0.00	1050[x]	0.0[f]	0[x]	
			31.71	1.76	0.00	1800[x]			
1506	34.83[r]	44.524[bb]	21.88[x]	48.20[x]	0.00[x]	900[x]	0.0[f]	0[x]	
			48.00[x]	0.00[x]	0.00[x]	1800[x]			
1110	9.50	16.674	11.67	1.08	1.56	2000			
1109	6.44	11.248	10.18	1.74	1.48	2100			
1123	22.5	40.38	18.51	8.65	0.88	1100			
1124	17.935	25.00	18.25	4.89	2.89	1000			
1505	9.88	22.688	11.22	8.20	2.70	848[x]	0.342[f]	290[x]	0.372[x]
			14.41	1.94	0.00	2000[x]			
1556	10.372[g]	25.74[n]	13.98[m]	3.34[m]	3.81[m]	543[g]	0.591[f]	321[g]	[v]
			17.39[m]	0.31[m]	9.89[m]	2000[g]			
1126	10.372[g]	25.74[n]	13.98[m]	3.34[m]	3.81[m]	1000[g]			
1127	11.963[g]	27.38[n,p]	17.39[m]	0.31[m]	9.89[m]	2000[g]			
1557	9.65[nnnn]	20.641[bb]	11.0[pppp]	8.2[pppp]	2.70[pppp]	848[pppp]			
			14.19[pppp]	1.94[pppp]	0.0[pppp]	2000[pppp]			
1128	9.88[q]	22.688[q]	11.22[q]	8.20[q]	2.70[q]	848[q]			
1125	14.34[s]	29.0[cc]	5.93[s]	47.20[s]	22.72[s]	622[s]			
1120	19.27[g]	39.71[bb]	36.773[m]	6.415[m]	9.709[m]	2000[g]			
1116	11.58[bb]	19.539[bb]	14.435[dd]	4.20[dd]	0.00[dd]	500[dd]			
1115	8.43[bb]	17.760[bb]	14.435[dd]	4.20[dd]	0.00[dd]	500[dd]			
1114	16.75[bb]	31.956[bb]	8.65[x]	45.6[x]	0.0[x]	425[x]			
1117	15.09[bb]	24.63[bb]	24.147[jjjj]	4.0124[jjjj]	6.11[jjjj]	900[jjjj]			
1073	22.15[bb]	36.934[bb]	24.98[x]	5.24[x]	6.20[x]	1200[x]			
1072	21.56[aaaa]	34.15[bb]	20.13[x]	10.24[x]	3.34[x]	600[x]			
1071	37.09[bb]	64.34[bb]	44.71	17.78	10.95	1000			
1070	39.84[uuu]	64.39[qqqq]	44.71[uuu]	17.78[uuu]	10.95[uuu]	1000[uuu]			
1075	37.09[bb]	64.365[rrrr]	41.557[uuu]	23.952[uuu]	9.884[uuu]	1000[uuu]			
1074	15.70[bb]	28.018[bb]	19.731[m]	12.539[m]	4.748[m]	1000			
1502	31.15[kkkk]	42.83[zzzz]	20.79[mmmm]	12.80[mmmm]	1.34[mmmm]	830[mmmm]			
			-141.40[mmmm]	210.0[mmmm]	0.0[mmmm]	930[mmmm]			
			41.22[mmmm]	0.0[mmmm]	0.0[mmmm]	1200[mmmm]			
1503	99.29[kkkk]	98.6[n]	49.76[mmmm]	35.08[mmmm]	1.35[mmmm]	485[mmmm]			
			-34.31[mmmm]	247.00[mmmm]	0.0[mmmm]	540[mmmm]			
			80.33[mmmm]	-2.04[mmmm]	0.0[mmmm]	1200[mmmm]			
1002	20.00[gg]	44.09[bb]	41.3931[m]	6.8165[m]	12.8821[m]	466[zzz]	2.238[zzz]	1043[zzz]	7.44[zzz]
1001	22.20[gg]	51.53[bb]	41.3103[m]	6.2926[m]	12.3921[m]	1043[zzz]	0.507[zzz]	529[zzz]	-1.63[zzz]
1003	23.13[gg]	49.90[bb]	40.0240[m]	7.3905[m]	11.6741[m]	1200[g]			
1047	48.1	90.24[bb]	63.74[hh]	8.00[hh]	15.12[hh]	1800[hh]			
1529	60.87[xxxx]	125.3	104.017[zzzz]	17.013[zzzz]	27.318[zzzz]	1000[zzzz]			

indicated otherwise, the values of ΔG°_f shown in this column were computed from experimental observations of high pressure/temperature phase equilibria (see text). [h]Maier-Kelley power function coefficients for equation (19). The upper temperature limit for the coefficients is designated by the value of T_t given for the mineral. The lower limit corresponds to 298.15°K, except where more than one set of coefficients is given. In the latter cases, the lower temperature limit of the first set is 298.15°K, but those for subsequent sets correspond to T_t for the preceeding set (see footnote e). Note that in the vicinity of the transition temperature, equation (19) fails to describe adequately the temperature dependence of $C^{\circ}_{P_r}$ (see text). [i]Except where indicated otherwise, the values shown in this column were taken from tables 2, 3, 7, or 9. [j]cal mole^{-1} (°K)$^{-2}$.

continued →

TABLE 8

Mineral Class	Name	Index Number[aa]	Formula	Gram Formula Weight[ffff]	ΔG°_f[c,g]	ΔH°_f[c,d]
Ortho and Ring Silicates	Andradite	1530	$Ca_3Fe_2Si_3O_{12}$	508.184	-1,297,479[ssss]	-1,381,005[ssss]
	Monticellite	1046	$CaMgSiO_4$	156.476	-512,829[ee]	-540,800[bb]
	Merwinite	1045	$Ca_3Mg(SiO_4)_2$	328.719	-1,037,186	-1,091,456
	Akermanite	1044	$Ca_2MgSi_2O_7$	272.640	-879,802	-926,937
	Fayalite	1049	Fe_2SiO_4	203.778	-330,233	-354,119
	Forsterite	1048	Mg_2SiO_4	140.708	-491,564	-520,000
	Cordierite	1065	$Mg_2Al_3(AlSi_5O_{18})$	584,969	-2,061,279	-2,183,199
	Hydrous Cordierite	1066	$Mg_2Al_3(AlSi_5O_{18})\cdot H_2O$	602.984	-2,121,350	-2,255,676
	Clinozoisite	1515	$Ca_2Al_3Si_3O_{12}(OH)$	622.882	-1,549,680	-1,644,221
	Zoisite	1519	$Ca_2Al_3Si_3O_{12}(OH)$	622.882	-1,549,619	-1,644,131
	Ordered Epidote	1545	$Ca_2FeAl_2Si_3O_{12}(OH)$	651.747	-1,451,346[ssss]	-1,544,456[ssss]
	Epidote[uuuu]	1559	$Ca_2FeAl_2Si_3O_{12}(OH)$	651.747	-1,451,346[ssss]	-1,544,432[ssss]
	Lawsonite	1516	$CaAl_2Si_2O_7(OH)_2\cdot H_2O$	314.2	-1,073,628	-1,158,324
Chain and Band Silicates	Wollastonite	1035	$CaSiO_3$	116.164	-369,445	-389,810
	Ca-Al Pyroxene	1040	$CaAl_2SiO_6$[jj]	218.125	-742,287	-784,013
	Jadeite	1067	$NaAl(SiO_3)_2$	202.140	-679,445	-722,116
	Enstatite[vvv]	1537	$MgSiO_3$	100.396	-348,930	-369,686
	Ferrosilite[vvv]	1508	$FeSiO_3$	131.931	-267,160	-285,625
	Diopside	1039	$CaMg(SiO_3)_2$	216.560	-724,000	-765,598
	Hedenbergite	1054	$CaFe(SiO_3)_2$	248.106	-639,218[ssss]	-678,496[ssss]
	Anthophyllite	1518	$Mg_7Si_8O_{22}(OH)_2$	780.872	-2,715,430	-2,888,749
	Tremolite	1517	$Ca_2Mg_5Si_8O_{22}(OH)_2$	812.410	-2,770,685	-2,944,478
	Pargasite	1538	$NaCa_2Mg_4Al(Al_2Si_6O_{22})(OH)_2$	835.858	-2,847,168	-3,017,064
Framework Silicates	Analcime	1022	$NaAlSi_2O_6\cdot H_2O$	220.155	-738,098	-790,193
	Dehydrated Analcime	1021	$NaAlSi_2O_6$	202.140	-674,989[ee]	-714,678[cccc]
	Albite[bbb]	1531	$NaAlSi_3O_8$	262.224	-886,308	-939,680
	Low Albite	1025	$NaAlSi_3O_8$	262.224	-886,308	-939,680
	High Albite	1560	$NaAlSi_3O_8$	262.224	-884,509[ee]	-937,050[dddd]
	Anorthite	1030	$CaAl_2Si_2O_8$	278.210	-954,298	-1,007,772
	K-feldspar[zz]	1028	$KAlSi_3O_8$	278.337	-895,374	-949,188
	Maximum Microcline	1027	$KAlSi_3O_8$	278.337	-895,374	-949,188

[k]cal $mole^{-1}(°K)$. [l]Stull and Prophet (1971). [m]Generated by regression of heat capacity or enthalpy data reported by Stull and Prophet (1971) with equations (19) or (26). [n]Roble and others (1966). [p]405°C. [q]Assumed to be equal to the corresponding values for α-quartz. [r]Haas and Roble (1973). [s]Walther and Helgeson (1977a). [t]Huber and Holley (1956). [u]O'Hare (1972). [v]Owing to ambiguities in the relative temperature dependence of V° for α and β cristobalite, no value of ΔV°_t is given for the α/β cristobalite transition. [w]Hemingway and Roble (1977a). [x]Computed from equation (1) using the Clausius-Clapeyron slope shown in figure 17 and the value of ΔS°_t shown above. [y]Kelley (1960). [z]The value of n may range from 0.14 to 0.83 (Frondel, 1962), but the thermodynamic properties of amorphous silica appear to be insensitive to the variation in H_2O content (Krauskopf, 1956; Walther and Helgeson, 1977). [aa]Identification number in computer program data file (see text). [bb]Roble and Waldbaum (1968). [cc]Iler (1955). [dd]Assumed equal to the values reported by Kelley for AlO(OH). [ee]Computed from equation (92) and the values of ΔH°_f and S° shown above together with the values of S° for the elements at 298.15°K and 1 bar given in footnote d. [ff]Christ, Hostetler, and Siebert (1974). The value shown for $\Delta G^\circ_{f,calcite}$ is consistent with log K = -8.52 for the reaction $CaCO_{3(calcite)} \rightleftharpoons Ca^{++} + CO_3^{--}$, which is slightly

(continued)

Index Number[aa]	S°[a,i]	V°[b,i]	$C^\circ_{P_r}$ Coefficients[h,i]			Transition Data (1 bar)			
			a[a]	b[a]×10³	c[k]×10⁻⁵	T_t[a,i]	ΔS°_t[a]	ΔH°_t[c]	ΔV°_t[b]
1530	70.13	131.85	113.532[aaaaa]	15.636[aaaaa]	30.889[aaaaa]	1100			
1046	26.4	51.47	36.82	5.34	8.00	1400			
1045	60.5[ii]	104.4[bb]	72.97[hh]	11.96[hh]	14.44[hh]	1700[hh]			
1044	50.03[ii]	92.81[bb]	60.09[hh]	11.40[hh]	11.40[hh]	1700[hh]			
1049	35.45[bb]	46.39[bb]	36.51[y]	9.36[y]	6.70[y]	1490[y]			
1048	22.75[bb]	43.79[bb]	35.81[y]	6.54[y]	8.52[y]	1800[y]			
1065	97.33[bb]	233.22[bb]	143.83[hh]	25.80[hh]	38.60[hh]	1700[hh]			
1066	111.43	241.22	155.23	25.80	38.60	1700			
1515	70.64	136.2	106.118[bbbbb]	25.214[bbbbb]	27.145[bbbbb]	700[bbbbb]			
1519	70.74[ccccc]	135.9[sssss]	106.118[ddddd]	25.214[ddddd]	27.145[ddddd]	700[ccccc]			
1545	75.2	139.2	113.78[eeeee]	14.69[eeeee]	28.92[eeeee]	1100[eeeee]			
1559	75.28[ssss]	139.2[tttt]	117.622[ssss]	12.816[ssss]	31.864[ssss]	1100[ssss]			
1516	55.8[eeee]	101.32[bb]	81.80 84.99	23.36 17.10	16.26 13.56	848 1000			
1035	19.60[bb]	39.93[bb]	26.64[y]	3.60[y]	6.52[y]	1400[y]			
1040	35.0	63.5	54.13	6.42	14.9	1400			
1067	31.9[bb]	60.4[bb]	48.16[y]	11.42[y]	11.87[y]	1400[y]			
1537	16.2[t]	31.276[kk]	24.55[y]	4.74[y]	6.28[y]	903[nn]	0.184[ff]	166[mm]	0.02[qq]
			28.765[m]	0.00[m]	0.00[m]	1258[pp]	0.31[ff]	390[mm]	1.09[qq]
			29.26[m]	0.00[m]	0.00[m]	1800[t]			
1508	22.6	32.952	26.49[yyy]	5.07[yyy]	5.55[yyy]	413[nn]	0.09[ff]	37[mm]	0.056[rr]
			21.0[bbbb]	9.0[bbbb]	0.0[bbbb]	1400[bbbb]			
1039	34.2[bb]	66.09[bb]	52.87[y]	7.84[y]	15.74[y]	1600[y]			
1054	40.7	68.27	54.81	8.17	15.01	1600			
1518	128.6	264.4	180.682	60.574	38.462	903			
			197.542	41.614	13.342	1258			
			199.522	41.614	13.342	1800			
1517	131.19[bb]	272.92[bb]	188.222	57.294	44.822	800			
1538	160.0	273.5	205.80	41.66	50.21	1000			
1022	56.0[tt]	97.1[ss]	53.49	24.14	8.88	1000			
1021	41.9[uu]	89.1[ww]	42.09[vv]	24.14[vv]	8.88[vv]	1000[vv]			
1531	49.51[xx]	100.25[ccc]	61.70[y]	13.90[y]	15.01[y]	473			
			81.880[ddd]	3.554[ddd]	50.154[ddd]	1200[ggg]			
1025	49.51[xx]	100.07[bb]	61.70[y]	13.90[y]	15.01[y]	1400[y]			
1560	52.30[aaa]	100.43[bb]	61.70[iiii]	13.90[iiii]	15.01[iiii]	623[ggg]			
			64.17[hhh]	13.90[hhh]	15.01[hhh]	1400			
1030	49.1[eeee]	100.79[bb]	63.311[fffff]	14.794[fffff]	15.44[fffff]	1700[fffff]			
1028	51.13[xx]	108.87[eee]	76.617[iii]	4.311[iii]	29.945[iii]	1400			
1027	51.13[xx]	108.741[fff]	63.83[y]	12.90[y]	17.05[iii]	1400[y]			

more negative than the values of -8.37, -8.40, and -8.41 given by Plummer and MacKenzie (1974), Langmuir (1968), and Berner (1967, 1976), respectively. The differences between these values result primarily from discrepancies in dissociation constants for aqueous species at 25°C and 1 bar. The values of ΔG°_f for Ca^{++} and CO_3^{--} used to calculate log K were taken from Wagman and others (1968) and Parker, Wagman, and Evans (1971). [qq]Kelley and King (1961) and Stull and Prophet (1971), modified slightly in the first and/or second decimals to achieve internal consistency (see text). [hh]Pankratz and Kelley (1964). [ii]Weller and Kelley (1963). [jj]Disordered Ca-Al pyroxene. [kk]Stephenson, Sclar, and Smith (1966). [ff]Computed from equation (1) using values of ΔV°_t given above and the Clausius-Clapeyron slopes shown in figures 22, 23 or 108A. [mm]Computed from equation (9) and the values of T_t and ΔS°_t given above. [nn]Computed from the curves shown in figures 22 or 108A. [pp]Atlas (1952). [qq]Computed from density data given by Smith (1959) and/or Stephenson, Sclar, and Smith (1966) using the gram formula weight of enstatite shown above. [rr]Computed from cell volumes given by Burnham (1965). [ss]Computed from cell parameters reported by Liou (1971b). [tt]King (1955). [uu]King and Weller (1961b). [vv]Pankratz (1968b). [ww]Estimated from $V^\circ_{analcime}$ using the value of V° for "zeolitic" H_2O in table 2 (see text). [xx]Openshaw (1974) and Openshaw and others

continued →

TABLE 8

Mineral Class	Name	Index Number[aa]	Formula	Gram Formula Weight[fff]	ΔG°_f[c,g]	ΔH°_f[c,d]
Framework Silicates	High Sanidine	1029	$KAlSi_3O_8$	278.337	-893,738	-946,538
	Nepheline	1031	$NaAlSiO_4$	145.227	-472,872	-500,241
	Kalsilite	1507	$KAlSiO_4$	158.167	-481,750	-509,408
	Wairakite	1130	$CaAl_2Si_4O_{12}\cdot 2H_2O$	434.411	-1,477,652	-1,579,553
	Laumontite	1132	$CaAl_2Si_4O_{12}\cdot 4H_2O$	470.441	-1,597,043	-1,728,884
Sheet Silicates	Kaolinite	1004	$Al_2Si_2O_5(OH)_4$	258.161	-905,614[www]	-982,221
	Pyrophyllite	1509	$Al_2Si_4O_{10}(OH)_2$	360.316	-1,255,997	-1,345,313
	Chrysotile	1007	$Mg_3Si_2O_5(OH)_4$	277.134	-964,871	-1,043,123
	Antigorite	1542	$Mg_{48}Si_{34}O_{85}(OH)_{62}$	4,536.299	-15,808,020	-17,070,891
	Talc	1510	$Mg_3Si_4O_{10}(OH)_2$	379.289	-1,320,188	-1,410,920
	Annite	1015	$KFe_3(AlSi_3O_{10})(OH)_2$	511.890	-1,147,156	-1,232,195
	Phlogopite	1014	$KMg_3(AlSi_3O_{10})(OH)_2$	417.286	-1,396,187	-1,488,067
	Muscovite	1012	$KAl_2(AlSi_3O_{10})(OH)_2$	398.313	-1,336,301	-1,427,408
	Paragonite	1013	$NaAl_2(AlSi_3O_{10})(OH)_2$	382.201	-1,326,012	-1,416,963
	7-A Clinochlore	1512	$Mg_5Al(AlSi_3O_{10})(OH)_8$	555.832	-1,957,101[ttt]	-2,113,197
	14-A Clinochlore	1513	$Mg_5Al(AlSi_3O_{10})(OH)_8$	555.832	-1,961,703	-2,116,964
	Prehnite	1532	$Ca_2Al(AlSi_3O_{10})(OH)_2$	412.389	-1,390,537	-1,482,089
	Margarite	1551	$CaAl_2(Al_2Si_2O_{10})(OH)_2$	398.187	-1,394,370	-1,486,023
	Sepiolite	1023	$Mg_4Si_6O_{15}(OH)_2(OH_2)_2\cdot(OH_2)_4$[hhhh]	647.861	-2,211,192[9999]	-2,418,000

(1976). [yy]Computed from $S^\circ_{microcline}$ using 3.4 cal mole $(°K)^{-1}$ for the entropy of substitutional disorder based on regression of Hovis' (1974) calorimetric data (see text). [zz]The term K-feldspar is used above to designate $KAlSi_3O_8$ in its stable ordering state at any given temperature and pressure. At 25°C and 1 bar K-feldspar is synonymous with maximum microcline, but at high temperatures K-feldspar corresponds to high sanidine (see text). [aaa]Computed from $S^\circ_{P_r,T_r}$ for low albite and the heat capacity power function coefficients for albite and high albite, which include provision for the calorimetric consequences of substitutional and displacive order/disorder (see text). [bbb]The term albite refers to $NaAlSi_3O_8$ in its stable state at any given temperature and pressure (see text). [ccc]Taken as the mean of the V° values shown for low and high albite (see text). [ddd]Generated by regression (eq. 26) of finite difference derivatives of $H^\circ_{P_r,T} - H^\circ_{P_r,T_r}$ computed from data reported by Holm and Kleppa (1968) and Thompson, Waldbaum, and Hovis (1974). The computed values of $H^\circ_{P_r,T} - H^\circ_{P_r,T_r}$ take into account the calorimetric consequences of substitutional and displacive order/disorder (see text). [eee]Taken to be the mean of the values of V° given above for maximum microcline and high sanidine. [fff]Hovis (1974). [ggg]Limit imposed by the monoclinic/triclinic transition (see text). [hhh]Computed (see text) from data reported by Holm and Kleppa (1968). [iii]Based on composite regression (eq. 26) of enthalpies of disorder computed from calorimetric data reported by Hovis (1974) and values of $H^\circ_{P_r,T} - H^\circ_{P_r,T_r}$ for microcline reported by Kelley (1960) -- see text. [jjj]The heat capacity coefficients and value of T_t shown for high sanidine correspond to those for maximum microcline (see text). [kkk]Obtained by composite regression of calorimetric data reported by Kelley and others (1953) for α, β, and γ-nepheline, which exhibit little or no enthalpies of transition (see (text). [lll]King and Weller (1961a). [mmm]Robie and others (1966). [nnn]King and others (1967). [ppp]Robie, Hemingway and Wilson (1976). [qqq]The heat capacity coefficients shown for chrysotile are those reported by King and others (1967) for antigorite (see text). [rrr]Generated by regression (eq. 26) of calorimetric data reported by Robie, R.A., 1976, written communication. [sss]Pankratz (1964b). [ttt]Computed from the value calculated by Helgeson (1969) from data reported by MacKenzie and Garrels (1965) -- see text. [uuu]The term dolomite refers to $CaMg(CO_3)_2$ in its stable ordering state. The Maier-Kelley heat capacity power function coefficients for disordered dolomite correspond to those for the ordered phase (see text). The entropy and enthalpy of disorder used to compute ΔH°_f and S° for disordered dolomite from observations of high pressure/temperature phase equilibria were

(continued)

Index Number[aa]	$S°$[a,i]	$V°$[b,i]	$C°_{P_r}$ Coefficients[h,i]			Transition Data (1 bar)[yyyy]			
			a[a]	$b \times 10^3$[j]	$c \times 10^{-5}$[k]	T_t[e,i]	$\Delta S°_t$[a]	$\Delta H°_t$[c]	$\Delta V°_t$[b]
1029	54.53[yy]	109.008	63.83[jjj]	12.90[jjj]	17.05[jjj]	1400[jjj]			
1031	29.72[bb]	54.16[bb]	35.908[kkk]	6.458[kkk]	7.328[kkk]	1500			
1507	31.85[bb]	59.89[bb]	29.43[vv]	17.36[vv]	5.32[vv]	810[vv]	0.198[vv]	160[vv]	
			42.5[vv]	0.0[vv]	0.0[vv]	1800[vv]			
1130	105.1	186.87[vvvv]	100.40	44.47	16.43	1000			
1132	116.1[eeee]	207.55	123.20	44.47	16.43	1000			
1004	48.53[ffff]	99.52[bb]	72.77	29.20	21.52	1000			
1509	57.2[w],[ppp]	126.6[mmm]	79.432[rrr]	39.214[rrr]	17.282[rrr]	800			
1007	52.9[nnn]	108.5[bb]	75.82[qqq]	31.60[qqq]	17.58[qqq]	1000[qqq]			
1542	861.36	1749.13	1228.45	513.76	286.68	848			
			1234.83	501.24	281.28	1000			
1510	62.34[bb]	136.25[bb]	82.48	41.61	13.34	800			
1015	95.2	154.32	106.43	29.77	19.31	1000			
1014	76.1	149.66	100.61	28.78	21.50	1000			
1012	68.8[w],[ppp]	140.71[bb]	97.56[sss]	26.38[sss]	25.44[sss]	1000[sss]			
1013	66.4	132.53	97.43	24.50	26.44	1000			
1512	106.5	211.5	162.82	50.62	40.88	848			
			166.01	44.36	38.18	900			
1513	111.2	207.11	166.50	42.10	37.47	900			
1532	65.0[eeee]	140.33[ssss]	91.60	37.82	19.60	848			
			101.17	19.04	11.50	1000			
1551	63.8	129.4	102.50	16.35	28.05	848			
			99.31	22.61	30.75	1000			
1023	146.6	285.6	157.92	104.30	18.68	800			

derived from the Bragg-Williams theory (see text). [vvv]The terms enstatite and ferrosilite are used above to refer to $MgSiO_3$ and $FeSiO_3$ in their stable structural states at all pressures and temperatures. [www]Based on the value of $\Delta G°_{f,gibbsite}$ shown above and equilibrium constraints imposed by the composition of surface waters (see text). [xxx]Computed from the solubility product constant given by Christ, Hostetler, and Siebert (1974) using data for Ca^{++} and CO_3^{--} given by Wagman and others (1968) and Parker, Wagman, and Evans (1971). [yyy]Taken to be equal to the $C°_{P_r}$ coefficients shown for clinoferrosilite (see text). [zzz]Computed from thermodynamic data given above. [aaaaa]Robie and Waldbaum (1968), modified slightly to achieve internal consistency (see text). [bbbb]Computed from data plotted in figure 98 (see text). [cccc]Calculated from calorimetric data reported by Barany (1962) for the reaction $NaAlSi_2O_6 \cdot H_2O \rightleftharpoons NaAlSi_2O_6 + H_2O_{(g)}$ using the value of $\Delta H°_f$ for analcime shown above and that for $H_2O_{(g)}$ in table 9. [dddd]Computed from the value of $\Delta H°_{f,low\ albite}$ shown above and calorimetric data reported by Thompson, Waldbaum and Hovis (1974) -- see text. [eeeee]Computed from observations of high pressure/temperature phase equilibria (see text). [ffff]Grams $mole^{-1}$. [gggg]Stoessell (ms). [hhhh]See footnote [uu] in Table 3. [iiii]Assumed to be equivalent to the corresponding coefficients for low albite at temperatures below 350°C (see text). [jjjj]King, Ferrante, and Pankratz (1975). [kkkk]Price (ms). [llll]Calculated from cell parameters reported by Deer, Howie, and Zussman (1962). [mmmm]Pankratz and King (1970). [nnnn]Holm, Kleppa, and Westrum (1967). [pppp]Computed from data reported by Holm, Kleppa, and Westrum (1967). [qqqq]Goldsmith, Graf, and Heard (1961). [rrrr]Approximated as the mean of V° for ordered and disordered dolomite. [ssss]Bird (ms) and Bird and Helgeson (1977)--see text. [tttt]Taken to be the same as ordered epidote. [uuuu]The term epidote is used above to refer to $Ca_2FeAl_2Si_3O_{12}(OH)$ in its stable state of substitutional order/disorder at all pressures and temperatures. [vvvv]Adjusted (see text). [wwww]Cryptocrystalline β-cristobalite. [xxxx]Perkins and others (1977). [yyyy]Thermodynamic properties shown for lambda transitions correspond to the apparent properties (see text). [zzzz]Computed from data reported by Perkins and others (1977). [aaaaa]Computed from high pressure/temperature phase equilibrium data together with experimental heat capacities at low temperatures reported by Kiseleva, Topor, and Mel'chakova (1972). [bbbbb]Taken to be the same as those for zoisite. [ccccc]Dexter Perkins III (1977, written communication). [ddddd]Generated by regression of calorimetric data reported by Dexter Perkins III (1977, written communication). [eeeee]Generated by regression of experimental data reported by Kiseleva, Topor, and Andreyenko (1974). [fffff]Generated by regression of calorimetric data reported by Krupka, Robie, and Hemingway (1977a).

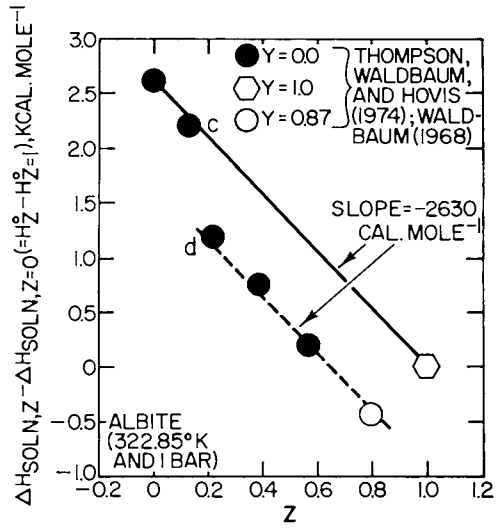

Fig. 50. Relative heat of solution at 49.7°C and 1 bar of albite as a function of the Z ordering parameter (see text).

and the Z ordering parameter are quenchable, but the high-temperature monoclinic symmetry of albite is not (Thompson, Waldbaum, and Hovis, 1974).

The standard molal enthalpy of substitutional disorder ($\Delta H°_{ds}$) represented by the upper curve in figure 50 can be expressed as

$$\Delta H°_{ds} = H°_Z - H°_{Z=1} = 2630(1 - Z) \tag{150}$$

As in the case of the monoclinic potassium feldspars (see below), it seems reasonable to assume that

$$\partial((\Delta H°_{ds})/\partial T)_Z = 0 \tag{151}$$

which permits calculation of the temperature distribution of $\Delta H°_{ds}$ from the curve depicting Z as a function of temperature in figure 51B. These calculations generated the curve representing $\Delta H°_{ds}$ for albite in figure 51D.

In contrast to the monoclinic/triclinic inversion in potassium feldspar, which is quenchable, occurs at relatively low temperatures, and has little or no effect on its thermodynamic behavior (see below), the displacive transformation in albite from monoclinic to triclinic symmetry is apparently accompanied by a relatively large heat of transition. Experimental data suggest that increasing displacive disorder caused by changes in bond angles with increasing temperature begins at temperatures well below $T_{m/a}$ (the highest temperature at which albite exhibits triclinic symmetry). It thus appears that albite undergoes two superimposed lambda transitions with increasing temperature: one caused by exchange of Al and Si atoms on the tetrahedral sites in the mineral,

and the other resulting from displacive changes in symmetry. As both substitutional and displacive disorder increase with increasing temperature to $T_{m/a}$ (which Thompson, Waldbaum, and Hovis, 1974, estimate to be 1238°K), the increasing heat of disorder affects the thermodynamic behavior of albite to an increasing degree.

The magnitude of the temperature corresponding to $T_{m/a}$ is still a matter of debate. Prewitt, Sueno, and Papike (1976) carried out experiments indicating that $T_{m/a}$ is greater than 1378°K, but Okamura and Ghose's (1975) experiments indicate that $T_{m/a} = 1203$°K. Recently, Winter and Ghose (1977) reported "a close approach to monoclinic symmetry at ~ 1333°K." The diversity of these values is consistent with the conclusion that the displacive change of symmetry in albite is a gradual lambda transition which is coupled both kinetically and thermodynami-

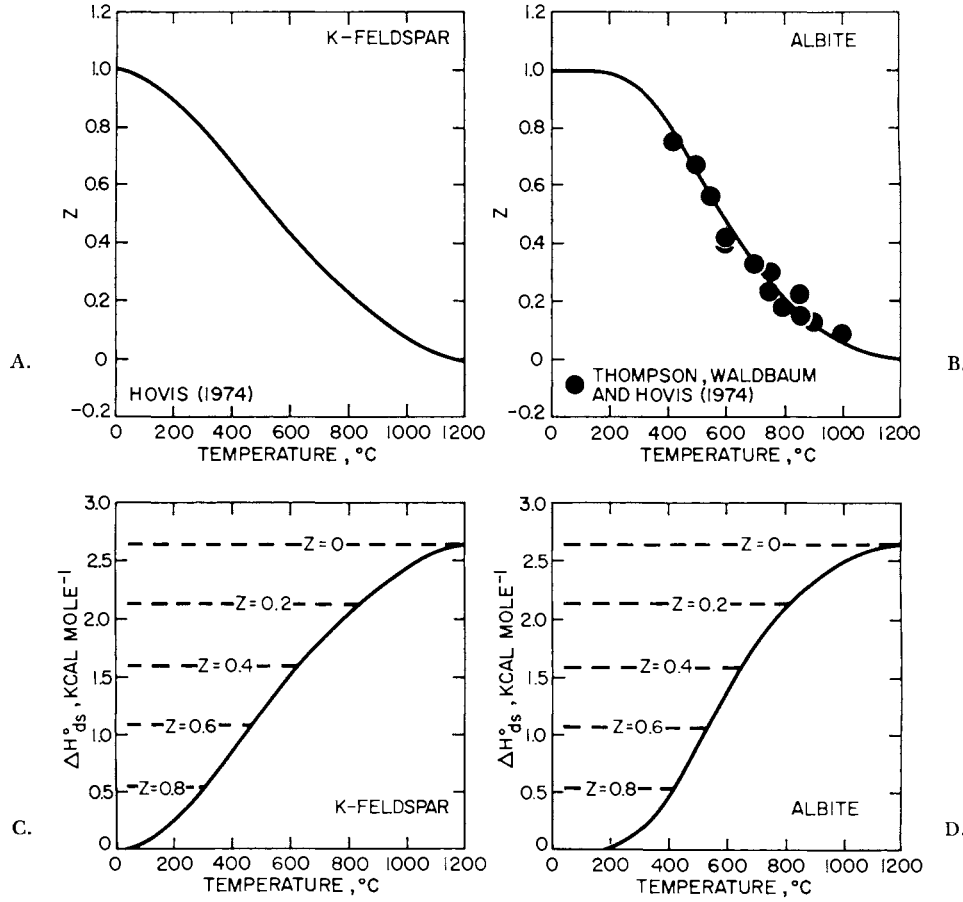

Fig. 51. Z ordering parameter and standard molal enthalpy of substitutional disorder (ΔH°_{ds}) in K-feldspar and albite as a function of temperature at 1 bar.

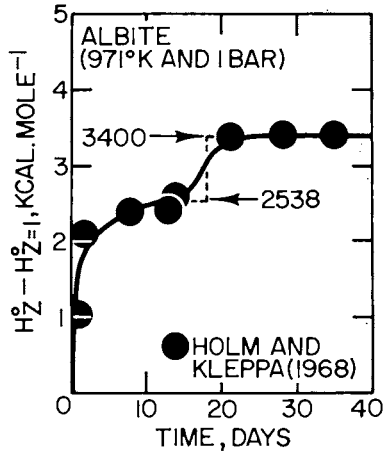

Fig. 52. Relative standard molal enthalpy of albite at 971°K and 1 bar as a function of annealing time at 1045°C and 1 bar (see text).

cally to substitutional disorder. The calculations summarized below are consistent with Thompson, Waldbaum, and Hovis' (1974) estimate of $T_{m/a}$ (1238°K).

The thermodynamic consequences of the displacive transformation in albite can be calculated from calorimetric data reported by Holm and Kleppa (1968), who measured heats of solution of Amelia albite in lead-cadmium-borate melts at 698°C and 1 bar.[13] The samples of albite were first heat-treated at 1045°C for different periods of time ranging up to 2 months. The results of the calorimetric experiments are summarized in figure 52, where it can be seen that $H^\circ_Z - H^\circ_{Z=1}$ increased rapidly with increasing annealing time up to ~ 5 days but then increased only slightly from 5 to ~ 14 days, where $H^\circ_Z - H^\circ_{Z=1}$ reached a "plateau" corresponding to ~2540 cal mole^{-1}. It can be deduced from figure 51B that the equilibrium value of the Z ordering parameter at 1045°C is ~ 0.035. Combining this value with eq (150) yields 2538 cal mole^{-1}. It thus appears that the albite samples that were annealed for 13 and 14 days reached their stable state of substitutional disorder at 1045°C. However, it can be seen in figure 52 that further heat treatment from 14 to 21 days caused $H^\circ_Z - H^\circ_{Z=1}$ to increase abruptly to 3400 cal mole. Because the displacive transformation is unquenchable, the latter increase

[13] On the basis of recent calorimetric investigation of the displacive transformation in albite by A. B. Thompson, J. B. Thompson, Jr. (1978, personal commun.) argues that the thermodynamic changes ascribed in the present communication to the displacive transformation in albite may be the result instead of undetected substitutional order/disorder among the T_{1o} and T_{1m} sites. However, distinction between the calorimetric consequences of the displacive transformation and differences in the Y ordering parameter requires comparative calorimetric annealing experiments, which have yet to be carried out. In any event, the thermodynamic analysis of order/disorder in albite summarized above is consistent with all the experimental data reported by Waldbaum (1968), Holm and Kleppa (1968), and Thompson, Waldbaum, and Hovis (1974).

(860 cal mole^{-1}) is almost certainly due to displacive disorder in high albite with Z $\approx$ 0.035 at 698°C. The observation that displacive disorder affected $H^\circ_Z - H^\circ_{Z=1}$ at 698°C only after the samples annealed at 1045°C reached their stable substitutional ordering state suggests that the kinetics of displacive disorder in albite depend on Z. If so, upon heating low albite, the displacive transformation should not take place until the phase achieves nearly complete substitutional disorder, which seems to constitute the rate-limiting step in the overall disordering process. Similarly, any substitutional ordering that occurs in metastable high albite at temperatures below $T_{m/a}$ would be expected to inhibit the displacive transformation at higher temperatures. Note that the increase in $H^\circ_Z - H^\circ_{Z=1}$ of 860 cal mole^{-1} after $\sim$ 14 days of heat treatment is nearly equal to the separation of the curves in figure 50.

The change in the standard molal enthalpy of displacive disorder (ΔH°_{dt}) can be expressed as

$$d(\Delta H^\circ_{dt}) = \left(\frac{\partial(\Delta H^\circ_{dt})}{\partial T}\right)_Z dT + \left(\frac{\partial(\Delta H^\circ_{dt})}{\partial Z}\right)_T dZ, \qquad (152)$$

which can be used to calculate the standard molal heat capacity of displacive disorder ($\Delta C^\circ_{P_r,dt}$). The drop calorimetry experiments reported by Holm and Kleppa (1968) indicate that $H^\circ_{P_r,971} - H_{P_r,T_r}$ for high albite is 790 $\pm$ 320 cal mole^{-1} (°K)$^{-1}$ greater than that for low albite.[14] However, if the abrupt increase in $H^\circ_Z - H^\circ_{Z=1}$ represented by the dashed line in figure 52 corresponds to the heat of displacive disorder in high albite at 971°K (which seems likely), it should also be equal to the difference in $H^\circ_{P_r,971} - H^\circ_{P_r,T_r}$ for high and low albite. The fact that this increase in $\Delta H^\circ_Z - \Delta H^\circ_{Z=1}$ (860 cal mole^{-1}) falls within the uncertainty range of the value of $H^\circ_{P_r,971} - \Delta H^\circ_{P_r,T_r}$ obtained by drop calorimetry supports the conclusion that the abrupt increase in $H^\circ_Z - H^\circ_{Z=1}$ after $\sim$ 14 days of annealing corresponds to the heat of displacive disorder in high albite at 971°K.

The samples of high albite used by Holm and Kleppa in their drop calorimetry experiments were obtained from Waldbaum and correspond to samples used in his calorimetric study of order/disorder (Waldbaum, ms). The degree of disorder in these samples may have been slightly different than that in the high albite produced in Holm and Kleppa's annealing experiments. Nevertheless, the Z ordering parameter was probably < 0.06 (which corresponds to that at $T_{m/a}$ = 1238°K) in both cases. It thus appears that 860 cal mole^{-1} is a reasonable estimate of $H^\circ_{P_r,971} - H^\circ_{P_r,T_r}$ for Z = 0.06. Because this value is consistent with

[14] Recent measurements of the heat capacities of low and high albite from 350° to 1000°K by Hemingway, Krupka, and Robie (1977, written commun.) apparently contradict the results of Holm and Kleppa's (1968) drop calorimetry experiments. However, this may be due to kinetic constraints on displacive disorder, which are coupled to annealing time and the rate at which the Z ordering parameter changes with increasing temperature (see above). The heat capacities of low albite reported by Hemingway, Krupka, and Robie are in close agreement with those given by Kelley (1960), which were adopted in the present study.

Holm and Kleppa's (1968) annealing experiments, it is used below in preference to the drop calorimetry results to calculate ΔH°_{dt} as a function of temperature.

The lowest temperature at which displacive disorder occurs in albite has yet to be determined. However, the magnitude of the interval separating the curves in figure 50 suggests that displacive disorder is negligible below 350°C (see below). This conclusion is consistent with the fact that no evidence of displacive disorder is apparent in the heat capacity data reported by Openshaw and others (1976) for temperatures below 373°K. If we take 350°C as the temperature at which displacive disorder becomes appreciable and assume $(\partial(\Delta H^\circ_{dt})/\partial T)_Z$ to be independent of temperature (which is likely), it follows from the value of $H^\circ_{P_r,971} - H^\circ_{P_r,T_r}$ for $Z = 0.06$ adopted above that

$$\left(\frac{\partial(\Delta H^\circ_{dt})}{\partial T}\right)_{Z=0.06} = \frac{860}{971 - 623} = 2.47 \text{ cal mole}^{-1} (^\circ K)^{-1} \tag{153}$$

Because $(\partial(\Delta H^\circ_{dt})/\partial Z)_T$ is apparently independent of Z (fig. 50) we can write for $623^\circ K < T < T_{m/a}$,

$$\Delta H^\circ_{dt,P_r,T} = (2.47 - 2.63(Z - 0.06))\,(T - 623) \tag{154}$$

and

$$\left(\frac{\partial(\Delta H^\circ_{dt})}{\partial Z}\right)_T = -2.63(T - 623) \tag{155}$$

where −2.63 corresponds to the slope of the curve in figure 53 and 10^{-3} of that of the curves in figure 50. Eq (152) can now be written as

$$\Delta C^\circ_{P_r,dt} \equiv \left(\frac{\partial(\Delta H^\circ_{dt})}{\partial T}\right)_{P_r} = 2.47 - 2.63(Z - 0.06) - 2.63(T - 623)\left(\frac{\partial Z}{\partial T}\right)_{P_r} \tag{156}$$

where $\Delta C^\circ_{P_r,dt}$ refers to the standard molal heat capacity of displacive disorder. Values of ΔH°_{dt} calculated from eq (154) are shown as a function of temperature in figure 54A, where it can be seen by comparison with figure 51D that the temperature dependence of ΔH°_{dt} is similar to that of ΔH°_{ds}.

Finite difference derivatives of ΔH°_{dt} are plotted in figure 54B to illustrate the extent to which $\Delta C^\circ_{P_r,dt}$ changes with increasing temperature. The curve in figure 54B exhibits the "classic" configuration of a lambda transition. It can be seen by comparison of this curve with that in figure 55B that $\Delta C^\circ_{P_r,dt}$ is only slightly smaller than $\Delta C^\circ_{P_r,ds}$ at the respective lambda points.

The total standard molal heat capacity of disorder ($\Delta C^\circ_{P_r,t}$) in albite is depicted as a function of temperature in figure 56. The values of

$\Delta C^\circ_{P_{r,t}}$ represented by the symbols were computed by taking finite difference derivatives of ΔH°_t, which is defined by

$$\Delta H^\circ_t \equiv \Delta H^\circ_{ds} + \Delta H^\circ_{dt} \tag{157}$$

and consistent with

$$\Delta C^\circ_{P_{r,t}} \equiv \Delta C^\circ_{P_{r,ds}} + \Delta C^\circ_{P_{r,dt}} \tag{158}$$

It can be seen in figure 56 that $\Delta C^\circ_{P_{r,t}}$ increases dramatically from 500° to 700°K, where it reaches 7 cal mole^{-1} (°K)$^{-1}$ at the lambda point. This sharp increase in $\Delta C^\circ_{P_{r,t}}$ is a consequence of the fact that the displacive and substitutional order/disorder transformations are superimposed on one another. Because the lambda points for the two transitions occur at low and high temperatures, respectively (figs. 54B and 55B), the slope of the curve in figure 56 changes only slightly from ~ 750° to ~ 1000°K.

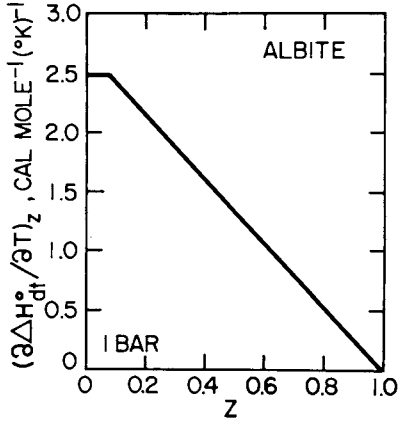

Fig. 53. Partial derivative of the standard molal enthalpy of displacive disorder in albite with respect to temperature at constant pressure and Z as a function of the Z ordering parameter at 1 bar (see text).

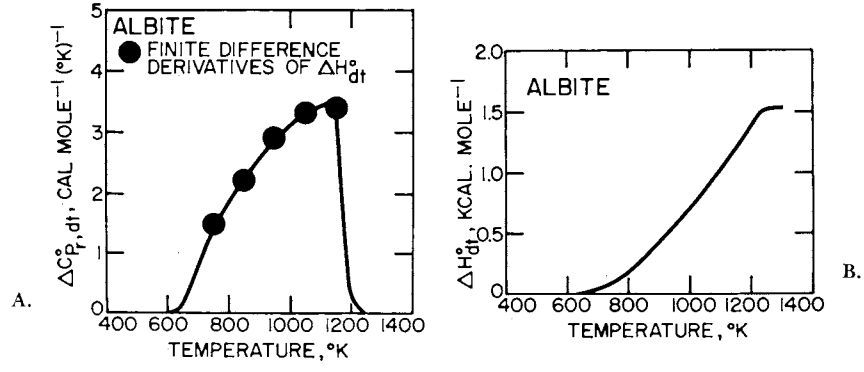

Fig. 54. Standard molal enthalpy and heat capacity of displacive disorder in albite as a function of temperature at 1 bar (see text).

It is not surprising in view of the configurations of the curves in figures 54B, 55B, and 56 that so much confusion has arisen over phase transitions in albite. For example, Holm and Kleppa (1968) considered the low/high albite transition to be first-order, and Orville (1974) estimated the temperature of transition as 575°C, which is not far from the lambda point in figure 56.

The separation of the two curves shown in figure 50 is probably a consequence of metastable cooling of intermediate albites. This can be demonstrated with the aid of figure 57. The solid curve in figure 57A represents albite in a state of stable homogeneous equilibrium at all

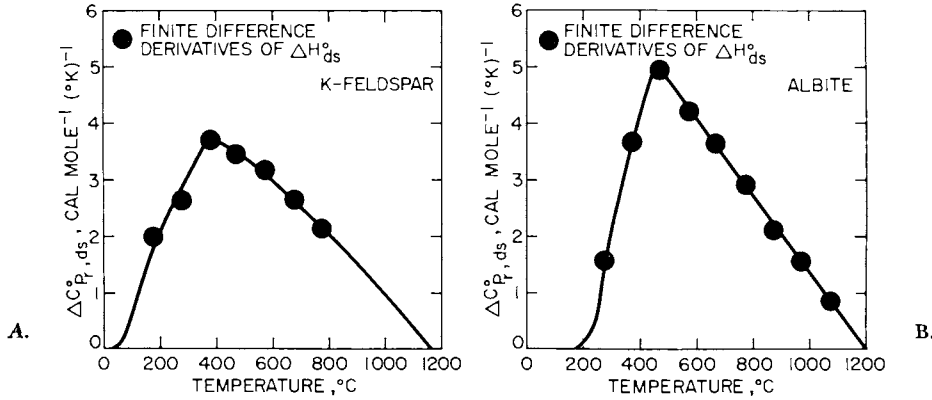

Fig. 55. Standard molal heat capacity of substitutional disorder in K-feldspar and albite as a function of temperature at 1 bar.

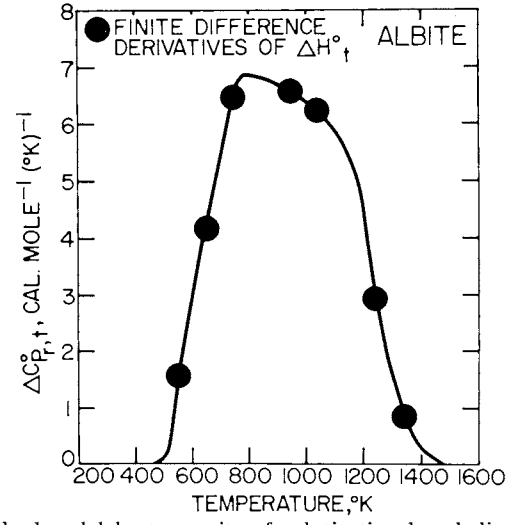

Fig. 56. Standard molal heat capacity of substitutional and displacive disorder in albite ($C^\circ_{P_r,t} = C^\circ_{P_r,ds} + C^\circ_{P_r,dt}$) as a function of temperature at 1 bar.

temperatures. The dashed curves designate displacive equilibrium cooling paths for albites with constant Z. In contrast, the dashed curves in figure 57B correspond to metastable cooling paths for constant Z, which have the same slope as the equilibrium cooling path for Z = 0.06. If an intermediate albite cools rapidly so that Z remains constant, it may not follow the dashed lines of constant order in figure 57A, which correspond to path *abc* in figure 57B. Instead, the kinetic observations noted above suggest it may follow a metastable cooling path like those labeled *ad* in figure 57B. As a consequence, $H°_Z - H°_{Z=1}$ at low temperatures would be smaller than the equilibrium value for constant Z by an amount corresponding to *cd* in figure 57B. The magnitude of *cd* in figures 50 and 57B, which is independent of Z, depends solely on $(\partial(\Delta H°_{dt})/\partial T)_Z$ for Z = 0.06.

The heat capacity power function coefficients given in table 8 for albite (which refers in the present communication to $NaAlSi_3O_8$ in its stable state of substitutional and displacive disorder) above 473°K were obtained by first adding $\Delta H°_{ds,P_r,T}$ and $\Delta H°_{dt,P_r,T}$ to values of $H°_{P_r,T} - H°_{P_r,473}$ calculated from eq (26) and the heat capacity coefficients reported by Kelley (1960) for albite. This procedure is based on the assumption that the high-temperature enthalpy differences given by Kelley and others (1953) for albite from Varuträsk, Sweden, closely approximate those of low albite with Z = Y = 1. The heat capacity coefficients reported by Kelley (1960) correspond to those shown in table 8 for low albite. The same coefficients are given in the table for albite in the temperature range 298.15° to 473°K, where both $\Delta C°_{P_r,dt}$ and $\Delta C°_{P_r,ds} \approx 0$. Regression of finite difference derivatives of the calculated values of $H°_{P_r,T} -$

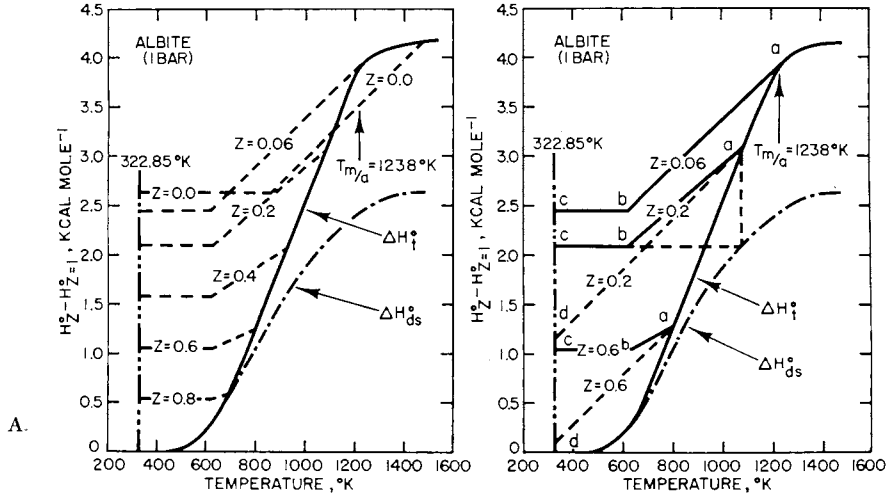

Fig. 57. Standard molal enthalpy of substitutional and displacive disorder ($\Delta H°_t = \Delta H°_{ds} + \Delta H°_{dt}$) in albite as a function of temperature at 1 bar. The dashed curves represent alternate possible cooling paths for albite in different states of order (see text).

$H°_{P_r,473}$ generated the second set of coefficients for albite in table 8. The corresponding set of heat capacity coefficients for high albite shown in the table were calculated by adding 2.47 to the *a* coefficient for low albite in the temperature range $T > 350°C$. The heat capacity coefficients for high albite at temperatures $< 350°C$ (where $\Delta C°_{P_r,dt} \approx 0$) correspond to those for low albite. Consequently, the heat capacity coefficients for high albite do not represent accurately $C°_{P_r}$ for high albite from 350°C to ~ 450°C, but the effect of this disparity on the accuracy of computed values of $H°_{P_r,T} - H°_{P_r,T_r}$ for high albite is negligible. Calculated values of $H°_{P_r,T} - H°_{P_r,T_r}$ for albite, low albite, and high albite are shown as a function of temperature in figure 58.

Finite difference derivatives of $H°_{P_r,T} - H°_{P_r,473}$ for albite are plotted in figure 59B, where they can be compared with the curves generated from the heat capacity coefficients in table 8. It can be seen that the calculations closely approximate the finite difference derivatives below the lambda point. However, the dashed curve above $T_{m/a}$, which corres-

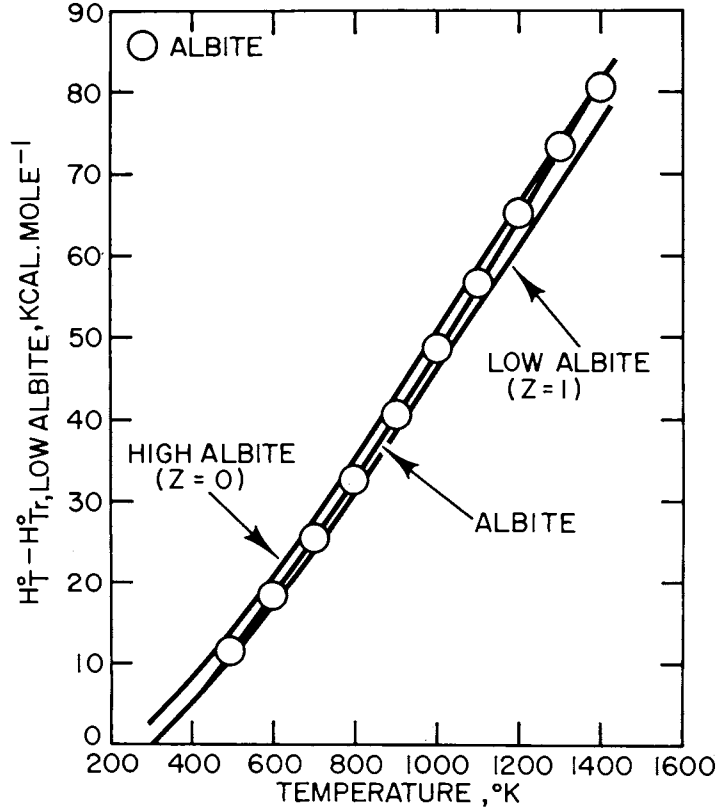

Fig. 58. Relative standard molal enthalpy of albite as a function of temperature at 1 bar.

ponds to calculated values of $C°_{P_r}$, differs significantly from that represented by the solid curve connecting the finite difference derivatives above the lambda point. This discrepancy limits the applicability of the heat capacity coefficients for albite in table 8 to temperatures < 1200°K.

Extrapolation of $S°_{P_r,1200} - S°_{P_r,T_r}$ computed from eq (27) and the coefficients for albite in table 8 to $T_{m/a}$ (1238°K) yields 97.74 cal mole^{-1} (°K)$^{-1}$ for $S°_{P_r,1438} - S°_{P_r,T_r}$. Similar extrapolation of $\Delta S°_{ds}$ from 1238° to 1473°K (T_{ds}) results in 0.13 cal mole^{-1} (°K)$^{-1}$. The difference in the sum of these values (97.87 cal mole^{-1} (°K)$^{-1}$) and $S°_{P_r,1238} - S°_{P_r,T_r}$ for low albite (92.95 cal mole^{-1} (°K)$^{-1}$) corresponds to $\Delta S°_{t,P_r,1473}$, which is the total standard molal entropy of displacive and substitutional disorder in albite caused by a temperature increase from $T_{Z=1}$ to $T_{Z=0}$. However, because the standard molal heat capacity of high albite is larger than that of low albite, this value (4.92 cal mole^{-1} (°K)$^{-1}$) is diminished by 2.13 cal mole^{-1} (°K)$^{-1}$ as temperature decreases to 298.15°K. It follows that the difference in the standard molal entropies of high and low albite at 25°C and 1 bar is 2.79 cal mole^{-1} (°K)$^{-1}$, which is close to that computed recently by Mazo (1977) from statistical mechanical considerations of Al/Si disorder (3.1 cal mole^{-1} (°K)$^{-1}$) but substantially less than the ideal configurational entropy (4.47 cal mole^{-1} (°K)$^{-1}$) adopted by Waldbaum (1968), Robie and Waldbaum (1968), and Hemingway and Robie (1977a). Adding this difference to the calorimetric third law entropy of low albite obtained by Openshaw (ms) leads to the value of $S°_{P_r,T}$ given in table 8 for high albite. The value of $V°_{P_r,T_r}$ for albite is approximated in table 8 by the mean of the corresponding values for high and low albite.

The calculations summarized above indicate that displacive disorder accounts for about a third of the total contribution of disorder to the thermodynamic behavior of albite. The maximum contribution by $\Delta H°_{ds}$ for Z = 0 (2630 cal mole^{-1}) corresponds to albite in its equilibrium ordering state at temperatures $\geqslant T_{ds}$ (1473°K), which is above the melt-

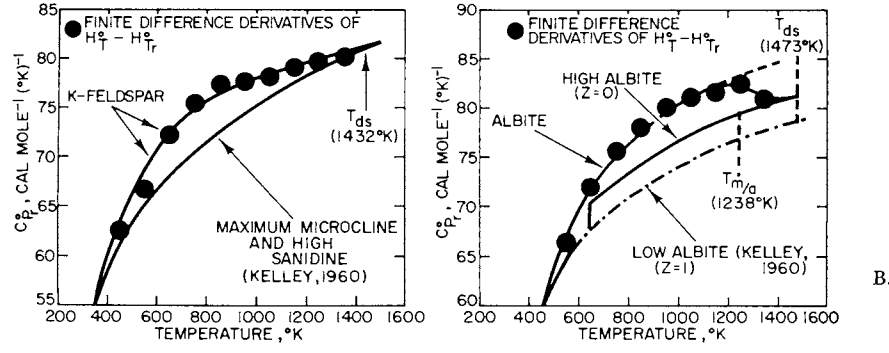

Fig. 59. Standard molal heat capacity of K-feldspar and albite as a function of temperature at 1 bar.

ing point of albite. Because there is no evidence of a first-order transition at $T_{m/a}$, the total heat of displacive and substitutional disorder at the melting point (1391°K at 1 bar, where $Z \approx 0.01$) is > 4000 cal mole^{-1}.

Order/disorder in K-feldspar.—The standard molal enthalpy of formation from the elements of high sanidine given by Robie and Waldbaum (1968) was taken from Waldbaum's (ms and 1968) calorimetric study of the alkali feldspars. Although this value was obtained using a sample of stoichiometric high sanidine (Waldbaum and Robie, 1971), it appears from the relation between the Z ordering parameter and the lattice constants for monoclinic potassium feldspar given by Hovis (1974) that the sample was not completely disordered. The Z ordering parameter is related to the b and c lattice constants by

$$Z \equiv 2(X_{Al,T_1} - X_{Al,T_2}) = 7.6344 - 4.3584b + 6.8615c \qquad (159)$$

where X_{Al,T_1} and X_{Al,T_2} refer to the mole fractions of aluminum on the T_1 and T_2 sites, respectively. Combining eq (159) with the cell parameters reported by Waldbaum (1968) for the sample of high sanidine used in his calorimetric experiments yields $Z = 0.098$. Taking account of the linear dependence of the heat of solution of K-feldspar on Z at 49.7°C (Hovis, 1974), the standard molal enthalpy of disorder ($\Delta H°_{ds}$) in cal mole^{-1} can be expressed as (fig. 60)

$$\Delta H°_{ds} = 2650(1 - Z). \qquad (160)$$

It follows that the standard molal enthalpy of formation from the elements at 25°C and 1 bar of high sanidine for which $Z = 0.098$ is more negative than that of its completely disordered counterpart by ~ 260 cal mole^{-1}.

It can be seen in figure 51 that the Z ordering parameters for K-feldspar and albite are nearly equal at equivalent temperatures. As in the case of albite, the dependence of Z on temperature is a function of the standard molal heat capacity of reaction ($\Delta C°_{P_r}$) for intracrystalline exchange of Al and Si among the energetically distinct tetrahedral sites

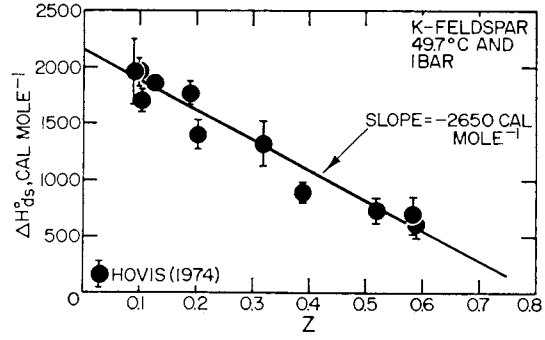

Fig. 60. Standard molal enthalpy of substitutional disorder ($\Delta H°_{d_s}$) in K-feldspar as a function of the Z ordering parameter at 49.7°C and 1 bar.

in K-feldspar. The intracrystalline exchange reaction for monoclinic potassium feldspars can be written as

$$Al_{T_1} + Si_{T_2} \rightleftharpoons Al_{T_2} + Si_{T_1} \tag{161}$$

for which

$$\frac{a_{Al,T_2}\, a_{Si,T_1}}{a_{Al,T_1}\, a_{Si,T_2}} = K \tag{162}$$

where K refers to the equilibrium constant for reaction (161). If as a first approximation we regard the activity coefficients for *Al* and Si on the tetrahedral sites as unity, it follows from the stoichiometry of $KAlSi_3O_8$ and eq (162) that we can write (Thompson, 1969)

$$ln\left(\frac{1-Z}{1+Z}\right) + ln\left(\frac{3-Z}{3+Z}\right) = -2(\text{arctanh } Z + \text{arctanh } (Z/3)) = ln\ K. \tag{163}$$

If $\Delta C^\circ_{P_r} = 0$ for reaction (161), which seems likely, *ln* K in eq (163) is a linear function of T^{-1}, and we can write,

$$ln\ K = -\frac{-\Delta H^\circ_r}{R}\left(\frac{1}{T} - \frac{1}{T_{ds}}\right) \tag{164}$$

where ΔH°_r refers to the standard molal enthalpy of reaction (which is independent of temperature) and T_{ds} designates the temperature in °K at which Z = 0 (1432°K). Eq (164) is represented by the curve in figure 61, which was generated from eq (163) and the curve shown in figure 51A. The slope of the curve in figure 61 is consistent with

$$\Delta H^\circ_r = \frac{\Delta H^\circ_{ds,Z}}{\nu_{Al,T_1,Z=1} - \nu_{Al,T_1,Z}} = \frac{2650}{0.5} = 5300 \text{ cal mole}^{-1} \tag{165}$$

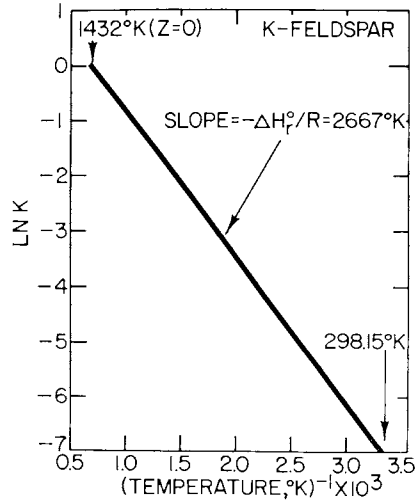

Fig. 61. Logarithm of the equilibrium constant for reaction (161) as a function of temperature^{-1} at 1 bar.

where $\nu_{Al,T_1,Z=1}$ and $\nu_{Al,T_1,Z}$ refer to the number of moles of Al on the T_1 sites (gram formula unit)$^{-1}$ of K-feldspar for Z = 1 and Z, respectively. The value of $\Delta S°_r$ for reaction (161) consistent with the linear curve in figure 61 is 5400 cal mole^{-1}/1432°K = 3.7 cal mole^{-1} (°K)$^{-1}$, which corresponds to that used by Hovis in his calculation of Z as a function of temperature.

Eqs (163) through (165) describe the temperature dependence of Z in figure 51A. The sigmoid configuration of the curves in figures 51A and B arise from constraints imposed by the limits of Z. As Z $\rightarrow$ 0, ln K $\rightarrow$ 0, but as Z $\rightarrow$ 1, ln K $\rightarrow -\infty$.

Waldbaum and Robie (1971) report −146,698 cal mole^{-1} for the heat of solution at 49.7°C of the slightly ordered sample of high sanidine discussed above. In contrast, Hovis' (1974) data indicate −148,200 cal mole^{-1} for the heat of solution of high sanidine with Z = 0.098. The two contradictory heats of solution (neither of which were used in the present study to compute $\Delta H°_f$ of high sanidine — see below) are plotted in figure 62, which was generated by taking account of the temperature dependence of the Z ordering parameter for monoclinic potassium feldspar (fig. 51A). Hovis (1974) and Hemingway and Robie (1977a) attribute the bulk of the discrepancy between the results of the two calorimetric studies to systematic differences in the data acquisition systems employed in the two investigations. Each system apparently yields accurate relative heats of solution as a function of composition or substitutional order/disorder, but the absolute heats of solution generated by the two systems are not comparable. It is of interest to note in this regard that the heats of solution reported recently by Hemingway and Robie (1977a) for Amelia

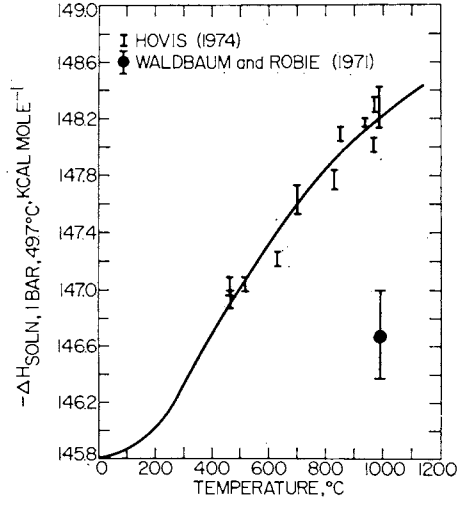

Fig. 62. Heats of solution at 49.7°C and 1 bar of monoclinic potassium feldspars in different states of substitutional disorder plotted at temperatures corresponding to the values of Z represented by the feldspars.

albite in a 20.1 wt percent hydrofluoric acid solution at 49.7°C are only ~ 500 cal mole^{-1} more negative than comparable values measured by Waldbaum and Robie (1971).

Because the calorimetric data given by Hovis (1974) are internally consistent and represent a range of Z from 0.093 to 0.590 for $X_{KAlSi_3O_8} > 0.9734$, the temperature dependence of the standard molal enthalpy of substitutional order/disorder in K-feldspar (ΔH°_{ds}) can be computed from his heats of solution and the curve representing Z as a function of temperature in figure 51A. Calculated values of ΔH°_{ds} for K-feldspar are plotted in figure 51C, where they can be compared with corresponding values for albite (figure 51D). The curve shown in figure 51C was generated from eq (160) and values of Z corresponding to a series of temperatures from 298.15°K (where Z = 1) to 1432°K (where Z = 0) in figure 51A.

Finite difference derivatives of ΔH°_{ds} for K-feldspar and albite can be compared in figure 55. Although the curves representing $\Delta C^\circ_{P_r,ds}$ as a function of temperature are similar in configuration, it can be seen that $\Delta C^\circ_{P_r,ds}$ of albite exceeds that of K-feldspar by more than a cal mole^{-1} (°K)$^{-1}$ at the respective lambda points.

The standard molal heat capacity of K-feldspar can be calculated by first combining the values of ΔH°_{ds} computed above with corresponding values of $H^\circ_{P_r,T} - H^\circ_{P_r,T_r}$ calculated from eq (26) and the heat capacity power function coefficients for maximum microline in table 8. Regression of the finite difference derivatives of these values of $H^\circ_{P_r,T} - H^\circ_{P_r,T_r}$ for K-feldspar in its stable ordering state with eq (19) generated the heat capacity coefficients shown for the mineral in table 8 and the curve depicted in figure 59A. It can be seen in this figure that eq (19) affords close approximation of the finite difference derivatives.

It is evident in figure 59 that the curves for K-feldspar and albite differ significantly, which is due primarily to the displacive transformation in albite. The corresponding change from triclinic to monoclinic symmetry in K-feldspar has no apparent effect on its thermodynamic behavior. Hovis (1974) estimated the triclinic/monoclinic temperature of transition for potassium feldspar to be 451° ± 47°C at 1 bar, which corresponds to Z ≈ 0.59. Because the difference in the heats of solution of maximum microcline and high sanidine measured by Waldbaum and Robie (1971) are consistent with Hovis' data for monoclinic K-feldspar, it appears that the triclinic/monoclinic transition in potassium feldspars is accompanied by a negligible heat of transition.

Values of ΔH°_{ds} and ΔS°_{ds} for Z = 1 to Z = 0 calculated from

$$\Delta H^\circ_{ds} = (H^\circ_{P_r,1432} - H^\circ_{P_r,298.15})_{K\text{-}feldspar} - (H^\circ_{P_r,1432} - H^\circ_{P_r,298.15})_{microcline} \quad (166)$$

and

$$\Delta S^\circ_{ds} = (S^\circ_{P_r,1432} - S^\circ_{P_r,298.15})_{K\text{-}feldspar} - (S^\circ_{P_r,1432} - S^\circ_{P_r,298.15})_{microcline} \quad (167)$$

using eqs (26) and (27) together with the heat capacity coefficients given in table 8 for K-feldspar and maximum microcline compare favorably with eq (160) and the value of $\Delta S°_{ds}$ estimated by Hovis for Z = 1 to Z = −1. Eqs (26) and (160) generate the same value of $\Delta H°_{ds}$ (2650 cal mole^{-1}), but eq (27) yields a value of $\Delta S°_{ds}$ (3.4 cal mole^{-1} (°K)$^{-1}$) for Z = 1 to Z = 0 which falls at the lower end of the uncertainty range given by Hovis for the estimate (3.7 ± 0.3 cal mole^{-1} (°K)$^{-1}$) he used to calculate Z as a function of temperature. Note that the value of $\Delta S°_{ds}$ for Z = 1 to Z = 0 is substantially less than the ideal configurational entropy of disorder (4.47 cal mole^{-1} (°K)$^{-1}$) adopted by Waldbaum (1968), Robie and Waldbaum (1968), and Hemingway and Robie (1977a).

The heat capacity power function coefficients given in table 8 for high sanidine are the same as those for maximum microcline. The coefficients for these two minerals were taken to be equal because Openshaw's (1974) calorimetric values of the standard molal third law entropies of microcline and high sanidine at 25°C and 1 bar differ by only 0.06 cal mole^{-1} (°K)$^{-1}$, and the difference in the corresponding heat capacities is only 0.07 cal mole^{-1} (°K)$^{-1}$ (Openshaw and others, 1976). Accordingly, the standard molal entropy of high sanidine in table 8 was calculated by adding $\Delta S°_{ds}$ = 3.4 cal mole^{-1} (°K)$^{-1}$ to the standard molal third law entropy of microcline (51.13 cal mole^{-1} (°K)$^{-1}$) reported by Openshaw (ms).

Paragonite, muscovite, K-feldspar, and albite.—The values of $\Delta G°_f$ and $\Delta H°_f$ given in table 8 for these minerals were calculated from equilibrium constants derived from high pressure/temperature experimental data for

$$\text{pyrophyllite} + \text{albite} \rightleftharpoons \text{paragonite} + 4\ SiO_{2(aq)}, \tag{168}$$

$$\text{albite} + K^+ \rightleftharpoons \text{K-feldspar} + Na^+, \tag{169}$$

$$2\ \text{muscovite} + 6\ \text{quartz} + 2\ H^+ \rightleftharpoons 3\ \text{pyrophyllite} + 2\ K^+, \tag{170}$$

and

$$\text{muscovite} + \text{quartz} \rightleftharpoons \text{K-feldspar} + \text{andalusite} + H_2O \tag{171}$$

using equations and data for the aqueous species given by Helgeson and Kirkham (1974a, 1976, and in press) and Walther and Helgeson (1977), and the values of $V°_{P_r,T_r}$, $S°_{P_r,T_r}$, and the standard molal heat capacity coefficients given in table 8 for the minerals appearing in these reactions.

Among the many pertinent equilibria for which experimental data are available (see below), reactions (168) through (171) were selected to optimize agreement of the computed values of $\Delta G°_f$ and $\Delta H°_f$ with both low and high-temperature solubility and phase equilibrium data and the compositions of interstitial waters in sediments. The experimental data used in the calculations are shown in figures 63A and B, 64, 65C, and 66A, where they can be compared with equilibrium con-

stants and univariant curves generated from thermodynamic data given in table 8.

Calculation of activity coefficients at high pressures and temperatures (Helgeson and Kirkham, in press) indicates that differences among $\bar{\gamma}_{K^+}$, $\bar{\gamma}_{Na^+}$, and $\bar{\gamma}_{H^+}$ are negligible (compared to experimental uncertainty) at the relatively low "true" ionic strengths of the electrolyte solutions considered by J. J. Hemley (1973, 1977, written commun.) and Montoya and Hemley (1975). It has also been demonstrated (Orville, 1963; J. J. Hemley, 1973, written commun.) that the activity coefficient of $SiO_{2(aq)}$ and the ratios of the activity coefficients of polar neutral species such as KCl, NaCl, and HCl in high temperature aqueous electrolyte solutions can be regarded as unity without introducing unacceptable uncertainties in computed equilibrium constants. Accordingly, all activity coefficients were set to one in the retrieval calculations.

The values of $\Delta G°_f$ and $\Delta H°_f$ for low albite in table 8 correspond to those for albite in its equilibrium state of order at 25°C and 1 bar, but the standard molal enthalpy of formation from the elements given for high albite is equal to the sum of $\Delta H°_f$ of low albite and $\Delta H°_{ds}$ for Z = 1 to Z = 0 (2630 cal mole^{-1}). This difference between the values of $\Delta H°_f$ for high and low albite is consistent with a corresponding difference of 2.79 cal mole^{-1} (°K)$^{-1}$ and 1799 cal mole^{-1} in $S°_{P_r,T_r}$ and $\Delta G°_f$, respectively. Similarly, the same values of $\Delta G°_f$ and $\Delta H°_f$ are given in

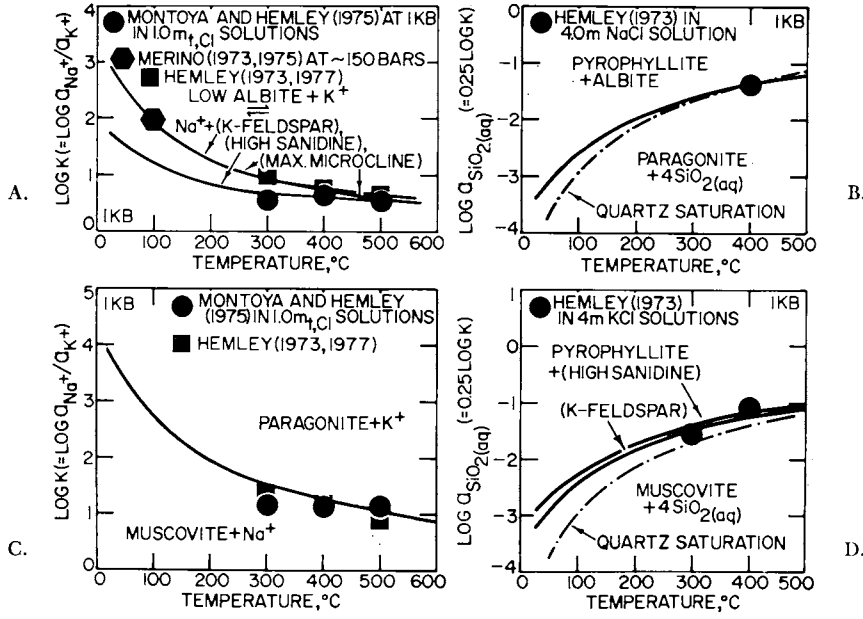

Fig. 63. Calculated (curves) and experimental (symbols) equilibrium constants for reactions in the system Na_2O–K_2O–Al_2O_3–SiO_2–H_2O as a function of temperature at 1 kb. Hemley (1973, 1977) refers to J. J. Hemley (1973, 1977, written commun.).

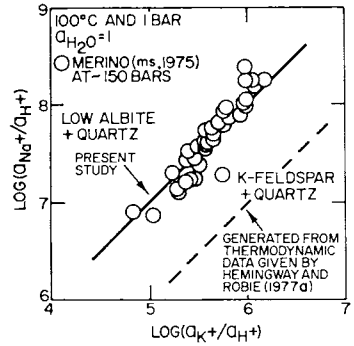

Fig. 64. Logarithmic activity diagram depicting log a_{Na^+}/a_{K^+} in interstitial waters coexisting with K-feldspar and albite in the Temblor and Upper McAdams sandstones, Kettleman North Dome, Calif. The solid curve is consistent with the thermodynamic data given in table 8, but the dashed curve was generated using data reported by Hemingway and Robie (1977a)—see text.

table 8 for maximum microcline and K-feldspar in its equilibrium state of order at 25°C and 1 bar, but those for high sanidine were computed by adding $\Delta H°_{ds} = 2650$ cal mole to $\Delta H°_f$ of microcline. The difference in the standard molal entropy of maximum microcline and high sanidine in table 8 corresponds to the value of ΔS_{ds} for Z = 1 to Z = 0 computed above (3.4 cal mole^{-1} °K^{-1}).

Despite the fact that relatively few experimental data were used in the retrieval calculations, it can be deduced from figures 63 through 68 that (with a few exceptions discussed below) the thermodynamic data given in table 8 are consistent with experimental equilibrium constants and univariant data for a large number of reactions at high pressures and temperatures. Separate curves are shown in figures 63A and D, 66, and 67 for maximum microcline, K-feldspar, high sanidine, low albite, albite, and high albite to illustrate the effects of order/disorder on solution compositions and reversal temperatures for reactions involving alkali feldspar.[15]

With a few exceptions (for example, Chelischev and Borutskaya, 1972; Chatterjee and Johannes, 1974), order/disorder in feldspars has received little attention in experimental studies of phase equilibria. Nevertheless, it appears likely from the distribution of the curves in figures 66 and 67 representing different states of order in feldspar, that discrepancies among experimental reversal temperatures reported by different investigators for the reactions shown in the figures can be attributed to different states of order in the feldspars produced and destroyed in the various laboratory studies. It can be seen that the decomposition

[15] As indicated in previous discussion, the terms K-feldspar and albite are used in the present communication to designate $KAlSi_3O_8$ and $NaAlSi_3O_8$ in their stable states of order at any temperature and pressure. Similarly, the names high sanidine and high albite connote complete disorder, whereas maximum microcline and low albite refer to the completely ordered phases.

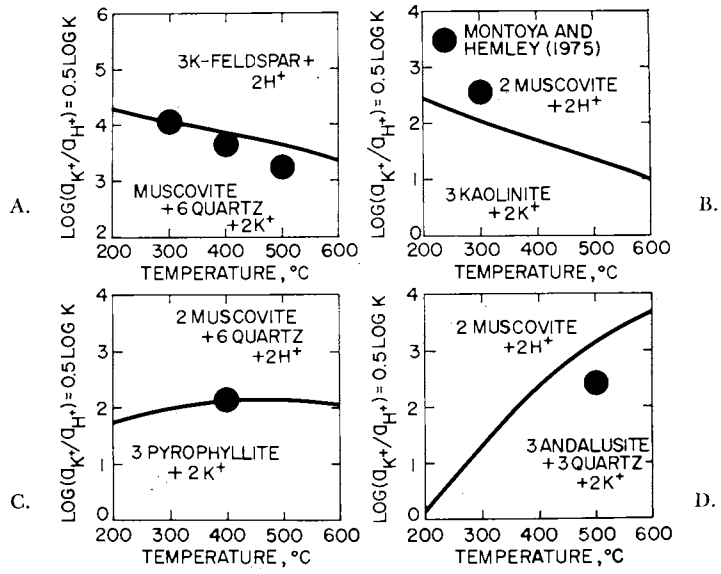

Fig. 65. Calculated (curves) and experimental (symbols) equilibrium constants for reactions in the system K_2O–Al_2O_3–SiO_2–HCl–H_2O as a function of temperature at 1 kb.

curves for muscovite generated from the thermodynamic calculations agree closely with the experimental reversals reported by Chatterjee and Johannes (1974), who calculated values of 0.11 to 0.19 for the Z ordering parameter in their reactant feldspars. The curve in figure 51A indicates that these values of Z correspond to equilibrium states of disorder for K-feldspar at temperatures ranging from ~ 800° to 950°C. Univariant curves representing reactions involving feldspars with these values of Z would thus lie between those for K-feldspar and high sanidine in figures 66 and 67C. In contrast, curves passing through Day's (1973) reversals and Velde's (1966) bracket at 2 kb would correspond to a more ordered state approaching that in metastable maximum microcline. It can be seen in figure 69 that $\Delta H°_{P,T}$ of a metastable ordered K-feldspar at 650°C is ~ 1 kcal mole^{-1} less negative than its stable counterpart.

Note that no provision for disorder in 2M muscovite is necessary to satisfy all the experimental data shown in figures 66 and 67C, which contradicts arguments and conclusions expressed by Ulbrich and Waldbaum (1976), Zen (1977), and Hemingway and Robie (1977a), who advocate adding an ideal mixing contribution to the standard molal third law entropy of muscovite. If in fact such a configurational contribution (4.47 cal mole^{-1} (°K)$^{-1}$) were added to the calorimetric standard molal entropy of muscovite in table 8, the Clapeyron slopes of the curves in figures 66 and 67C would be inconsistent with the experimental reversals. It can also be seen in figure 67A and B that no provision for disorder in paragonite is necessary to reproduce Chatterjee's (1970, 1972) experi-

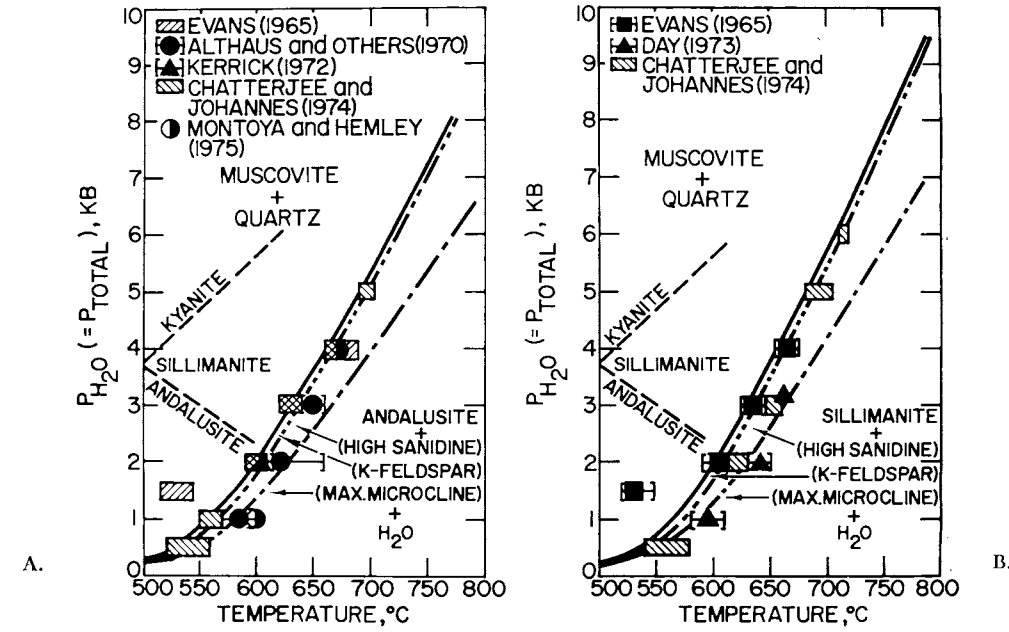

Fig. 66. Univariant equilibrium curves (generated from thermodynamic data given in table 8) and experimental observations of phase relations (symbols) in the system K_2O–Al_2O_3–SiO_2–H_2O at high pressures and temperatures.

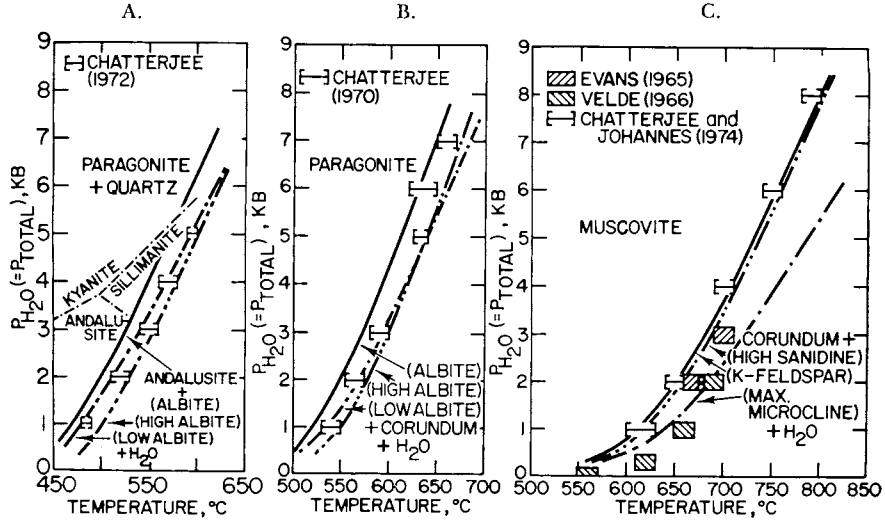

Fig. 67. Univariant equilibrium curves (generated from thermodynamic data given in table 8) and experimental observations of phase relations (symbols) in the systems Na_2O–Al_2O_3–SiO_2–H_2O and K_2O–Al_2O_3–SiO_2–H_2O at high pressures and temperatures.

mental reversals. However, it appears from figure 67B that the synthetic albite used in Chatterjee's (1970) experiments did not achieve its equilibrium state of disorder at high temperatures. This conclusion is supported by the somewhat erratic pressure distribution of the experimental temperature brackets in figure 67B and the relatively short duration of Chatterjee's (1970) experiments, which ranged from 17 to 152 days at 1 and 2 kb, but (with 3 exceptions) from 10 to 45 days at higher pressures. The fact that both 1M and 2M paragonite appeared in these experiments also introduces ambiguities in the results. In the case of figure 67A, the cell parameters reported by Chatterjee (1972) and eq (148) indicate a state of equilibrium disorder corresponding to ~ 750°C. Taking these observations into account, together with the nonstoichiometry of the albite in Chatterjee's (1972) experiments with albite, paragonite, and andalusite, the curves generated in the present study appear to be in excellent agreement with the experimental data.

The symbols shown in figures 63A and D, 64, and 65A represent equilibrium with adularia or microcline, and those shown in figures 63A and B and 68B refer to low albite. It is apparent in these figures that (with a few exceptions discussed below) the equation of state for aqueous species given by Helgeson and Kirkham (1976 and in press) and the thermodynamic properties of low albite, maximum microcline, high sanidine, and K-feldspar in table 8 afford close approximation of the equilibrium constants derived from experimental data and the com-

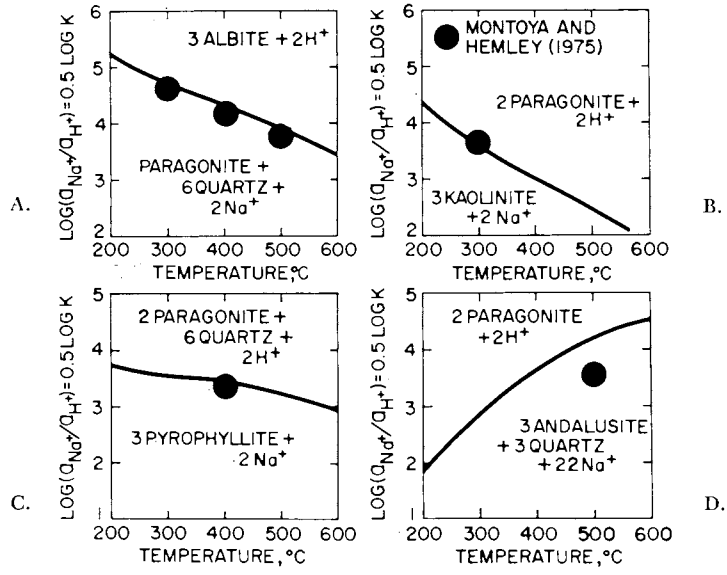

Fig. 68. Calculated (curves) and experimental (symbols) equilibrium constants for reactions among phases in the system Na_2O–Al_2O_3–SiO_2–HCl–H_2O as a function of temperature at 1 kb.

positions of natural waters. In contrast, it can be seen in figure 64 and deduced by comparison of figures 63A and 64 that the values of $\Delta G°_f$ and $\Delta H°_f$ given by Hemingway and Robie (1977a) for low albite and microcline are inconsistent with both Merino's (1973, 1975) data and those reported by Montoya and Hemley (1975) and J. J. Hemley (1973, 1977, written commun.). Hemingway and Robie report −948,301 ± 805, −940,515 ± 816, and −1,428,475 ± 773 cal mole^{-1} for $\Delta H°_f$ of microcline, low albite, and muscovite. These calorimetric values of $\Delta H°_f$ differ from those generated in the present study (table 8) by 887, 835, and 1067 cal mole^{-1}, respectively, which are only slightly larger than the uncertainty limits given by Hemingway and Robie.

The small discrepancies between the curves in figure 63 and the symbols representing Montoya and Hemley's (1975) calculated values of a_{Na^+}/a_{K^+} almost certainly arise from the relatively large uncertainties in the dissociation constants for NaCl and KCl employed in their calculations. For example, it can be deduced from consideration of figures 63C, 65B, and 68B that Montoya and Hemley's (1975) log K value for the

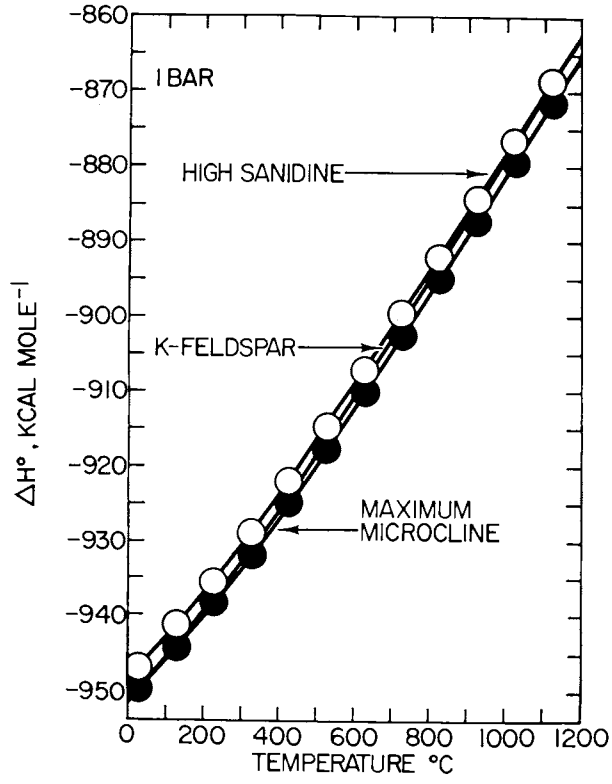

Fig. 69. Apparent standard molal enthalpy of formation of high sanidine (open symbols), K-feldspar (which refers to $KAlSi_3O_8$ in its stable state of order/disorder), and microcline (solid symbols) as a function of temperature at 1 bar.

reaction shown in figure 65B is inconsistent with J. J. Hemley's (1973, 1977, written commun.) values of log K for the reaction shown in figure 63C. In most instances the curves shown in figures 65 and 68 are in excellent agreement with the experimental equilibrium constants shown in the figures, but relatively large discrepancies are apparent in figures 65A, B, and D and 68D. Owing to the fact that these discrepancies are limited to certain reactions at a few temperatures, it seems unlikely that they can be attributed to noncompensating activity coefficients or errors in the equation of state coefficients employed in the present study to calculate $\Delta G°_{P,T,Na^+}$ and $\Delta G°_{P,T,K^+}$. Large uncertainties in the values adopted by Montoya and Hemley (1975) for the dissociation constant of KCl at 300° and 500°C (see Helgeson and Kirkham, 1976) are probably responsible for most of the disagreement in figures 65B and D. However, the fact that the discrepancies in figures 65D and 68D do not appear in figure 63C suggests compensating errors in Montoya and Hemley's calculation of a_{H^+} for the two reactions at 500°C. This calculation is sensi-

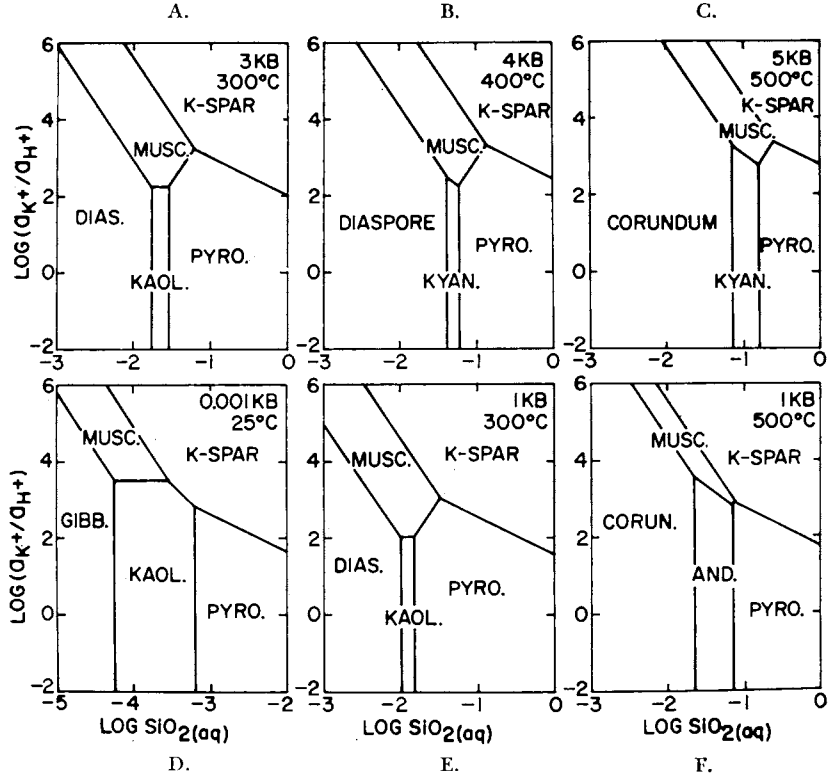

Fig. 70. Logarithmic activity diagrams for the system K_2O–Al_2O_3–HCl–H_2O at high pressures and temperatures. The positions of the stability field boundaries were computed for $a_{H_2O} = 1$ using thermodynamic equations and data for minerals summarized in the text and those for aqueous species given by Helgeson and Kirkham (1974a, 1976, and in press) and Walther and Helgeson (1977).

tive to the value adopted for the dissociation constant of HCl, which is uncertain to the extent of a log unit or more at 500°C and 1 kb (Chou and Frantz, 1977).

Activity diagrams generated from the thermodynamic data given in table 8 for minerals in the systems K_2O–Al_2O_3–SiO_2–HCl–H_2O and Na_2O–K_2O–Al_2O_3–SiO_2–HCl–H_2O are depicted in figures 70 and 71 for pressures and temperatures to 500°C and 5 kb. The thermodynamic properties of the aqueous species shown in the diagrams were computed from equations and data summarized by Helgeson and Kirkham (1974a, 1976, and in press) and Walther and Helgeson (1977). It can be seen that the stability field of paragonite in the presence of quartz appears only at high pressures or intermediate temperatures at low pressures. In the absence of quartz, the stability fields of kaolinite, kyanite, and andalusite are restricted to a few tenths of a log unit in $a_{SiO_{2(aq)}}$ at high pressures and temperatures. Note also that at high temperatures and low

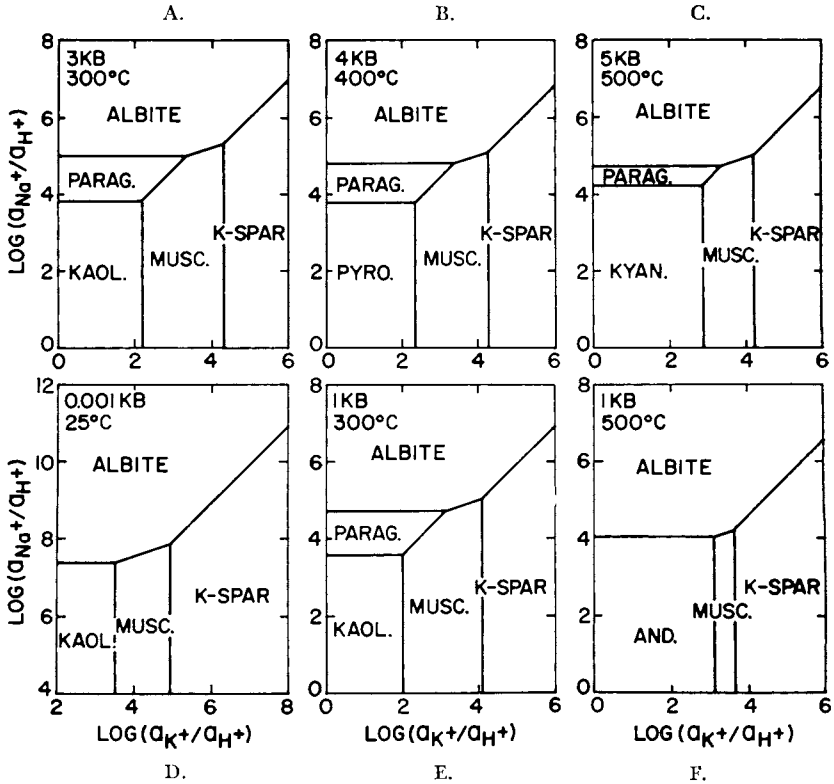

Fig. 71. Logarithmic activity diagrams for the system K_2O–Na_2O–Al_2O_3–SiO_2–HCl–H_2O at high pressures and temperatures. The positions of the stability field boundaries were computed for $a_{H_2O} = 1$ at quartz saturation using thermodynamic equations and data for minerals summarized in the text and those for aqueous species given by Helgeson and Kirkham (1974a, 1976, and in press).

pressures, the stability field of muscovite decreases dramatically in size with increasing temperature and/or decreasing pressure. Observations such as these underscore likely causes of the many difficulties encountered in both experimental and theoretical investigation of stability relations among aluminosilicates and aqueous solutions at high pressures and temperatures.

Although it might appear at first glance that the values of log a_{K^+}/a_{H^+} and log $a_{SiO_{2(aq)}}$ corresponding to the muscovite/kaolinite and K-feldspar/pyrophyllite boundaries in figure 70A are inconsistent with the compositions of natural waters presumed to be in equilibrium with montmorillonite and mixed layer clays, thermodynamic correlations of this kind depend on the ordering states and compositions of the minerals in the sediments and soils being considered. For example, if clay minerals coexist with metastable disordered feldspar, montmorillonite would be stable at much higher values of a_{K^+}/a_{H^+} for a given $a_{SiO_{2(aq)}}$ than those shown for the pyrophyllite/K-feldspar boundary in figure 70A. Considerations of this kind (Aagaard, Helgeson, and Benson, 1978) suggest that the phase relations shown in figure 70A are generally compatible with analytical data for clay minerals and ground waters in natural systems.

Kalsilite, analcime, nepheline, and jadeite.—High pressure/temperature experimental data reported by Hemley (1973, written commun.), Greenwood (1961), Liou (1971b), Kim and Burley (1971), Robertson, Birch, and MacDonald (1957), and Bell (1964) for

$$\text{muscovite} \rightleftharpoons \text{kalsilite} + \text{corundum} + 2\ SiO_{2(aq)} + H_2O, \quad (172)$$

$$\text{analcime} + SiO_{2(aq)} \rightleftharpoons \text{albite} + H_2O, \quad (173)$$

$$2\ \text{analcime} \rightleftharpoons \text{nepheline} + \text{albite} + 2\ H_2O, \quad (174)$$

and

$$2\ \text{jadeite} \rightleftharpoons \text{nepheline} + \text{low albite} \quad (175)$$

were used to retrieve values of ΔG°_f and ΔH°_f for kalsilite, analcime, nepheline, and jadeite. It can be deduced from figure 72 that the standard molal Gibbs free energies and enthalpies of formation retrieved for the first three of these minerals (table 8) are consistent with Hemley's (1973, written commun.) solubility data. However, those for analcime generate log K values for reaction (173) at temperatures and pressures corresponding to the vapor/liquid equilibrium curve for H_2O that differ slightly from those reported by Apps (ms). The latter discrepancy is probably a consequence of solid solution in the samples of analcime used by Apps.

The composition of both synthetic and natural analcime is highly variable (Saha, 1959, 1961; Greenwood, 1961; Wilkinson and Whetten, 1964; Coombs and Whetten, 1967; Thompson, 1971). Phase relations in the system $NaAlSiO_4$–SiO_2–H_2O are depicted in figure 73, where it can be seen that stoichiometric analcime cannot coexist with albite at any

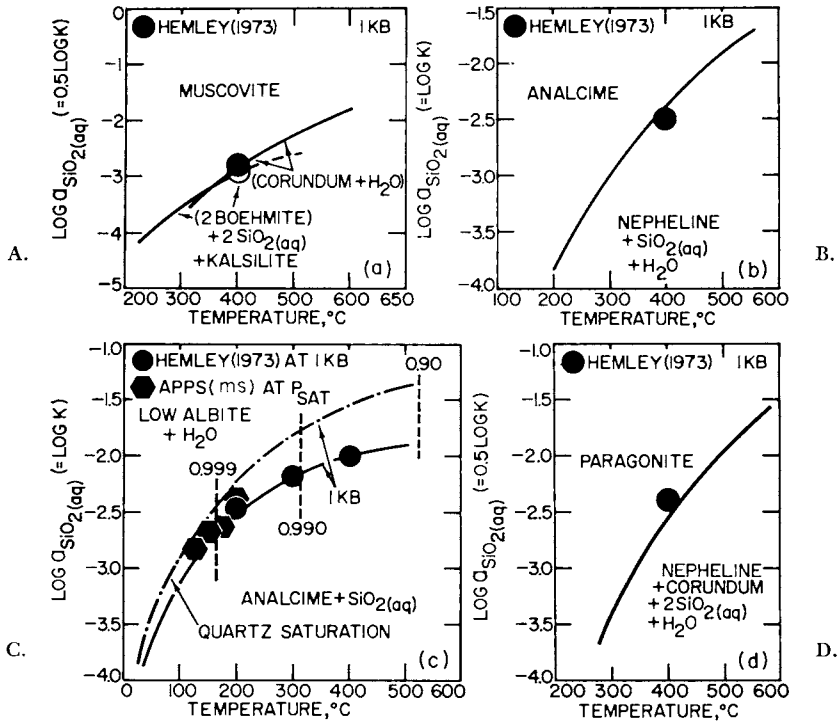

Fig. 72. Calculated (curves) and experimental (symbols) equilibrium constants for reactions in the system Na_2O–Al_2O_3–SiO_2–HCl–H_2O and K_2O–Al_2O_3–SiO_2–HCl–H_2O as a function of temperature at 1 kb and pressures corresponding to the vapor/liquid equilibrium curve for H_2O (P_{SAT}). Hemley (1973) refers to J. J. Hemley (1973, written commun.).

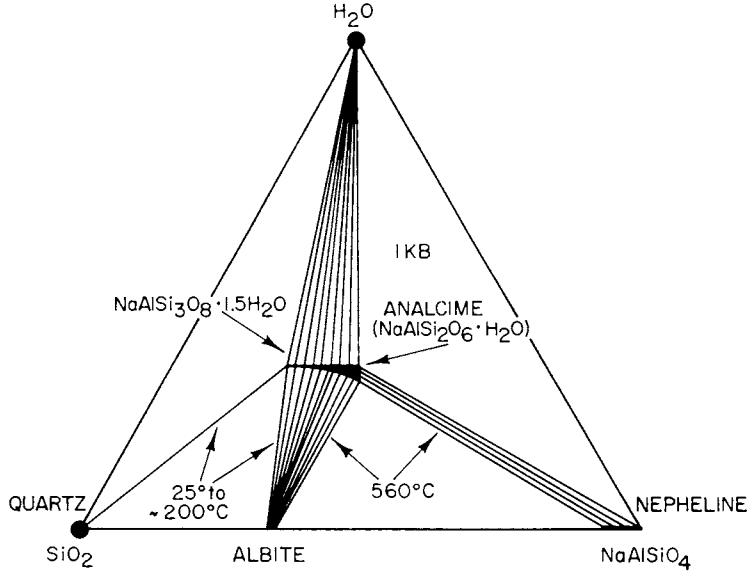

Fig. 73. Phase relations in the system $NaAlSiO_4$–SiO_2–H_2O (see text).

temperature. The compositional relations shown in figure 73 are based on data reported by Saha (1959, 1961), Mackenzie (1954), and Kim and Burley (1971), which were also used to construct the diagram shown in figure 74.

The extent to which analcime dehydrates with increasing temperature is shown in figure 75. The curves in figure 75A represent equilibrium constants pertaining to

$$\text{analcime} \rightleftharpoons \text{dehydrated analcime} + H_2O \tag{176}$$

for which the law of mass action can be written as

$$\frac{1 - X_a}{X_a} = \frac{\lambda_a K}{a_{H_2O}\lambda_d} \tag{177}$$

where the subscripts a and d refer to $NaAlSi_2O_6 \cdot H_2O$ and $NaAlSi_2O_6$, respectively. The values of $\Delta G°_f$ and $\Delta H°_f$ for dehydrated analcime in table 8 were computed from the value of $\Delta H°_r$ reported by Barany (1962) for reaction (176) at 25°C and 1 bar. Assuming $\lambda_a = \lambda_d = 1$ in eq (177), which seems likely, calculation of log K for reaction (176) as a function of temperature using the thermodynamic data given in table 8 for analcime and dehydrated analcime indicates that the activity of the $NaAlSi_2O_6 \cdot H_2O$ component in analcime decreases from unity at 25°C and 1 bar to ~ 0.9 at 500°C and 1 kb (fig. 75).

Taking account of the dehydration of analcime and the temperature dependence of the equilibrium compositions of coexisting albite and nepheline (fig. 74) permits calculation of the equilibrium constant for reaction (174), which can be expressed as

$$\frac{X_n X_{ab}}{X_a^2} = \frac{K \lambda_a^2}{a_{H_2O}\lambda_n \lambda_{ab}} \tag{178}$$

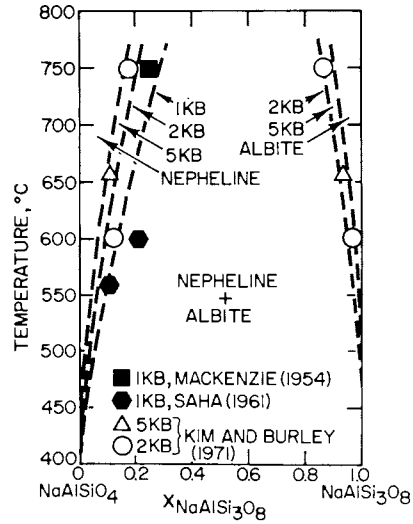

Fig. 74. Temperature-composition diagram for the system $NaAlSiO_4$–$NaAlSi_3O_8$.

where the subscripts *a*, *ab*, and *n* refer to $NaAlSi_2O_6 \cdot H_2O$, $NaAlSi_3O_8$, and $NaAlSiO_4$, respectively. Although solid solutions among nepheline and albite are obviously nonideal (fig. 74), the extent to which these two minerals dissolve in each other at temperatures below ~ 650°C is relatively small. Under these conditions λ_{ab} at $X_n << 1$ and λ_n at $X_{ab} << 1$ are probably close to unity. Hence, in a first approximation the activity coefficients in eq (178) can be set to one, which permits calculation of K for reaction (174) from the curves shown in figures 74 and 75. It can be deduced from figure 73 that analcime can be regarded as a solid solution of $NaAlSi_2O_6 \cdot H_2O$ and $NaAlSi_2O_6$ for the purpose of the calculation. It is evident in figure 76 that this procedure and the thermodynamic data for albite, analcime, and nepheline in table 8 yield equilibrium constants consistent with experimental reversal temperatures for reaction (174) at high pressures and temperatures. As noted above, the values of $\Delta H°_f$ and $\Delta G°_f$ for analcime and nepheline in table 8 are also consistent with J. J. Hemley's (1973, written commun.) solubility data (fig. 72), which refer to stoichiometric analcime.

Experimental reversal temperatures reported in the literature for

$$\text{analcime} + \text{quartz} \rightleftharpoons \text{albite} + H_2O \qquad (179)$$

are shown in figure 77B. Unless solid solution is taken into account, the experimental data plotted in figure 77B cannot be reconciled with those shown for other reactions involving analcime in figures 72 and 76. No indication is given by Thompson (1971) or Liou (1971b) of nonstoichiometry in the analcime produced in their experiments, but unambiguous determination of excess silica in analcime by X-ray methods requires evaluation of the angle of the $\bar{6}39$ peak, which is not part of the X-ray pattern normally used to identify the phase. Liou used cell

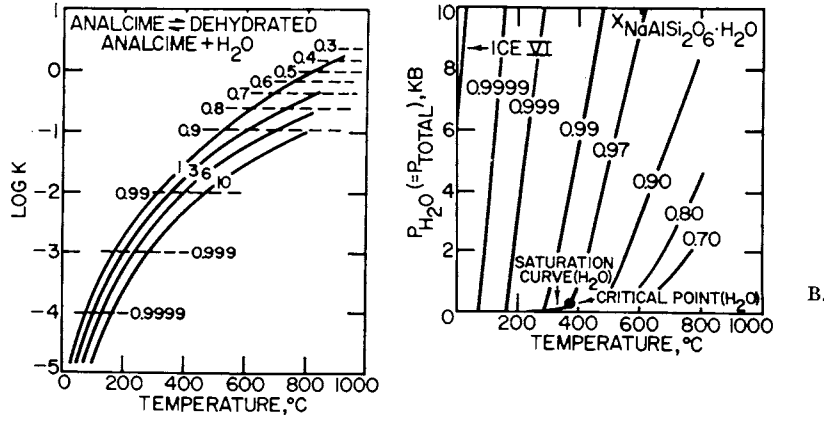

Fig. 75. Equilibrium constant for reaction (176) as a function of temperature at constant pressure (labeled in kb) and mole fraction isopleths for analcime-dehydrated analcime solid solutions as a function of pressure and temperature. The dashed curves in diagram A and the solid curves in diagram B designate $X_{NaAlSi_2O_6 \cdot H_2O}$.

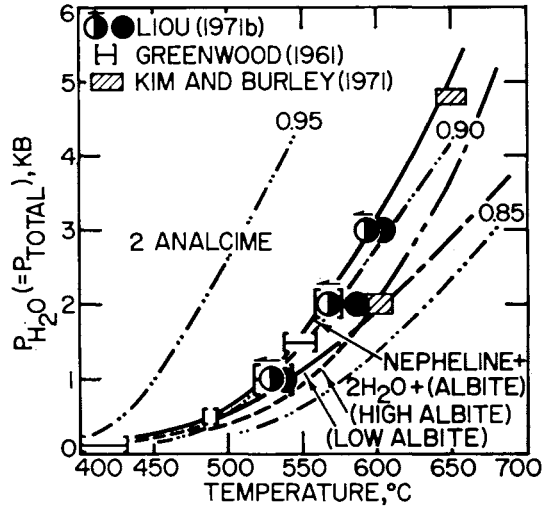

Fig. 76. Univariant equilibrium curves (generated from thermodynamic data given in table 8) and experimental observations of phase relations (symbols) in the system Na_2O–Al_2O_3–SiO_2–H_2O at high pressures and temperatures. The double-dot-dash curves represent isopleths of analcime composition designated by $X_{NaAlSi_2O_6 \cdot H_2O}$.

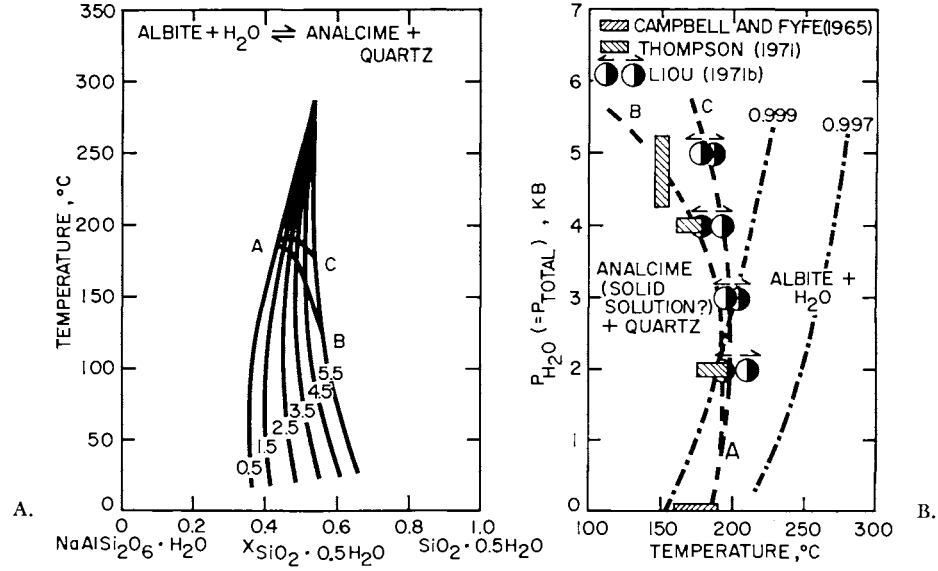

Fig. 77. Univariant equilibrium curves and temperature/composition relations in the system Na_2O–Al_2O_3–SiO_2–H_2O generated from thermodynamic data given in table 8 and the experimental observations of phase relations represented by the symbols in diagram B. The dot-dash curves represent isopleths of analcime composition in the system $NaAlSi_2O_6 \cdot H_2O$ – $NaAlSi_2O_6$ designated by $X_{NaAlSi_2O_6 \cdot H_2O}$.

edge determinations to monitor changes (or lack thereof) in analcime, but the cell edge of analcime is a function of both temperature and composition. In contrast, Thompson (1971) relied on a reversal criterion (see below) to assess the composition of the analcime produced in his experiments.

Because $\Delta S°_r$ and $\Delta V°_r$ for reaction (179) are small, it is not surprising that the reaction is sluggish and difficult to investigate experimentally. The amount of solid solution in analcime required to satisfy the various experimental reversals along curves AB and AC in figure 77B corresponds to that represented by curves AB and AC in figure 77A, which were generated by assuming ideal solid solution of $SiO_2 \cdot 0.5H_2O$ in $NaAlSi_2O_6 \cdot H_2O$. It can be seen that the discrepancies among the reversal temperatures reported by Thompson (1971) and those given by Liou (1971b) can be accounted for by slight differences (of the order of 0.01) in the mole fraction of $SiO_2 \cdot H_2O$ in the analcime produced in the two experimental studies. However, the analcime in both cases must have approached the composition of sodium phillipsite.

In analyzing the results of his weight-loss experiments, Thompson (1971) concluded that the equilibrium composition of analcime under the conditions of his experiments corresponded to that of the near-stoichiometric analcime in his starting materials. His conclusion is based on the observation that the temperatures at which the albite and quartz crystals showed no gain or loss in the experiments were essentially the same. However, this is not a valid criterion because the analcime in the starting materials could have changed composition without affecting

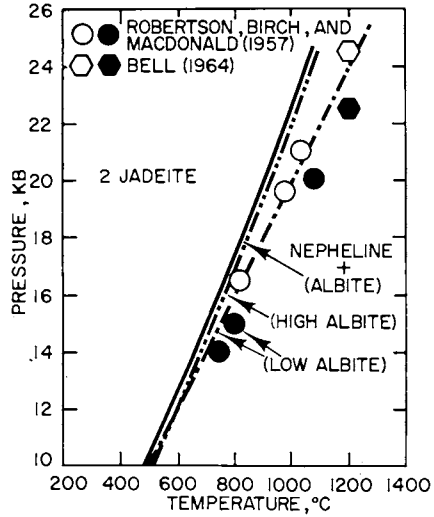

Fig. 78. Univariant equilibrium curves (generated from thermodynamic data given in table 8) and experimental observations of phase relations (symbols) in the system Na_2O–Al_2O_3–SiO_2 at high pressures and temperatures.

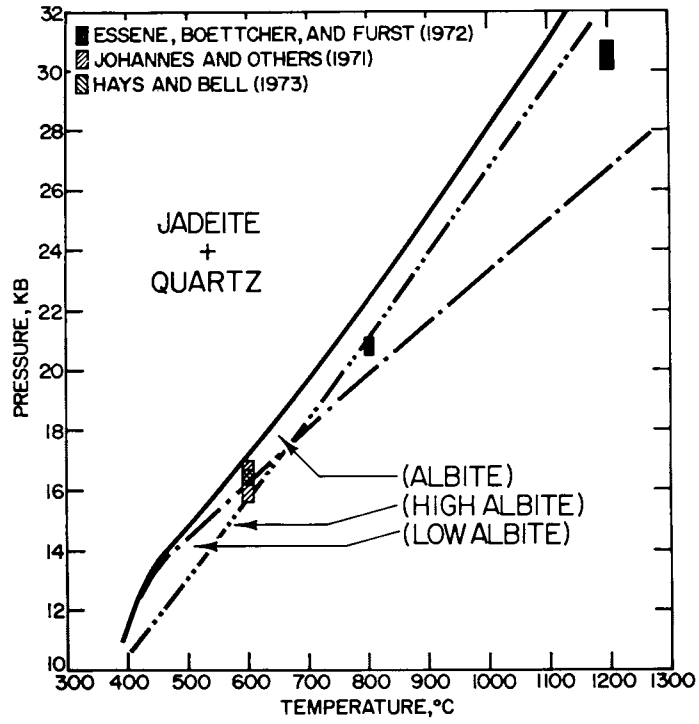

Fig. 79. Univariant equilibrium curves (generated from thermodynamic data given in table 8) and experimental observations of phase relations (symbols) in the system Na_2O–Al_2O_3–SiO_2 at high pressures and temperatures.

the reversible nature of the reaction. In fact, the relative gains and losses in the weight of the albite and quartz crystals reported by Thompson for a given increase or decrease in temperature at 2 kb (the only pressure where both minerals were monitored) are almost perfectly consistent with the compositional curves shown in figure 77A. These curves indicate an equilibrium composition of $NaAlSi_{2.82}O_{7.64} \cdot 1.41H_2O$ for analcime at Thompson's 2 kb reversal temperatures, which would require destruction of $\sim 1 \times 10^{-6}$ g of quartz to produce $\sim 26 \times 10^{-6}$ g of albite. This relative weight gain and loss is approximately equal to that observed by Thompson in the vicinity of his reversal temperatures.

The standard molal Gibbs free energy and enthalpy of formation of jadeite in table 8 were generated from the experimental data shown in figure 78. Because these data, as well as those shown in figure 79 were obtained from experiments of short duration using low albite, the thermodynamic properties of the latter mineral were used in the calculations instead of those of albite in its equilibrium state of order. However, it can be deduced from the distribution of the curves in figure 79 that the discrepancies at pressures > 20 kb between the calculated univariant curve for

$$\text{low albite} \rightleftharpoons \text{jadeite} + \text{quartz} \qquad (180)$$

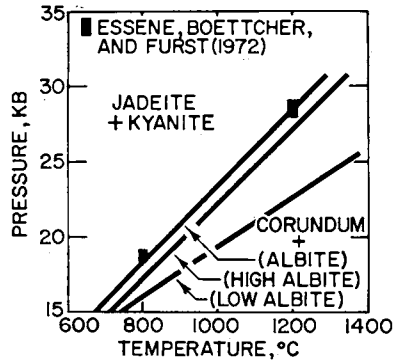

Fig. 80. Univariant equilibrium curves (generated from thermodynamic data given in table 8) and experimental observations of phase relations (symbols) in the system Na_2O–Al_2O_3–SiO_2 at high pressures and temperatures.

and the experimental reversals reported by Essene, Boettcher, and Furst (1972) probably result from differences in order/disorder in the feldspars produced and destroyed in the high-pressure experiments.

The effect of order/disorder in albite on equilibrium pressures and temperatures for reactions involving nepheline, analcime, and jadeite can be assessed in figures 76 and 78 through 80. Note also in the latter figure that the univariant curve generated from the thermodynamic data in table 8 for

$$\text{jadeite} + \text{kyanite} \rightleftharpoons \text{corundum} + \text{albite} \qquad (181)$$

is in close agreement with experimental observations of equilibrium pressures and temperatures for the coexistence of these minerals. Taking account of the difference in the value of $\Delta H°_f$ for corundum adopted by Robie and Waldbaum (1968) and that shown in table 8, the standard molal enthalpy of formation from the elements of jadeite derived in the present study is well within the uncertainty range of the value calculated by Robie and Waldbaum (1968). In contrast, the values of $\Delta H°_f$ for nepheline, analcime, and kalsilite in table 8 differ substantially from their calorimetric counterparts (see, for example, Hemingway and Robie, 1977a).

CaO–Al_2O_3–SiO_2–CO_2–H_2O

The thermodynamic properties of 11 calcium aluminum silicates are given in table 8. In each case the values of $\Delta G°_f$ and $\Delta H°_f$ were derived from experimental high pressure/temperature phase equilibrium data using the heat capacity coefficients and values of $V°_{P_r,T_r}$ and $S°_{P_r,T_r}$ given in the table for the minerals in this system.

Anorthite, grossular, zoisite, gehlenite, and Ca–Al pyroxene.—The standard molal enthalpies and Gibbs free energies of formation of these minerals in table 8 were calculated in the manner described above using experimental data for

$$\text{grossular} + \text{quartz} \rightleftharpoons \text{anorthite} + 2\ \text{wollastonite}, \qquad (182)$$

$$4 \text{ zoisite} + \text{quartz} \rightleftharpoons \text{grossular} + 5 \text{ anorthite} + 2\ H_2O, \quad (183)$$

$$2 \text{ grossular} \rightleftharpoons \text{anorthite} + 3 \text{ wollastonite} + \text{gehlenite}, \quad (184)$$

$$\text{grossular} + 2 \text{ kyanite} + \text{quartz} \rightleftharpoons 3 \text{ anorthite}, \quad (185)$$

and

$$\text{grossular} + 2 \text{ corundum} \rightleftharpoons 3 \text{ Ca–Al pyroxene}. \quad (186)$$

It can be seen in figures 81 and 82 that the univariant curves generated in the present study for these reactions are in close agreement with all the experimental reversals taken from the literature. Similar agreement is apparent in figure 83, where equilibrium pressures and temperatures are shown for the decomposition of zoisite to anorthite, grossular, corundum, and H_2O, and the reaction of zoisite, quartz, and kyanite or sillimanite to give anorthite and H_2O.

Calorimetric standard molal entropies and heat capacities are available for all the minerals other than Ca–Al pyroxene appearing in the reactions shown in figures 81 through 83. With the exception of $S°_{P_r,T_r}$ for gehlenite and anorthite, these values (table 8) were used in the retrieval calculations. In the case of gehlenite, a configurational contribution of 0.7 cal mole^{-1} (°K)$^{-1}$ was added to the calorimetric entropy cited by Robie and Waldbaum (1968) to optimize the Clapeyron slope of the curve in figure 82B. This value is considerably smaller than the ideal entropy of substitutional disorder (2.75 cal mole^{-1} (°K)$^{-1}$) assigned to gehlenite by Waldbaum (1973). In contrast, it appears that the configurational contribution to $S°_{P_r,T_r}$ for Ca–Al pyroxene is close to the ideal value. The standard molal entropy of Ca–Al pyroxene shown in table 8 (35.0 cal mole^{-1} (°K)$^{-1}$), which was derived from the Clapeyron slope of the curve in figure 82A, is ~ 2 to 5 cal mole^{-1} larger than that

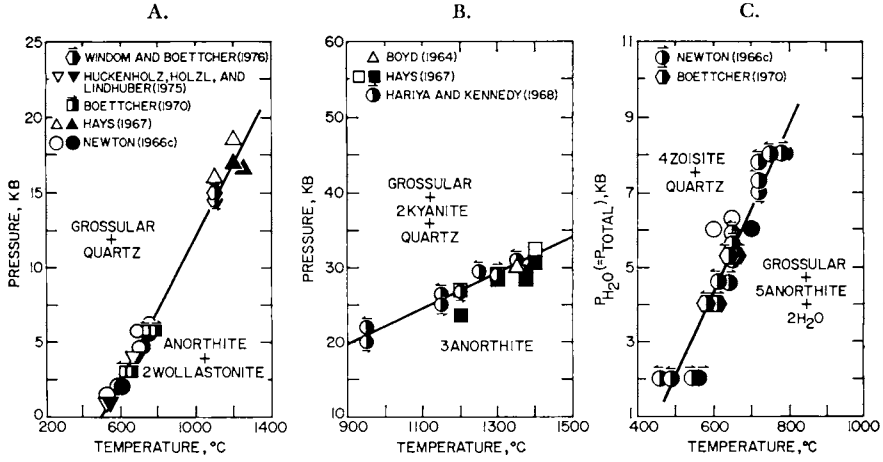

Fig. 81. Univariant equilibrium curves (generated from thermodynamic data given in table 8) and experimental observations of phase relations (symbols) in the system CaO–Al_2O_3–SiO_2–H_2O at high pressures and temperatures.

estimated from any of the algorithms cited above. These differences are consistent with complete disorder of Al and Si among the tetrahedral sites in Ca–Al pyroxene (Okamura, Ghose, and Ohashi, 1974).

Repeated attempts were made in the present study to satisfy all the Clapeyron slope constraints represented by the pressure distribution of the experimental reversals in figures 81 and 83 with the calorimetric standard molal entropies and heat capacities of all the minerals shown in the figures. Comparative analysis using alternate adjustments in the calorimetric entropies and heat capacities of these minerals led to the conclusion that all the calorimetric values of $S°_{P_r,T_r}$ for anorthite are too small to satisfy the high pressure/temperature phase equilibrium data. This conclusion is a consequence of the fact that anorthite is the only mineral that appears in all the reactions, and its reaction coefficient is different in each of them. Because the value of $S°_{P_r,T_r}$ for anorthite in table 8 (49.1 cal mole^{-1} (°K)$^{-1}$) optimizes the slopes of the curves in figures 81 and 83, it was adopted in the present study.

The standard molal entropy of anorthite given in table 8 is 0.65 cal mole^{-1} (°K)$^{-1}$ larger than that given by Robie and Waldbaum (1968), which is 0.82 cal mole^{-1} (°K)$^{-1}$ larger than the value adopted recently by Hemingway and Robie (1977a). However, it is 2 cal mole^{-1} (°K)$^{-1}$ smaller than the estimate (51.0 cal mole^{-1} (°K)$^{-1}$) afforded by eq (75) for the reference reaction,

$$\text{anorthite} + Na_2O + 4\ \text{quartz} \rightleftharpoons 2\ \text{low albite} + CaO \qquad (187)$$

Similarly, the standard molal entropy of grossular in table 8, which

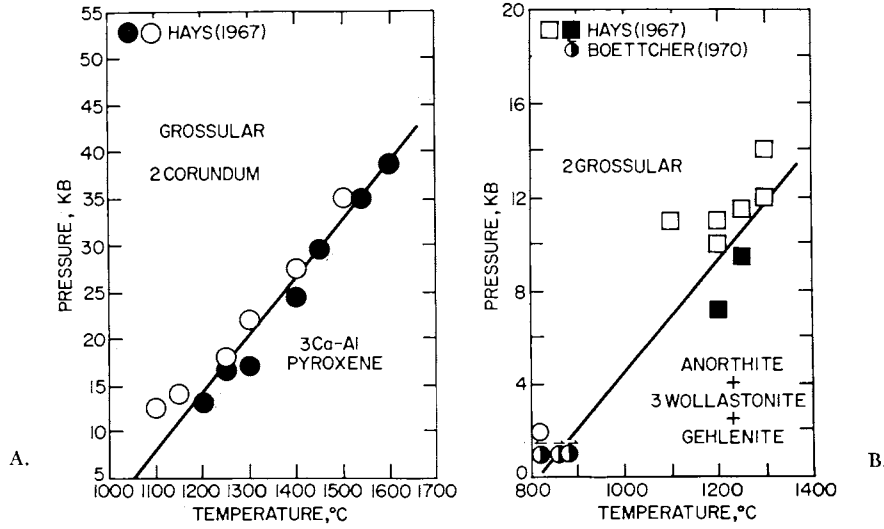

Fig. 82. Univariant equilibrium curves (generated from thermodynamic data given in table 8) and experimental observations of phase relations (symbols) in the system CaO–Al_2O_3–SiO_2–H_2O at high pressures and temperatures.

was derived from calorimetric measurements by Perkins and others (1977), differs from the estimate calculated from eq (73) by 1.8 cal mole^{-1} (°K)$^{-1}$. The value of $S°_{P_r,T_r}$ for zoisite reported by Dexter Perkins III (1977, written commun.) and adopted in the present study is nearly identical to that given by Kiseleva and Topor (1973).

The value of $\Delta H°_f$ for anorthite derived in the present study is 6435 cal mole^{-1} less negative than that adopted by Hemingway and Robie (1977a), which apparently represents a "correction" of Barany's (1962) calorimetric value. In contrast, the calculated value of the standard molal enthalpy of formation of anorthite from its oxides at 970°K and 1 bar using thermodynamic data taken from table 8 is ~ 1670 cal mole^{-1} more negative than that for synthetic anorthite obtained calorimetrically by Charlu, Newton, and Kleppa (1978). However, it is only 876 cal mole^{-1} more negative than the value they report for natural anorthite. The standard molal enthalpies of formation from the oxides of synthetic and natural anorthite reported by Charlu, Newton, and Kleppa are ~ 430 and ~ 1220 cal mole^{-1} more negative, respectively, than that obtained by Shearer (ms) at 965°K and 1 bar.

The value of $\Delta H°_f$ for anorthite that best satisfies the high pressure/temperature phase equilibrium data shown in figures 81 through 83 (table 8) is closer to that given by Hemingway and Robie (1977a) for hexagonal anorthite (which is metastable with respect to its triclinic counterpart) than it is to the value they report for anorthite. Furthermore, the value of $S°_{P_r,T_r}$ for anorthite in table 8 is almost identical to the calorimetric value of $S°_{P_r,T_r}$ for ordered hexagonal anorthite, which can be

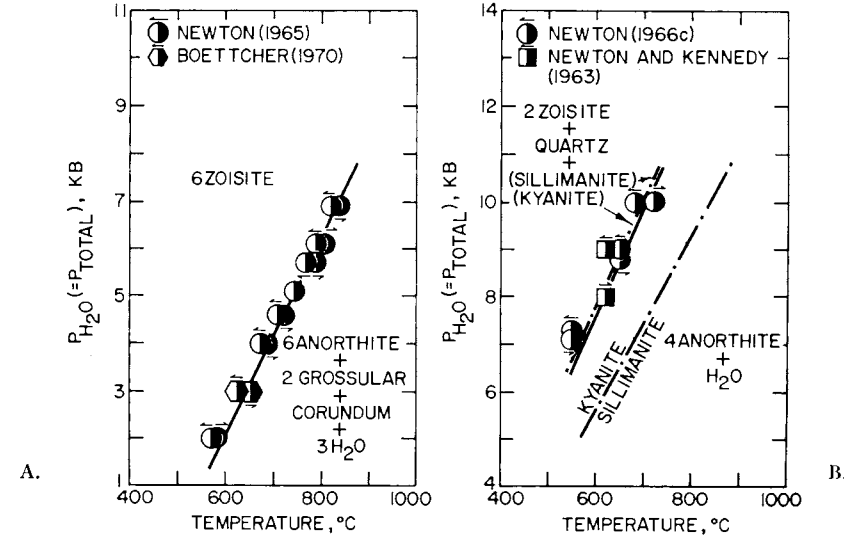

Fig. 83. Univariant equilibrium curves (generated from thermodynamic data given in table 8) and experimental observations of phase relations (symbols) in the system $CaO–Al_2O_3–SiO_2–H_2O$ at high pressures and temperatures.

computed from that given for its disordered counterpart by Hemingway and Robie (1977a). These observations suggest that unquenchable displacive disorder may occur in anorthite with increasing temperature. Although the aluminum avoidance principle requires anorthite to be in a state of complete substitutional order at low temperatures, displacive disorder corresponding to subtle changes in bond angles may permit substitutional disorder in anorthite at higher temperatures. If so, both kinds of disorder may contribute to the thermodynamic behavior of anorthite, even in the absence of obvious changes in symmetry. It should perhaps be emphasized in this regard that if the coupled disordering process is sluggish, it would be difficult to detect in short-term laboratory experiments.

The value of $\Delta H°_f$ for Ca–Al pyroxene in table 8 differs by only $\sim$ 350 and $\sim$ 600 cal mole^{-1}, respectively, from those calculated from Charlu, Newton, and Kleppa's (1978) and Shearer's (ms) calorimetric data, but the standard molal enthalpy of formation of gehlenite derived in the present study is 1075 and 6167 cal mole^{-1} less negative than the respective values given by Robie and Waldbaum (1968) and Hemingway and Robie (1977a). Although the value of $\Delta H°_f$ for grossular given in table 8 is in close agreement with Shearer's (ms) calorimetric value as well as with that adopted by Perkins and others (1977), it differs by $\sim$ 2 kcal mole^{-1} from the value for synthetic grossular computed from Charlu, Newton, and Kleppa's (1978) calorimetric data. The latter difference is of the order of magnitude of the variation in the heats of solution of natural and synthetic garnets at 965°K (Shearer, ms).

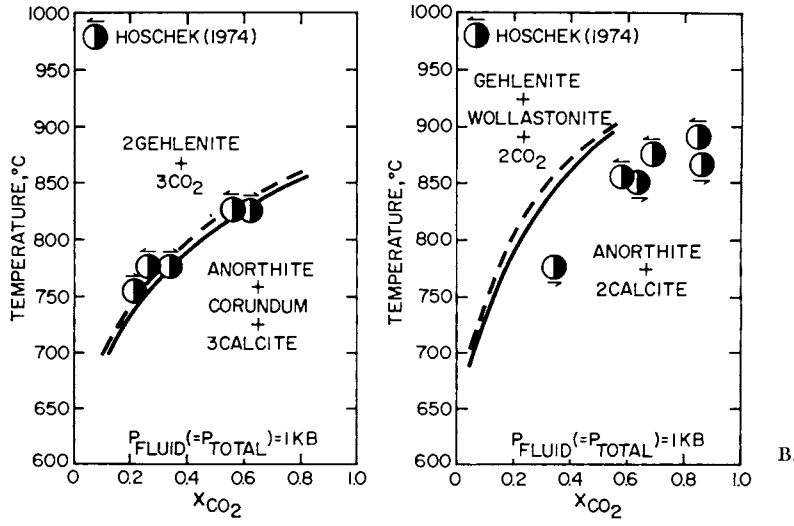

Fig. 84. Calculated (curves) and experimental (symbols) equilibrium temperatures and fluid compositions at 1 kb for coexisting mineral assemblages in the system CaO–Al_2O_3–SiO_2–CO_2–H_2O. The calculations were carried out assuming, alternately, ideal (solid curves) and nonideal (dashed curves) mixing of CO_2 and H_2O (see text).

Equilibrium temperatures and fluid compositions computed from thermodynamic data taken from table 8 can be compared with their experimental counterparts for a large number of reactions among calcite, wollastonite, corundum, grossular, anorthite, gehlenite, and CO_2 at 1 or 2 kb in figures 84 through 87. The solid and unevenly dashed curves in these figures were generated assuming ideal mixing of CO_2 and H_2O, but the evenly dashed curves represent calculations incorporating Holloway's (1977) provisions for nonideal mixing of CO_2 and H_2O. It can be seen in figures 84 through 87 that in all but two of the cases (figures 85 and 86A), the calculated effects of nonideal mixing of CO_2 and H_2O have only a slight effect on the predicted equilibrium temperatures and fluid compositions. In contrast, provision for nonideal mixing of CO_2 and H_2O for the reactions shown in figures 85 and 86A eliminates all the discrepancies between the experimental reversals and the curves based on the assumption of ideality in CO_2–H_2O mixtures. The fact that the effects of providing for nonideality in CO_2–H_2O mixtures are large in figure 86A and slight in figure 86B and C is a consequence of the relatively small value of $\Delta H°_r$ for the reaction shown in figure 86A.

In contrast to the close agreement between the calculated and experimental fluid compositions and equilibrium temperatures in figures 84A, 85, and 86A and B, large discrepancies are apparent between the curves and experimental data shown in figures 84B and 86C. The cause

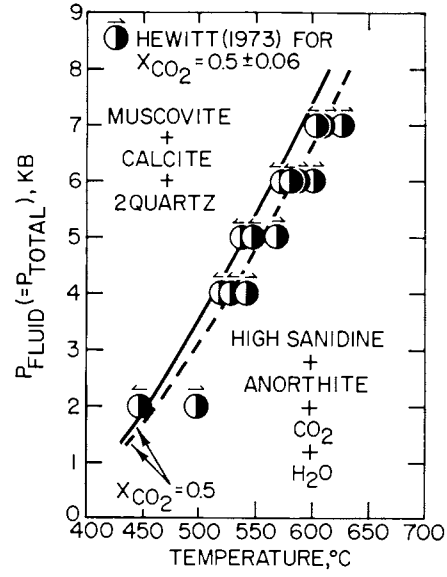

Fig. 85. Calculated (curves) and experimental (symbols) equilibrium temperatures and pressures for muscovite, calcite, quartz, high sanidine, and anorthite coexisting with a CO_2–H_2O fluid in which $X_{CO_2} \approx 0.05$. The calculations were carried out assuming, alternately, ideal (solid curve) and nonideal (dashed curve) mixing of CO_2 and H_2O (see text).

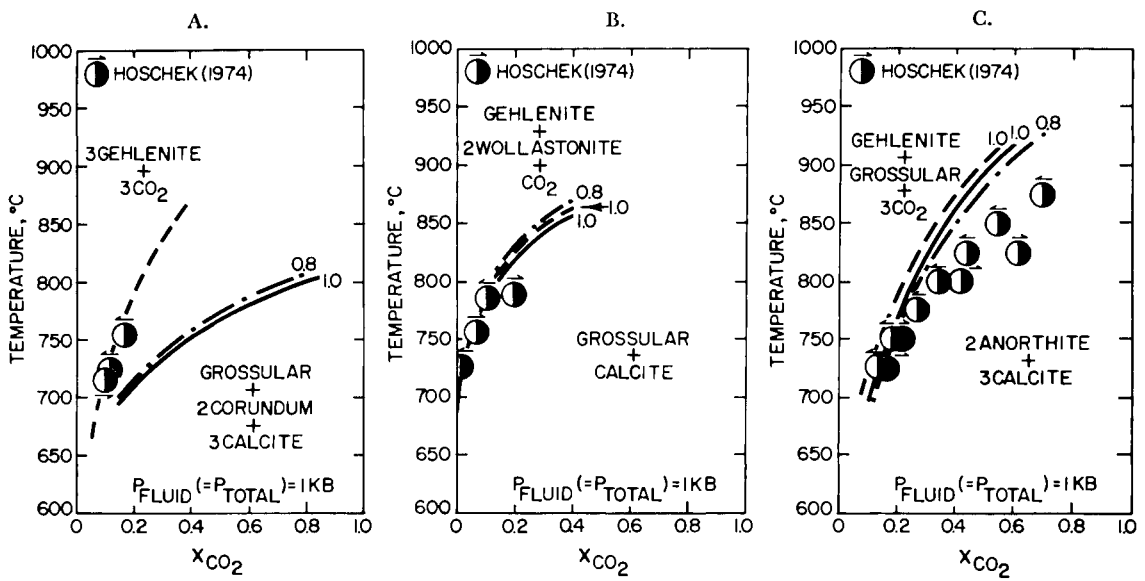

Fig. 86. Calculated (curves) and experimental (symbols) equilibrium temperatures and fluid compositions at 1 kb for coexisting mineral assemblages in the system CaO–Al_2O_3–SiO_2–CO_2–H_2O. The labels on the curves designate the activity of $Ca_3Al_2Si_3O_{12}$. The evenly dashed curves were generated assuming nonideal mixing of CO_2 and H_2O, but the others are based on the assumption that these two species mix ideally.

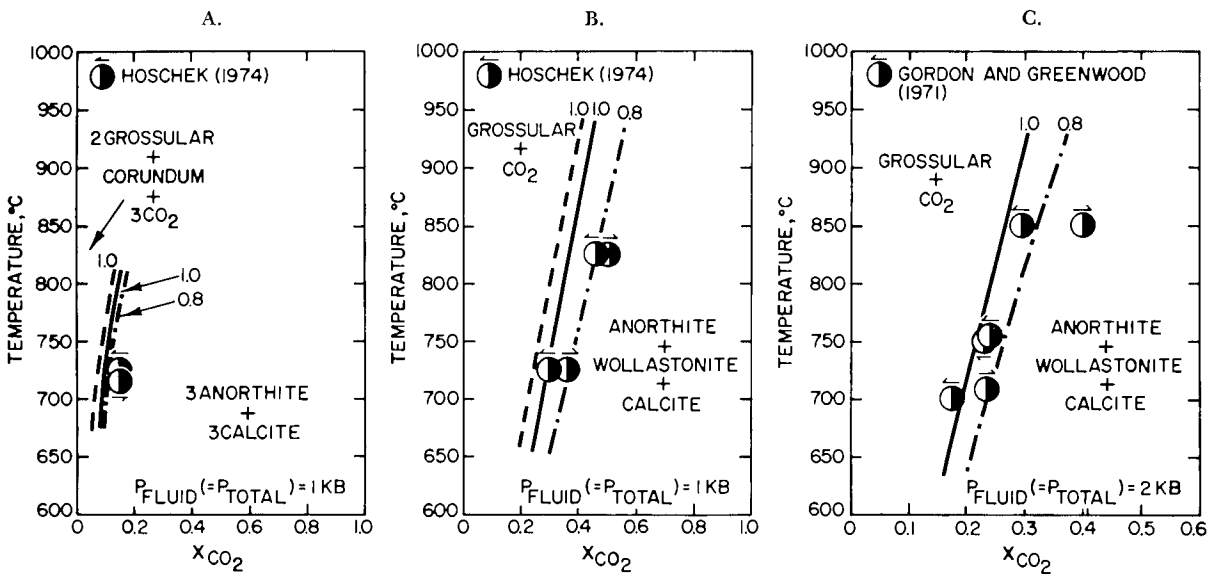

Fig. 87. Calculated (curves) and experimental (symbols) equilibrium temperatures and fluid compositions at 1 and 2 kb for coexisting mineral assemblages in the system $CaO–Al_2O_3–SiO_2–CO_2–H_2O$. The labels on the curves designate the activity of $Ca_3Al_2Si_3O_{12}$. The evenly dashed curves were generated assuming nonideal mixing of CO_2 and H_2O, but the others are based on the assumption that these two species mix ideally.

of these discrepancies is not readily apparent, but they appear to represent inconsistencies in the experimental data reported by Hoschek (1974) for the reactions shown in figures 84, 86, and 87. On the other hand, the discrepancies between the solid curves and symbols in figure 87 can be attributed to the effects of solid solution in grossular.

The unevenly dashed curves shown in figures 86 and 87 represent equilibrium temperatures and fluid compositions for reactions involving grossular with an activity of $Ca_3Al_2Si_3O_{12}$ equal to 0.8. This activity is consistent with slight compositional variation with respect to hydrogrossular, which reportedly occurred in Hoschek's (1974) and Gordon and Greenwood's (1971) experiments.

Hydrogrossular can be regarded as a solid solution of $Ca_3Al_2Si_3O_{12}$ and $Ca_3Al_2Si_2O_8(OH)_4$ (which corresponds to the mineral hibschite). Assuming random mixing of atoms on energetically equivalent sites in a solid solution of these components, it follows from eq (46) that an activity of $Ca_3Al_2Si_3O_{12}$ equal to 0.8 corresponds to a grossular solid solution in which the mole fraction of the hibschite component is only 0.015. It can be deduced from figure 87B and C that provision for this order of magnitude of compositional variation is closely consistent with the experimental reversals shown in the figures. On the other hand, resolution of the discrepancies in figure 87A would require a substantially greater mole fraction of the hibschite component in the grossular solid solution. Owing to the relatively large standard molal entropy changes accompanying the reactions shown in figures 81 through 83A,

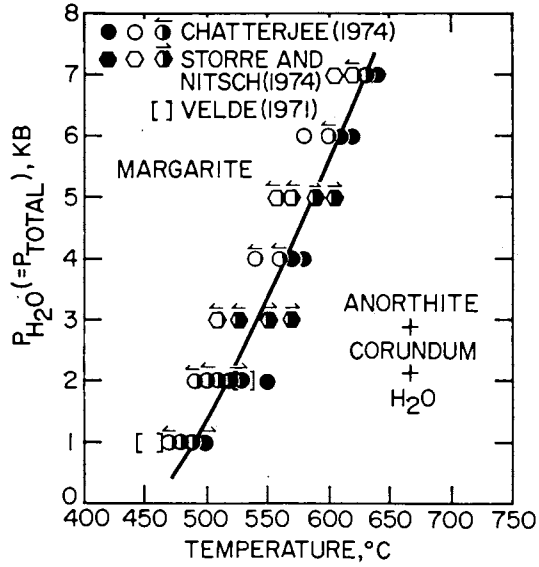

Fig. 88. Univariant equilibrium curve (generated from thermodynamic data given in table 8) and experimental observations of phase relations (symbols) in the system CaO–Al_2O_3–SiO_2–H_2O at high pressures and temperatures.

the presence of a few mole percent hibschite in grossular has a negligible effect on calculated equilibrium temperatures for these reactions.

It should perhaps be emphasized that thermodynamic analysis of the experimental data shown in figures 81 through 87, together with those reported by Hays (1967), Boettcher (1970), and Huckenholz, Hölzl, and Lindhuber (1975) for

$$\text{grossular} + 3\ \text{Ca–Al pyroxene} \rightleftharpoons 2\ \text{anorthite} + 2\ \text{gehlenite} \qquad (186A)$$

$$3\ \text{Ca–Al pyroxene} \rightleftharpoons \text{anorthite} + \text{gehlenite} + \text{corundum} \qquad (186B)$$

and

$$\text{grossular} + \text{corundum} \rightleftharpoons \text{anorthite} + \text{gehlenite} \qquad (186C)$$

reveals serious inconsistencies between the data reported for these reactions and those shown in the figures. The explanation of these discrepancies remains obscure, but the fact that no systematic departures of the curves from the experimental data are evident in figures 84 through 87 suggests that the inconsistencies arise from kinetic factors affecting reactions (186A) through (186C).

Clinozoisite.—The values of $\Delta G°_f$ and $\Delta H°_f$ for clinozoisite in table 8 were computed by taking the temperature of the clinozoisite/zoisite transition at 1 bar to be 900°K on the basis of Holdaway's (1972) experimental observations. An estimated entropy of transition of 0.1 cal mole^{-1} (°K)$^{-1}$ was then used together with the approximation $C°_{P_r,T,clinozoisite} = C°_{P_r,T,zoisite}$ to calculate $\Delta H°_f$ for clinozoisite from that of zoisite. The small difference between these values (90 cal mole^{-1}) is consistent with the sluggish nature of the transition, both in the laboratory and in natural systems.

Margarite and prehnite.—The values of $\Delta H°_f$ and $\Delta G°_f$ listed in table 8 for these minerals were retrieved from the experimental data shown in figures 88 and 89A using the values of $V°_{P_r,T_r}$, $S°_{P_r,T_r}$ and the heat capacity coefficients for the minerals given in the table. Despite the apparent discrepancy in the Clapeyron slope of the curve in figure 89A and the pressure distribution of the experimental data shown in the figure, the experimental data for

$$5\ \text{prehnite} \rightleftharpoons 2\ \text{zoisite} + 2\ \text{grossular} + 3\ \text{quartz} + 4\ H_2O, \qquad (186D)$$

were used in the present study to retrieve values of $\Delta H°_f$ and $\Delta G°_f$ for prehnite. This reaction was chosen for the retrieval calculations in preference to that in figure 89B because thermodynamic analysis indicates that the experimental data shown in the latter figure are inconsistent with the occurrence of prehnite in geothermal systems (Bird, ms; Bird and Helgeson, 1977). Comparison of the curves in figures 81A and 89B indicates that curve A in the latter figure represents a metastable equi-

librium state, which is consistent with the large differences in reaction rates noted by Liou (1971a).

The standard molal entropy given in table 8 for prehnite, which was generated from the experimental data shown in figure 89A, is of the order of 5 cal mole^{-1} (°K)$^{-1}$ smaller than corresponding values estimated from the various algorithms discussed above. This observation, together with the Clapeyron slope discrepancy noted above suggests that the values of $S°_{P_r,T_r}$, $\Delta H°_f$, and $\Delta G°_f$ given for prehnite in table 8 should be regarded as provisional approximations. Fortunately, calorimetric work currently under way (E. F. Westrum, Jr., 1977, personal commun.) should soon resolve these uncertainties. The curve labeled B in figure 89B, which was generated from thermodynamic data taken from table 8, represents the stable equilibrium analog of curve A. The latter curve simply connects the experimental reversals shown in the figure. The temperature interval between the curves in figure 89B represents the region where anorthite and wollastonite apparently persisted metastably (relative to grossular and quartz) in Liou's (1971a) experiments.

It can be seen in figure 90 that the thermodynamic data given in table 8 for margarite satisfy Storre and Nitsch's (1974) reversals only if their data apply to the metastable equilibria represented by

$$\text{margarite} + \text{quartz} \rightleftharpoons \text{anorthite} + \text{andalusite} + H_2O \qquad (186E)$$

and

$$4\ \text{margarite} + 3\ \text{quartz} \rightleftharpoons 2\ \text{zoisite} + 5\ \text{andalusite} + 3\ H_2O. \qquad (187F)$$

Because both kyanite and andalusite were used together as reactants in their experiments, it seems likely that this was indeed the case. In fact, if it were not, their experimental data in figure 90 would be thermo-

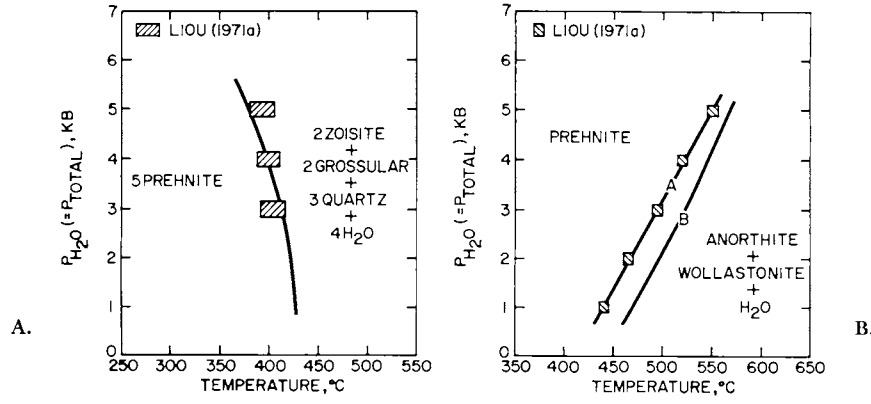

Fig. 89. Univariant equilibrium curves (generated from thermodynamic data given in table 8) and experimental observations of phase relations (symbols) in the system CaO–Al_2O_3–SiO_2–H_2O at high pressures and temperatures. Curve B is consistent with the curve in diagram A, but curve A was drawn simply to connect the symbols shown in diagram B (see text).

dynamically inconsistent with the reversals they report for the reaction in figure 88, which was used to retrieve the values of $\Delta H°_f$ and $\Delta G°_f$ for margarite in table 8.

Wairakite, laumontite, and lawsonite.—Repeated efforts in the present study to retrieve reliable values of $\Delta G°_f$ and $\Delta H°_f$ for these minerals (as well as epistilbite and disordered wairakite) from experimental data reported by Coombs and others (1959), Koizumi and Roy (1960), Liou (1970, 1971c), Thompson (1970b), and Newton and Kennedy (1963) using the values of $S°_{P_r,T_r}$ and $V°_{P_r,T_r}$ in table 3 were unsuccessful, owing to ambiguities and uncertainties concerning compositional variation, partial dehydration, and the temperature and pressure dependence of the standard molal volumes of the zeolites. For example, the values of $S°_{P_r,T_r}$ and the standard molal heat capacity coefficients of wairakite, anorthite, and quartz in table 8, together with the values of $V°_{P_r,T_r}$ given in table 3 for wairakite and table 8 for anorthite and quartz require a Clapeyron slope corresponding to that of curve A in figure 91A for

$$\text{wairakite} \rightleftharpoons \text{anorthite} + 2\ \text{quartz} + 2\ H_2O. \qquad (190)$$

The discrepancy between curve A and the curve that satisfies Liou's (1970) reversal temperatures is a function solely of $\Delta V°_r$ for the reaction. Alternate calculations indicate that $\Delta V°_r$ for reaction (190) must be 5.3 $cm^3\ mole^{-1}$ more positive than that computed from the values of $V°_{P_r,T_r}$ for wairakite, anorthite, and quartz in table 8 in order to satisfy Liou's data and the assumption that $(\partial \Delta V°_r/\partial P)_T = (\partial V°_{H_2O}/\partial P)_T$ and $(\partial \Delta V°_r/\partial T)_P = (\partial V°_{H_2O}/\partial T)_P$ for reaction (190). The difficulties en-

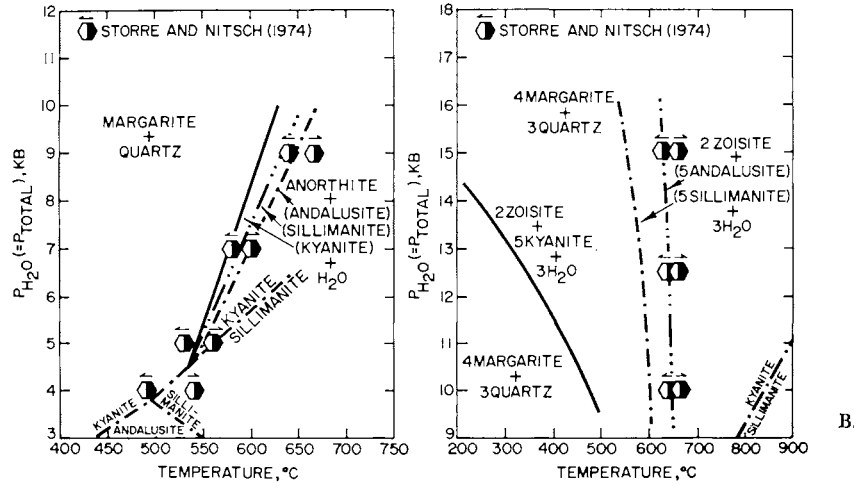

Fig. 90. Univariant equilibrium curves (generated from thermodynamic data given in table 8) and experimental observations of phase relations (symbols) in the system CaO–Al_2O_3–SiO_2–H_2O at high pressures and temperatures.

countered in thermodynamic analysis of these data suggest that the latter assumptions fail to represent adequately the thermodynamic behavior of zeolites as a function of pressure. This observation is consistent with the "loosely" bound character of the H_2O in zeolite channels, which is minimally inhibited by structural constraints from expansion and compression in response to increasing temperature and pressure. As a consequence, zeolites might be expected to exhibit abnormally large expansibilities and compressibilities.

Although several factors may be responsible for the discrepancy between the two curves in figure 91A, the value of $S°_{P_r,T_r}$ and the heat capacity coefficients for wairakite in table 8 can be reconciled with Liou's experimental data by subtracting 5.3 cm^3 $mole^{-1}$ from the experimental value of $V°_{P_r,T_r}$ for wairakite in table 3. This procedure and Liou's (1971c) data lead to the values of $V°_{P_r,T_r}$, $\Delta G°_f$, and $\Delta H°_f$ for wairakite in table 8 and the univariant curve for reaction (190) consistent with Liou's reversals in figure 91A. These data were used together with the experimental reversals shown in figures 91B and C to generate the values of $\Delta G°_f$ and $\Delta H°_f$ for laumontite and lawsonite in table 8 and the univariant curves shown in the figure for

$$\text{laumontite} \rightleftharpoons \text{wairakite} + 2\ H_2O \qquad (191)$$

and

$$\text{lawsonite} + 2\ \text{quartz} + 2\ H_2O \rightleftharpoons \text{laumontite} \qquad (191A)$$

The experimental data shown in figure 91C were selected for this purpose because (in contrast to those reported by Crawford and Fyfe, 1965; and Nitsch, 1972), they are consistent with both the experimental data shown in figure 81 and the absence of lawsonite in low-pressure metamorphic rocks. The values of $S°_{P_r,T_r}$ given for laumontite and lawsonite in table 8 were derived by optimizing agreement of the Clapeyron slopes

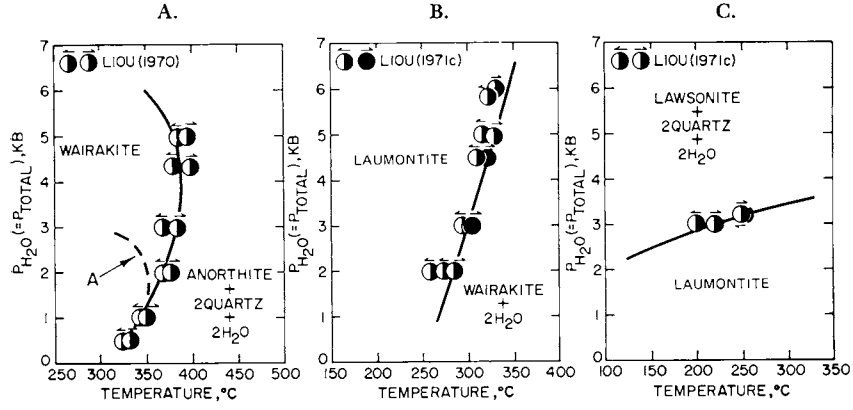

Fig. 91. Univariant equilibrium curves (generated from thermodynamic data given in table 8) and experimental observations of phase relations (symbols) in the system CaO–Al_2O_3–SiO_2–H_2O at high pressures and temperatures.

of the curves shown in figures 91B and C with the pressure distribution of the experimental data represented by the symbols. The standard molal entropy of laumontite in table 8 differs from the estimate shown in table 3 by 1 cal $mole^{-1}$ $(°K)^{-1}$, which is also the difference between the value of $S°_{P_r,T_r}$ adopted in the present study for lawsonite and the calorimetric value given by Robie and Waldbaum (1968).

It can be seen in figure 91 that with the exception of the experimental reversal at 6 kb in figure 91B, the curves generated in the present study are in close agreement with the experimental data shown in the figure. Similar agreement is evident in figure 92B, but discrepancies are apparent in figures 92A and C between the curves and a number of the temperature brackets reported by Thompson (1970b) and Newton and Kennedy (1963). Comparison of the curves and experimental data in figures 92A and 91A indicates that those in the latter figure represent a metastable assemblage, which mitigates to some extent the lack of agreement between the curve and Thompson's data in figure 92A. In the case of figure 92C, the discrepancies can almost certainly be attributed to metastable persistence of sillimanite in the experiments reported by Newton and Kennedy (1963).

K_2O–MgO–Al_2O_3–SiO_2–H_2O

Relatively large uncertainties attend retrieval of thermodynamic data for the minerals in this system from either calorimetric or high-pressure/temperature phase equilibrium data. These uncertainties, for example, are manifested by the many experimental values of the heats of solution of anhydrous cordierite, pyrope, and spinel in lead borate melts at 970°K, which vary considerably depending on the sample and calorimeter used in the experiments (Newton, 1972; Shearer, ms; Shearer and Kleppa, 1973; Charlu, Newton, and Kleppa, 1975; Newton, Charlu, and Kleppa, 1974, 1977). Similarly, many of the available experimental

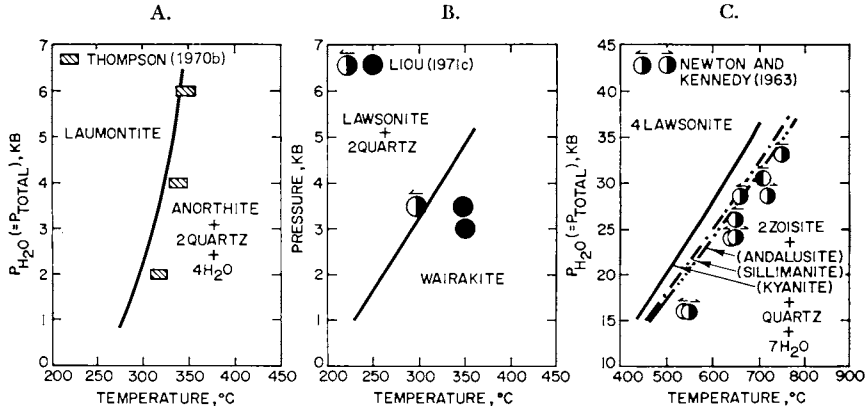

Fig. 92. Univariant equilibrium curves (generated from thermodynamic data given in table 8) and experimental observations of phase relations (symbols) in the system CaO–Al_2O_3–SiO_2–H_2O.

high pressure/temperature phase equilibrium data for this system are inconsistent with one another. As a consequence, subjective judgement is required to retrieve values of $\Delta H°_f$ and $\Delta G°_f$ from these data.

Cordierite, hydrous cordierite, spinel, 14A-clinochlore, 7A-clinochlore, and phlogopite.—With the exception of 7A-clinochlore, the values of $\Delta G°_f$ and $\Delta H°_f$ for these minerals in table 8 were calculated from high pressure/temperature experimental data for

$$3 \text{ 14A-clinochlore} + 5 \text{ muscovite} \rightleftharpoons 5 \text{ phlogopite} + 8 \text{ kyanite} + \text{quartz} + 12 \text{ } H_2O, \quad (192)$$

$$14\text{A-clinochlore} + \text{muscovite} + 2 \text{ quartz} \rightleftharpoons \text{phlogopite} + \text{cordierite} + 4 \text{ } H_2O, \quad (193)$$

$$5 \text{ 14A-clinochlore} \rightleftharpoons \text{cordierite} + 3 \text{ spinel} + 10 \text{ forsterite} + 20 \text{ } H_2O, \quad (194)$$

$$2 \text{ 14A-clinochlore} + 6 \text{ enstatite} \rightleftharpoons 7 \text{ forsterite} + \text{cordierite} + 8 \text{ } H_2O \quad (195)$$

and

$$\text{hydrous cordierite} \rightleftharpoons \text{cordierite} + H_2O. \quad (196)$$

Equilibrium constants computed from observations reported in the literature for these reactions were considered simultaneously in the retrieval calculations. Implicit in this approach is the assumption that the cordierite studied experimentally was in its stable state of hydration.

It is widely recognized that cordierite incorporates "zeolitic" H_2O in its structure (for example, see Schreyer and Yoder, 1964; Weisbrod, 1973a and b), but the dependence of the process on temperature and pressure has yet to be defined quantitatively. The thermodynamic consequences of the hydration of cordierite can be computed from data given by Schreyer and Yoder (1964), who report the H_2O content of cordierite synthesized at 600°C and 2 and 5 kb after reaction times at 64 and 139 hrs, respectively. A third determination of H_2O in a sample synthesized over a period of 1 hr at 950°C and 1 kb is not suitable for this purpose, owing to questionable equilibration after such a short reaction time. The standard molal Gibbs free energy and enthalpy of formation of hydrous cordierite from its elements at 25°C and 1 bar can be calculated, together with the corresponding properties of anhydrous cordierite, from experimental data for reactions (192) through (195) and the compositional data cited above by adopting the values of $S°_{P_r,T_r}$, $V°_{P_r,T_r}$, and the heat capacity coefficients for hydrous and anhydrous cordierite in table 8. Assuming ideal solid solution between the two minerals leads to

$$\frac{(1 - X_h)a_{H_2O}}{X_h} = K \quad (197)$$

where X_h stands for the mole fraction of hydrous cordierite, and K represents the equilibrium constant for reaction (196). Evaluation of eq (197)

yields 3590 and 3178 cal mole^{-1} for $\Delta G°_r$ of reaction (196) at 25°C and 1 bar using the two analyses reported by Schreyer and Yoder (1964) for 600°C at 2 and 5 kb. The mean of these, together with experimental values for $\Delta G°_{r,P,T}$ for reactions (192) through (195) leads to the values of $\Delta H°_f$ and $\Delta G°_f$ given in table 8 for cordierite, anhydrous cordierite, 14A-clinochlore, spinel, and phlogopite.

The thermodynamic data shown in the table for cordierite and anhydrous cordierite were used to generate the equilibrium constants and isopleths plotted in figure 93. The latter calculations yield values of X_h for reaction (196) at 600°C and 2 and 5 kb that are within the analytical uncertainty of the compositional data reported by Schreyer and Yoder (1964), but a significant discrepancy occurs between the value calculated from their data at 950°C and 1 kb and the corresponding value in figure 93. This discrepancy is almost certainly due to nonequilibration in the 1 hr experiment.

It can be seen in figures 94 through 97A that the thermodynamic calculations described above afford close approximation of experimental data for reactions (192) through (195). However, similar calculations for a number of other reactions reveal discrepancies (like those apparent in fig. 97B) among computed equilibrium constants and those generated from experimental data taken from the literature. It appears that these discrepancies can be attributed to formation of metastable cordierite–hydrous cordierite solid solutions and/or clinochlore with basal spacings significantly less than 14A.

The relative stability of clinochlore has received considerable attention in recent years (Fawcett and Yoder, 1966; Seifert, 1970; Seifert and Schreyer, 1970; Bird and Fawcett, 1973; Bird and Anderson, 1973; Zen, 1973; Chernosky, 1974, 1975, 1976a), and it has been pointed out (Zen, 1973) that experimentally determined reversal temperatures for uni-

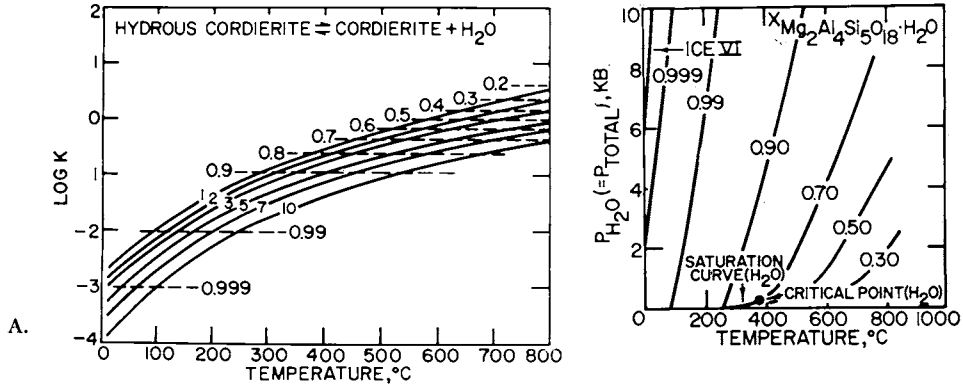

Fig. 93. Equilibrium constant for reaction (196) as a function of temperature at constant pressures (labeled in kb) and mole fraction isopleths for cordierite–hydrous cordierite solid solutions as a function of pressure and temperature. The dashed curves in diagram A and the solid curves in diagram B designate $X_{Mg_2Al_4Si_5O_{18}\cdot H_2O}$.

variant phase equilibria at high pressures and temperatures are inconsistent with the value of $\Delta G°_f$ for clinochlore calculated by Helgeson (1969) from low-temperature solubility data reported by Mackenzie and Garrels (1965). It appears from the calculations carried out in the present study that this apparent inconsistency can be attributed to different basal spacings in chlorites formed at high and low temperatures. It has been observed repeatedly in experimental phase equilibrium studies that 7A-chlorite commonly forms initially as a reaction product in the vicinity of 500°C, but it later inverts to its 14A counterpart. At higher temperatures, 14A-chlorite forms immediately, but at lower temperatures, only 7A-chlorite forms. It is interesting to note in this regard that chlorites found in modern sediments and weathering profiles are almost invariably of the 7A variety. However, with burial and increasing age, 7A-chlorite apparently transforms to 14A-chlorite. This observation is consistent with the occurrence of 14A-chlorites in Mississippian sediments of the Cumberland Plateau (Peterson, 1962).

The clinochlore sample used by Mackenzie and Garrels (1965) in their solubility experiments had a 7A basal spacing. The value of $\Delta G°_f$ for clinochlore computed by Helgeson (1969) thus refers to the 7A variety. This value was corrected in the present study to be consistent with the values of $\Delta G°_f$ for the other aluminosilicates in table 8 and combined with the revised estimate of the standard molal entropy of 7A-clinochlore shown in the table to calculate $\Delta H°_f$ for the mineral. The thermodynamic properties of 7A-clinochlore in table 8 afford close approximation of ob-

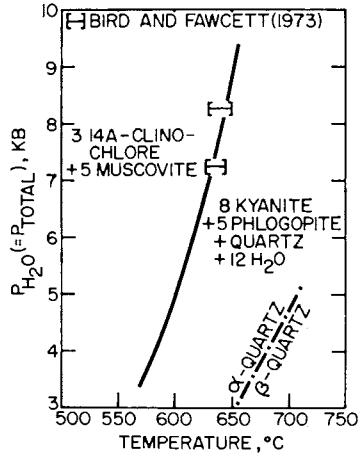

Fig. 94. Univariant equilibrium curve (generated from thermodynamic data given in table 8) and experimental observations of phase relations (symbols) in the system K_2O–MgO–Al_2O_3–SiO_2–H_2O at high pressures and temperatures.

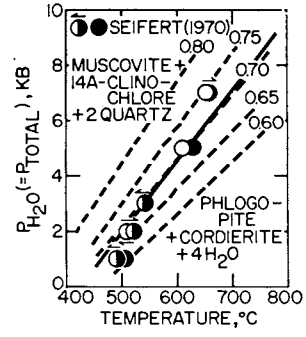

Fig. 95. Univariant equilibrium curve (generated from thermodynamic data given in table 8) and experimental observations of phase relations (symbols) in the system K_2O–MgO–Al_2O_3–SiO_2–H_2O at high pressures and temperatures. The dashed curves represent isopleths of cordierite composition designated by $X_{Mg_2Al_4Si_5O_{18} \cdot H_2O}$.

served phase relations in hydrothermal, geothermal, and diagenetic systems (Helgeson, 1967, 1970; Helgeson and Mackenzie, 1970).

The calculations summarized above indicate that 7A-clinochlore is metastable with respect to its 14A counterpart at all temperatures and pressures. This conclusion is consistent with observations summarized by Nelson and Roy (1958). Conversion of 7A-clinochlore to the 14A variety probably requires a relatively high activation energy, which could account for the persistence of 7A clinochlore in weathering profiles, sedimentary environments, hydrothermal alteration zones, and laboratory experiments at temperatures $< 400°$ to 500°C.

It appears from the discrepancies in figure 97B between the reversal temperatures reported by Chernosky (1975) for

$$6\ \text{14A-clinochlore} + 29\ \text{quartz} \rightleftharpoons 3\ \text{cordierite} + 8\ \text{talc} + 16\ H_2O \tag{198}$$

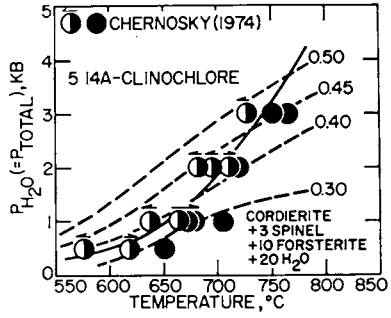

Fig. 96. Univariant equilibrium curve (generated from thermodynamic data given in table 8) and experimental observations of phase relations (symbols) in the system MgO–Al_2O_3–SiO_2–H_2O at high pressures and temperatures. The dashed curves represent isopleths of cordierite composition designated by $X_{Mg_2Al_4Si_5O_{18} \cdot H_2O}$.

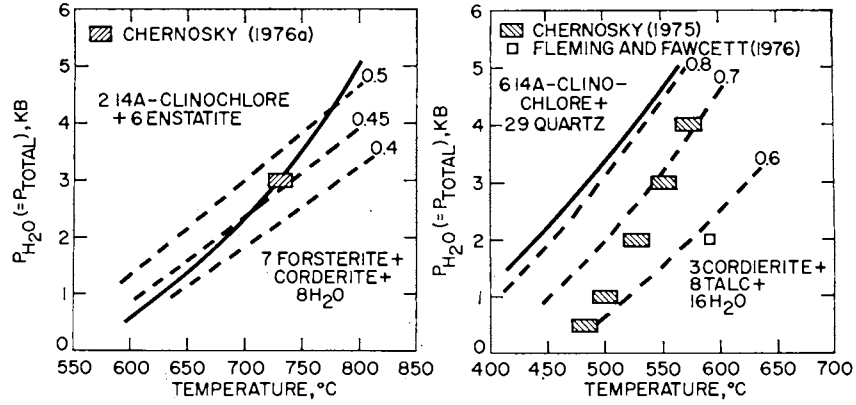

Fig. 97. Univariant equilibrium curves (generated from thermodynamic data given in table 8) and experimental observations of phase relations (symbols) in the system MgO–Al_2O_3–SiO_2–H_2O at high pressures and temperatures. The dashed curves represent isopleths of cordierite composition designated by $X_{Mg_2Al_4Si_5O_{18} \cdot H_2O}$.

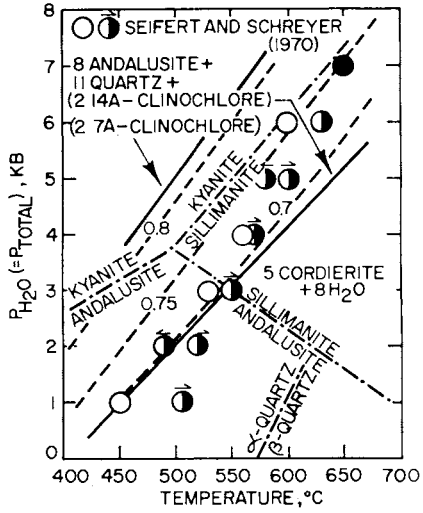

Fig. 98. Univariant equilibrium curves (generated from thermodynamic data given in table 8) and experimental observations of phase relations (symbols) in the system MgO–Al_2O_3–SiO_2–H_2O at high pressures and temperatures. The dashed curves represent isopleths of cordierite composition designated by $X_{Mg_2Al_4Si_5O_{18} \cdot H_2O}$.

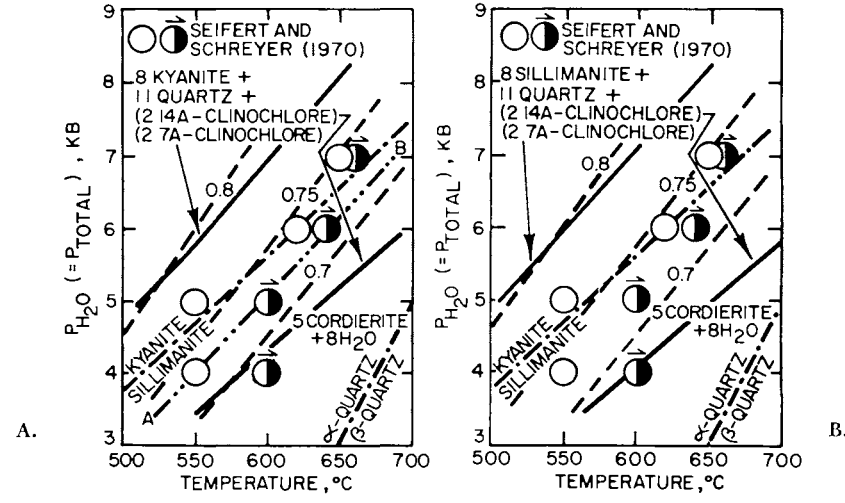

Fig. 99. Univariant equilibrium curves (generated from thermodynamic data given in table 8) and experimental observations of phase relations (symbols) in the system MgO–Al_2O_3–SiO_2–H_2O at high pressures and temperatures. The dashed curves represent isopleths of cordierite composition designated by $X_{Mg_2Al_4Si_5O_{18} \cdot H_2O}$.

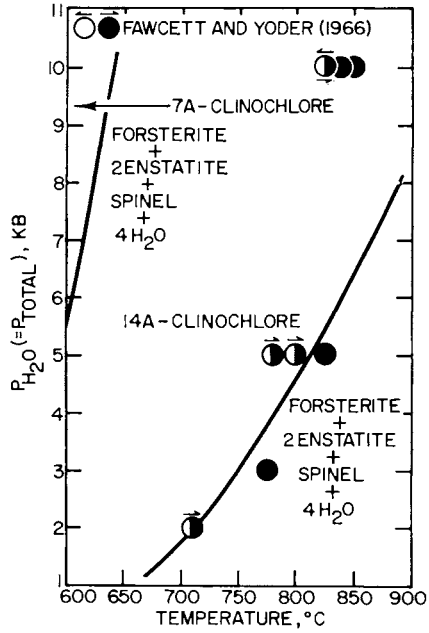

Fig. 100. Univariant equilibrium curves (generated from thermodynamic data given in table 8) and experimental observations of phase relations (symbols) in the system MgO–Al_2O_3–SiO_2–H_2O at high pressures and temperatures.

and the univariant curve generated from the data in table 8 for the minerals in reaction (198), that the experimental data shown in figure 97B are inconsistent with those in figures 96 and 97A. The discrepancies cannot be explained by formation of metastable 7A-clinochlore, but they could result from formation of metastable cordierite with excess H_2O. Similar disagreement between calculated and experimental reversal temperatures is apparent in figures 98 through 100. In each of these cases, the somewhat erratic pressure distribution of the experimental reversal temperatures implies Clapeyron slopes that are too large to be consistent with any reasonable estimate of the standard molal entropy and heat capacity of 14A-clinochlore. It can be seen in figures 98 through 100 that the univariant curves generated from the thermodynamic calculations are in agreement with the experimental reversals at or below ~ 4 kb, but serious discrepancies are apparent at higher pressures. The cause of these discrepancies is not obvious, but it appears likely that stable equilibrium was not achieved in the experimental studies at the higher pressures.

It can be deduced from figures 101 and 102 (where the effects of ideal and nonideal mixing of CO_2 and H_2O can be compared) that the thermodynamic data given in table 8 for phlogopite are in close agreement with Hewitt's (1975) experimental data for

$$5 \text{ phlogopite} + 6 \text{ calcite} + 24 \text{ quartz} \rightleftharpoons 5 \text{ sanidine} + 3 \text{ tremolite} + 6\ CO_2 + 2\ H_2O, \qquad (198A)$$

which contradict Hoschek's (1973) measurements of X_{CO_2} in fluids coexisting with K-feldspar, phlogopite, calcite, and quartz. The differences in the two experimental results can be attributed to several factors. Hoschek's experiments were carried out using synthetic tremolite, which may be metastable by as much as several kcal mole^{-1} with respect to its natural counterpart (see above). In contrast, Hewitt used both natural and synthetic tremolite. The discrepancies could also be a consequence of Al/Si disorder in the phlogopite formed in Hoschek's experiments, which probably accounts for the differences between the three curves on the left side of figure 103 (which were generated using data taken from table 8) and the reversal reported by Wones and Dodge (1966, 1977) for

phlogopite + 3 quartz $\rightleftharpoons$ 3 enstatite + high sanidine + H_2O. (199)

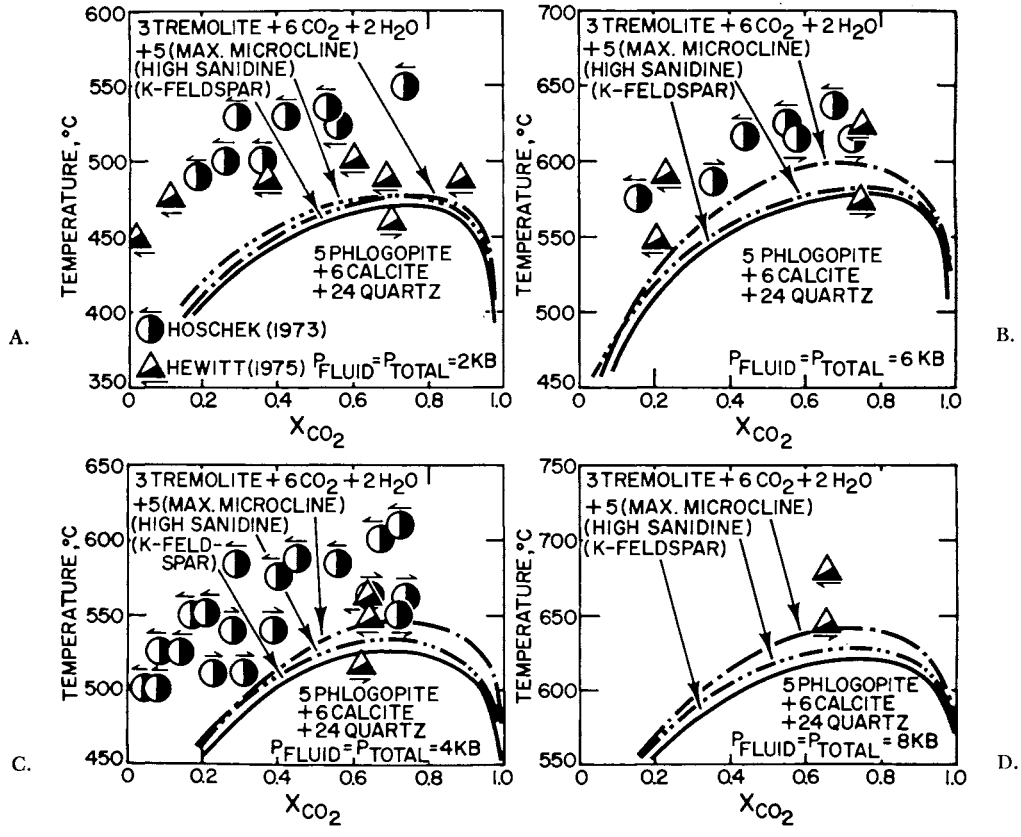

Fig. 101. Calculated (curves) and experimental (symbols) equilibrium temperatures and fluid composition for coexisting tremolite, K-feldspar (or alternately, maximum microcline or high sanidine), phlogopite, calcite, quartz, and CO_2–H_2O solutions at high pressures and temperatures. The curves were generated assuming ideal mixing of CO_2 and H_2O.

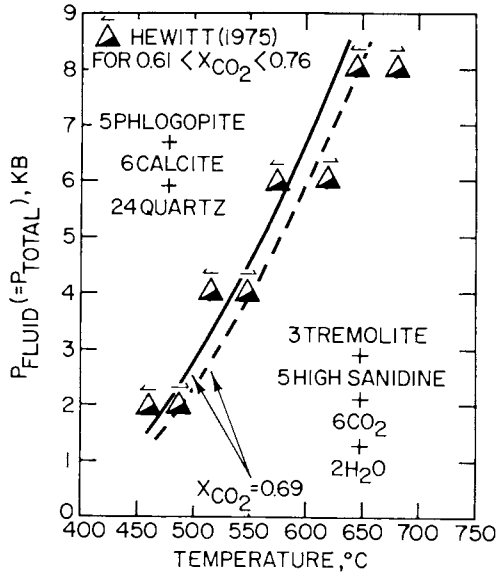

Fig. 102. Calculated (curves) and experimental (symbols) equilibrium temperatures and pressures for tremolite, high sanidine, phlogopite, calcite, and quartz coexisting with a CO_2-H_2O fluid in which $X_{CO_2} \approx 0.7$. The calculations were carried out assuming, alternately, ideal (solid curve) and nonideal (dashed curve) mixing of CO_2 and H_2O (see text).

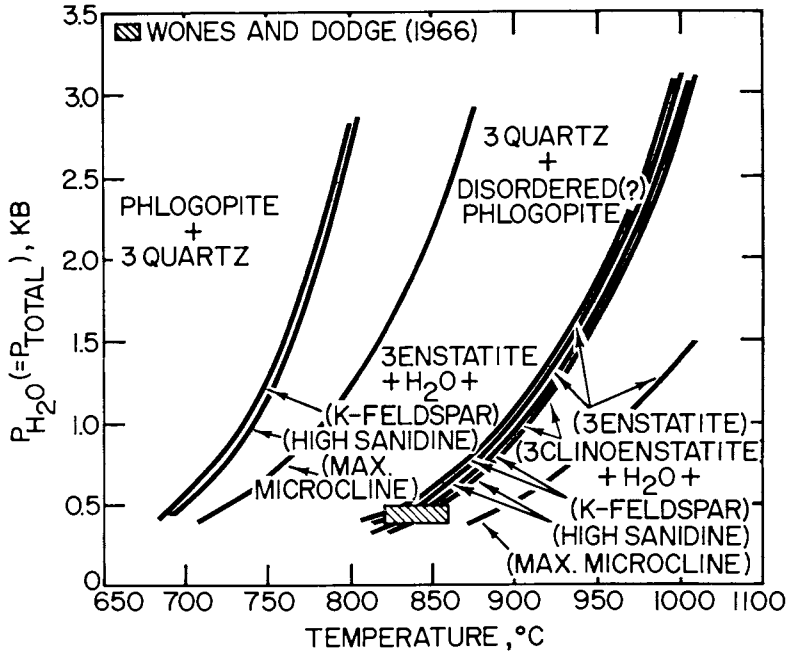

Fig. 103. Univariant equilibrium curves (generated from thermodynamic data given in table 8 for phlogopite, quartz, enstatite, K-feldspar, microcline, and sanidine and experimental observations of phase relations (symbol) in the system K_2O–MgO–Al_2O_3–SiO_2–H_2O at high pressures and temperatures (see text).

The extent to which phlogopite disorders at high temperatures is poorly understood, but there is no evidence of disorder in the experimental data reported by Bird and Fawcett (1973), Seifert (1970), and Hewitt (1975), all of which are consistent with one another.

The values of $\Delta H°_f$ given in table 8 for spinel and cordierite are nearly equal to those computed from calorimetric data reported by Charlu, Newton, and Kleppa (1975). Consequently, the corresponding values of $\Delta H°_f$ for 14A-clinochlore and phlogopite derived above are also consistent with these data.

PARGASITE

Experimental reversal temperatures for the decomposition of pargasite to anorthite, nepheline, aluminous diopside, forsterite, spinel, and H_2O are shown in figure 104, where it can be seen that the recent data reported by Westrich, Navrotsky, and Holloway (1976) are in substantial agreement with earlier observations by Boyd (1959).

The composition of aluminous diopside in equilibrium with forsterite and spinel at high pressures and temperatures has been determined experimentally by MacGregor (1965), who reports the aluminum content of the diopside as weight percent Al_2O_3. If aluminous diopside is regarded as a solid solution of $CaMg(SiO_3)_2$, $MgAl_2O_4$, and Mg_2SiO_4 with Mg_2SiO_4 as a negative component, conservation of mass and charge for a unit framework of 6 oxygen atoms requires

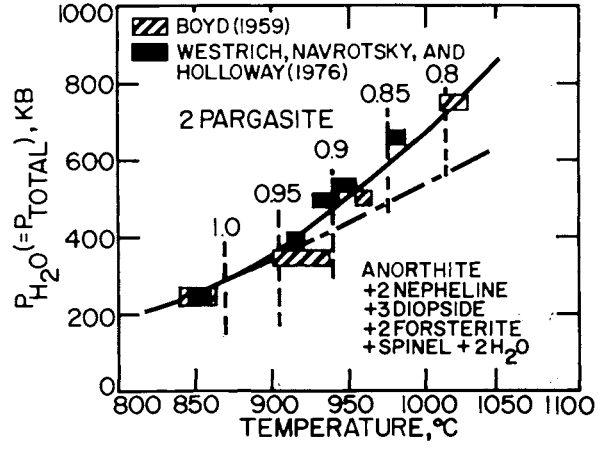

Fig. 104. Univariant equilibrium curve (generated from thermodynamic data given in table 8) and experimental observations of phase relations (symbols) in the system Na_2O–CaO–MgO–Al_2O_3–SiO_2–H_2O at high pressures and temperatures. The dashed curves represent activity isopleths for diopside–forsterite–spinel solid solutions designated by $a_{CaMg(SiO_3)_2}$. The solid curve represents pargasite in equilibrium with aluminous diopside, but the dot-dash curve refers to pargasite coexisting with pure diopside (see text).

$$CaMg(SiO_3)_2 + nMgAl_2O_4 - nMg_2SiO_4 = CaMg_{(1-n)}Al_n(Al_{(n/2)}Si_{(1-(n/2))}O_3)_2 \quad (200)$$

where n stands for the number of moles of the spinel component (mole of the aluminous diopside solid solution)$^{-1}$. The weight percent of Al_2O_3 in the aluminous diopside (w) can be expressed as

$$w = \frac{100nM_a}{M_c + (1-n)M_m + nM_a + (2-n)M_s} \quad (201)$$

where M_a, M_c, M_m, and M_s stand for the molecular weight of Al_2O_3, CaO, MgO, and SiO_2, respectively. Rearranging eq (201) and factoring n results in

$$n = \frac{M_d}{M_m + M_s - M_a(1 - (100/w))} \quad (202)$$

where M_d refers to the molecular weight of $CaMg(SiO_3)_2$. If the Al and Si atoms mix randomly on both tetrahedral sites in aluminous diopside, eq (46) can be written for the activity of the diopside component (a_d) as

$$a_d = X_{Mg,M(1)} X_{Si,T}^2 = \frac{(1-n)(2-n)^2}{4} \quad (203)$$

where $X_{Mg,M(1)}$ and $X_{Si,T}$ refer to the mole fractions of magnesium and silicon on the octahedral (M(1)) and tetrahedral (T) sites, respectively. On the other hand, if the Al and Si atoms mix randomly on only one kind of tetrahedral site, eq (203) becomes

$$a_d = X_{Mg,M(1)} X_{Si,T} = \frac{(1-n)(2-n)}{2} \quad (204)$$

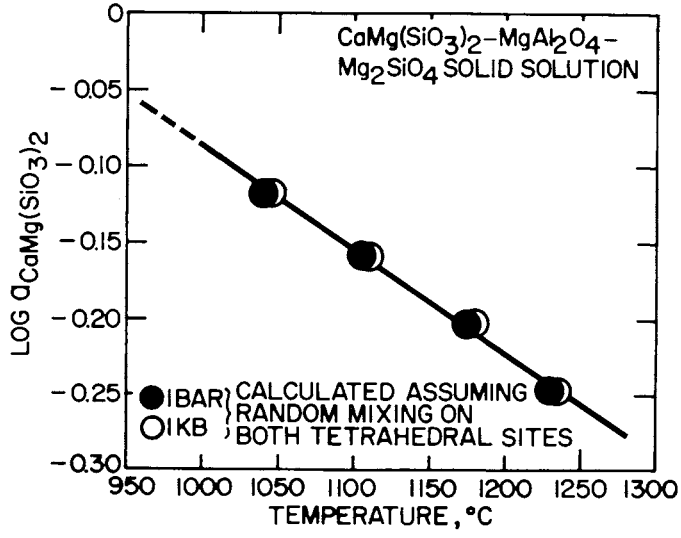

Fig. 105. Activity of $CaMg(SiO_3)_2$ in aluminous diopside as a function of temperature at 1 bar (see text).

where $X_{Si,T}$ refers to the mole fraction of silicon on the tetrahedral sites where mixing occurs. Graphic extrapolation and interpolation of MacGregor's (1965) data yield values of w which can be combined with eqs (202) through (204) to calculate a_d as a function of temperature and pressure. Comparative extrapolations, interpolations, and calculations of this kind indicate that mixing of Al and Si on both tetrahedral sites is most compatible with the experimental reversal temperatures shown in figure 93. Accordingly, eqs (202) and (203) were used to generate the curves in figure 105, where it can be seen that log a_d exhibits a linear dependence on temperature at constant pressure. The curves in figure 105 are based on numerical analysis of MacGregor's data to optimize agreement between the extrapolated values of w and the experimental data plotted in figure 104. Because pressure has a negligible effect on log a_d at pressures below a kilobar, values of a_d computed from the equation of the curve in figure 105 can be used to calculate equilibrium constants for the reaction shown in figure 104, which can be expressed as

$$a_d^3 = \mathrm{K} \tag{205}$$

These calculations, together with the experimental reversal temperatures shown in the figure were used to compute the values of $\Delta G°_f$ and $\Delta H°_f$ for pargasite in table 8.

It can be seen in figure 104 that the curves generated from the thermodynamic data in table 8 using the solid solution model described above for aluminous diopside coexisting with pargasite, anorthite, nepheline, forsterite, and H_2O agree closely with the experimental reversal temperatures at all pressures. Because $\Delta S°_r$ for the reaction is of the order of 20 cal mole^{-1} at high temperatures and low pressures, calculated equilibrium temperatures and pressures are highly sensitive to small errors in a_d. Although not conclusive, this observation, together with the close agreement of the curve and experimental data shown in the figure, strongly supports the validity of the solid solution model used in the calculations. The effect of solid solution in diopside on the equilibrium temperatures can be assessed by comparing the two curves shown in the figure. The lower curve represents pargasite in equilibrium with anorthite, nepheline, forsterite, spinel, H_2O, and pure diopside.

K_2O–CaO–FeO–Fe_2O_3–Al_2O_3–SiO_2–CO_2–H_2O

Relatively few published experimental data are suitable for calculating reliable values of $\Delta G°_f$ and $\Delta H°_f$ for aluminosilicates containing ferrous and/or ferric iron. In addition to ambiguities concerning the oxidation state of the iron in such minerals, many of the pertinent equilibria that have been studied experimentally involve multiple solid solutions for which few compositional data are available. In certain cases, it is not at all clear that the experimental system was adequately buffered by the presence of such minerals as magnetite and hematite or quartz, fayalite, and magnetite.

Magnetite, hematite, and fayalite.—The calorimetric data for magnetite in table 8 were used in the present study together with the recent experimental data obtained by I-Ming Chou and H. P. Eugster (1977, personal and written commun.) and Chou (1978) for the hematite–magnetite buffer (fig. 106) to calculate the standard molal enthalpy and Gibbs free energy of formation of hematite from its elements at 298.15°K and 1 bar. The value of $\Delta H°_f$ for hematite retrieved in this manner (table 8) is 370 cal mole^{-1} more negative than the standard molal enthalpy of formation adopted by Haas and Robie (1973), and it differs from the calorimetric value reported by Stull and Prophet (1971) and Robie and Waldbaum (1968) by 420 cal mole^{-1}. The latter difference is only 120 cal mole^{-1} greater than the uncertainty range given for the calorimetric value.

The thermodynamic data for magnetite in table 8 were also used to retrieve values of $\Delta G°_f$ and $\Delta H°_f$ for fayalite from the quartz–fayalite–magnetite reversals reported by Hewitt (1976), I-Ming Chou and H. P. Eugster (1977, personal and written commun.), and Chou (1978), which are consistent with those at 1 bar given by Chou and Williams (1977) but differ somewhat from earlier data obtained by Wones and Gilbert (1969). The latter temperature brackets have since been found to be in error (D. R. Wones, 1976, personal commun.). It can be seen in figures

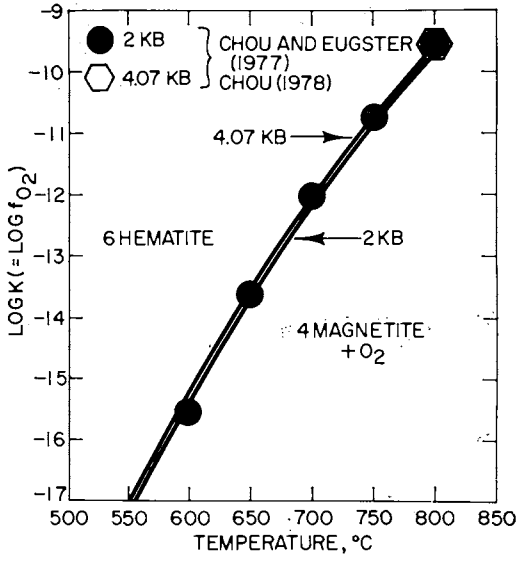

Fig. 106. Calculated (curves) and experimental (symbols) fugacities of oxygen corresponding to equilibrium constants for the hematite/magnetite buffer as a function of temperature at constant pressure. Chou and Eugster (1977) refers to I-Ming Chou and H. P. Eugster (1977, personal and written commun.).

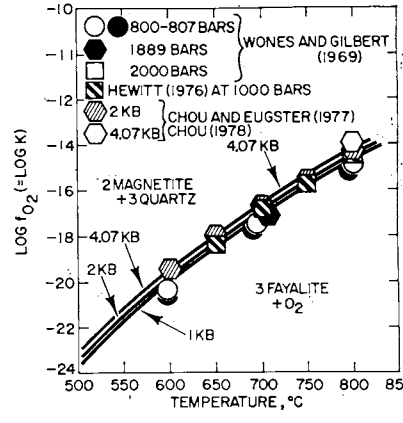

Fig. 107. Calculated (curves) and experimental (symbols) equilibrium constants for the quartz–fayalite–magnetite buffer at a function of temperature at constant pressure. Chou and Eugster (1977) refers to I-Ming Chou and H. P. Eugster (1977, personal and written commun.).

106 and 107 that the curves generated from the thermodynamic data in table 8 agree closely with the experimental observations represented by the symbols. The value of $\Delta H°_f$ for fayalite given in the table falls within the uncertainty range of its calorimetric counterpart given by Robie and Waldbaum (1968).

Ferrosilite.—The transition of clinoferrosilite to ferrosilite at high pressures and temperatures has been investigated experimentally by Lindsley (1965) and Akimoto and others (1965), but the results of these studies are in serious disagreement with one another. It can be seen in figure 108 that the Clapeyron slope of the univariant curve required by the distribution of data reported by Akimoto and others (1965) is considerably smaller than that of the curve drawn through Lindsley's (1965) experimental reversals. Taking account of the standard molal volumes of the two polymorphs (Burnham, 1965), the latter curve requires a standard molal entropy of transition > 0.8 cal mole^{-1} (°K)$^{-1}$, which is much larger than the corresponding entropy of transition for clinoenstatite/enstatite at 1 bar (0.18 cal mole^{-1} (°K)$^{-1}$). In contrast, the standard molal entropy of transition required by these volume data and the slope of the univariant curve in figure 108A is only 0.09 cal mole^{-1} (°K)$^{-1}$. Because the latter value is much more reasonable than that calculated from Lindsley's observations, the data reported by Akimoto and others (1965) were used to compute the thermodynamic properties of transition shown for clinoferrosilite/ferrosilite in table 8. The values of $\Delta H°_f$ and $\Delta G°_f$ for ferrosilite (which is used in the present communication to refer to $FeSiO_3$ in its stable structural configuration at all

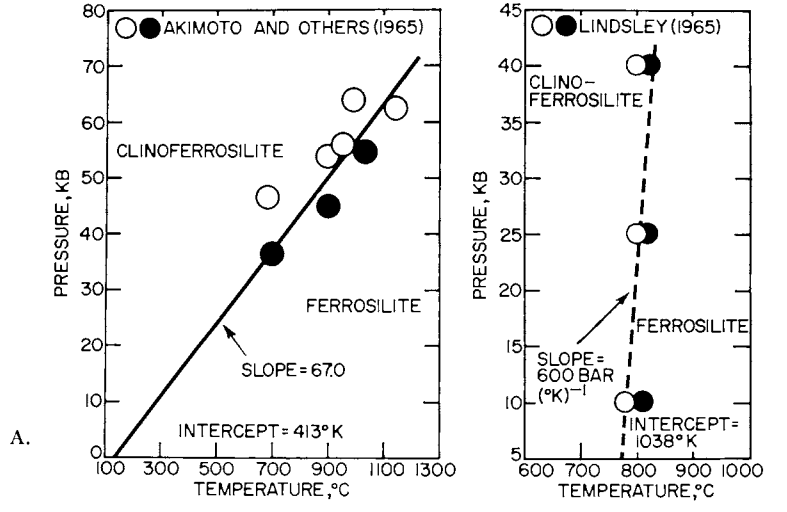

Fig. 108. Calculated equilibrium pressures and temperatures (solid curve) and experimental data (symbols) documenting the clinoferrosilite/ferrosilite transition at high pressures and temperatures (see text).

pressures and temperatures) were calculated from the experimental reversal temperatures shown in figure 109 for

$$\text{fayalite} + \text{quartz} \rightleftharpoons 2 \text{ ferrosilite} \qquad (206)$$

using data taken from table 8. The heat capacity coefficients for ferrosilite above the transition temperature at 1 bar were computed from Clapeyron slope constraints imposed by the experimental data. It can be seen in figure 109 that the univariant curves generated from the thermodynamic data in table 8 are in close agreement with all the experimental temperature reversals.

Annite.—Oxygen fugacities calculated from experimentally determined hydrogen pressures for coexisting annite, high sanidine, magnetite, and H_2O are shown in figures 110 and 111. The equilibrium composition of the annite in three of the four mineral assemblages represented by the symbols in these figures has been determined by D. R. Wones (1976, personal commun.), who reports 0.58 at ~ 440°C and 2 kb, 0.81 at ~ 631°C and 1 kb, and 0.89 at ~ 746°C and 1 kb for the mole fraction of the annite component in the binary system, $KFe^{++}{}_3(AlSi_3O_{10})(OH)_2$ – $KFe^{++}\,Fe^{+++}{}_2(AlSi_3O_{10})O_2$. The corresponding mole fractions of the annite component in the system $KFe^{++}{}_3(AlSi_3O_{10})(OH)_2$ – $KFe^{+++}{}_3(AlSi_3O_{10})O_2H_{-1}$, where the latter component corresponds to proton deficient annite (PD-oxyannite), are 0.72, 0.87, and 0.93. Activity coefficients of the annite component in the latter system can be computed from Beane's (in preparation) Margules parameters obtained by regression of experimental data reported by Eugster and Wones (1962) and Wones and Eugster (1965) for annite–phlogopite–PD-oxyannite solid solutions. Beane's regression calculations were carried out using thermodynamic data taken from table 8, which insures compatibility of the mixing parameters generated in his study with the calculations summarized below.

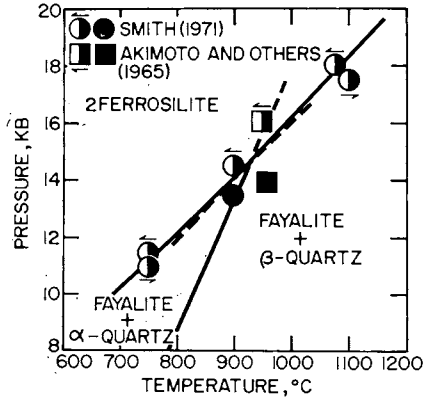

Fig. 109. Univariant equilibrium curves (generated from thermodynamic data given in table 8) and experimental observations of phase relations (symbols) in the system FeO–SiO_2 at high pressures and temperatures.

Alternate regression of the experimental data with parabolic athermal and regular solution equations resulted in (Beane, in preparation)

$$\log \lambda_{an} = -9.38X_{PD}^2 \tag{207}$$

and

$$\log \lambda_{an} = \frac{-7799X_{PD}^2}{T} \tag{208}$$

where λ_{an} refers to the activity coefficient of the annite component and X_{PD} stands for the mole fraction of the PD-oxyannite component in the solid solution. Evaluating eqs (207) and (208) for the three compositions given above leads to 0.13, 0.60, and 0.84 for the activity of the annite component in the case of the athermal model and 0.10, 0.62, and 0.85 for the regular solution approximation at 440°, 631°, and 746°C, respectively. Note that both equations give essentially the same results, which can be compared with activities computed from eq (46) by assuming (1) random mixing of Fe^{++} and Fe^{+++} among all the octahedral sites in the solid solution, (2) random mixing of OH^- and O^{--}, and (3) no substitution of Fe^{+++} for Al^{+++} on the tetrahedral sites. Eq (46) can then be written as

$$a_{an} = X_{Fe^{+++}}{}^3 \, X_{OH^-}{}^2 \tag{209}$$

which yields 0.13, 0.43, and 0.64 for the three compositions determined by Wones.

The values of $\Delta G°_f$ and $\Delta H°_f$ for annite in table 8 were retrieved from the experimental data shown in figure 110 by optimizing agreement

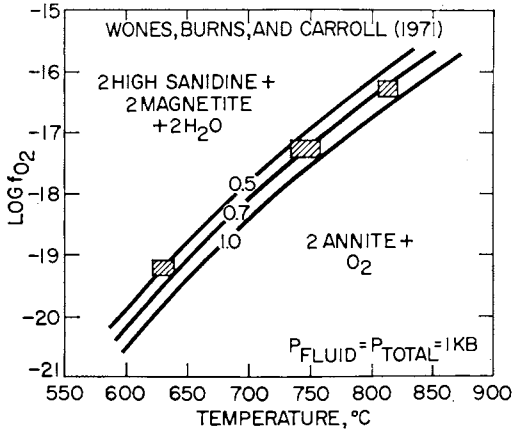

Fig. 110. Calculated (curves) and experimental (symbols) fugacities of oxygen for coexisting sanidine, magnetite, annite, and H_2O at high pressures and temperatures. The numbers on the curves designate activities of $KFe_3AlSi_3O_{10}(OH)_2$ in annite–PD-oxyannite solid solutions (see text).

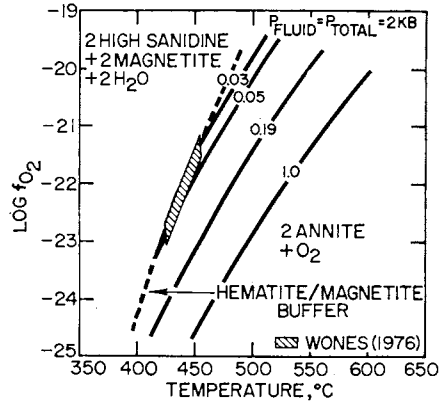

Fig. 111. Calculated (curves) and experimental (symbols) fugacities of oxygen for coexisting sanidine, magnetite, annite, and H_2O at high pressures and temperatures. The numbers on the curves designate activities of $KFe_3AlSi_3O_{10}(OH)_2$ in annite–PD-oxyannite solid solutions. Wones (1976) refers to D. R. Wones (1976, personal commun.).

of the activities computed from the various solution models with the experimental reversal temperatures and oxygen fugacities. It can be deduced from the distribution of the curves in figure 110, which were generated from the thermodynamic data given in table 8 for annite, high sanidine, and magnetite, that the values of $\Delta G°_f$ and $\Delta H°_f$ for annite as well as the activities of annite computed for 631° and 746°C from all three solution models are consistent (within experimental uncertainty) with the data reported by Wones, Burns, and Carroll (1971). In the case of figure 111, the calculations require slightly smaller activities of annite than those computed above to satisfy the experimental observation. This is not surprising in view of the relatively large mole fraction of PD-oxyannite in the solid solution represented by the symbol in figure 111 (0.28), which is higher than that in any of the samples considered in Beane's regression calculations. The value of $\Delta H°_f$ for annite in table 8 is within the uncertainty of that calculated by Beane (1978), who reports $-1{,}231{,}735 \pm 465$ cal mole^{-1} for the value of $\Delta H°_{f,annite}$ generated from his parabolic athermal regression calculations.

Andradite, hedenbergite, and epidote.—The values of $\Delta G°_f$ and $\Delta H°_f$ for these minerals, together with the heat capacity power function coefficients given in table 8 for epidote (which is used in the present study to refer to $Ca_2FeAl_2Si_3O_{12}(OH)$ in its stable state of substitutional order/disorder at any pressure and temperature) were retrieved by Bird (ms) and Bird and Helgeson (1977) from high pressure/temperature experimental data reported by Liou (1973, 1974) and Gustafson (1974) for

$$6 \text{ andradite} \rightleftharpoons 4 \text{ magnetite} + 18 \text{ wollastonite} + O_2, \quad (210)$$

$$2 \text{ andradite} + 4 \text{ quartz} \rightleftharpoons 4 \text{ hedenbergite} + 2 \text{ wollastonite} + O_2, \quad (211)$$

and

$$2 \text{ epidote} \rightleftharpoons \text{grossular} + \text{anorthite} + \text{hematite} + \text{quartz} + H_2O. \quad (212)$$

Compositional uncertainties in the experimental data reported by Chatterjee (1967) and Holdaway (1972) for the decomposition of epidote and the reaction of calcite, wollastonite, and epidote to give grossular-andradite garnet precludes use of their data in retrieval calculations of the thermodynamic properties of stoichiometric epidote. It should be noted that reaction (212) representing the coexistence of epidote–clinozoisite and grossular–andradite–almandine solid solutions can also be written as

$$6 \text{ epidote} \rightleftharpoons 2 \text{ andradite} + 6 \text{ anorthite} + \text{hematite} + 3 H_2O \quad (212A)$$

However, because the standard molal entropy of this reaction is ~ 4 times larger than that of reaction (212), it was not used to retrieve values of $\Delta H°_f$ and $\Delta G°_f$ for epidote and andradite.

It can be seen in figures 112 and 113 that the curves generated by Bird (ms) and Bird and Helgeson (1977) are consistent with all the experimental data reported by Gustafson (1974) and Liou (1973, 1974). The calculations took account simultaneously of the thermodynamic consequences of both compositional variation and order/disorder in epidote, as well as the effect of grossular–andradite–almandine solid solution on the experimental reversal temperatures for reactions (210) through (212).

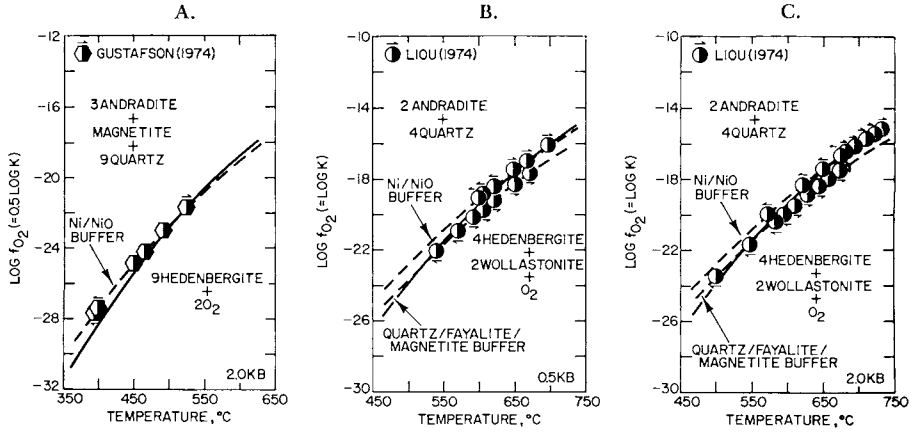

Fig. 112. Calculated (curves) and experimental (symbols) equilibrium constants for coexisting mineral assemblages in the system CaO–FeO–Fe_2O_3–SiO_2–H_2O as a function of temperature at 0.5 and 2 kb.

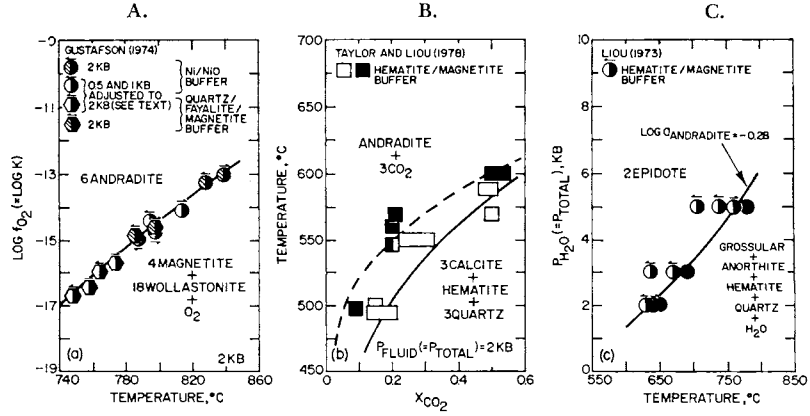

Fig. 113. Calculated (curves) and experimental (symbols) equilibrium constants, fluid compositions, temperatures, and pressures for coexisting mineral assemblages in the system CaO–FeO–Fe_2O_3–Al_2O_3–SiO_2–CO_2–H_2O. The calculations for diagram B were carried out assuming, alternately, ideal (solid curve) and nonideal (dashed curve) mixing of CO_2 and H_2O (see text).

Three energetically distinct octahedral (M) sites are occupied by Al^{+++} and Fe^{+++} in epidote. Crystal structure refinements (Dollase, 1971) and Mössbauer spectral data (DeCoster, Pollack, and Amelinckx, 1963; Bancroft, Maddock, and Burns, 1967; Dollase, 1973) indicate that Fe^{+++} is preferentially distributed among the M(3) sites. Minor amounts of Fe^{+++} are also present on the M(1) sites, but the M(2) sites contain only Al^{+++}.

Octahedral disordering of stoichiometric epidote (which corresponds to $X_{pistacite} = 0.33$ $Ca_2Fe_3Si_3O_{12}(OH)$ in the binary system, pistacite–clinozoisite ($Ca_2Al_3Si_3O_{12}(OH)$)) with increasing temperature can be represented by:

$$\underset{(\textit{ordered epidote})}{Ca_2Al^{M(1)}Al^{M(2)}Fe^{M(3)}Si_3O_{12}(OH)} \rightarrow \underset{(\textit{disordered epidote})}{Ca_2(Al_{(1-x)}Fe_x)^{M(1)}Al^{M(2)}(Al_xFe_{(1-x)})^{M(3)}Si_3O_{12}(OH)} \qquad (212B)$$

where x stands for the number of moles of Fe^{+++} on the M(1) sites in one mole (gram formula unit) of stoichiometric disordered epidote. The intracrystalline exchange reaction representing equilibrium among Al^{+++} and Fe^{+++} on the M(1) and M(3) sites can be written as

$$Fe^{+++}{}_{M(3)} + Al^{+++}{}_{M(1)} \rightleftharpoons Fe^{+++}{}_{M(1)} + Al^{+++}{}_{M(3)} \qquad (212C)$$

Assuming random mixing of Fe^{+++} and Al^{+++} on each of the energetically distinct sites, the law of mass action for reaction (212C) reduces to

$$\frac{X_{Fe,M(1)}\, X_{Al,M(3)}}{X_{Fe,M(3)}\, X_{Al,M(1)}} = K \qquad (212D)$$

where $X_{Fe,M(3)}$, $X_{Fe,M(1)}$, $X_{Al,M(3)}$, and $X_{Al,M(1)}$ stand for mole fractions defined by eq (47), and K refers to the equilibrium constant for reaction (212C). Because x and $1-x$ are equal to the mole fractions of Fe^{+++} and Al^{+++} on the M(1) and M(3) sites in stoichiometric epidote, an ordering parameter, σ, which approaches 0 for complete disorder and unity for complete order, can be defined as

$$\sigma \equiv 1 - 2x \qquad (212E)$$

which permits eq (212D) to be written as

$$-4 \operatorname{arctanh} \sigma = \ln K \qquad (212F)$$

Note that x and K are by definition independent of composition, so that σ is a function only of temperature and pressure.

Experimental distribution coefficients for epidote–clinozoisite solid solutions are shown in figure 114. Because the standard molal heat capacity of reaction (212C) is probably negligible, it would not be unreasonable to expect $\ln K$ for the exchange reaction to be a linear function of T^{-1}. This observation, together with the assumption that substitutional order/disorder in the solid solution is independent of composi-

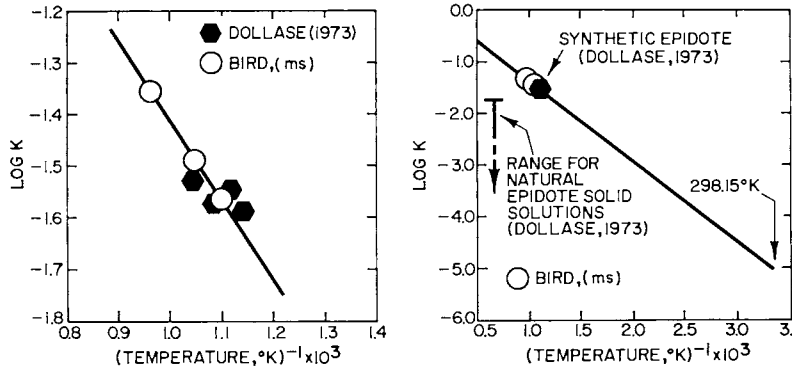

Fig. 114. Equilibrium constant for reaction (212C) as a function of temperature^{-1} (see text).

tion (which is supported by experimental evidence), permits calculation of *ln* K as a function of temperature by simultaneous evaluation of material balance constraints, activity-composition relations, and epidote compositions and garnet cell parameters reported by Liou (1973). The temperature dependence of *ln* K computed in this manner is depicted in figure 114, which is consistent with the experimental data shown in figure 113E. Note that $x \approx 0$ at 25°C. Calculated values of K and σ (*fig.* 115) can be used together with $\Delta H°_f$ for the exchange reaction computed from the slope of the curve in figure 114 to calculate the standard molal heat capacity, enthalpy, Gibbs free energy, and entropy of disorder. Computed values of the first two of these properties ($\Delta C°_{P_r,ds}$ and $\Delta H°_{ds}$) are shown in figure 116.

The standard molal heat capacities of disorder in figure 116B were added to the calorimetric heat capacities of epidote reported by Kiseleva, Topor, and Andreyenko (1974), which were assumed to represent the ordered phase. These values were then regressed with eq (19) to generate

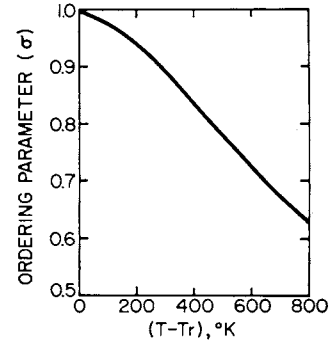

Fig. 115. Ordering parameter for stoichiometric epidote as a function of temperature at 1 bar computed from eq (212F)—see text.

the heat capacity coefficients shown for epidote in table 8 and the heat capacities of epidote plotted in figure 117B. The heat capacity coefficients given in the table for ordered epidote were obtained by regression of Kiseleva, Topor, and Andreyenko's (1974) data (fig. 117B), but those for andradite were derived by optimizing the computed and experimental equilibrium temperatures for reactions (210), (211), and (212A). Standard molal heat capacities of andradite computed in this manner are shown in figure 117A, where they can be compared with those estimated from eq (85).

Compositional variation in epidote was taken into account in the retrieval calculations described above by assuming random intrasite mixing of Al^{+++} and Fe^{+++} on the M(1) and M(3) sites in the epidote–clinozoisite solid solution. Similarly, in the grossular–andradite–almandine solid solution, Ca^{++} and Fe^{++} on the X sites and Al^{+++} and Fe^{+++} on the Y sites were assumed to mix ideally on the respective sites. These assumptions, together with that implicit in eq (212C), which requires σ to be independent of composition, permits calculation of the activities of the grossular and disordered epidote components in the two coexisting solid solutions from eqs (46) and (48) using compositional data and cell dimensions reported by Liou (1973) for the experimental reversal temperatures shown in figure 113C. Calculated equilibrium compositions of coexisting epidote and garnet solid solutions consistent with the curve in figure 113C are shown in figure 118. Activities and equilibrium constants consistent with these compositions for the reversal temperatures shown in figure 113C were used to retrieve the values of $\Delta G°_f$ and $\Delta H°_f$ for epidote and its ordered counter-

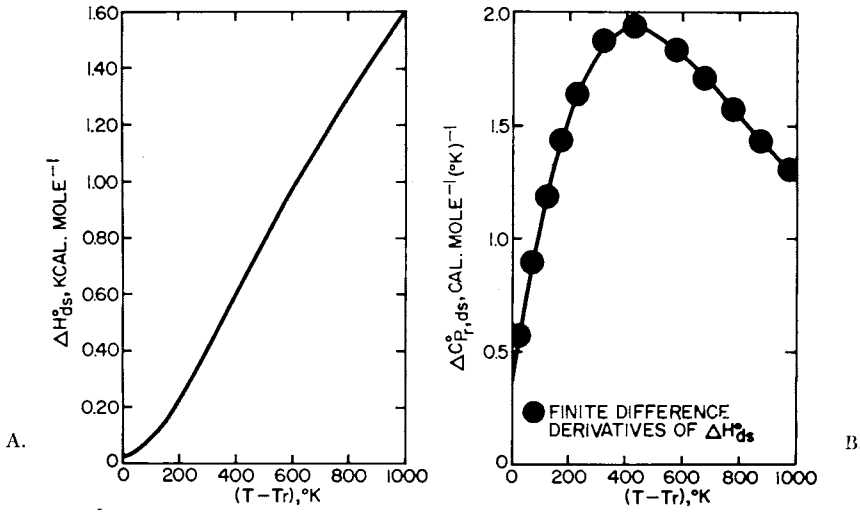

Fig. 116. Standard molal enthalpy and heat capacity of disorder in stoichiometric epidote as a function of temperature at 1 bar (see text).

part in table 8. The thermodynamic properties of hedenbergite, andradite, ordered epidote, and epidote given in the table are consistent with those of the other minerals. The value of $\Delta G°_f$ for hedenbergite in table 8 differs by only 585 cal mole^{-1} from that estimated by Navrotsky and Coons (1976).

Owing to compensation of the thermodynamic consequences of compositional variation with respect to the almandine and grossular components of andradite–almandine–grossular solid solutions in equilibrium with epidote from ~ 550° to ~ 800°C, the activity of the andradite component (but not its mole fraction — see fig. 118) is essentially constant at pressures and temperatures corresponding to those along the curve shown in figure 113C. The activity of the epidote component of the coexisting epidote–clinzoisite solid solution is also nearly constant, but in contrast to that of andradite (which is ~ 0.5) it differs only slightly from unity. At high temperatures, the activity of epidote in epidote–clinozoisite solid solutions is relatively insensitive to compositional variation at $X_{pistacite} > 0.3$.

Although estimated values of $S°_{P_r,T_r}$ for hedenbergite, epidote, and andradite, as well as estimated heat capacity coefficients for hedenbergite were used in the retrieval calculations, it can be seen in figures 112 and 113 that the estimates afford close approximation of experimental equilibrium constants over a wide temperature interval (~ 350° to ~ 800°C). The symbols representing Gustafson's (1974) data at 0.5 and 1 kb in figure 113A were adjusted to 2 kb by taking account of the standard molal volumes of andradite, magnetite, and wollastonite in table 8.

The effect of nonideal mixing of CO_2 and H_2O on equilibrium temperatures and fluid compositions for coexisting andradite, calcite, hematite, and quartz can be assessed in figure 113B. It can be seen that the experimental reversals are bracketed by the solid curve representing ideal mixing and the dashed curve, which was generated with the aid

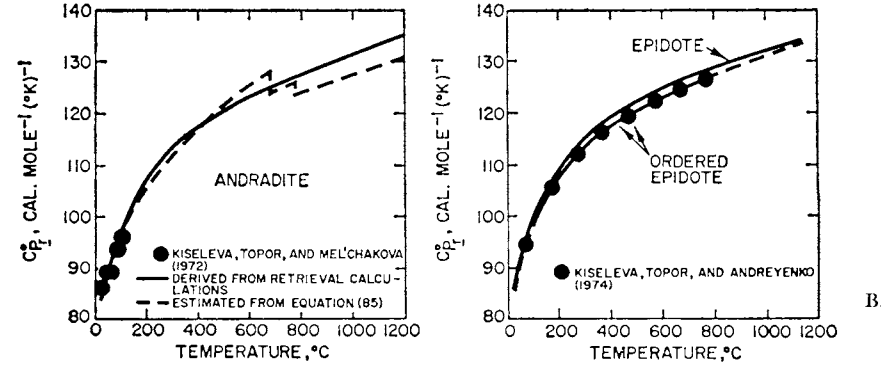

Fig. 117. Standard molal heat capacities of andradite and epidote as a function of temperature at 1 bar (see text).

of Holloway's (1977) equations describing nonideality in the system CO_2–H_2O.

BORNITE AND CHALCOPYRITE

The values of $S°_{P_r,T_r}$, $\Delta H°_f$, and $\Delta G°_f$ given in table 8 for these minerals were retrieved by Price (ms) from experimental data reported by Schneeberg (1973) and Yund and Kullerud (1966) for

$$5 \text{ chalcopyrite} + S_{2(g)} \rightleftharpoons 4 \text{ pyrite} + \text{bornite} \qquad (213)$$

and

$$\text{chalcopyrite} + 2 \text{ chalcocite} \rightleftharpoons \text{bornite} \qquad (214)$$

where the subscript (g) designates the gas state. The retrieval calculations were carried out assuming ideal mixing of Cu and Fe atoms among energetically equivalent sites in coexisting bornite and chalcopyrite solid solutions. The standard molal heat capacity coefficients for bornite and chalcopyrite in table 8 were used in the calculations together with the thermodynamic properties of pyrite, chalcocite, and $S_{2(g)}$ summarized in table 9.

It can be seen in figure 119 that equilibrium constants for reaction (213) computed from the thermodynamic data for chalcopyrite and bornite in table 8 are in close agreement with their experimental counterparts. The values of $\Delta G°_f$ for these two minerals in table 8 are within the uncertainties given by Bartholome (1958) for his estimates (Young, 1967) of $\Delta G°_f$ of bornite ($-89{,}000 \pm 6000$ cal mole^{-1}) and chalcopyrite ($-45{,}000 \pm 3500$ cal mole^{-1}). Although the value of $S°_{P_r,T_r}$ shown in table 8 for chalcopyrite is close to that estimated by Helgeson (1969) using Latimer's (1952) algorithm, that shown for bornite differs by more than 9 cal mole^{-1} (°K)$^{-1}$ from the corresponding estimate calculated by

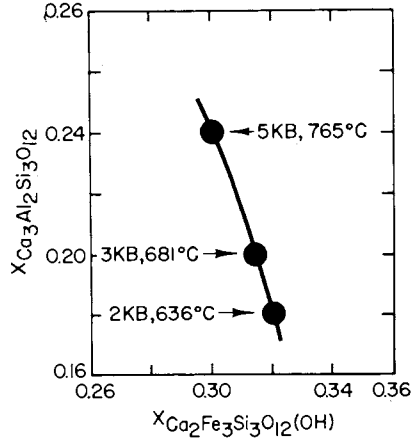

Fig. 118. Calculated compositions of coexisting epidote and garnet solid solutions in the system CaO–FeO–Fe_2O_3–Al_2O_3–SiO_2–H_2O as a function of temperature and pressure.

Helgeson. The latter difference almost certainly stems from ambiguities concerning the oxidation state of the copper, iron, and sulfur in stoichiometric bornite, which must be known accurately to obtain a reliable entropy estimate from Latimer's algorithm.

Calculation of the equilibrium constant for

$$10 \text{ chalcopyrite} + 4\ H^+ + CO_{2(g)} \rightleftharpoons 2 \text{ bornite} + 6 \text{ pyrite} + \text{graphite} + Fe^{+++} + H_2O \qquad (215)$$

using data taken from table 8, together with thermodynamic equations and data for H_2O and Fe^{++} given by Helgeson and Kirkham (1974a, 1976, and in press) yields values at high temperature which are inconsistent with those determined experimentally by Crerar and Barnes (1976). In fact, the calculated values of $\Delta H°_r$ (and thus $(\partial \ ln\ K/\partial T)_P$) for reaction (215) are opposite in sign to those required by Crerar and Barnes' experimental data. The cause of this discrepancy is not clear, but it may be due to lack of graphite–CO_2 equilibration in the experimental study (D. A. Crerar, 1976, written commun.). In any event, the thermodynamic data given for bornite and chalcopyrite in table 8 are more reliable than those given by Helgeson (1969).

SUMMARY OF SELECTED CALORIMETRIC DATA

Thermodynamic data are given in table 9 for selected elements, oxides, halides, sulfates, carbonates, and sulfides which can be used together with those in table 8 to calculate equilibrium constants for a

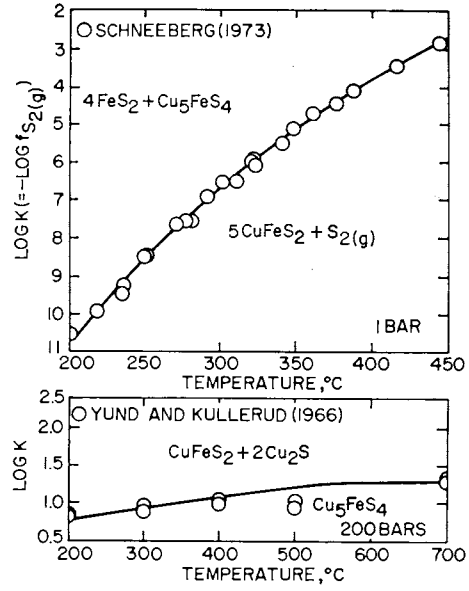

Fig 119. Calculated (curves) and experimental (symbols) equilibrium constants for reactions (213) and (214) as a function of temperature at constant pressure (Price, ms).

large number of metasomatic reactions among these minerals and silicates at high pressures and temperatures. Because the thermodynamic data given in table 9 were selected from a multitude of sources of varying reliability and have not been subjected to critical comparison with other experimental observations, they are subject to more uncertainty than those in table 8. Nevertheless, they appear to be more consistent with observed phase relations in geologic systems than those adopted previously (Helgeson, 1969).

ESTIMATION AND CORRELATION OF ΔG°_f and ΔH°_f OF MINERALS

Many algorithms have been used to estimate standard molal enthalpies and Gibbs free energies of formation of minerals from the elements at 298.15°K and 1 bar (for example, Latimer, 1952; Slaughter, 1966; Karpov and Kashik, 1968; Helgeson, *in* Eugster and Chou, 1973; Chen, 1975; Nriagu, 1975; Tardy and Garrels, 1974, 1976, 1977). However, because such estimates are uncertain to the extent of $\sim$ 2 kcal mole^{-1} or more, none of them affords sufficient accuracy to predict equilibrium temperatures for univariant reactions. Nevertheless, in the absence of experimental data, all of them offer approximations of reality that can be used to advantage in estimating the chemical environment in which various mineral assemblages form in geologic systems.

Perhaps the simplest and most generally applicable approach to estimating ΔG°_f for silicates is that taken by Tardy and Garrels (1974), who computed intracrystalline contributions by oxide and hydroxide formula groups to the standard molal Gibbs free energies of formation of layer silicates. This procedure can be generalized by writing

$$G^\circ_\psi = \sum_i \nu_{i,\psi}\, \mu^\bullet_{i,\psi} \tag{216}$$

where G°_ψ stands for the standard molal Gibbs free energy of the ψth mineral, $\nu_{i,\psi}$ refers to the number of moles of the ith oxide or hydroxide formula group (gram formula unit)$^{-1}$ of the mineral, and $\mu^\bullet_{i,\psi}$ represents the standard molal intracrystalline chemical potential of the formula group in the mineral. Taking account of constraints imposed by conservation of mass, eq (216) can also be written as

$$\Delta G^\circ_{f,\psi} = \sum_i \nu_{i,\psi}\, \Delta G^\bullet_{f,i,\psi} \tag{217}$$

where $\Delta G^\circ_{f,\psi}$ refers to the standard molal Gibbs free energy of formation from the elements of the ψth mineral, and $\Delta G^\bullet_{f,i,\psi}$ designates the intracrystalline standard molal Gibbs free energy of formation of the ith formula group in the mineral. If we now assume $\Delta G^\bullet_{f,i,\psi}$ to be equal in all minerals of a given structural class designated by the index c ($c = 1, 2, \ldots \hat{c}$) and let $\psi = 1, 2, \ldots \Psi$ and $i = 1, 2, \ldots \hat{\imath}$, Ψ statements of eq (217) can be solved simultaneously to generate $\hat{\imath}$ values of

TABLE 9

Summary of selected calorimetric data for minerals and gases at 298.15°K and 1 bar

Mineral Class	Name[a]	Index Number	Formula	Gram Formula Weight[pp]	$S°$[b]	$V°$[c]	$\Delta G°_f$[d,e]	$\Delta H°_f$[d]	$C°_{P_r}$ Coefficients[f,m]			Transition Data (1 bar)[uu]			
									a[b]	b[g]×10³	c[h]×10⁻⁵	T_t[i,m]	$\Delta S°_t$[b,j]	$\Delta H°_t$[d,m]	ΔV_t[c]
Elements	Silver$_{(c)}$	1101	Ag	107.870	10.17[k]	10.272[ℓ]	0	0	5.09	2.04	-0.36	1234			
	Gold$_{(c)}$	1100	Au	196.967	11.33[k]	10.215[ℓ]	0	0	5.66	1.24	0.0	1336			
	Copper$_{(c)}$	1102	Cu	63.54	7.923[k]	7.113[ℓ]	0	0	5.41	1.50	0.0	1357			
	Mercury$_{(ℓ)}$	1552	Hg	200.59	18.17[k]	14.822[ℓ]	0	0	6.44	0.0	-0.19	629[n]	22.48	14,140	
									4.97	0.0	0.0	3000			
	Nickel	1553	Ni	58.71	7.14[k]	6.588[ℓ]	0	0	4.06	7.04	0.0	633[p]		0	
									6.00	1.80	0.0	1725			
	Graphite	1103	C	12.011	1.372[s]	5.2982[ℓ]	0	0	4.03	1.14	2.04	2500			
	Oxygen$_{(g)}$	1302	O_2	31.999	49.003[k]	24,465[q]	0	0	7.16	1.0	0.4	3000			
	Hydrogen$_{(g)}$	1303	H_2	2.016	31.208[k]	24,465[q]	0	0	6.52	0.78	-0.12	3000			
Oxides	Carbon Dioxide$_{(g)}$	1305	CO_2	44.01	51.072[r]	24,465[q]	-94,262	-94,054[r]	10.57	2.10	2.06	2500			
	Steam	1301	H_2O	18.0153	45.104[k]	24,465[q]	-54,634	-57,796[k]	7.30	2.46	0.0	2750			
	Water	69	H_2O	18.0153	16.71[k]	18.068[u]	-56,687[k]	-68,315[k]							
	Bunsenite	1554	NiO	74.709	9.08[k]	10.97[ℓ]	-50,573	-57,300[k]	-4.99	37.58	-3.89	525[p]	0	0	
									13.88	0.0	0.0	565[t]	0	0	
									11.18	2.02	0.0	2000			
	Tenorite	1111	CuO	79.539	10.18[r]	12.22[ℓ]	-30,568	-37,200[w]	11.53[v]	1.88[v]	1.76[v]	1600[v]			
	Cuprite	1112	Cu_2O	143.079	22.08[v]	23.437[ℓ]	-35,384	-40,830[v]	14.08[v]	5.88[v]	0.76[v]	1515[v]			
Halides	Sylvite	1107	KCl	74.555	19.73[r]	37.524[ℓ]	-97,735	-104,370[r]	9.89	5.20	-0.77	1043			
	Halite	1106	NaCl	58.443	17.24[r]	27.015[ℓ]	-91,807	-98,260[r]	10.98	3.90	0.0	1073			
	Fluorite	1079	CaF_2	78.077	16.39[r]	24.542[ℓ]	-280,493	-293,000[r]	14.30	7.28	-0.47	1424			

Mineral Class	Name[a]	Index Number	Formula	Gram Formula Weight[pp]	$S°$[b]	$\bar{V}°$[c]	$\Delta G°_f$[d,e]	$\Delta H°_f$[d]	$C°_{P_r}$ Coefficients[f,m]			Transition Data (1 bar)[uu]			
									a[b]	b[g] $\times 10^3$	c[h] $\times 10^{-5}$	T_t[i,m]	$\Delta S°_t$[b,j]	$\Delta H°_t$[d,m]	V_t[c]
Sulfates	Barite	1080	$BaSO_4$	233.402	31.6[k]	52.10[ℓ]	-325,563	-352,100[k]	33.80	0.0	3.43	1422			
	Anhydrite	1078	$CaSO_4$	136.142	25.5[x]	45.94[ℓ]	-315,925	-342,760[k]	16.78	23.60	0.0	1453			
	Anglesite	1081	$PbSO_4$	303.252	35.51[k]	47.95[ℓ]	-194,353	-219,870[k]	10.96	31.0	-4.20	1100			
	Celestite	1082	$SrSO_4$	183.682	28.0[k]	46.25[ℓ]	-320,435	-347,300[k]	21.80	13.30	0.0	1500			
	Alunite	1083	$KAl_3(OH)_6(SO_4)_2$	414.220	78.4[y]	293.6[ℓ]	-1,113,600	-1,235,600[y]	153.45	0.0	54.95	650			
Carbonates	Witherite	1084	$BaCO_3$	197.349	26.8[k]	45.81[ℓ]	-278,400	-297,500[z]	21.50	11.06	3.91	1079			
	Siderite	1076	$FeCO_3$	115.856	25.1[ℓ]	29.378[ℓ]	-162,390[aa]	-179,172[bb]	11.63	26.80	0.0	885			
	Rhodachrosite	1085	$MnCO_3$	114.947	23.9[ℓ]	31.075[ℓ]	-195,045	-212,521[k]	21.99	9.30	4.69	700			
	Cerussite	1068	$PbCO_3$	267.199	31.3[k]	40.59[ℓ]	-150,370	-168,000[z]	12.39	23.60	0.0	800			
	Strontianite	1069	$SrCO_3$	147.629	23.2[k]	39.01[ℓ]	-275,470	-294,600[z]	23.52	6.32	5.08	1197			
	Smithsonite	1064	$ZnCO_3$	125.379	19.7[k]	28.275[ℓ]	-174,850	-194,260[k]	9.30	33.00	0.0	780			
	Malachite	1059	$Cu_2(OH)_2CO_3$	221.104	44.5[k]	54.86[ℓ]	-214,204	-251,900[cc]	27.76[ff]	43.78[ff]	1.34[ff]	780[gg]			
	Azurite	1060	$Cu_3(OH)_2(CO_3)_2$	344.653	66.97[dd]	91.01[ℓ]	-334,417	-390,100[k]	36.88[ff]	77.44[ff]	0.92[ff]	780[gg]			
	Huntite	1050	$CaMg_3(CO_3)_4$	353.052	71.59[ii]	122.90[jj]	-1,004,710	-1,082,600[ii]	84.17[ss]	42.86[ss]	20.44[ss]	1000[ss]			
	Nesquehonite	1558	$MgCO_3 \cdot 3H_2O$	138.367	46.76[hh]	74.79[kk]	-412,035	-472,576[hh]	-1574.804[tt]	3099.173[tt]	-417.325[tt]	306.5[tt]	0.60	184[tt]	
									25.246[tt]	91.289[tt]	-4.222[tt]	340[tt]			
	Artinite	1053	$Mg_2(OH)_2CO_3 \cdot 3H_2O$	196.693	55.67[ii]	96.9[kk]	-613,915	-698,043[ii]	70.87[ss]	27.66[ss]	7.43[ss]	1000[ss]			
	Hydromagnesite	1062	$Mg_5(OH)_2(CO_3)_4 \cdot 4H_2O$	467.671	129.38[hh]	208.8[kk]	-1,401,687	-1,557,090[hh]	141.46[ss]	65.28[ss]	21.67[ss]	1000[ss]			
Sulfides	Acanthite	1501	Ag_2S	247.804	34.3[ll]	34.2[jj]	9,446	7,550[ll]	15.63[ll]	8.6[ll]	0.0[ll]	450[ll,mm]	2.111	950[ll]	
									1.819[ll]	53.0[ll]	0.0[ll]	620[ll,nn]	0.963	600[ll]	
									21.6[ll]	0.0[ll]	0.0[ll]	1000[ll]			
	Chalcocite	1504	Cu_2S	159.144	28.9[ll]	27.48[jj]	-20,626	-19,000[ll]	12.63[ll]	18.82[ll]	0.0[ll]	376[p,ℓ]	2.447	920[ll]	
									26.78[ll]	-7.35[ll]	0.0[ll]	717[t,ll]	0.402	287[ll]	
									20.32[ll]	0.0[ll]	0.0[ll]	1400[ll]			
	Covellite	1086	CuS	95.604	15.9[ll]	20.42[ℓ]	-12,612	-12,500[ll]	10.60	2.64	0.0	1273			

continued →

TABLE 9 (continued)

Mineral Class	Name[a]	Index Number	Formula	Gram Formula Weight[pp]	$S°$[b]	$V°$[c]	$\Delta G°_f$[d,e]	$\Delta H°_f$[d]	$C°_P$ Coefficients[f,m] a[b]	$b \times 10^3$[b,g]	$c \times 10^{-5}$[h]	Transition Data (1 bar)[uu] T_t[i,m]	$\Delta S°_t$[b,j]	$\Delta H°_t$[d,m]	$\Delta V°_t$[c]
Sulfides	Pyrrhotite	1555	FeS	87.92	14.41[ll]	18.20[l]	-24,084	-24,000[ll]	5.19	26.40	0.0	411[p]	1.387	570	
									17.40	0.0	0.0	598[t]	0.201	120	
									12.20	2.38	0.0	1468			
	Pyrite	1093	FeS_2	119.98	12.65[ll]	23.940[l]	-38,293	-41,000[ll]	17.88	1.32	3.05	1000			
	Galena	1087	PbS	239.25	21.8[kk]	31.49[l]	-23,115	-23,500[ll]	11.17[ll]	2.2[ll]	0.0[ll]	1388[ll]			
	Sphalerite	1088	ZnS	97.434	14.019[qq]	23.830[c]	-47,947	-49,000[rr]	11.77[rr]	1.26[rr]	1.16[rr]	1300[rr]			
	Wurtzite	1089	ZnS	97.434	14.064[qq]	23.846[l]	-44,810	-45,850[rr]	11.82[rr]	1.16[rr]	1.04[rr]	1300[rr]			
	Cinnibar	1091	HgS	232.654	19.7[ll]	28.416[l]	-10,940	-12,750[rr]	10.46[rr]	3.72[ll]	0.0[ll]	618[ll]			
	Metacinnibar	1090	HgS	232.654	21.2[ll]	30.169[l]	-10,437	-11,800[rr]	10.52[ll]	3.63[ll]	0.0[ll]	1000[ll]			
	Alabandite	1092	MnS	87.002	19.20[ll]	21.46[l]	-52,178	-51,000[ll]	11.40[rr]	1.8[ll]	0.0[ll]	1803[ll]			
	Sulfur$_{(g)}$	1307	S_2	64.128	54.51[k]	24,465[q]	18,960	30,680[k]	8.72	0.16	0.90	3000			
	Hydrogen sulfide$_{(g)}$	1304	H_2S	34.0799	49.16[k]	24,465[q]	-8,016	-4,930[k]	7.81	2.96	0.46	2300			
Hydrocarbons	Methane$_{(g)}$	1308	CH_4	16.043	44.492[ee]	24,465[q]	-12,127	-17,880[k]	5.65	11.44	0.46	1500			

[a] Subscripts in this column refer to liquid (l), gas (g) and crystalline (c) states. [b] cal mole^{-1} (°K)$^{-1}$. [c] Standard molal volume and volume of transition at 25°C and 1 bar in cm^3 mole^{-1}. [d] cal mole^{-1}. [e] Except where indicated otherwise, the values shown in this column were computed from $\Delta G°_f = \Delta H°_f - T\Delta S°_f$ using values of $\Delta H°_f$ and $S°$ shown above together with standard molal third law entropies of the elements for $Na_{(c)}$, $K_{(c)}$, $Ca_{(c)}$, $Mg_{(c)}$, $Ba_{(c)}$, $Pb_{(c)}$, $Sr_{(c)}$, $Al_{(c)}$, $S_{(c)}$, $Fe_{(c)}$, $Mn_{(c)}$, $Zn_{(c)}$, $As_{(c)}$, $Cl_{2(g)}$, and $F_{2(g)}$ (12.24, 15.34, 9.9, 7.81, 15.0, 15.49, 12.50, 6.769, 7.60, 6.529, 7.65, 9.95, 8.4, 53.288, and 48.44 cal mole^{-1} (°K)$^{-1}$, respectively) taken from Wagman and others (1968, 1969), Parker, Wagman, and Evans (1971), and (in the case of $Fe_{(c)}$, Stull and Prophet, 1971). [f] Maier-Kelley power function coefficients for equation (19). The upper temperature limit for the coefficients is designated by the value of T_t given for the mineral. The lower limit corresponds to 298.15°K, except where more than one set of coefficients is given. In the latter cases, the

lower temperature limit of the first set is 298.15°K, but those for subsequent sets corresponds to T_t for the preceding set. Note that in the vicinity of the transition temperature, equation (19) fails to describe adequately the temperature dependence of $C°_{P_r}$ (see text). [g] cal mole^{-1} (°K)$^{-2}$. [h] cal mole^{-1} (°K). [i] Transition temperature at 1 bar in °K, except where no values of $\Delta S°_t$, $\Delta H°_t$, and $\Delta V°_t$ are shown. In the latter cases T_t refers to the upper temperature limit (in °K) for the heat capacity power function coefficients for the mineral. [j] Computed from equation (9) using the values of T_t and $\Delta H°_t$ shown above. [k] Wagman and others (1968, 1969); Parker, Wagman, and Evans (1971). [l] Robie and Waldbaum (1968). [m] Unless indicated otherwise, the values shown in this column were taken from Kelley (1960). [n] Liquid/gas transition. [p] α/β transition. [q] Standard molal volume of an ideal gas. [r] Stull and Prophet (1971). [s] CODATA (1976). [t] β/γ transition. [u] Helgeson and Kirkham (1974a). [v] Mah, Pankratz, Weller, and King (1967). [w] King, Mah, and Pankratz (1973). [x] Stern and Weise (1966). [y] Kelley and others (1946). [z] Adami and Conway (1966). [aa] Langmuir (1969). [bb] Computed from $\Delta H°_f = \Delta G°_f - T\Delta S°_f$ using values of $\Delta G°_f$ and S° shown above together with standard molal third law entropies of the elements given in footnote [e]. [cc] Richardson and Brown (1974). [dd] Estimated from equation (62) for azurite $\rightleftharpoons$ malachite + $CuCO_{3(c)}$ using $S°_{CuCO_{3(c)}}$ = 21.0 cal mole^{-1} (°K)$^{-1}$ (Stern and Weise, 1969), $V°_{CuCO_3}$ = 30.95 cm^3 mole^{-1}. (computed from cell parameters reported by Donnay and Ondik, 1973) using the standard molal entropy of malachite and the values of V° for malachite and azurite shown above. [ee] Din (1961). [ff] Computed from equations (86) through (88) assuming $\Delta C°_{P_r} = 0$ for $Cu_2(OH)_2CO_3 + ZnO \rightleftharpoons ZnCO_3 + H_2O_{(s)}$ and $Cu_3(OH)_2(CO_3)_2 + ZnO \rightleftharpoons Cu_2(OH)_2 + CO_3 + ZnCO_3 + CuO$ using $C°_{P_r}$ coefficients given above and in table 2. [gg] Limit imposed by the lowest temperature limit for the heat capacity coefficients used to estimate a, b, and c for azurite and malachite. [hh] Robie and Hemingway (1972, 1973). [ii] Hemingway and Robie (1972, 1973). [jj] Robie and others (1966). [kk] Computed from densities reported in references given in footnotes [hh] and [ii]. [ll] Mills (1974). [mm] β/α transition. [nn] α/γ transition. [pp] grams mole^{-1}. [qq] Stuve (1974). [rr] Pankratz and King (1965). [ss] Estimated from equations (86) through (88) assuming $\Delta C°_{P_r} = 0$ for the reactions $CaMg_3(CO_3)_4 \rightleftharpoons CaCO_3 + 3MgCO_3$, $Mg_2(OH)_2CO_3 \cdot 3H_2O \rightleftharpoons MgCO_3 + Mg(OH)_2 + 3H_2O_{(z)}$, and $Mg_5(OH)_2(CO_3)_4 \cdot 4H_2O \rightleftharpoons 4MgCO_3 + Mg(OH)_2 + 4H_2O_{(z)}$ using heat capacity coefficients given in tables 2 and 8. [tt] generated from regression of calorimetric values taken from Robie and Hemingway (1973). [uu] thermodynamic properties given for lambda transitions correspond to the apparent properties (see text).

$\Delta G^\bullet_{f,i,c}$ if $\Psi = i$ and Ψ experimental values of $\Delta G^\circ_{f,\psi,c}$ are known. The calculated values of $\Delta G^\bullet_{f,i,c}$ can then be used to estimate $\Delta G^\circ_{f,\psi,c}$ for other minerals in the cth structural class for which experimental data are lacking.

As might be expected, the success of Tardy and Garrels' approach is highly sensitive to structural differences among minerals. For example, eq (217) and thermodynamic data given in table 8 for the mineral pairs, gibbsite and brucite, kaolinite and chrysotile, pyrophyllite and talc, and muscovite and phlogopite result in significantly different values of $\Delta G^\bullet_{f,Al_2O_3,c} - 3\Delta G^\bullet_{f,MgO,c}$ (46.6, 59.3, 64.2, and 59.9 kcal mole^{-1}, respectively) for hypothetical intracrystalline exchange of trioctahedral MgO and dioctahedral Al_2O_3 groups in clay minerals. The general progression of these values is consistent with Chen's (ms and 1975) stochastic estimates, but not with the generalizations advocated by Tardy and Garrels. The differences in the last three values of $\Delta G^\bullet_{f,Al_2O_3,c} - 3\Delta G^\bullet_{f,MgO,c}$ computed above result from subtle structural differences like those responsible for the distinction between chrysotile and the structural analog of kaolinite, lizardite.

The algorithm represented by eq (217) can be improved substantially by replacing the oxide and hydroxide formula units designated by the subscript i with structural components corresponding to minerals in a given polysomatic series, which is defined by J. B. Thompson (1970, 1977, personal commun., 1978) as a series of minerals composed of different combinations of chemically and structurally distinct layers with a common structural plane. For example, $\Delta G^\circ_{f,tremolite}$ would be estimated by adding $2\Delta G^\bullet_{f,diopside}$ to $\Delta G^\bullet_{f,talc}$. Similarly, $\Delta G^\circ_{f,anthophyllite}$ would be taken as the sum of $\Delta G^\bullet_{f,talc}$ and $4\Delta G^\bullet_{f,enstatite}$. These relations and the values of ΔG°_f for tremolite and anthophyllite in table 8 result in $2\Delta G^\bullet_{f,enstatite} - \Delta G^\bullet_{f,diopside} = 27{,}628$ cal mole, which is $\sim$ 1490 cal mole^{-1} greater than $2\Delta G^\circ_{f,enstatite} - \Delta G^\circ_{f,diopside}$ (table 8). The difference corresponds to the intracrystalline Gibbs free energy associated with bonding the enstatite and diopside structural components in the minerals.

An alternate approach, and one consistent with eq (46), involves calculation of relative intracrystalline standard molal enthalpies of formation of different cations or anions on energetically equivalent sites in minerals of the same structural class. For example, $\Delta H^\bullet_{f,Fe^{++}(c)} - \Delta H^\bullet_{f,Mg^{++}(c)}$ in olivines can be computed by assuming the standard molal enthalpy of reaction to be zero for hypothetical intracrystalline exchange of Mg^{++} and Fe^{++} represented by

$$0.5 \text{ fayalite} + Mg^{++}{}_{(c)} \rightleftharpoons 0.5 \text{ forsterite} + Fe^{++}{}_{(c)} \qquad (218)$$

which leads to

$$\Delta H^\bullet_{f,Fe^{++}(c)} - \Delta H^\bullet_{f,Mg^{++}(c)} = \Delta H^\circ_{f,fayalite} - \Delta H^\circ_{f,forsterite} \qquad (219)$$

where $Fe^{++}{}_{(c)}$ and $Mg^{++}{}_{(c)}$ refer to pure Fe^{++} and Mg^{++} in a hypothetical crystalline state. Values of $\Delta H^\bullet_{f,Fe^{++}(c)} - \Delta H^\bullet_{f,Mg^{++}(c)}$ and

$\Delta H^{\bullet}_{f,Mg^{++}(c)} - \Delta H^{\bullet}_{f,Ca^{++}(c)}$ computed in this manner from data taken from table 8 are shown in figures 120 and 121, where it can be seen that these differences exhibit a linear correlation with the ratio of the number of tetrahedral sites to the number of moles of oxygen (other than that in OH^-) in minerals representing different structural groups. The equations of the curves in figures 120 and 121 can be written as

$$\Delta H^{\bullet}_{f,Fe^{++}(c)} - \Delta H^{\bullet}_{f,Mg^{++}(c)} = 78{,}780 + \frac{16{,}290\,(\nu_{Al,t} + \nu_{Si,t})}{\nu_O} \qquad (220)$$

and

$$\Delta H^{\bullet}_{f,Mg^{++}(c)} - \Delta H^{\bullet}_{f,Ca^{++}(c)} = 7990 + \frac{54{,}600\,(\nu_{Al,t} + \nu_{Si,t})}{\nu_O} \qquad (221)$$

respectively, where $\nu_{Al,t}$ and $\nu_{Si,t}$ stand for the stoichiometric number of moles of tetrahedral Al and Si atoms (gram formula unit of the minerals)$^{-1}$ and ν_O refers to the corresponding number of moles of oxygen (excluding that in OH^-).

Eqs (220) and (221) yield values of $\Delta H^{\bullet}_{f,Fe^{++}(c)} - \Delta H^{\bullet}_{f,Mg^{++}(c)}$ and $\Delta H^{\bullet}_{f,Mg^{++}(c)} - \Delta H^{\bullet}_{f,Ca^{++}(c)}$ within 150 cal mole^{-1} or less of those represented by the symbols in figures 120 and 121. Nevertheless, care must be exercised in using the equations to estimate values of ΔH°_f for minerals. For example, eq (220) and the value of ΔH°_f in table 8 for diopside yield an estimate of ΔH°_f for hedenbergite (which is not an exact structural analog of diopside at high temperatures[16]) of −681,388 cal mole^{-1}. This estimate differs by ~ 2900 cal mole^{-1} from the value of ΔH°_f for hedenbergite shown in table 8. Similarly, because wollastonite is not a pyroxene, the estimate for wollastonite afforded by eq (221) and the value of ΔH°_f for enstatite in table 8 differ from the corresponding value of ΔH°_f for wollastonite shown in the table by 6066 cal mole^{-1}. Such discrepancies would also be expected to result from estimates of ΔH°_f for ferrotremolite and minnesotaite, which are not exact structural analogs of tremolite and talc, respectively. In the case of minnesotaite, the estimate of ΔH°_f generated from eq (220) and the value of ΔH°_f for talc in table 8 is −1,155,032 cal mole^{-1}, which can be combined with entropy data taken from table 3 to give $\Delta G^{\circ}_{f,minnesotaite} = -1{,}070{,}609$ cal mole^{-1}. The latter value is ~ 650 cal mole^{-1} more negative than that given by Mel'nik (1972).

Compositional variation in montmorillonites, illites, glauconites, chlorites, and amphiboles.—Although Helgeson (1969), Tardy and Garrels (1974), Nriagu (1975), Nesbitt (1977), and others generated estimates of ΔG°_f for montmorillonites, illites, and other minerals which have no stoichiometric compositions, this practice leaves much to be desired. If standard molal Gibbs free energies of formation are to be assigned to all such minerals, it would take an infinite number to account adequately for all the compositions of montmorillonites, illites, glauconites, chlorites,

[16] At high temperatures the structure of hedenbergite is more closely related to that of bustamite (Rutstein, 1971; Rapport and Burnham, 1973).

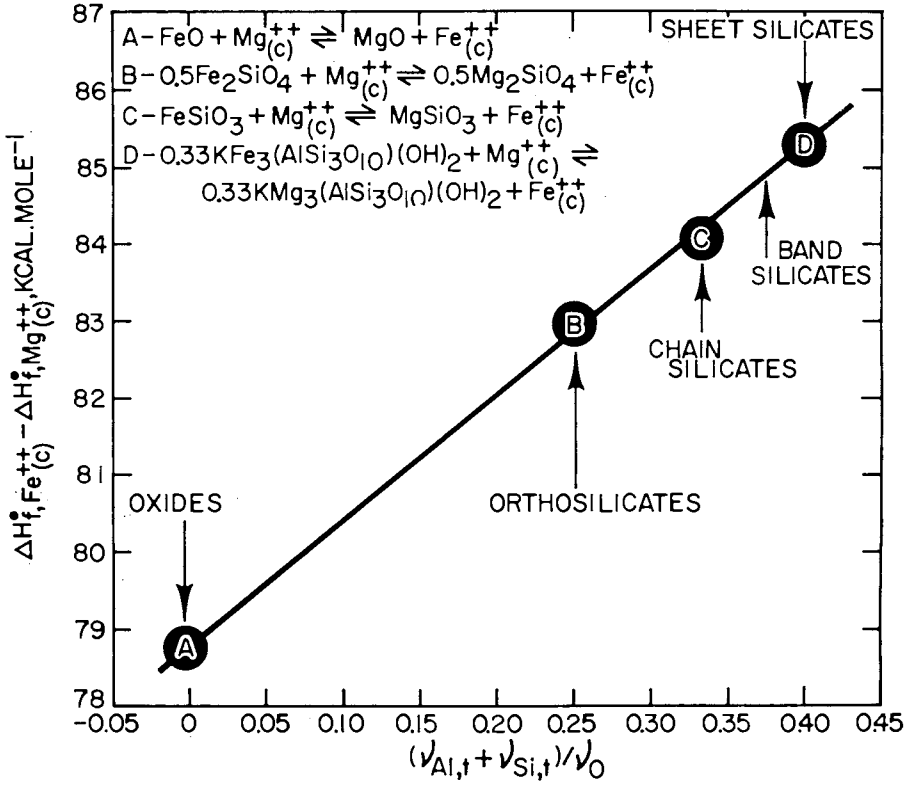

Fig. 120. Corresponding states relation represented by eq (220).

and amphibole solid solutions observed in nature. Because large numbers of components are required to describe the compositions of these minerals, it is advantageous to take them into account in geochemical calculations by computing the activities of the thermodynamic components of the minerals from site mixing approximations, such as those represented by eq (46) or its nonideal counterparts. This approach permits calculation from lattice parameters and Mössbauer data of the activities of components corresponding in stoichiometry to pyrophyllite, muscovite, paragonite, phlogopite, margarite, clinochlore, anthophyllite, tremolite, and other minerals for which thermodynamic data are available. The activities of these components can then be correlated with the compositions of the minerals and used as descriptive variables in activity diagrams, thereby obviating the practice of assigning values of ΔG°_f to one or another solid solution mineral with a specified composition. This procedure has been used recently to calculate activity/composition relations among aqueous solutions and montmorillonites, illites, and mixed layer clays (Aagaard, Helgeson, and Benson, in preparation). Because it is comprehensive, simple, and offers far more versatility and reliability

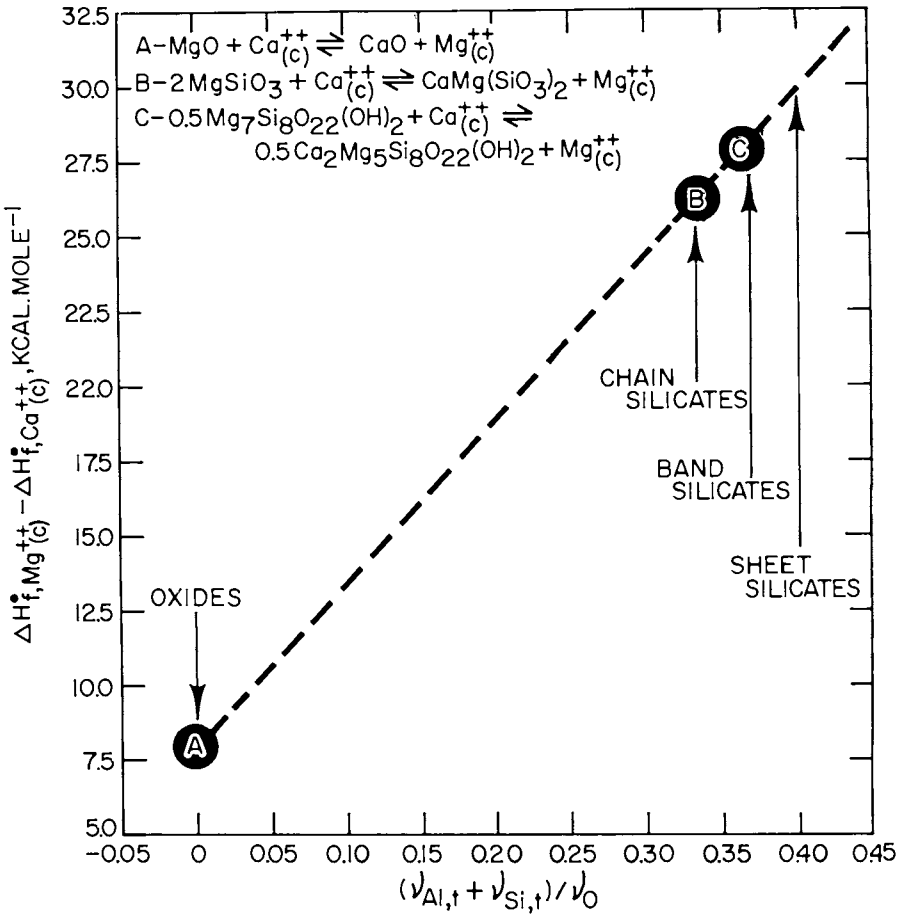

Fig. 121. Corresponding states relation represented by eq (221).

than the approach taken by Helgeson (1969), Helgeson and Mackenzie (1970), Kittrick (1971b, c, and d), Weaver, Jackson, and Syers (1971), Routson and Kittrick (1971), Huang and Keller (1973), Tardy and Garrels (1974, 1976, 1977), Nriagu (1975), Nesbitt (1977), and others, no thermodynamic data are given for these minerals in tables 8 and 9.

CONCLUDING REMARKS

The equations and data summarized above permit comprehensive calculation of the chemical and thermodynamic consequences of reactions among aqueous solutions and the bulk of the abundant minerals in the Earth's crust. Preliminary calculations of this kind (Delany and Helgeson, 1978; Bird and Helgeson, 1977) indicate a close correspondence between predicted phase relations and those observed in nature. The agreement is due primarily to the fact that the thermodynamic data summarized

in table 8 are internally consistent and compatible with both laboratory and field observations, as well as with general equations of state for aqueous and gaseous species. It should perhaps be emphasized that the thermodynamic data in tables 8 and 9 should not be used together with data taken from other sources without making sure that the two sources are consistent with one another. Similarly, any modification of the values of $\Delta G°_f$ and $\Delta H°_f$ in table 8 must be accompanied by modification of the corresponding values for all other minerals involved in the retrieval calculations responsible for the values given in the table, and these must be consistent with all pertinent experimental data.

The thermodynamic equations and data for minerals and gases discussed in the preceding pages have been combined with their analogs for aqueous species (Helgeson and Kirkham, 1974, 1976, and in press) to calculate hydrolysis constants for > 130 minerals at pressures and temperatures to 5 kb and 600°C. These equilibrium constants will be used to generate comprehensive activity diagrams for a wide variety of geologic systems at high pressures and temperatures. The equations and data employed in the calculations have been incorporated in a computer program (SUPCRT) which provides for up to 5 solid/solid phase transitions mineral^{-1} and contains a univariant/divariant curve-finding option. If only minerals, $H_2O_{(l)}$, and/or gases are involved in the reactions, the program can be used to compute equilibrium constants and fugacity coefficients at pressures and temperatures to 100 kb and 1000°C. Copies of the program and data file (which incorporates the thermodynamic data given in tables 8 and 9), together with a program description can be obtained at cost from the senior author before July 1, 1979. The program description, program (which is written in FORTRAN IV for CDC 6400, 6600, and 7600 computers), and data file are stored on magnetic tape: 7 track, 800 binary bits inch^{-1}, 132 characters record^{-1}, 1 record block^{-1}.

As more and better experimental data become available, the calculations described above will undoubtedly require revision, which hopefully will generate more accurate values of the thermodynamic properties of minerals. The first such revision (to be undertaken in 1979) will incorporate recent calorimetric measurements of the high-temperature heat capacities of talc, tremolite, dolomite, prehnite, lawsonite, and margarite, none of which was available at the time the retrieval calculations reported in the present communication were carried out. Although taking account of these and other new data may lead to values of $\Delta H°_f$ and $\Delta G°_f$ that differ from those computed above by several hundred calories or more, the revised values (like those in table 8) will be internally consistent and compatible with the experimental observations summarized in the preceding pages. Plans call for the results of all future retrieval calculations to be incorporated in the SUPCRT data file, which will be updated and distributed periodically to interested laboratories. In this way we hope to accelerate scientific progress toward

a better and more comprehensive understanding of the chemical and thermodynamic behavior of minerals in geochemical processes.

ACKNOWLEDGMENTS

The research described above has been supported over the past 5 years by the National Science Foundation (NSF grants GA 25314, GA 21509, GA 35888, GA 36023, EAR 74-14280, and EAR 77-14492), the donors of the Petroleum Research Fund administered by the American Chemical Society (PRF grants 5356 AC2 and 8927 AC2C), and the Miller Institute and Committee on Research at the University of California, Berkeley. We are indebted to these agencies and also to the Division of Physical Research of the U.S. Energy Research and Development Administration for financial support derived from the Geoscience Programs at the Lawrence Berkeley Laboratory (ERDA Contract Nos. 7405-ENG-48 and UCB-ENG-4288) and the Lawrence Livermore Laboratory (ERDA Contract No. W-7405-ENG. 48). In addition, we are grateful to our many friends and colleagues at Berkeley who contributed much in the way of ideas, suggestions, and critical comment, as well as assistance with calculations, data analysis, literature search, plotting, drafting, and reproduction. In particular we would like to thank D. H. Kirkham, J. V. Walther, G. C. Flowers, P. Aagaard, R. Reeder, M. Ghiorso, C. Schnake, K. Jackson, D. Wolfgram, C. Frisch, M. Reed, R. Stoessell, J. Price, P. Behrman, W. MacKenzie, M. Lee, T. Boleslawski, L. Bridges, D. Maskell, P. Mullen, and J. Hampel. Thanks are also due to G. B. Skippen, E. G. King, K. K. Kelley, R. E. Beane, J. Holloway, R. E. Openshaw, A. Pabst, D. Wones, H. P. Eugster, C. L. Christ, I-Ming Chou, R. A. Robie, B. Hemingway, Charles E. Holley, Jr., C. Herrick, A. Navrotsky, P. Orville, R. M. Garrels, O. Kleppa, H.-R. Wenk, I. S. E. Carmichael, B. Wood, H. J. Greenwood, D. Hewitt, Dexter Perkins III, H. Oterdoom, V. Trommsdorff, J. B. Thompson, Jr., L. Cohen, and especially J. J. Hemley, who made available unpublished data and/or offered many helpful suggestions during the course of the research. D. Aoki and T. Brooks more than deserve our gratitude for their outstanding patience and skill in typing and retyping the manuscript.

The calculations reported in the preceding pages could not have been carried out without the computer programs generated by D. H. Kirkham and J. V. Walther. These programs were revised and updated time and time again by J. V. Walther and G. C. Flowers, who are largely responsible for successful completion of the project. We gratefully acknowledge their expertise and generous contributions of time and effort.

The present communication benefited greatly from critical reviews by H. J. Greenwood, G. B. Skippen, R. A. Robie, T. H. Brown, Enrique Merino, Dugald Carmichael, H. Oterdoom, E-an Zen, J. R. Fisher, Dexter Perkins III, A. B. Thompson, G. M. Anderson, J. J. Hemley, F. J. Turner, Alex Navrotsky, and J. B. Thompson, Jr., who made many constructive suggestions for improvement. We are indebted to these individuals for

their valuable contributions to the review process but hasten to absolve them of responsibility for any omissions, errors, and erroneous conclusions that may have escaped their attention. Our thanks also to J. Hower, the National Science Foundation, the editorial staff of the American Journal of Science, and in particular, Marie Casey and P. M. Orville for facilitating and expediting publication of this paper. Finally we would like to express our appreciation to the many experimentalists who overcame what must have seemed at times to be insurmountable experimental difficulties in order to contribute to the literature much needed data on phase relations at high pressures and temperatures. We find it both remarkable and commendable that so many diverse observations by a multitude of scientists in different laboratories over several decades are not only consistent with one another but also with observations of geologic systems and independent advances in theoretical research concerned with the physical chemistry of high-pressure/temperature electrolyte solutions.

References

Aagaard, P., and Helgeson, H. C., 1977, Thermodynamic and kinetic constraints on the dissolution of feldspars [abs.]: Geol. Soc. America Abs. with Programs, v. 9, p. 873.

Adami, L. H., and Conway, K. C., 1966, Heats and free energies of formation of anhydrous carbonates of barium, strontium, and lead: U.S. Bur. Mines Rept. Inv. 6822, 7 p.

Akimoto, S., Katsura, T., Syono, Y., Fujisawa, H., and Komada, E., 1965, Polymorphic transition of pyroxenes $FeSiO_3$ and $CoSiO_3$ at high pressures and temperatures: Jour. Geophys. Research, v. 70, p. 5269-5278.

Althaus, Egon, 1966, Der stabilitätsbereich des Pyrophyllits unter dem einflux von Säuren: Contr. Mineralogy Petrology, v. 13, p. 31-50.

———— 1967, The triple point andalusite–sillimanite–kyanite: Contr. Mineralogy Petrology, v. 16, p. 29-44.

———— 1969, Experimental evidence that reaction of kyanite to form sillimanite is at least bivariant: Am. Jour. Sci., v. 267, p. 273-277.

Althaus, Egon, Karotke, E., Nitsch, K. H., and Winkler, H. G. F., 1970, An experimental re-examination of the upper stability limit of muscovite plus quartz: Neues Jahrb. Mineralogie, p. 325-336.

Anderson, G. M., 1970, Some thermodynamics of dehydration equilibria: Am. Jour. Sci., v. 269, p. 392-401.

———— 1976, Error propagation by the Monte Carlo method in geochemical calculations: Geochim. et Cosmochim. Acta, v. 40, p. 1533-1538.

———— 1977, The accuracy and precision of calculated mineral dehydration equilibria, *in* Fraser, D. G., ed., Thermodynamics in Geology: Netherlands, D. Reidel Pub. Co., p. 115-136.

Anderson, P. A. M., Newton, R. C., and Kleppa, O. J., 1977, The enthalpy change of the andalusite–sillimanite reaction and the Al_2SiO_5 diagram: Am. Jour. Sci., v. 277, p. 585-593.

Apps, J. A., ms, 1970, The stability field of analcine: Ph.D. dissert., Harvard Univ., Cambridge, Mass., 347 p.

Atlas, L., 1952, The polymorphism of $MgSiO_3$ and solid-state equilibria in the system $MgSiO_3$–$CaMgSi_2O_6$: Jour. Geology, v. 60, p. 125-147.

Bailey, S. W., 1972, Determination of chlorite compositions by X-ray spacings and intensities: Clays and Clay Minerals, v. 20, p. 381-388.

Bancroft, G. M., Maddock, A. G., and Burns, R. G., 1967, Application of the Mossbauer effect to silicate mineralogy: I: Iron silicates of known crystal structure: Geochim et Cosmochim. Acta., v. 31, p. 2219-2246.

Barany, R., 1962, Heats and free energies of formation of some hydrated and anhydrous sodium and calcium aluminum silicates: U.S. Bur. Mines. Rept. Inv. 5900, 17 p.

———— 1963, Heats of formation of gehlenite and talc: U.S. Bur. Mines, Rept. Inv. 6251, 9 p.

———— 1964, Heat and free energy of formation of muscovite: U.S. Bur. Mines Rept. Inv. 6356, 6 p.

Barany, R., and Adami, L. H., 1966, Heats of formation of lithium sulfate and five potassium– and lithium–aluminum silicates: U.S. Bur. Mines Rept. Inv. 6873, 18 p.

Barany, R., and Kelley, K. K., 1961, Heats and free energies of formation of gibbsite, kaolinite, halloysite, and dickite: U.S. Bur. Mines Rept. Inv. 5825, 13 p.

Barnes, H. L., and Ernst, W. G., 1963, Ideality and ionization in hydrothermal fluids: The system MgO–H_2O–NaOH: Am. Jour. Sci., v. 261, p. 129-150.

Barnes, Ivan, and Back, W., 1964, Dolomite solubility in ground water: U.S. Geol. Survey Prof. Paper 475-D, p. 179-180.

Bartholomé, 1958, On the paragenesis of copper ores: Leopoldville, Belgian Congo, Studia Univ. Lovanium.

Beane, R. E., ms, 1972, A thermodynamic analysis of the effect of solid solution on the hydrothermal stability of biotite: Ph.D. thesis, Northwestern Univ., Evanston, Ill.

Bell, P. M., 1964, High-pressure melting relations for jadeite composition: Carnegie Inst. Washington Year Book 63, p. 171.

Benson, S. W., 1968, Thermochemical kinetics: New York, John Wiley & Sons, 223 p.

Berner, R. A., 1967, Comparative dissolution characteristics of carbonate minerals in the presence and absence of aqueous magnesium ions: Am. Jour. Sci., v. 265, p. 45-70.

Berry, L. G., 1974, Powder diffraction file search manual, minerals: Joint Comm. Powder Diffraction Standards, Pub. M-1-23, 833 p.

Bird, D. K., ms, 1978, Chemical interaction of aqueous solutions with epidote/feldspar mineral assemblages in geologic systems: Ph.D. dissert., Univ. California, Berkeley, California.

Bird, D. K., and Helgeson, H. C., 1977, Prediction of the chemical characteristics of geothermal reservoir fluids from authigenic mineral assemblages [abs.]: Geol. Soc. America Abs. with Programs, v. 9, p. 898-899.

Bird, G. W., and Anderson, G. M., 1973, The free energy of formation of magnesian cordierite and phlogopite: Am. Jour. Sci., v. 273, p. 84-91.

Bird, G. W., and Fawcett, J. J., 1973, Stability relations of Mg–chlorite–muscovite and quartz between 5 and 10 kb water pressure: Jour. Petrology, v. 14, p. 415-428.

Blander, M., 1970, The partitioning of cations between co-existing one-site-two-site phases: Geochim. et Cosmochim. Acta, v. 34, p. 515-518.

————1972, Thermodynamic properties of orthopyroxenes and clinopyroxenes based on the ideal two-site model: Geochim. et Cosmochim. Acta, v. 36, p. 787-799.

Boettcher, A. L., 1970, The system CaO–Al_2O_3–SiO_2–H_2O at high pressures and temperatures: Jour. Petrology, v. 11, p. 337-379.

Boettcher, A. L., and Wyllie, P. J., 1968, The quartz–coesite transition measured in the presence of a silicate liquid and calibration of piston-cylinder apparatus: Contr. Mineralogy Petrology, v. 17, p. 224-232.

Boyd, F. R., 1959, Hydrothermal investigations of amphiboles, *in* Abelson, P. H., ed., Researches in Geochemistry, v. 1: New York, John Wiley & Sons, Inc., p. 377-396.

———— 1964, Geological aspects of high pressure research: Science, v. 145, p. 13-20.

Boyd, F. R., and England, J. L., 1960, The quartz–coesite transition: Jour. Geophys. Research, v. 65, p. 749-756.

———— 1965, The rhombic enstatite–clinoenstatite inversion: Carnegie Inst. Washington Year Book 64, p. 117-123.

Boyd, F. R., England, J. L., and Davis, B. T. C., 1964, Effects of pressure on the melting and polymorphism of enstatite, $MgSiO_3$: Jour. Geophys. Research, v. 69, p. 2101-2109.

Bragg, L., and Claringbull, G. F., 1965, Crystal structures of minerals: London, G. Bell and Sons, 409 p.

Bragg, W. L., and Williams, E. J., 1934, The effect of thermal agitation on atomic arrangements in alloys: Royal Soc. London Proc., v. 145A, p. 699-730.

———— 1935, The effect of thermal agitation on atomic arrangement in alloys, Pt. 2: Royal Soc. London Proc., v. 151A, p. 540-566.

Breedveld, G. J. F., and Prausnitz, J. M., 1973, Thermodynamic properties of supercritical fluids and mixtures at very high pressures: Am. Inst. Chem. Eng. Jour., v. 19, p. 783-795.

Bricker, O. P., and Garrels, R. M., 1967, Mineralogic factors in natural water equilibria, *in* Faust, S. D., and Hunter, J. V., eds., Principles and Applications of Water Chemistry: New York, John Wiley & Sons, Inc., p. 449-469.

Bricker, O. P., Nesbitt, H. W., and Gunter, W. D., 1973, The stability of talc: Am. Mineralogist, v. 58, p. 64-72.

Bridgman, P. W., 1948a, Rough compressions of 177 substances to 40,000 kg/cm²: Am. Acad. Arts and Sci. Proc., v. 76, p. 71-87.

———— 1948b, The compression of 39 substances to 100,000 kg/cm²: Am. Acad. Arts and Sciences Proc., v. 76, p. 55-87.

———— 1949, Linear compressions to 30,000 kg/cm², including relatively incompressible substances: Am. Acad. Arts and Sci. Proc., v. 77, p. 187-234.

Burnham, C. W., 1965, Ferrosilite: Carnegie Inst. Washington Year Book 64, p. 202-204.

Burns, R. G., 1970, Mineralogical applications of crystal field theory: London, Cambridge Univ. Press, 224 p.

Burns, R. G., and Fyfe, W. S., 1967, Crystal field theory and the geochemistry of transition elements *in* Abelson, P. H., ed., Researches in Geochemistry, v. 2: New York, John Wiley & Sons, p. 259-285.

Cameron, M., Sueno, S., Prewitt, C. T., and Papike, J. J., 1973, High-temperature crystal chemistry of acmite, diopside, hedenbergite, jadeite, spodumene, and ureyite: Am. Mineralogist, v. 58, p. 594-618.

Campbell, A. S., and Fyfe, W. S., 1965, Analcime–albite equilibria: Am. Jour. Sci., v. 263, p. 807-816.

Cantor, S., 1977, Entropy estimates of garnets and other silicates: Science, v. 198, p. 206-207.

Charlu, T. V., Newton, R. C., and Kleppa, O. J., 1975, Enthalpies of formation at 970 K of compounds in the system $MgO–Al_2O_3–SiO_2$ from high temperature solution calorimetry: Geochim. et Cosmochim. Acta, v. 39, p. 1487-1498.

———— 1978, Enthalpy of formation of some lime silicates by high-temperature solution calorimetry, with discussion of high-pressure phase equilibria: Geochim. et Cosmochim. Acta, v. 42, p. 367-375.

Chase, M. W., Cornutt, J. L., Prophet, H., McDonald, R. A., and Syverud, A. N., 1975, JANAF thermochemical tables, 1975 supplement: Jour. Phys. and Chem. Ref. Data, v. 4, p. 1-175.

Chatterjee, N. D., 1967, Experiments on the phase transition calcite + wollastonite + epidote = grossular–andradite$_{ss}$ + CO_2 + H_2O: Contr. Mineralogy Petrology, v. 14, p. 114-122.

———— 1970, Synthesis and upper stability of paragonite: Contr. Mineralogy Petrology, v. 27, p. 244-257.

———— 1972, The upper stability limit of the assemblage paragonite + quartz and its natural occurrences: Contr. Mineralogy Petrology, v. 34, p. 288-303.

———— 1974, Synthesis and upper thermal stability limit of 2M–margarite, $CaAl_2[Al_2Si_2O_{10}(OH)_2]$: Schweizer min. pet. Mitt., v. 54, p. 753-767.

———— 1977, Thermodynamics of dehydration equilibria, *in* Fraser, D. G., ed., Thermodynamics in Geology: Netherlands, D. Reidel Pub. Co., p. 137-159.

Chatterjee, N. D., and Johannes, W., 1974, Thermal stability and standard thermodynamic properties of synthetic $2M_1$–muscovite, $KAl_2[AlSi_3O_{10}(OH)_2]$: Contr. Mineralogy Petrology, v. 48, p. 89-114.

Chelischev, N. F., and Borutskaya, V. L., 1972, Dependence of potassic feldspar ion exchange capacity on the degree of ordering under supercritical conditions: Geochim. Internat., v. 1972, p. 194-198.

Chen, C. H., ms, 1973, Stochastic estimation of standard free energies of formation of silicate minerals: M.S. Thesis, Univ. California, Berkeley.

———— 1975, A method of estimation of standard free energies of formation of silicate minerals at 298.15°K: Am. Jour. Sci., v. 275, p. 801-817.

Chernosky, J. V., Jr., 1973, The stability of chrysotile, $Mg_3Si_2O_5(OH)_4$, and the free energy of formation of talc, $Mg_3Si_4O_{10}(OH)_2$ [abs.]: Geol. Soc. America Abs. with Programs, v. 5, p. 575.

———— 1974, The stability field of anthophyllite—an experimental redetermination [abs.]: Geol. Soc. America Abs. with Programs, v. 6, p. 687.

———— 1975, The stability of the assemblage clinochlore + quartz at low pressure [abs.]: Am. Geophys. Union Trans., v. 56, p. 466.

———— 1976a, Gibbs free energy of enstatite, clinochlore, and hydrous Mg-cordierite evaluated from phase equilibrium data [abs.]: Am. Geophys. Union Trans., v. 57, p. 1020.

———— 1976b, The stability of anthophyllite—A reevaluation based on new experimental data: Am. Mineralogist, v. 61, p. 1145-1155.

Chernosky, J. V., and Knapp, L. A., 1977, The stability of anthophyllite plus quartz [abs.]: Geol. Soc. America Abs. with Programs, v. 9, p. 927.

Chou, I., 1978, Calibration of oxygen buffers at elevated P and T by the hydrogen fugacity sensor: Am. Mineralogist, v. 63, in press.

Chou, I. M., and Frantz, J. D., 1977, Recalibration of Ag + AgCl acid buffer at elevated pressures and temperatures: Am. Jour. Sci., v. 277, p. 1067-1072.

Chou, I. M., and Williams, R. J., 1977, Hydrogen fugacity sensor measurements of the quartz–fayalite–magnetite and hematite–magnetic buffer reactions [abs.]: Am. Geophys. Union Trans., v. 58, p. 520.

Christ, C. L., Hostetler, P. B., and Siebert, R. M., 1973, Studies in the system MgO–SiO_2–CO_2–H_2O(III): The activity-product constant of sepiolite: Am. Jour. Sci., v. 273, p. 65-83.

———— 1974, Stabilities of calcite and aragonite: U.S. Geol. Survey Jour. Research, v. 2, p. 175-184.

CODATA, 1976, CODATA recommended key values for thermodynamics, 1975, Report of the CODATA task group on key values for thermodynamics, 1975: Jour. Chem. Thermodynamics, v. 8, p. 603-605.

Cohen, L. H., and Klement, W., Jr., 1967, High-low quartz inversion: determination to 35 kilobars: Jour. Geophys. Research, v. 72, p. 4245-4251.

Coombs, D. S., Ellis, A. J., Fyfe, W. S., and Taylor, A. M., 1959, The zeolite facies. With comments on the interpretation of hydrothermal synthesis: Geochim. et Cosmochim. Acta, v. 17, p. 53-107.

Coombs, D. S., and Whetten, J. T., 1967, Composition of analcime from sedimentary and buried metamorphic rocks: Geol. Soc. America Bull., v. 78, p. 269-282.

Coughlin, J. P., 1958, Heats of formation of cryolite and sodium fluoride: Am. Chem. Soc. Jour., v. 80, p. 1802-1804.

Crawford, W. A., and Fyfe, W. S., 1965, Lawsonite equilibria: Am. Jour. Sci., v. 263, p. 262-270.

Crawford, W. A., and Hoersh, A. L., 1972, Calcite–aragonite equilibrium from 50°C to 150°C: Am. Mineralogist, v. 57, p. 995-997.

Crerar, D. A., and Barnes, H. L., 1976, Ore solution chemistry. V. Solubilities of chalcopyrite and chalcocite assemblages in hydrothermal solution at 200° to 350°C: Econ. Geology, v. 71, no. 4, p. 773-794.

Day, H. W., 1970, Redetermination of the stability of muscovite + quartz: Geol. Soc. America Abs. with Programs, v. 2, p. 535.

———— 1973, The high temperature stability of muscovite plus quartz: Am. Mineralogist, v. 58, p. 255-262.

DeCoster, M., Pollack, H., and Amelinckx, S., 1963, A study of Mössbauer Absorption in iron silicates: Physica stat. solidi, v. 3, p. 283-288.

Deer, W. A., Howie, R. A., and Zussman, J., 1962, Rock-forming minerals, v. 3, Sheet Silicates: New York, John Wiley & Sons, Inc. 270 p.

———— 1962, Rock-forming minerals, v. 5, Non-silicates: New York, John Wiley & Sons, Inc., 371 p.

Delany, J. M., and Helgeson, H. C., 1978, Calculation of the thermodynamics of dehydration in subducting oceanic crust to 100 kb and 800°C: Am. Jour. Sci., v. 278, p. 638-686.

Demarest, H. H., Jr., 1972, Lattice model calculation of elastic and thermodynamic properties at high pressure and temperature: Physics Earth Planetary Interiors, v. 6, p. 146-153.

Denbigh, K., 1971, The principles of chemical equilibrium, 3d ed.: Cambridge, Cambridge Univ. Press, 494 p.

Din, F., 1961, Thermodynamic functions of gases, v. 3: London, Butterworths, 218 p.

Dollase, W. A., 1971, Refinement of the crystal structures of epidote, allanite, and hancockite: Am. Mineralogist, v. 56, p. 447-464.

———— 1973, Mössbauer spectra and iron distribution in the epidote group minerals: Zeitschr. Kristallographie, v. 138, p. 41-63.

Donnay, J. D. H., and Ondik, H. M., 1973, Crystal data determinative tables, 3d ed.: U.S. Dept. Commerce, Natl. Bur. Standards, Joint Comm. Powder Diff. Standards, v. 2, 1580 p.

Ernst, W. G., 1968, Amphiboles: New York, Springer-Verlag, 125 p.

Essene, E. J., Boettcher, A. L., and Furst, G. A., 1972, Indirect measurement of ΔG for quartz + corundum = kyanite [abs.]: Am. Geophys. Union Trans., v. 53, p. 554.

Eugster, H. P., and Chou, I. -M., 1973, The depositional environments of Precambrian banded iron-formations: Econ. Geology, v. 68, p. 1144-1168.

Eugster, H. P., and Skippen, G. B., 1967, Igneous and metamorphic reactions involving gas equilibria, *in* Abelson, P. H., ed., Researches in Geochemistry, v. 2: New York, John Wiley & Sons, p. 492-520.

Eugster, H. P., and Wones, D. R., 1962, Stability relations of the ferruginous biotite, annite: Jour. Petrology, v. 3, no. 1, p. 82-125.

Evans, B. W., 1965, Application of a reaction-rate method to the breakdown equilibria of muscovite plus quartz: Am. Jour. Sci., v. 263, p. 647-667.

Evans, B. W., Johannes, W., Oterdoom, H., and Trommsdorff, V., 1976, Stability of chrysotile and antigorite in the serpentinite multisystem: Schweizer min. pet. Mitt., v. 56, p. 79-93.

Fawcett, J. J., and Yoder, H. S., Jr., 1966, Phase relationships of chlorites in the system $MgO–Al_2O_3–SiO_2–H_2O$: Am. Mineralogist, v. 51, p. 353-380.

Ferrier, A., 1966, Influence de l'état de division de la goethite et de l'oxyde ferrique sur leurs chaleurs de réaction: Rev. Chimie minérale, v. 3, p. 587-615.

Fisher, J. R., and Zen, E., 1971, Thermodynamic calculations from hydrothermal phase equilibrium data and the free energy of H_2O: Am. Jour. Sci., v. 270, p. 297-314.

Fleming, P. D., and Fawcett, J. J., 1976, Upper stability of chlorite + quartz in the system $MgO–FeO–Al_2O_3–SiO_2–H_2O$ at 2 kbar water pressure: Am. Mineralogist, v. 61, p. 1175-1193.

Foland, K. A., 1974, Alkali diffusion in orthoclase, *in* Hoffman, A. W., Giletti, B. J., Yoder, H. S., Jr., and Yund, R. A., eds., Geochemical Transport and Kinetics: Washington, Carnegie Inst., p. 77-98.

Frink, C. R., and Peech, M., 1962, The solubility of gibbsite in aqueous solutions and soil extracts: Soil Sci. Soc. Am. Proc., v. 26, p. 346-347.

Frondel, C. F., 1962, The system of mineralogy of James Dwight Dana and Edward Salisbury Dana, 7th ed., v. III, Silica Minerals: New York, John Wiley & Sons, 334 p.

Fyfe, W. S., and Hollander, M. A., 1964, Equilibrium dehydration of diaspore at low temperatures: Am. Jour. Sci., v. 262, p. 709-712.

Fyfe, W. S., Turner, F. J., and Verhoogen, John, 1958, Metamorphic reactions and metamorphic facies: Geol. Soc. America Mem. 75, 253 p.

Garrels, R. M., and Mackenzie, F. T., 1967, Origin of the chemical compositions of some springs and lakes, *in* Equilibrium Concepts in Natural Water Systems: Am. Chem. Soc., Advances in Chemistry ser. 67, p. 222-242.

Garrels, R. M., Thompson, M. E., and Siever, R., 1960, Stability of some carbonates at 25°C and one atmosphere total pressure: Am. Jour. Sci., v. 258, p. 402-481.

Ghosh, D. S., 1976, Electrochemical determination of the standard free energy of formation of alumina at steel-making temperatures [abs.]: Dissert. Abs. Internatl., B., v. 37, p. 416.

Goldsmith, J. R., Graf, D. L., and Heard, H. C., 1961, Lattice constants of the calcium magnesium carbonates: Am. Mineralogist, v. 46, p. 453-457.

Goldsmith, J. R., and Heard, H. C., 1961, Subsolidus phase relations in the system $CaCO_3–MgCO_3$: Jour. Geology, v. 69, p. 45-74.

Goldsmith, J. R., and Newton, R. C., 1969, P-T-X relations in the system $CaCO_3–MgCO_3$ at high temperatures and pressures: Am. Jour. Sci., Schairer v. (267-A), p. 160-190.

Gordon, T. M., 1973, Determination of internally consistent thermodynamic data from phase equilibrium experiments: Jour. Geology, v. 81, p. 199-208.

Gordon, T. M., and Greenwood, H. J., 1970, The reaction: dolomite + quartz + water = talc + calcite + carbon dioxide: Am. Jour. Sci., v. 268, p. 225-242.

———— 1971, The stability of grossularite in $H_2O–CO_2$ mixtures: Am Mineralogist, v. 56, p. 1674-1688.

Green, T. H., Ringwood, A. E., and Major, A., 1966, Friction effects and pressure calibration in a piston-cylinder apparatus at high pressure and temperature: Jour. Geophys. Research, v. 71, p. 3589-3594.

Greenwood, H. J., 1961, The system $NaAlSi_2O_6$–H_2O–Argon: Total pressure and water pressure in metamorphism: Jour. Geophys. Research, v. 66, p. 3923-3946.

———— 1962, Metamorphic reactions involving two volatile components: Carnegie Inst. Washington Year Book 61, p. 82-85.

———— 1963, The synthesis and stability of anthophyllite: Jour. Petrology, v. 4, p. 317-351.

———— 1967a, Mineral equilibria in the system MgO–SiO_2–H_2O–CO_2, *in* Abelson, P. H., ed., Researches in Geochemistry, v. 2: New York, John Wiley & Sons, p. 542-592.

————1967b, Wollastonite: stability in H_2O–CO_2 mixtures and occurrence in a contact-metamorphic aureole near Salemo, British Columbia, Canada: Am. Mineralogist, v. 52, p. 1669-1680.

———— 1969, The compressibility of gaseous mixtures of carbon dioxide and water between 0 and 500 bars pressure and 450° and 800° centigrade: Am. Jour. Sci., Schairer v. (267-A), p. 191-208.

———— 1971, Anthophyllite. Corrections and comments on its stability: Am. Jour. Sci., v. 270, p. 151-154.

———— 1973, Thermodynamic properties of gaseous mixtures of H_2O and CO_2 between 450° and 800° and 0 to 500 bars: Am. Jour. Sci., v. 273, p. 561-571.

Grover, J. E., and Orville, P. M., 1969, The partitioning of atoms between coexisting single- and multi-site phases with application to the assemblages: orthopyroxene–clinopyroxene and orthopyroxene–olivine: Geochim. et Cosmochim. Acta, v. 33, p. 205-226.

Gustafson, W. I., 1974, Stability relations of andradite, hedenbergite, and related minerals in the system Ca–Fe–Si–O–H: Jour. Petrology, v. 15, p. 455-496.

Haas, H. H., 1972, Diaspore–corundum equilibrium determined by epitaxis of diaspore on corundum: Am. Mineralogist, v. 57, p. 1375-1385.

Haas, H. H., and Holdaway, M. J., 1973, Equilibria in the system Al_2O_3–SiO_2–H_2O involving the stability limits of pyrophyllite, and thermodynamic data of pyrophyllite: Am. Jour. Sci., v. 273, p. 449-464.

Haas, J. L., and Fisher, J. R., 1976, Simultaneous evaluation and correlation of thermodynamic data: Am. Jour. Sci., v. 276, p. 525-545.

Haas, J. L., and Robie, R. A., 1973, Thermodynamic data for wustite, $Fe_{.947}O$, Magnetite, Fe_3O_4, and Hematite, Fe_2O_3 [abs.]: Am. Geophys. Union Trans., v. 54, p. 483.

Hariya, Y., and Kennedy, G. C., 1968, Equilibrium study of anorthite under high pressure and high temperature: Am. Jour. Sci., v. 266, p. 193-203.

Harker, R. I., and Tuttle, O. F., 1955, Studies in the system CaO–MgO–CO_2. Pt. 1, The thermal dissociation of calcite, dolomite, and magnesite: Am. Jour. Sci., v. 253, p. 209-224.

———— 1956, Experimental data on the P_{CO_2}–T curve for the reaction: calcite + quartz = wollastonite + carbon dioxide: Am. Jour. Sci., v. 254, p. 239-256.

Hays, J. F., 1967, Lime–alumina–silica: Carnegie Inst. Washington Year Book 65, p. 234-239.

Hays, J. F., and Bell, P. M., 1973, Albite–jadeite–quartz equilibrium: A hydrostatic determination. The reaction: albite = jadeite + quartz [abs.]: Am. Geophys. Union Trans., v. 54, p. 482.

Helgeson, H. C., 1967, Thermodynamics of complex dissociation in aqueous solution at elevated temperatures: Jour. Phys. Chemistry, v. 71, p. 3121-3136.

———— 1969, Thermodynamics of hydrothermal systems at elevated temperatures and pressures: Am. Jour. Sci., v. 267, p. 729-804.

———— 1970, A chemical and thermodynamic model of ore deposition in hydrothermal systems: Mineralog. Soc. America Spec. Pub. 3, p. 155-186.

———— 1978, Mass transfer among minerals and hydrothermal solutions, *in* Barnes, H. L., ed., Geochemistry of Hydrothermal Ore Deposits, v. II: New York, Holt, Rinehart, and Winston, Inc., in press.

Helgeson, H. C., and Kirkham, D. H., 1974a, Theoretical prediction of the thermodynamic behavior of aqueous electrolytes at high pressures and temperatures. I. Summary of the thermodynamic/electrostatic properties of the solvent: Am. Jour. Sci., v. 274, p. 1089-1198.

———— 1974b, Theoretical prediction of the thermodynamic behavior of aqueous electrolytes at high pressures and temperatures. II. Debye-Hückel parameters for activity coefficients and relative partial molal properties: Am. Jour. Sci., v. 274, p. 1199-1261.

———— 1976, Theoretical prediction of the thermodynamic behavior of aqueous electrolytes at high pressures and temperatures: III. Equation of state for aqueous species at infinite dilution: Am. Jour. Sci., v. 276, p. 97-240.

———— in preparation, Theoretical prediction of the thermodynamic behavior of aqueous electrolytes at high pressures and temperatures. IV. Calculation of activity coefficients, osmotic coefficients, and apparent molal and standard and relative partial molal properties to 5 kb and 600°C: Am. Jour. Sci., in preparation.

Helgeson, H. C., and MacKenzie, F. T., 1970, Silicate-sea water equilibria in the ocean system: Deep-Sea Research, v. 17, p. 877-892.

Hemingway, B. S., and Robie, R. A., 1972, The heat capacities at low temperatures and entropies at 298.15°K of huntite, $CaMg_3(CO_3)_4$, and artinite, $Mg_2(OH)_2CO_3 \cdot 3H_2O$: Am. Mineralogist, v. 57, p. 1754-1767.

———— 1973, A calorimetric determination of the standard enthalpies of formation of huntite, $CaMg_3(CO_3)_4$, and artinite, $Mg(OH)_2CO_3 \cdot 3H_2O$, and their standard Gibbs free energies of formation: U.S. Geol. Survey Jour. Research, v. 1, no. 5, p. 535-541.

———— 1977a, Enthalpies of formation of low albite ($NaAlSi_3O_8$), Gibbsite ($Al(OH)_3$) and $NaAlO_2$: revised values for $\Delta H^\circ_{f,298}$ and $\Delta G^\circ_{f,298}$ of some alumino-silicate minerals: U.S. Geol. Survey Jour. Research, v. 5, p. 413-429.

———— 1977b, The entropy and Gibbs free energy of formation of the aluminum ion: Geochim. et Cosmochim. Acta, v. 41, p. 1402-1404.

Hemley, J. J., 1959, Some mineralogical equilibria in the system K_2O–Al_2O_3–SiO_2–H_2O: Am. Jour. Sci., v. 257, p. 241-270.

———— 1967, Stability relations of pyrophyllite, andalusite, and quartz at elevated temperatures: Am. Geophys. Union Trans., v. 48, p. 224.

Hemley, J. J., Meyer, C., and Richter, D. H., 1961, Some alteration reactions in the system Na_2O–Al_2O_3–SiO_2–H_2O: U.S. Geol. Survey Prof. Paper 424D, p. 338-340.

Hemley, J. J., Montoya, J. W., Christ, C. L., and Hostetler, P. B., 1977a, Mineral equilibria in the MgO–SiO_2–H_2O system: I. Talc-chrysotile-forsterite-brucite stability relations: Am. Jour. Sci., v. 277, p. 322-351.

Hemley, J. J., Montoya, J. W., Nigrini, A., and Vincent, H. A., 1971, Some alteration reactions in the system CaO–Al_2O_3–SiO_2–H_2O: Soc. Mining Geol. Japan, Spec. issue 2, p. 58-63.

Hemley, J. J., Montoya, J. W., Shaw, D. R., and Luce, R. W., 1977b, Mineral equilibria in the MgO–SiO_2–H_2O system: II. Talc–antigorite–forsterite–anthophyllite–enstatite stability relations and some geologic implications in the system: Am. Jour. Sci., v. 277, p. 353-383.

Hemley, J. J., Shapiro, L., Shaw, D. R., and Luce, R. L., 1975, Stability relations of anthophyllite [abs.]: Geol. Soc. America Abs. with Programs, v. 7, p. 1109.

Hewitt, D. A., 1973, Stability of the assemblage muscovite–calcite–quartz: Am. Mineralogist, v. 58, p. 785-791.

———— 1975, Stability of the assemblage phlogopite–calcite–quartz: Am. Mineralogist, v. 60, p. 391-397.

———— 1976, A redetermination of the fayalite–magnetite–quartz equilibrium between 650 and 850°C [abs.]: Am. Geophys. Union Trans., v. 57, p. 1020.

Hill, V. G., and Ellington, A. C., 1961, Chemical characteristics of the ground water resources of Jamaica, W. I.: Econ. Geology, v. 56, p. 533-541.

Hlabse, T., and Kleppa, O. J., 1968, The thermochemistry of jadeite: Am. Mineralogist, v. 53, p. 1281-1292.

Holdaway, M. J., 1971, Stability of andalusite and the aluminum silicate phase diagram: Am. Jour. Sci., v. 271, p. 97-131.

———— 1972, Thermal stability of aluminum-iron epidote as a function of f_{O_2} and iron content: Contr. Mineralogy Petrology, v. 36, p. 307-340.

Holder, J., and Granato, A. V., 1969, Thermodynamic properties of solids containing defects: Phys. Rev., v. 182, p. 729-741.

Holland, H. D., Kirsipu, T. V., Hueber, J. S., and Oxburgh, U. M., 1964, On some aspects of the chemical evolution of cave waters: Jour. Geology, v. 72, p. 36-67.

Holley, C. E., and Huber, E. J., Jr., 1951, The heats of combustion of magnesium and aluminum: Am. Chem. Soc. Jour., v. 73, p. 5577-5579.

Holloway, J. R., 1977, Fugacity and activity of molecular species in supercritical fluids, *in* Fraser, D. G., ed., Thermodynamics in Geology: Netherlands, D. Reidel Pub. Co., p. 161-181.

Holloway, J. R., and Reese, R. L., 1974, The generation of N_2–CO_2–H_2O fluids for use in hydrothermal experimentation. I. Experimental method and equilibrium calculations in the system C–O–H–N: Am. Mineralogist, v. 59, p. 587-597.

Holm, J. L., and Kleppa, O. J., 1966, The thermodynamic properties of the aluminum silicates: Am. Mineralogist, v. 51, p. 1608-1622.

———— 1968, Thermodynamics of the disordering process in albite: Am. Mineralogist, v. 53, p. 123-133.

Holm, J. L., Kleppa, O. J., and Westrum, E. F., Jr., 1967, Thermodynamics of polymorphic transformations in silica. Thermal properties from 5° to 1070°K and pressure-temperature stability fields for coesite and stishovite: Geochim. et Cosmochim. Acta, v. 31, p. 2289-2307.

Hoschek, G., 1973, Die Reaktion Phlogopit + Calcit + Quarz = Tremolit + Kalifeldspat + H_2O + CO_2: Contr. Mineralogy Petrology, v. 39, p. 231-237.

———— 1974, Gehlenite stability in the system CaO–Al_2O_3–SiO_2–H_2O–CO_2: Contr. Mineralogy Petrology, v. 47, p. 245-254.

Hovis, G. L., 1974, A solution calorimetric and X-ray investigation of Al–Si distribution in monoclinic potassium feldspars, *in* MacKenzie, W. S., and Zussman, J., eds., The Feldspars: New York, Crane, Russak and Co., Inc., p. 114-144.

Hsu, K. J., 1963, Solubility of dolomite and composition of Florida ground waters: Jour. Hydrology, v. 1, p. 288-310.

Huang, W. H., and Keller, W. D., 1973, Gibbs free energies of formation calculated from dissolution data using specific mineral analyses. III. Clay minerals: Am. Mineralogist, v. 58, p. 1023-1028.

Huber, E. J., Jr., and Holley, C. E., Jr., 1956, The heat of combustion of calcium: Jour. Phys. Chemistry, v. 60, p. 498-499.

Huckenholz, H. G., Hölzl, E., and Lindhuber, W., 1975, Grossularite, its solidus and liquidus relations in the CaO–Al_2O_3–SiO_2–H_2O system up to 10 kbar: Neues Jahrb. Mineralogie Abh., v. 124, p. 1-46.

Iler, R. K., 1955, The colloid chemistry of silica and silicates: Ithaca, N. Y., Cornell Univ. Press.

Johannes, W., 1967, Zur bildung und stabilität von forsterit, talk, serpentin, quarz und magnesit im system MgO–SiO_2–H_2O–CO_2: Contr. Mineralogy Petrology, v. 15, p. 233-250.

———— 1968, Experimental investigation of the reaction forsterite + H_2O $\rightleftharpoons$ serpentine + brucite: Contr. Mineralogy Petrology, v. 19, p. 309-315.

Johannes, W., Bell, P. M., Mao, H. K., Boettcher, A. L., Chipman, D. W., Hays, J. F., Newton, R. C., and Seifert, S., 1971, An interlaboratory comparison of piston-cylinder pressure calibration using the albite-breakdown reaction: Contr. Mineralogy Petrology, v. 32, p. 24-38.

Karpov, I. K. and Kashik, S. A., 1968, Computer calculation of standard isobaric-isothermal potentials of silicates by multiple regression from a crystallochemical classification: Geochem. Internat., v. 5, no. 4, p. 706-713.

Kelley, K. K., 1960, Contributions to the data on theoretical metallurgy. XIII. High temperature heat content, heat capacity and entropy data for the elements and inorganic compounds: U.S. Bur. Mines Bull. 584, 232 p.

———— 1962, Heats and free energies of formation of anhydrous silicates: U.S. Bur. Mines Rept. Inv. 5091, 32 p.

Kelley, K. K., and King, E. G., 1961, Contributions to the data on theoretical metallurgy XIV. Entropies of the elements and inorganic compounds: U.S. Bur. Mines Bull. 592, 149 p.

Kelley, K. K., Shomate, C. H., Young, F. E., Naylor, B. F., Salo, A. E., and Juffman, E. H., 1946, Thermodynamic properties of ammonium and potassium alums and related substances with reference to extraction of alumina from clay and alunite: U.S. Bur. Mines Tech. Paper No. 688, 104 p.

Kelley, K. K., Todd, S. S., Orr, R. L., King, E. G., and Bonnickson, K. R., 1953, Thermodynamic properties of sodium-aluminum and potassium-aluminum silicates: U.S. Bur. Mines Rept. Inv. 4955, 21 p.

Kerrick, D. M., 1968, Experiments on the upper stability limit of pyrophyllite at 1.8 kilobars and 3.9 kilobars water pressure: Am. Jour. Sci., v. 266, p. 204-214.

———— 1972, Experimental determination of muscovite + quartz stability with $P_{H_2O} < P_{total}$: Am. Jour. Sci., v. 272, p. 946-958.

Kerrick, D. M., and Darken, L. S., 1975, Statistical thermodynamic models for ideal oxide and silicate solid solutions, with application to plagioclase: Geochim. et Cosmochim. Acta, v. 39, p. 1431-1442.

Kim, Ki-Tae, and Burley, B. J., 1971, Phase equilibria in the system $NaAlSi_3O_8$–$NaAlSiO_4$–H_2O with special emphasis on the stability of analcite: Canadian Jour. Earth Sci., v. 8, p. 311-337.

King, E. G., 1955, Low-temperature heat capacity and entropy at 298.16°K of analcite: Am. Chem. Soc. Jour., v. 87, p. 2192-2193.

King, E. G., Barany, R., Weller, W. W., and Pankratz, L. B., 1967, Thermodynamic properties of forsterite and serpentine: U.S. Bur. Mines Rept. Inv. 6962, 18 p.

King, E. G., Ferrante, M. J., and Pankratz, L. B., 1975, Thermodynamic data for $Mg(OH)_2$ (brucite): U.S. Bur. Mines Rept. Inv. 8041, 13 p.

King, E. G., Mah, A. D., and Pankratz, L. B., 1973, Thermodynamic properties of copper and its inorganic compounds: New York, Internat. Copper Research Assoc., 257 p.

King, E. G., and Weller, W. W., 1961a, Low-temperature heat capacities and entropies at 298.15°K of diaspore, kaolinite, dickite, and halloysite: U.S. Bur. Mines Rept. Inv. 5810, 6 p.

———— 1961b, Low-temperature heat capacities and entropies at 298.15°K of some sodium- and calcium-aluminum silicates: U.S. Bur. Mines Rept. Inv. 5855, 8 p.

Kiseleva, I. A., and Topor, N. D., 1973, On the thermodynamic properties of zoisite: Geochem. Internat., v. 10, p. 1555.

Kiseleva, I. A., Topor, N. D., and Andreyenko, E. D., 1974, Thermodynamic parameters of minerals of the epidote group: Geochem. Internat., v. 11, p. 389-398.

Kiseleva, I. A., Topor, N. D., and Mel'chakova, L. V., 1972, Experimental determination of the heat content and heat capacity of grossularite, andradite, and pyrope [abs.]: Geochem. Internat., v. 9, p. 1087.

Kitahara, S., and Kennedy, G. C., 1964, The quartz–coesite transition: Jour. Geophys. Research, v. 69, p. 5395-5400.

Kittrick, J. A., 1966a, The free energy of formation of gibbsite and $Al(OH)_3$ from solubility measurements: Soil Sci. Soc. America Proc., v. 30, no. 5, p. 595-598.

———— 1966b, Free energy of formation of kaolinite from solubility measurements: Am. Mineralogist, v. 51, p. 1457-1466.

———— 1967, Gibbsite-kaolinite equilibria: Soil Sci. Soc. America Proc., v. 31, p. 314-316.

———— 1969, Soil minerals in the Al_2O_3–SiO_2–H_2O system and a theory of their formation: Clays and Clay Minerals, v. 17, p. 157-167.

———— 1970, Precipitation of kaolinite at 25°C and 1 atm: Clays and Clay Minerals, v. 18, p. 261-267.

———— 1971a, Soil solution composition and stability of clay minerals: Soil Sci. Soc. America Proc., v. 35, no. 3, p. 450-454.

———— 1971b, Montmorillonite equilibria and the weathering environment: Soil Sci. Soc. America Proc., v. 35, p. 815-820.

———— 1971c, Stability of montmorillonites: I. Belle Fourche and Clay Spur montmorillonites: Soil Sci. Soc. America Proc., v. 35, no. 1, p. 140-145.

———— 1971d, Stability of montmorillonites: II. Aberdeen montmorillonites: Soil Sci. Soc. America Proc., v. 35, no. 5, p. 820-823.

Koizumi, M., and Roy, R., 1960, Zeolite studies. I. Synthesis and stability of the calcium zeolites: Jour. Geology, v. 68, p. 41-53.

Kracek, F. C., 1953, Thermochemical properties of minerals: Carnegie Inst. Washington Year Book 52, p. 69-74.

Kracek, F. C., Neuvonen, K. J., and Burley G., 1951, Thermochemistry of mineral substances. Part I. A thermodynamic study of the stability of jadeite: Washington Acad. Sci. Jour., v. 41, p. 373-383.

Kramer, J. R., 1959, Correction of some earlier data on calcite and dolomite in sea water: Jour. Sed. Petrology, v. 29, p. 465-467.

Krauskopf, K. B., 1956, Dissolution and precipitation of silica at low temperatures: Geochim. et Cosmochim. Acta, v. 10, p. 1-26.

Krupka, K. M., Kerrick, D. M., and Robie, R. A., 1977, High temperature heat capacities of dolomite, talc, and tremolite, and implications to equilibrium in the siliceous dolomite system [abs.]: Geol. Soc. America Abs. with Programs, v. 9, p. 1060.

Krupka, K. M., Robie, R. A., and Hemingway, B. S., 1977, The heat capacities of corundum, periclase, anorthite, $CaAl_2Si_2O_8$ glass, muscovite, pyrophyllite, $KAlSi_3O_8$ glass, grossular, and $NaAlSi_3O_8$ glass between 350 and 1000 K [abs.]: Am. Geophys. Union Trans., v. 58, p. 523.

Kunze, G., 1961, Antigorit. Struktur theoretische Grundlagen und ihre praktische Bedeutung für weitere Serpentin-Forschung: Fortschr. Mineralogie, v. 39, p. 206-324.

Langmuir, D., 1964, Thermodynamic properties of phases in the system CaO–MgO–CO_2–H_2O: Geol. Soc. America Abs. with Programs, p. 120.

———— 1968, Stability of calcite based on aqueous solubility measurements: Geochim. et Cosmochim. Acta, v. 32, p. 835-851.

———— 1969, The Gibbs free energies of substances in the system Fe–O_2–H_2O–CO_2 at 25°C: U.S. Geol. Survey Prof. Paper 650-B, p. B180-B184.

———— 1971a, Particle size effect on the reaction goethite = hematite + water: Am. Jour. Sci., v. 271, p. 147-156.

———— 1971b, The geochemistry of some carbonate groundwaters in central Pennsylvania: Geochim. et Cosmochim. Acta, v. 35, p. 1023-1045.

Latimer, W. M., 1952, The oxidation states of the elements and their potentials in aqueous solutions: Englewood Cliffs, N.J., Prentice-Hall, Inc., 392 p.

Lietzke, M. H., and Stoughton, R. W., 1974, The prediction of osmotic and activity coefficients for electrolyte mixtures at elevated temperatures: Oak Ridge Natl. Lab. ORNL-4999, 16 p.

Lindsley, D. H., 1965, Ferrosilite: Carnegie Inst. Washington Year Book 64, p. 148-150.

Liou, J. G., 1970, Synthesis and stability relations of wairakite, $CaAl_2Si_4O_{12} \cdot 2H_2O$: Contr. Mineralogy Petrology, v. 27, p. 259-282.

———— 1971a, Synthesis and stability of prehnite, $Ca_2Al_2Si_3O_{10}(OH)_2$: Am. Mineralogist, v. 56, p. 507-531.

———— 1971b, Analcime equilibria: Lithos, v. 4, p. 389-402.

———— 1971c, P-T stabilities of laumontite, wairakite, lawsonite, and related minerals in the system $CaAl_2Si_2O_8$–SiO_2–H_2O: Jour. Petrology, v. 12, pt. 2, p. 379-411.

———— 1973, Synthesis and stability relations of epidote, $Ca_2Al_2FeSi_3O_{12}(OH)$: Jour. Petrology, v. 14, p. 381-413.

———— 1974, Stability relations of andradite–quartz in the system Ca–Fe–Si–O–H: Am. Mineralogist, v. 59, p. 1016-1025.

Liu, C., and Lindsay, W. T., Jr., 1972, Thermodynamics of sodium chloride solutions at high temperatures: Jour. Solution Chemistry, v. 1, p. 45-70.

MacGregor, I. D., 1965, Stability fields of spinel and garnet peridotites in the synthetic system MgO–CaO–Al_2O_3–SiO_2: Carnegie Inst. Washington Year Book 64, p. 126-134.

MacKenzie, F. T., 1954, The system $NaAlSiO_4$–$NaAlSi_3O_8$–H_2O: Carnegie Inst. Washington Year Book 53, p. 119-124.

MacKenzie, F. T., and Garrels, R., 1965, Silicates: reactivity with sea water: Science, v. 150, p. 57-58.

Mah, A. D., 1957, Heats of formation of alumina, molybdenum trioxide and molybdenum dioxide: Jour. Phys. Chemistry, v. 61, p. 1572-1576.

Mah, A. D., Pankratz, L. B., Weller, W. W., and King, E. G., 1967, Thermodynamic data for cuprous and cupric oxides: U.S. Bur. Mines Rept. Inv. 7026, 20 p.

Maier, C. G., and Kelley, K. K., 1932, An equation for the representation of high temperature heat content data: Am. Chem. Soc. Jour., v. 54, p. 3243-3246.

Matsui, U., and Banno, S., 1965, Intracrystalline exchange equilibrium in silicate solid solutions: Japanese Acad. Proc., v. 41, p. 461-466.

Mazo, R. M., 1977, Statistical mechanical calculation of aluminum–silicon disorder in albite: Am. Mineralogist, v. 62, p. 1232-1237.

Mel'nik, Y. P., 1972, Thermodynamic constants for the analysis of conditions of formation of iron ores (in Russian): Ukranian U.S.S.R., Kiev Acad. Sci., Inst. Geochemistry and Physics of Minerals, 193 p.

Mel'nik, Y. P., and Onopriyenko, V. L., 1969, Thermodynamic properties of anthophyllite: Geochem. Internat., v. 6, p. 994-999.

Merino, Enrique, ms, 1973, Diagenetic mineralogy and water chemistry in Tertiary sandstones from Kettleman North Dome, San Joaquin Valley, California: Ph.D. thesis, Geology Dept., Univ. California, Berkeley.

———— 1975, Diagenesis in tertiary sandstones from Kettleman North Dome, California—II. Interstitial solutions: chemical relation to the diagenetic mineralogy: Geochim. et Cosmochim. Acta, v. 39, p. 1629-1645.

Mills, K. C., 1974, Thermodynamic data for inorganic sulphides, selenides, and tellurides: London, Butterworths, 845 p.

Moelwyn-Hughes, A. E., 1961, Physical chemistry, 2d ed.: Oxford, Pergamon Press, p. 667-679.

Montoya, J. W., and Hemley, J. J., 1975, Activity relations and stabilities in alkali feldspar and mica alteration reactions: Econ. Geology, v. 70, p. 577-594.

Morey, G. W., 1957, The solubility of solids in gases: Econ. Geology, v. 52, p. 225-251.

Mueller, R. F., 1962, Energetics of certain silicate solid solutions: Geochim. et Cosmochim. Acta, v. 26, p. 581-598.

Naumov, G. B., Ryzhenko, B. N., and Khodakovskii, Y. L., 1971, Handbook of thermodynamic quantities for geology (in Russian): Moscow, Atomic Press, 240 p.

Navrotsky, A., 1971, The intracrystalline cation distribution and the thermodynamics of solid solution formation in the system $FeSiO_3$–$MgSiO_3$: Am Mineralogist, v. 56, p. 201-211.

Navrotsky, A., and Coons, E., 1976, Thermochemistry of some pyroxenes and related compounds: Geochim. et Cosmochim. Acta, v. 40, p. 1281-1288.

Navrotsky, A., and Loucks, D., 1977, Calculation of subsolidus phase relations in carbonates and pyroxenes: Physics and Chemistry of Minerals, v. 1, p. 109-127.

Nelson, B. W., and Roy, R., 1958, Synthesis of the chlorites and their structural and chemical constitution: Am. Mineralogist, v. 43, p. 707-710.

Nesbitt, H. W., 1977, Estimation of the thermodynamic properties of Na–Ca– and Mg–beidellites: Canadian Mineralogist, v. 15, p. 22-29.

Neuvonen, K. J., 1952, Heat of formation of merwinite and monticellite: Am. Jour. Sci., Bowen v., p. 373-380.

Newton, R. C., 1965, The thermal stability of zoisite; Jour. Geology, v. 73, p. 431-441.

———— 1966a, Kyanite–sillimanite equilibrium at 750°C: Science v. 151, p. 1222-1225.

———— 1966b, Kyanite–andalusite equilibrium from 700° to 800°C: Science, v. 153, p. 170-172.

———— 1966c, Some calc–silicate equilibrium relations: Am. Jour. Sci., v. 264, p. 204-222.

———— 1969, Some high-pressure hydrothermal experiments on severely ground kyanite and sillimanite: Am. Jour. Sci., v. 267, p. 278-284.

———— 1972, An experimental determination of the high pressure stability limits of magnesium cordierite under wet and dry conditions: Jour. Geology, v. 80, p. 398-420.

Newton, R. C., Charlu, T. V., and Kleppa, O. J., 1974, A calorimetric investigation of the stability of anhydrous magnesium cordierite with application to granulite facies metamorphism: Contr. Mineralogy Petrology, v. 44, p. 295-311.

———— 1977, Thermochemistry of high pressure garnets and clinopyroxenes in the system CaO–MgO–Al_2O_3–SiO_2: Geochim. et Cosmochim. Acta, v. 41, p. 369-377.

Newton, R. C., and Kennedy, G. C., 1963, Some equilibrium reactions in the join $CaAl_2Si_2O_8$–H_2O: Jour. Geophys. Research, v. 68, p. 2967-2983.

Nitsch, K. H., 1972, Das P–T–X_{CO_2}–stabilitätsfeld von lawsonit: Contr. Mineralogy Petrology, v. 34, p. 116-134.

Nriagu, J. O., 1975, Thermochemical approximations for clay minerals: Am. Mineralogist, v. 60, p. 834-839.

O'Hare, P. A. G., 1972, Thermochemical and theoretical investigations of the sodium–oxygen system. I. The standard enthalpy of formation of sodium oxide (Na_2O): Jour. Chem. Physics, v. 56, p. 4513-4516.

Okamura, F. P., and Ghose, S., 1975, Analbite-monalbite transition in a heat-treated twinned Amelia albite: Contr. Mineralogy Petrology, v. 50, p. 211-216.

Okamura, F. P., Ghose, S., and Ohashi, H., 1974, Structure and crystal chemistry of calcium Tschermak's pyroxene, $CaAlAlSiO_6$: Am. Mineralogist, v. 59, p. 549-557.

O'Neill, M. J., and Fyans, R. L., ms, 1971, Design of differential scanning calorimeters and the performance of a new system: Norwalk, Conn., Perkin-Elmer Corp., 38 p.

Openshaw, R., ms, 1974, The low temperature heat capacities of analbite, low albite, microcline, and sanidine: Ph.D. dissert., Princeton Univ., Princeton, N.J., 312 p.

Openshaw, R. E., Hemingway, B. S., Robie, R. A., Waldbaum, D. R., and Krupka, K. M., 1976, The heat capacities at low temperatures and entropies at 298.15 K of low albite, microcline, and high sanidine: U.S. Geol. Survey Jour. Research, v. 4, p. 195-204.

Orville, P. M., 1963, Alkali ion exchange between vapor and feldspar phases: Am. Jour. Sci., v. 261, p. 201-237.

———— 1967, Unit-cell parameters of the microcline-low albite and the sanidine-high albite solid solution series: Am. Mineralogist, v. 52, p. 55-86.

———— 1972, Plagioclase cation exchange equilibria with aqueous chloride solution: results at 700°C and 2000 bars in the presence of quartz: Am. Jour. Sci., v. 272, p. 234-272.

———— 1974, The "peristerite gap" as an equilibrium between ordered albite and disordered plagioclase solid solution: Soc. franç minéralogie cristallographie Bull., v. 97, p. 386-392.

Pankratz, L. B., 1964a, High-temperature heat contents and entropies of andalusite, kyanite, and sillimanite: U.S. Bur. Mines Rept. Inv. 6370, 7 p.

———— 1964b, High-temperature heat contents and entropies of muscovite and dehydrated muscovite: U.S. Bur. Mines Rept. Inv. 6371, 6 p.

———— 1968a, High-temperature heat contents and entropies of four crystalline sodium–calcium silicates: U.S. Bur. Mines Rept. Inv. 7201, 8 p.

———— 1968b, High-temperature heat contents and entropies of dehydrated analcite, kaliophilite, and leucite: U.S. Bur. Mines Rept. Inv. 7073, 8 p.

Pankratz, L. B., and Kelley, K. K., 1964, High-temperature heat contents and entropies of akermanite, cordierite, gehlenite, and merwinite: U.S. Bur. Mines Rept. Inv. 6555, 5 p.

Pankratz, L. B., and King, E. G., 1965, High-temperature heat contents and entropies of two zinc sulfides and for solid solutions of zinc and iron sulfides: U.S. Bur. Mines Rept. Inv. 6708, 8 p.

———— 1970, High-temperature enthalpies and entropies of chalcopyrite and bornite: U.S. Bur. Mines Rept. Inv. 7435, 10 p.

Parker, V. B., Wagman, D. D., and Evans, W. H., 1971, Selected values of chemical thermodynamic properties, Pt. 6: Natl. Bur. Standards Tech. Note 270-6, 106 p.

Parks, G. A., 1972, Free energies of formation and aqueous solubilities of aluminum hydroxides and oxide hydroxides at 25°C: Am. Mineralogist, v. 57, p. 1163-1189.

Patterson, S. H., and Roberson, C. E., 1961, Weathered basalt in the eastern part of Kauai, Hawaii: U.S. Geol. Survey, Short Papers in the Geol. and Hydrologic Sci., Art. 219, p. C195-C198.

Perkins, D., III, Essene, E. J., and Westrum, E. F., Jr., 1978, New thermodynamic data for diaspore, α-AlO(OH), and its application to the system Al_2O_3–SiO_2–H_2O: Am. Mineralogist, v. 63, in press.

Perkins, D., III, Essene, E. J., Westrum, E. F., Jr., and Wall, V. J., 1977, Application of new thermodynamic data to grossular phase relations: Contr. Mineralogy Petrology, v. 64, p. 137-147.

Peterson, M. N. A., 1962, The mineralogy and petrology of upper Mississippian carbonate rocks of the Cumberland Plateau in Tennessee: Jour. Geology, v. 70, p. 1-31.

Petrović, R., 1974, Diffusion of alkali ions in alkali feldspars, *in* MacKenzie, W. S., and Zussman, J., eds., The Feldspars: New York, Crane, Russak and Co. Inc., p. 174-182.

Pitzer, K. S., and Brewer, L., 1961, Thermodynamics: New York, McGraw-Hill Book Co., 723 p.

Plummer, L. N., and MacKenzie, F. T., 1974, Predicting mineral solubility from rate data: application to the dissolution of magnesian calcites: Am. Jour. Sci., v. 274, p. 61-83.

Powell, R., 1977, Activity-composition relationships for crystalline solutions, *in* Fraser, D., ed., Thermodynamics in Geology: Netherlands, Reidel Pub. Co., p. 57-65.

Preisinger, A., 1959, X-ray study of the structure of sepiolite: Natl. Cong. on Clays and Clay Minerals, 6th, p. 61-67.

Prewitt, C. T., Sueno, S., and Papike, J. J., 1976, The crystal structure of high albite and monalbite at high temperatures: Am. Mineralogist, v. 61, p. 1213-1225.

Price, J. G., ms, 1977, Geological history of alteration and mineralization at the Yerington porphyry copper deposit, Nevada: Ph.D. dissert., Univ. California, Berkeley.

Prigogine, I., 1967, Introduction to the thermodynamics of irreversible processes, 3d ed.: New York, Intersci., 147 p.

Rapoport, P. A., and Burnham, C. W., 1973, Ferrobustamite; the crystal structure of two Ca, Fe bustamite type pyroxenoids: Zeitschr. Kristallographie, v. 138, p. 419-438.

Reed, B. L., and Hemley, J. J., 1966, Occurrence of pyrophyllite in the Kekiktuk conglomerate, Brooks Range, Northeastern Alaska: U.S. Geol. Survey Prof. Paper 550-C, p. C162-C166.

Richardson, D. W., and Brown, R. R., 1974, Enthalpy of formation of malachite [$Cu_2(CO_3)(OH)_2$]: U.S. Bur. Mines Rept. Inv. 7851, 5 p.

Richardson, S. W., Bell, P. M., and Gilbert, M. C., 1968, Kyanite–sillimanite equilibrium between 700° and 1500°C: Am. Jour. Sci., v. 266, p. 513-541.

Richardson, S. W., Gilbert, M. C., and Bell, P. M., 1969, Experimental determination of kyanite–andalusite and andalusite–sillimanite equilibria; the aluminum silicate triple point: Am. Jour. Sci., v. 267, p. 259-272.

Rittner, E. S., Hutner, R. A., and du Pré, F. K., 1949a, The work of polarization in ionic crystals of the sodium chloride type: I. Polarization around a single charge in the rigid lattice: Jour. Chem. Physics, v. 17, p. 198-203.

———— 1949b, The work of polarization in ionic crystals of the sodium chloride type. II. Polarization around two adjacent charges in the rigid lattice: Jour. Chem. Physics, v. 17, p. 204-208.

Robertson, E. C., Birch, F., and MacDonald, G. J. F., 1957, Experimental determination of jadeite stability relations to 25000 bars: Am. Jour. Sci., v. 255, p. 115-137.

Robie, R. A., Bethke, P. M., Toulmin, M. S., and Edwards, J. L., 1966, X-ray crystallographic data, densities, and molar volumes of minerals, *in* Clark, S., ed., Handbook of Physical Constants: Geol. Soc. America Mem. 97, p. 27-73.

Robie, R. S., and Hemingway, B. S., 1972, Calorimeters for heat of solution and low-temperature heat capacity measurements: U.S. Geol. Survey Prof. Paper 755, 32 p.

———— 1973, The enthalpies of formation of nesquehonite, $MgCO_3 \cdot 3H_2O$, and hydromagnesite, $5MgO \cdot 4CO_2 \cdot 5H_2O$: U.S. Geol. Survey Jour. Research, v. 1, p. 543-547.

Robie, R. A., Hemingway, B. S., and Fisher, J. R., 1978, Thermodynamic properties of minerals and related substances at 298.15°K and 1 bar (10^5 pascals) pressure and at higher temperatures: U.S. Geol. Survey Bull. 1452, 456 p.

Robie, R. A., Hemingway, B. S., and Wilson, W. H., 1976, The heat capacities of calorimetry conference copper and of muscovite $KAl_2(AlSi_3)O_{10}(OH)_2$, pyrophyllite $Al_2Si_4O_{10}(OH)_2$, and illite $K_3(Al_7Mg)(Si_{14}Al_2)O_{40}(OH)_8$ between 15 and 375 K and their standard entropies at 298.15 K: U.S. Geol. Survey Jour. Research, v. 4, p. 631-644.

Robie, R. A., and Waldbaum, D. R., 1968, Thermodynamic properties of minerals and related substances at 298.15°K (25°C) and one atmosphere (1.013 bars) pressure and at higher temperatures: U.S. Geol. Survey Bull. 1259, 256 p.

Routson, R. C., and Kittrick, J. A., 1971, Illite solubility: Soil Soc. America Proc., v. 35, p. 714-718.

Rutstein, M. S., 1971, Re-examination of the wollastonite–hedenbergite equilibria: Am. Mineralogist, v. 56, p. 2040-2052.

Ryzhenko, B. N., and Malinin, S. D., 1971, The fugacity rule for the systems CO_2–H_2O, CO_2–CH_4–CO_2–N_2, and CO_2–H_2: Geochim. Internat., v. 8, p. 899-913.

Ryzhenko, B. N., and Volkov, V. P., 1971, Fugacity coefficients of some gases in a broad range of temperatures and pressures: Geochem. Internat., v. 1971, p. 468-481.

Saha, P., 1959, Geochemical and X-ray investigation of natural and synthetic analcites: Am. Mineralogist, v. 44, p. 300-313.

———— 1961, The system $NaAlSiO_4$ (nepheline)–$NaAlSi_3O_8$ (albite)–H_2O: Am. Mineralogist, v. 46, p. 859-884.

Saxena, S. K., 1969, Silicate solid solution geothermometry. I. Use of the regular solution model: Contr. Mineralogy Petrology, v. 21, p. 338-345.

———— 1973, Thermodynamics of rock-forming crystalline solutions: New York, Springer-Verlag, 190 p.

———— 1976, Entropy estimates for some silicates at 298°K from molar volumes: Science, v. 193, p. 1241-1242.

Saxena, S. K., and Ghose, S., 1971, Mg^{2+}–Fe^{2+} order-disorder and the thermodynamics of the ortho-pyroxene crystalline solution: Am. Mineralogist, v. 56, p. 532-559.

Schneeberg, E. P., 1973, Sulfur fugacity measurements with the electrochemical cell $Ag|AgI|Ag_{2+x}S,f_{S_2}$: Econ. Geology., v. 68, p. 507-517.

Schneider, A., and Gattow, G., 1954, Zur Bildungswärme des Aluminomoxyds: Zeitschr. anorg. allgem. Chemie, v. 277, p. 41-48.

Schreyer, W., and Yoder, H. S., Jr., 1964, The system Mg–cordierite–H_2O and related rocks: Neues Jahrb. Mineralogie Abh., v. 101, p. 271-342.

Sclar, C. B., Young, A. P., Carrison, L. C., and Schwartz, C. M., 1962, Synthesis and optical crystallography of stishovite, a very high pressure polymorph of SiO_2: Jour. Geophys. Research, v. 67, p. 4049-4054.

Seifert, F., 1970, Low-temperature compatibility relations of cordierite in haplopelites of the system K_2O–MgO–Al_2O_3–SiO_2–H_2O: Jour. Petrology, v. 11, p. 73-99.

Seifert, F., and Schreyer, W., 1970, Lower temperature stability limit of Mg cordierite in the range 1-7 Kb water pressure: A redetermination: Contr. Mineralogy Petrology, v. 27, p. 225-238.

Shearer, J. A., ms, 1973, The thermochemistry of garnets and some related compounds: Ph.D., dissert., Univ. Chicago, 176 p.

Shearer, J. A., and Kleppa, O. J., 1973, The enthalpies of formation of $MgAl_2O_4$, $MgSiO_3$, Mg_2SiO_4, and Al_2SiO_5 by oxide melt solution calorimetry: Jour. Inorg. Nuclear Chemistry, v. 35, p. 1073-1078.

Sheppard, R. A., and Gude, A. J., III, 1970, Chemical composition and physical properties of phillipsite from the Pacific and Indian oceans: Am. Mineralogist, v. 55, p. 2053-2063.

Silvester, L. F., and Pitzer, K. S., 1977, Thermodynamics of electrolytes. 8. High-temperature properties, including enthalpy and heat capacity with application to sodium chloride: Jour. Phys. Chemistry, v. 81, p. 1822-1828.

Skinner, B. J., 1966, Thermal expansion, *in* Clark, S., ed., Handbook of Physical Constants: Geol. Soc. America Mem. 97, p. 75-96.

Skippen, G. B., 1971, Experimental data for reactions in siliceous marbles: Jour. Geology, v. 79, p. 457-481.

———— 1974, An experimental model for low pressure metamorphism of siliceous dolomitic marble: Am. Jour. Sci., v. 274, p. 487-509.

Slaughter, J., Kerrick, D. M., and Wall, V. J., 1975, Experimental and thermodynamic study of equilibria in the system CaO–MgO–SiO_2–H_2O–CO_2: Am. Jour. Sci., v. 275, p. 143-162.

Slaughter, M., 1966, Chemical binding in silicate minerals, Parts I, II, III: Geochim. et Cosmochim. Acta, v. 30, p. 299-339.

Smith, D., 1971, Stability of the assemblage iron-rich orthopyroxene–olivine–quartz: Am. Jour. Sci., v. 271, p. 370-382.

Smith, J. V., 1959, The crystal structure of proto-enstatite, $MgSiO_3$: Acta Cryst., v. 12, p. 515-517.

Snyder, P. E., and Seltz, H., 1945, The heat of formation of aluminum oxide: Am. Chem. Soc. Jour., v. 67, p. 683-685.

Spetzler, H., 1970, Equation of state of polycrystalline and single crystal MgO to 8 kilobars and 800°K: Jour. Geophys. Research, v. 75, p. 2073-2087.

Spetzler, H., Sammis, C. G., and O'Connell, R. J., 1972, Equation of state of NaCl: Ultrasonic measurements to 8 kbar and 800°C and static lattice theory: Jour. Phys. Chemistry Solids, v. 33, p. 1727-1750.

Staveley, L. A. K., and Linford, R. G., 1969, The heat capacity and entropy of calcite and aragonite, and their interpretation: Jour. Chem. Thermodynamics, v. 1, p. 1-11.

Steinfink, H., 1958, The crystal structure of chlorite. I. A monoclinic polymorph: Acta. Cryst., v. 11, p. 191-195.

Stephenson, D. A., Sclar, C. B., and Smith, J. V., 1966, Unit cell volumes of synthetic orthoenstatite and low clinoenstatite: Mineralog. Mag., v. 35, p. 838-846.

Stern, K. H., and Weise, E. L., 1966, High temperature properties and decomposition of inorganic salts: Part 1. Sulfates: Natl. Bur. Standards, Natl. Standard Ref. Data Ser. NBS7, 38 p.

———— 1969, High temperature properties and decomposition of inorganic salts: Part 2. Carbonates: Natl. Bur. Standards, Natl. Standard Ref. Data Ser. NBS30, 27 p.

Stishov, S. M., 1963, Equilibrium between coesite and the rutile-like modification of silica: Akad. Nauk. SSSR, Doklady, v. 148, p. 1186-1188.

Stoessell, R., ms, 1977, Low temperature geochemistry of sepiolite and kerolite: Ph.D. Thesis, Dept. Geology and Geophysics, Univ. California, Berkeley.

Storre, B., and Nitsch, K. H., 1974, Zur stabilität von Margarit im System $CaO–Al_2O_3–SiO_2–H_2O$: Contr. Mineralogy Petrology, v. 43, p. 1-24.

Stull, D. R., 1965, JANAF thermochemical tables, processing copy: Springfield, Va., Clearinghouse for Federal Sci. and Tech. Info.

Stull, D. R., and Prophet, H., 1971, JANAF thermochemical tables, 2d ed.: Natl. Bur. Standards, Natl. Standards Ref. Data Ser., NBS37, 1141 p.

Stuve, J. M., 1974, Low-temperature heat capacities of sphalerite and wurtzite: U.S. Bur. Mines. Rept. Inv., 1974, 8 p.

Sueno, S., Cameron, M., Papike, J. J., and Prewitt, C. T., 1973, The high temperature crystal chemistry of tremolite: Am. Mineralogist, v. 58, p. 649-664.

Tardy, Yves, and Garrels, R. M., 1974, A method of estimating the Gibbs energies of formation of layer silicates: Geochim. et Cosmochim. Acta., v. 38, p. 1101-1116.

———— 1976, Prediction of Gibbs energies of formation—I. Relationships among Gibbs energies of formation of hydroxides, oxides, and aqueous ions: Geochim. et Cosmochim. Acta., v. 40, p. 1051-1056.

———— 1977, Prediction of Gibbs energies of formation of compounds from the elements—II. Monovalent and divalent metal silicates: Geochim. et Cosmochim. Acta, v. 41, p. 87-92.

Taylor, B. E., and Liou, J. G., 1978, The low-temperature stability of andradite in C–O–H fluids: Am. Mineralogist, v. 63, p. 378-393.

Thompson, A. B., 1970a, A note on the kaolinite–pyrophyllite equilibrium: Am. Jour. Sci., v. 268, p. 454-458.

———— 1970b, Laumontite equilibria and the zeolite facies: Am. Jour. Sci., v. 269, p. 267-275.

———— 1971, Analcite–albite equilibria at low temperatures: Am. Jour. Sci., v. 271, p. 72-92.

———— 1973a, Gibbs energy of Al_2SiO_5 polymorphs, corundum and other aluminous minerals [abs.]: Am. Geophys. Union Trans., v. 54, p. 482.

———— 1973b, Analcime: free energy from hydrothermal data. Implications for phase equilibria and thermodynamic quantities for phases in $NaAlO_2–SiO_2–H_2O$: Am. Mineralogist, v. 58, p. 277-286.

———— 1974a, Gibbs energy of aluminous minerals: Contr. Mineralogy Petrology, v. 48, p. 123-136.

———— 1974b, Calculation of muscovite–paragonite–alkali feldspar phase relations: Contr. Mineralogy Petrology, v. 44, p. 173-194.

Thompson, J. B., Jr., 1967, Thermodynamic properties of simple solutions, *in* Abelson, P. H., ed., Researches in Geochemistry, v. II.: New York, John Wiley & Sons, p. 340-361.

———— 1969, Chemical reactions in crystals: Am. Mineralogist, v. 54, p. 341-375.

———— 1970, Geometrical possibilities for amphibole structures: Model biopyriboles [abs.]: Am. Mineralogist, v. 55, p. 292-293.

———— 1978, Biopyriboles and polysomatic series: Am. Mineralogist, v. 63, p. 239-249.

Thompson, J. B., Jr., Waldbaum, D. R., and Hovis, G. L., 1974, Thermodynamic properties related to ordering in end-member alkali feldspars, *in* MacKenzie, W. S., and Zussman, J., eds., The Feldspars: New York, Crane, Russak, and Co., Inc., p. 218-248.

Tödheide, K., and Franck, E. U., 1963, Das Zweiphasengebiet und die kritische Kurve im System Kohlendioxid—Wasser bis zu Drucken von 3500 bar: Zeitschr. Physik. Chemie Neue Folge, v. 37, p. 387-401.

Ulbrich, H. H., and Merino, E., 1974, An examination of standard enthalpies of formation of selected minerals in the system $SiO_2–Al_2O_3–K_2O–Na_2O–H_2O$: Am. Jour. Sci., v. 274, p. 510-542.

Ulbrich, H., and Waldbaum, D. R., 1976, Structural and other contributions to the third-law entropies of silicates: Geochim. et Cosmochim. Acta., v. 40, p. 1-24.

Van Tassel, R., 1962, Personal communication cited by Halla, G., Chilingar, G. V., and Bissel, H. J., 1962, Thermodynamic studies on dolomite formation and their geologic implications: an interim report: Sedimentology, v. 1, p. 296-303.

Velde, Bruce, 1966, Upper stability of muscovite: Am. Mineralogist, v. 51, p. 924-929.

———— 1971, The stability and natural occurrence of margarite: Mineralog. Mag., v. 38, p. 317-323.

Wagman, D. D., Evans, W. H., Parker, V. B., Halow, I., Bailey, S. M., and Schwinn, R. H., 1968, Selected values of chemical thermodynamic properties, Part 3: Natl. Bur. Standards Tech. Note 270-3, 264 p.

———— 1969, Selected values of chemical thermodynamic properties, Part 4: Natl. Bur. Standards Tech Note 270-4, 141 p.

Waldbaum, D. R., 1965, Thermodynamic properties of mullite, andalusite, kyanite and sillimanite: Am. Mineralogist, v. 50, p. 186-195.

———— ms, 1966, Calorimetric investigation of the alkali feldspars: Ph.D. thesis, Harvard Univ., 247 p.

———— 1968, High-temperature thermodynamic properties of alkali feldspars: Contr. Mineralogy Petrology, v. 17, p. 71-77.

———— 1971, On the enthalpy of formation of alpha–Al_2O_3 (corundum): Princeton Univ., N.J., Thermochem. Project Rept. 71-02.

———— 1973, The configurational entropies of $Ca_2MgSi_2O_7$–$Ca_2SiAl_2O_7$ melilites and related minerals: Contr. Mineralogy Petrology, v. 39, p. 33-54.

Waldbaum, D. R., and Robie, R. A., 1971, Calorimetric investigation of Na–K mixing and polymorphism in the alkali feldspars: Zeitschr. Kristallographie, v. 134, p. 381-420.

Walter, L. S., 1963a, Experimental studies on Bowen's decarbonation series: I: P-T univariant equilibria of the "monticellite" and "akermanite" reactions: Am. Jour. Sci., v. 261, p. 488-500.

———— 1963b, Experimental studies on Bowen's decarbonation series: II: P-T univariant equilibria of the reaction: forsterite + calcite = monticellite + periclase + CO_2: Am. Jour. Sci., v. 261, p. 773-779.

Walther, J. V., and Helgeson, H. C., 1977, Calculation of the thermodynamic properties of aqueous silica and the solubility of quartz and its polymorphs at high pressures and temperatures: Am. Jour. Sci., v. 277, p. 1315-1351.

Weaver, R. M., Jackson, M. L., and Syers, J. K., 1971, Magnesium and silica activities in matrix solutions of montmorillonite containing soils in relation to clay mineral stability: Soil Sci. Soc. America Proc., v. 35, p. 823-830.

Weeks, W. F., 1956, Heats of formation of metamorphic minerals in the system CaO–MgO–SiO_2–H_2O and their petrological significance: Jour. Geology, v. 64, p. 456-472.

Weisbrod, A., 1973a, Cordierite–garnet equilibrium in the system Fe–Mn–Al–Si–O–H: Carnegie Inst. Washington Year Book 72, p. 515-521.

———— 1973b, The problem of water in cordierite: Carnegie Inst. Washington Year Book 72, p. 521-523.

Weller, W. W., and Kelley, K. K., 1963, Low-temperature heat capacities and entropies at 298.15°K of akermanite, cordierite, gehlenite, and merwinite: U.S. Bur. Mines Rept. Inv., 6343, 7 p.

Wentorf, R. H., Jr., 1962, Stishovite synthesis: Jour. Geophys. Research, v. 67, p. 3648.

Westrich, H., Navrotsky, A., and Holloway, J., 1976, Thermodynamic data for pargasite, fluorpargasite, fluorapatite, and fluorphlogopite: Am. Geophys. Union Trans., v. 57, p. 1020-1021.

Westrum, E. F., Jr., Essene, E. J., and Perkins, D., III, 1977, Thermophysical properties of the garnet, grossularite $Ca_3Al_2Si_3O_{12}$: Jour. Chem. Thermodynamics, v. 10, in press.

Wilkinson, J. F. G., and Whetten, J. T., 1964, Some analcime-bearing pyroclastic and sedimentary rocks from New South Wales: Jour. Sed. Petrology, v. 34, p. 543-553.

Windom, K. E., and Boettcher, A. L., 1976, The effect of reduced activity of anorthite on the reaction grossular + quartz = anorthite + wollastonite: a model for plagioclase in the earth's lower crust and upper mantle: Am. Mineralogist, v. 61, p. 889-896.

Winter, J. K., and Ghose, S., 1977, A reinvestigation of the analbite → monalbite transition at high temperatures [abs.]: Am. Geophys. Union Trans., v. 58, p. 522.

Wones, D. R., Burns, R. G., and Carroll, B. M., 1971, Stability and properties of synthetic annite [abs.]: EOS, Am. Geophys. Union Trans., v. 52, p. 369-370.

Wones, D. R., and Dodge, F. C., 1966, On the stability of phlogopite [abs.]: Geol. Soc. America Spec. Paper 101, p. 242.

———— 1977, The stability of phlogopite in the presence of quartz and diopside, *in* Fraser, D. G., ed., Thermodynamics in Geology: Netherlands, D. Reidel Pub. Co., p. 229-247.

Wones, D. R., and Eugster, H. P., 1965, Stability of biotite: experiment, theory, and application: Am. Mineralogist, v. 50, p. 1228-1272.

Wones, D. R., and Gilbert, M. C., 1969, The fayalite–magnetite–quartz assemblage between 600° and 800°C: Am. Jour. Sci., v. 267-A (Schairer V.), p. 480-488.

Wood, B. J., and Banno, S., 1973, Garnet–orthopyroxene and orthopyroxene–clinopyroxene relationships in simple and complex systems: Contr. Mineralogy Petrology, v. 42, p. 109-124.

Wood, B. J., and Strens, R. G. J., 1971, The orthopyroxene geobarometer: Earth Planetary Sci. Letters, v. 11, p. 1-6.

———— 1972, Calculation of crystal field splitting in distorted coordination polyhedra: spectra and thermodynamic properties of minerals: Mineralog. Mag., v. 38, p. 910-917.

Yoder, H. S., Jr., 1950, High-low quartz inversion up to 10,000 bars: Am. Geophys. Union Trans., v. 31, p. 827-835.

———— 1968, Akermanite and related melilite-bearing assemblages: Carnegie Inst. Washington Year Book 66, p. 471-477.

Young, P. A., 1967, The stability of the copper–iron sulphides: Australian Min. Dev. Lab. Bull., no. 3, p. 1-19.

Yund, R. A., and Kullerud, G., 1966, Thermal stability of assemblages in the Cu–Fe–S system: Jour. Petrology, v. 7, p. 454-488.

Zen, E-an, 1969a, Free energy of formation of pyrophyllite from hydrothermal data: Values, discrepancies, and implications: Am. Mineralogist, v. 54, p. 1592-1606.

———— 1969b, The stability relations of the polymorphs of aluminum silicate: a survey and some comments: Am. Jour. Sci., v. 267, p. 297-309.

———— 1971, Comments on the thermodynamic constants and hydrothermal stability relations of anthophyllite: Am. Jour. Sci., v. 270, p. 136-150.

———— 1972, Gibbs free energy, enthalpy, and entropy of ten rock-forming minerals: calculations, discrepancies, implications: Am. Mineralogist, v. 57, p. 524-553.

———— 1973, Thermodynamical parameters of minerals from oxygen-buffered hydrothermal equilibrium data: Method and application to annite and almandine: Contr. Mineralogy Petrology, v. 39, p. 65-80.

———— 1977, The phase equilibrium calorimeter, the petrogenetic grid, and a tyranny of numbers: Am. Mineralogist, v. 62, p. 189-204.

Zen, E-an, and Chernosky, J. V., Jr., 1976, Correlated free energy values of anthophyllite, brucite, clinochrysotile, enstatite, forsterite, quartz, and talc: Am. Mineralogist, v. 61, p. 1156-1166.

Subject Index to Volume 278-A